

CHEMIA

**STUDIA UNIVERSITATIS BABEȘ-BOLYAI
CHEMIA**

4/2019

EDITORIAL BOARD OF STUDIA UNIVERSITATIS BABEȘ-BOLYAI CHEMIA

ONORARY EDITOR:

IONEL HAIDUC – Member of the Romanian Academy

EDITOR-IN-CHIEF:

LUMINIȚA SILAGHI-DUMITRESCU

EXECUTIVE EDITOR:

CASTELIA CRISTEA

EDITORIAL BOARD:

PAUL ȘERBAN AGACHI, Babeș-Bolyai University, Cluj-Napoca, Romania

LIVAIN BREAU, UQAM University of Quebec, Montreal, Canada

HANS JOACHIM BREUNIG, Institute of Inorganic and Physical Chemistry,
University of Bremen, Bremen, Germany

JEAN ESCUDIE, HFA, Paul Sabatier University, Toulouse, France

ION GROSU, Babeș-Bolyai University, Cluj-Napoca, Romania

EVAMARIE HEY-HAWKINS, University of Leipzig, Leipzig, Germany

FLORIN DAN IRIMIE, Babeș-Bolyai University, Cluj-Napoca, Romania

FERENC KILAR, University of Pecs, Pecs, Hungary

BRUCE KING, University of Georgia, Athens, Georgia, USA

ANTONIO LAGUNA, Department of Inorganic Chemistry, ICMA, University
of Zaragoza, Zaragoza, Spain

JURGEN LIEBSCHER, Humboldt University, Berlin, Germany

KIERAN MOLLOY, University of Bath, Bath, UK

IONEL CĂTĂLIN POPESCU, Babeș-Bolyai University, Cluj-Napoca, Romania

CRISTIAN SILVESTRU, Babeș-Bolyai University, Cluj-Napoca, Romania

[http://chem.ubbcluj.ro/~studiachemia/;](http://chem.ubbcluj.ro/~studiachemia/)
studiachemia@chem.ubbcluj.ro
http://www.studia.ubbcluj.ro/serii/chemia/index_en.html

YEAR
MONTH
ISSUE

Volume 64 (LXIV) 2019
DECEMBER
4

STUDIA UNIVERSITATIS BABEȘ-BOLYAI CHEMIA

4

ISSUE DOI:10.24193/subbchem.2019.4

STUDIA UBB EDITORIAL OFFICE: B.P. Hasdeu no. 51, 400371 Cluj-Napoca, Romania,
Phone + 40 264 405352

CUPRINS – CONTENT – SOMMAIRE – INHALT

ȘTEFAN CRISTIAN GALUSNYAK, SIMION DRĂGAN, Mathematical Modeling of Steam Methane Reforming Process	7
ADRIAN CATALIN SOIT, IONELA DUMBRAVA, VLAD-CRISTIAN SANDU, ANA-MARIA CORMOS, Modelling and Simulation of Water Gas Shift Reactor Using COMSOL Multiphysics	19
SORINA BORAN, ANDRA TĂMĂȘ, GIANNIN MOȘOARCĂ, Soybean Bioester Obtained in a Bubble Column Esterification Reactor – A Rheological Study	31
ANDRADA S. MĂICĂNEANU, RALUCA PLEȘA CHICINAȘ, HOREA BEDELEAN, Treated Diatomite for Toluidine Blue Removal from Wastewater. Is it Worth it?	37
SHIN-LEEI OOI, SIEW-TENG ONG, Remediation of Lead (II) and Malachite Green from Aqueous Solution using Palm Oil Fruit Fibre.....	55

DANA CRĂCIUN, DANIELA DASCĂLU, ADRIANA ISVORAN, Computational Assessment of the ADME-TOX Profiles and Harmful Effects of the Most Common Used Phthalates on the Human Health	71
CORINA VOINA, ADRIANA MURESAN, ADA DELEAN, AMALIA IONELA MOLDOVAN, LAURA SILAGHI DUMITRESCU, ANDRADA VOINA TONEA, MADALINA VALEANU, Effect of an Experimental Green Tea Extract Bleaching Gel on the Color Changes of a Composite Resin	93
LAURA SILAGHI-DUMITRESCU, ANA MARIA MIHĂILESCU, ALEXANDRINA MUNTEAN, CODRUTA SAROSI, DOINA PRODAN, MEDA ROMANA SIMU, MARIOARA MOLDOVAN, ANDREA KUI, MIHAELA PASTRAV, Remineralization Products Effect on Human Enamel in Vitro Study	107
ÖZLEM AKSU DÖNMEZ, Multivariate Calibration Method for Simultaneous Estimation of Fluocortolone Caproate, Fluocortolone Pivalate and Cinchocaine HCl in Suppository	121
ROXANA T. PATRUT, ADRIAN PATRUT, JEAN-MICHEL LEONG POCK-TSY, STEPHAN WOODBORNE, LASZLO RAKOSY, PASCAL DANTHU, ILEANA-ANDREEA RATIU, JENÖ BODIS, KARL VON REDEN, Radiocarbon Investigation of a Superlative Grandidier Baobab, the Big Reniala of Isosa	131
THOMAS DIPPONG, ALEXANDRA AVRAM, CRISTINA MIHALI, GAS-Chromatography Assessments of the Major Volatile Compounds in Traditional Fruit Brandies Throughout Fruit and Wood Maturation.....	141
FLORIN DUMITRU BORA, ANAMARIA CĂLUGĂR, CLAUDIU IOAN BUNEA, VALENTIN PETRESCU MAG, CLAUDIA CIMPOIU, RĂZVAN VASILE FILIMON, Trace Metal Concentration and Human Health Risk Assessment in Distilled Alcoholic Beverages in Romania	157
KANAGAT KAZHMUKHANOVICH KISHIBAYEV, ZHANIBEK SERIKOVICH ASSYLHANOV, DARIA BAZARBEOVNA MARKINA, SERGEY VITALIEVICH NECHIPURENKO, AZHAR AIDAROVNA ATCHABAROVA, RUSTAM RISHATOVICH TOKPAYEV, SERGEY ANATOLIEVICH YEFREMOV, SERGEY NIKOLAEVICH KALUGIN, VLADIMIR LEONIDOVICH RUSSINOV, KAZHMUKHAN ORAZOVICH KISHIBAYEV, Preparation and Study of Growth Stimulating Activity of 1-Propyl-4-(3'-Amino-1', 2', 4'-Triazolo-3'-Thiopropinyl) Piperidin-4-ol	177

SIMONA CODRUȚA AURORA COBZAC, DORINA CASONI, MIHAELA BADEA, BILJANA BALABANOVA, NATALIJA MARKOVA RUZDIK, Ultraviolet-Visible (UV-VIS) Spectroscopy and Cluster Analysis as a Rapid Tool for Classification of Medicinal Plants.....	191
CARMEN SOCACIU, From Phytochemistry to Metabolomics: Eight Decades of Research in Plant and Food Science	205

Studia Universitatis Babes-Bolyai Chemia has been selected for coverage in Thomson Reuters products and custom information services. Beginning with V. 53 (1) 2008, this publication is indexed and abstracted in the following:

- Science Citation Index Expanded (also known as SciSearch®)
- Chemistry Citation Index®
- Journal Citation Reports/Science Edition

MATHEMATICAL MODELING OF STEAM METHANE REFORMING PROCESS

ȘTEFAN CRISTIAN GALUSNYAK^a, SIMION DRĂGAN^{a*}

ABSTRACT. This article presents the mathematical model of mass balance, the mathematical model at equilibrium for steam methane reforming process and the analysis of the equilibrium model for different operating conditions (T , P , X_{feed}). The optimal operating conditions were established based on the analysis of the equilibrium model. It was also developed the mathematical model of heat balance, while the optimal size of catalyst granules was determined. The optimal working conditions were set by the equilibrium process' analysis, the reactor feed ratio, $\text{H}_2\text{O}:\text{CH}_4$, 3:1, the temperature in the range of 780-1140 K and the pressure of about 30 atm.

Keywords: *steam methane reforming, mathematical modeling, stoichiometric independent reaction, equilibrium process analysis*

INTRODUCTION

During the last years, the demand of crops has increased, thus the production of fertilizers seems to be very suitable for countries with a well-developed agriculture. Ammonia is a very important product of chemical industry due to its various uses, both as finite or as intermediate product. According to a study made by Jeenchary and Siemanond [1], about 88% of the ammonia production is used for the production of fertilizers, synthetic fibers and coolers. Ammonia is obtained through the Haber-Bosch process, where, in most cases, the source of hydrogen is the natural gas while the nitrogen is taken from the air. The overall energy consumption for ammonia process is somewhere around $1.1 \cdot 10^{12}$ kJ/hr. This process consumes 1% of annual energy production and generates over 3% of the total greenhouse gases [1]. Given the high thermal input needed, even the slightest improvement would translate into major benefits, both from an economic standpoint, as well as regarding environmental issues.

^a Babes-Bolyai University, Faculty of Chemistry and Chemical Engineering, 11 Arany Janos str., RO-400028, Cluj-Napoca, Romania

* Corresponding author: sdragan@chem.ubbcluj.ro

Numerous researches are currently being carried out to find new, more economical and cleaner sources, such as obtaining hydrogen through the water electrolysis process using renewable energy (solar or wind power). From the environmental point of view, water electrolysis has been proved to be one of the most propitious alternatives in the production of hydrogen, as long as the power sources are renewable [2,3]. Nevertheless, the results show that the hydrogen source in the synthesis of ammonia will remain, at least in the upcoming decades, the natural gas.

The European Commission foresees an increase in the amount of world's hydrogen production. That will come as a consequence of the costs reduction in hydrogen technologies as well as an increased demand of hydrogen in the transport sector [4]. Uyar and Besiki [5] mention that hydrogen could meet 18% of the total energy demand, reduce, at the same time, about 6 Gt of carbon dioxide emissions annually. As presented by Pashchenko [6], steam reforming of hydrocarbons represents the leading route for producing hydrogen and syngas. Ewan and Allen [7] point out that 96% of the hydrogen produced has fossil fuels as raw materials, while Calisan et al [8], show that approximately 50% of the world's hydrogen production is achieved by the steam methane reforming process despite the fact that different other production routes are well developed and well known.

The methane reforming reaction takes place between 800°C - 1000°C, in the presence of catalysts, and in a pressure range of 20-30 bar, according to Nielsen [9].

Acknowledging aforementioned problems concerning the environment, we employed the values mentioned above for the physical parameters in modeling and optimizing the steam methane reforming process.

RESULTS AND DISCUSSION

Mathematical model of mass balance

The characteristic equation for the steam methane reforming process is presented below [10]:

$[CH_4 + H_2O + A'']_g + [K]_s = [H_2 + CO_2 + CO + CH_4 + A'']_g + [K]_s$, where A'' represents the inert and K the catalyst.

Using the Graham-Schmidt algebraic method we established how many and which of the four possible reactions are stoichiometric independent.

The possible reactions for this process are:



Stoichiometric independent are those reactions for which the condition presented below is fulfilled:

$$A_{Ri}^T \cdot A_e = 0 \quad (1)$$

where A_{Ri}^T represents the transposed matrix of the considered reaction and A_e represents the matrix of the elements.

For the reactions of our process, we obtain:

$$A_{R1}^T \cdot A_e = (-1 \ 3 \ 1 \ 0 \ -1) \cdot A_e = 0 \quad (2)$$

$$A_{R2}^T \cdot A_e = (0 \ 1 \ -1 \ 1 \ -1) \cdot A_e = 0 \quad (3)$$

$$A_{R3}^T \cdot A_e = (-1 \ 4 \ 0 \ 1 \ -2) \cdot A_e = 0 \quad (4)$$

$$A_{R4}^T \cdot A_e = (-1 \ 2 \ 2 \ -1 \ 0) \cdot A_e = 0 \quad (5)$$

As it can be seen, all four reactions fulfil this condition, thus, in order to find out which reactions are stoichiometric independent we did a thermodynamic analysis. As a result, it was found that R1 and R2 are the only one who satisfy the thermodynamic condition, $\Delta_R G < 0$.

The methane conversion, for the first reaction, and the carbon monoxide conversion, in the second reaction are defined:

$$\eta_{CH_4} = \frac{n_{CH_4}^{01} - n_{CH_4}^{11}}{n_{CH_4}^{01}} = \frac{n_{H_2O}^{01} - n_{H_2O}^{11}}{n_{CH_4}^{01}} = \frac{n_{CO}^{01} - n_{CO}^{11}}{n_{CH_4}^{01}} = \frac{n_{H_2}^{01} - n_{H_2}^{11}}{3 \cdot n_{CH_4}^{01}} \quad (6)$$

$$\eta_{CO} = \frac{n_{CO}^{02} - n_{CO}^{22}}{n_{CO}^{02}} = \frac{n_{H_2O}^{02} - n_{H_2O}^{22}}{n_{CO}^{02}} = \frac{n_{CO_2}^{02} - n_{CO_2}^{22}}{n_{CO}^{02}} = \frac{n_{H_2}^{02} - n_{H_2}^{22}}{n_{CO}^{02}} \quad (7)$$

The concretization relations for the two stoichiometric independent reactions are:

$$\begin{aligned} n_{CH_4}^{01} &= n_{CH_4}^0 & n_{CO}^{02} &= n_{CO}^1 & n_{H_2O}^{02} &= n_{H_2O}^1 & n_{H_2O}^2 &= n_{H_2O} & n_{CO_2}^2 &= n_{CO_2} \\ n_{H_2O}^{01} &= n_{H_2O}^0 & n_{H_2}^{02} &= n_{H_2}^1 & n_{CH_4}^1 &= n_{CH_4} & n_{CO}^2 &= n_{CO} & n_{H_2}^2 &= n_{H_2} \end{aligned}$$

Some simplifications were made also for the algebraic mass balance equations described below, the conversion of methane was replaced with α , $\eta_{CH_4} = \alpha$, whereas with β it is represented the product between the conversion of methane and carbon monoxide $\eta_{CH_4} \cdot \eta_{CO} = \beta$.

The algebraic mass balance equations expressed in moles and in mole fractions are shown in Table 1 and Table 2. Those expressed in mole fractions (b), are deduced from the first type (a), by replacing the next ratios:

$$\dot{X}_{H_2O}^0 = \frac{n_{H_2O}^0}{n_{CH_4}^0}; \dot{X}_{CO_2}^0 = \frac{n_{CO_2}^0}{n_{CH_4}^0}; \dot{X}_{H_2}^0 = \frac{n_{H_2}^0}{n_{CH_4}^0}; \dot{X}_{A''}^0 = \frac{n_{A''}^0}{n_{CH_4}^0} \quad (8)$$

Table 1. Algebraic mass balance equations expressed in moles

Crt. Nr	Comp	IN	Form of algebraic mass balance equation	
			a	b
1	CH ₄	n _{CH₄} ⁰	n _{CH₄} = n _{CH₄} ⁰ · (1 - η _{CH₄})	n _{CH₄} = n _{CH₄} ⁰ · (1 - α)
2	H ₂ O	n _{H₂O} ⁰	n _{H₂O} = n _{H₂O} ⁰ - n _{CH₄} ⁰ · η _{CH₄} · (1 + η _{CO})	n _{H₂O} = n _{CH₄} ⁰ · (X _{H₂O} ⁰ - α - β)
3	CO ₂	n _{CO₂} ⁰	n _{CO₂} = n _{CO₂} ⁰ + n _{CH₄} ⁰ · η _{CH₄} · η _{CO}	n _{CO₂} = n _{CH₄} ⁰ · (X _{CO₂} ⁰ + β)
4	CO	n _{CO} ⁰	n _{CO} = n _{CH₄} ⁰ · η _{CH₄} · (1 - η _{CO})	n _{CO} = n _{CH₄} ⁰ · (α - β)
5	H ₂	n _{H₂} ⁰	n _{H₂} = n _{H₂} ⁰ + n _{CH₄} ⁰ · η _{CH₄} · (3 + η _{CO})	n _{H₂} = n _{CH₄} ⁰ · (X _{H₂} ⁰ + 3 · α - β)
6	A''	n _{A''} ⁰	n _{A''} = n _{A''} ⁰	n _{A''} = n _{CH₄} ⁰ · X _{A''} ⁰
Total			n _T = n _T ⁰ · (1 + 2 · X _{CH₄} ⁰ · η _{CH₄})	n _T = n _{CH₄} ⁰ · (A + 2 · α)

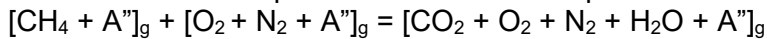
Table 2. Algebraic mass balance equations expressed in mole fractions

Crt Nr	Comp	IN	Form of algebraic mass balance equations	
			a	b
1	CH ₄	n _{CH₄} ⁰	$X_{CH_4} = \frac{X_{CH_4}^0 \cdot (1 - \alpha)}{1 + 2 \cdot X_{CH_4}^0 \cdot \alpha}$	$X_{CH_4} = \frac{1 - \alpha}{A + 2 \cdot \alpha}$
2	H ₂ O	n _{H₂O} ⁰	$X_{H_2O} = \frac{X_{H_2O}^0 - X_{CH_4}^0 \cdot \alpha - X_{CH_4}^0 \cdot \beta}{1 + 2 \cdot X_{CH_4}^0 \cdot \alpha}$	$X_{H_2O} = \frac{X_{H_2O}^0 - \alpha - \beta}{A + 2 \cdot \alpha}$
3	CO ₂	n _{CO₂} ⁰	$X_{CO_2} = \frac{X_{CO_2}^0 + X_{CH_4}^0 \cdot \beta}{1 + 2 \cdot X_{CH_4}^0 \cdot \alpha}$	$X_{CO_2} = \frac{X_{CO_2}^0 + \beta}{A + 2 \cdot \alpha}$
4	CO	n _{CO} ⁰	$X_{CO} = \frac{X_{CH_4}^0 \cdot \alpha - X_{CH_4}^0 \cdot \beta}{1 + 2 \cdot X_{CH_4}^0 \cdot \alpha}$	$X_{CO} = \frac{\alpha - \beta}{A + 2 \cdot \alpha}$
5	H ₂	n _{H₂} ⁰	$X_{H_2} = \frac{X_{H_2}^0 + 3 \cdot X_{CH_4}^0 \cdot \alpha + X_{CH_4}^0 \cdot \beta}{1 + 2 \cdot X_{CH_4}^0 \cdot \alpha}$	$X_{H_2} = \frac{X_{H_2}^0 + 3 \cdot \alpha + \beta}{A + 2 \cdot \alpha}$
6	A''	n _{A''} ⁰	$X_{A''} = \frac{X_{A''}^0}{1 + 2 \cdot X_{CH_4}^0 \cdot \alpha}$	$X_{A''} = \frac{X_{A''}^0}{A + 2 \cdot \alpha}$

Mathematical model of heat balance

The oxidation process takes place with an excess of air, thus the oxidation process is complete. The methane's conversion equals 1.

The characteristic equation for the oxidation process is:



The mathematical model of heat balance is described by two equations. The equation number (8) express the heat needed to take place the reaction, while equation number (9) shows the heat which must be brought from the outside, taking into consideration that the steam methane reforming reaction is an endothermic reaction.

$$\begin{aligned} \Delta H_{nec} = & 41100 \cdot \alpha - 10320 \cdot \beta + (32.5 \cdot \alpha - 0.522 \cdot \beta + 3.422 + \\ & 7.219 \cdot X_{H_2O}) \cdot T - (17.93 \cdot \alpha - 4.134 \cdot \beta - 8.922 - 1.87 \cdot X_{H_2O}) \cdot 10^{-3} \cdot T^2 + \\ & (2.85 \cdot \alpha - 1.336 \cdot \beta - 1.388 + 0.089 \cdot X_{H_2O}) \cdot 10^{-6} \cdot T^3 - (3.422 + 7.219 \cdot \\ & X_{H_2O}) \cdot T_0 - (8.922 - 1.187 \cdot X_{H_2O}) \cdot 10^{-3} \cdot T_0^2 + (1.388 - 0.089 \cdot X_{H_2O}) \cdot \\ & 10^{-6} \cdot T_0^3 \end{aligned} \quad (9)$$

$$Q_{ex} = n_{CH_4}^0 \cdot \Delta H_{nec} \quad (10)$$

The optimal size of catalyst granules was determined on the basis of the following algorithm:

$$\frac{\partial K_T}{\partial d} = 0 \Rightarrow \left(\frac{d}{D}\right)_{optim} \quad (11)$$

$$Nu = \frac{K_T \times D}{\lambda} = 0.542 \times Re^{0.93} \times e^{\frac{-6 \times d}{D}} \quad (12)$$

$$\frac{K_T \times D}{\lambda} = 0.542 \times \left(\frac{\rho \times w_0 \times d}{\eta}\right)^{0.93} \times d^{0.93} \times e^{\frac{-6 \times d}{D}} \quad (13)$$

$$\left(\frac{d}{D}\right)_{optim} = 0.155 \quad (14)$$

Kinetic model of steam methane reforming process

The basic structural diagram for the transport and transfer process is depicted in Figure 1.

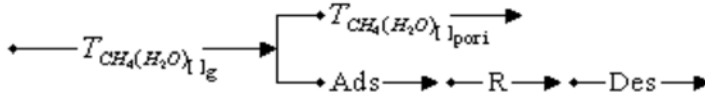


Figure 1. Schematic overview of the mass transport and transfer process

By comparing the rate of the processes showed in the above scheme, there are three possible macro-kinetic mechanisms:

- > Macro-kinetic mechanism of transfer through the gaseous phase defined by the equation obtained by integrating the steady-state one:

$$n_{AK} = \frac{4 \times D}{r} \times \int_{C_{AK}^0}^{C_{AK}} -\bar{r} \times dC_{AK} \times r^2 \times \pi \quad (15)$$

- > Macro-kinetic model of transformation which is described by the following equation:

$$\frac{d\eta}{d\tau_c} = K(1) \times \frac{C_{A1}^0 \times (1-\eta)}{(1+\alpha \times \eta)} \times \left(\frac{\eta}{1+\alpha \times \eta} \times \frac{\eta^e}{1+\alpha \times \eta^e} \right) \quad (16)$$

- > Combined transfer and transport process described through a more complex equation which was not taken into consideration

It has been shown that at an industrial level, mass transport and transfer reaches equilibrium, and the steam methane reforming process, as a whole, is most accurately described by a macro-kinetic model of heat transfer from the reactor's surface towards the reaction mixture [10].

Mathematical model of the equilibrium process

Steam methane reforming is a contact process, therefore, the equilibrium is described through chemical equilibrium [11]. The equilibrium constants for the stoichiometric independent reactions are defined with respect to the partial pressure of each component:

$$K_{p1} = \frac{p_{CO} \cdot p_{H_2}^3}{p_{CH_4} \cdot p_{H_2O}} \quad (17)$$

$$K_{p2} = \frac{p_{CO_2} \cdot p_{H_2}}{p_{CO} \cdot p_{H_2O}} \quad (18)$$

The partial pressure of each component was substituted according to Dalton's law with the total pressure and his concentration in the reaction mixture. This leads to the following relations:

$$K_{p1} = \frac{x_{CO} \cdot x_{H_2}^3}{x_{CH_4} \cdot x_{H_2O}} \cdot p^2 \quad (19)$$

$$K_{p2} = \frac{x_{CO_2} \cdot x_{H_2}}{x_{CO} \cdot x_{H_2O}} \quad (20)$$

Using the mathematical model of mass balance, the final relations for the equilibrium constants are:

$$K_{p1} = \frac{(\alpha - \beta) \cdot (3 \cdot \alpha + \beta)^3 \cdot p^2}{(x_{H_2O}^0 - \alpha - \beta) \times (1 - \alpha) \cdot (1 + x_{H_2O}^0 + 2 \cdot \alpha)^2} \quad (21)$$

$$K_{p2} = \frac{\beta \cdot (3 \cdot \alpha + \beta)}{(\alpha - \beta) \cdot (x_{H_2O}^0 - \alpha - \beta)} \quad (22)$$

$$\lg K_{p1} = \frac{-9861.11}{T} - 11.87 - 2.05 \cdot 10^{-3} \cdot T + 0.1779 \cdot 10^{-6} \cdot T^2 + 8.3432 \cdot \lg T \quad (23)$$

$$\lg K_{p2} = \frac{2217.18}{T} - 3.27467 + 0.3524 \cdot 10^{-3} \cdot T - 0.0507 \cdot 10^{-6} \cdot T^2 + 0.2969 \cdot \lg T \quad (24)$$

These two relations, (21) and (22), which describe how the equilibrium constants depend on the conversion of methane and carbon monoxide, together with the computational expressions, (23) and (24), which allows us to see the variation of the equilibrium constants with temperature, constitute the mathematical model of the equilibrium process.

Solving these equations will help us to better understand how the conversion, for both components, vary with respect to pressure, temperature and feed ration. All the thermodynamic computations which are needed for describing the process were made using MatLab.

Table 3 presents the values of the enthalpy [cal/mol], entropy [cal/mol·K] and free Gibbs energy [cal/mol] for the two stoichiometric independent reactions.

Table 3. Variation of the thermodynamic parameters with respect to temperature for both stoichiometric independent reactions

T [K]	R1			R2		
	$\Delta_R H_T$	$\Delta_R S_T$	$\Delta_R G_T$	$\Delta_R H_T$	$\Delta_R S_T$	$\Delta_R G_T$
780	53093.95	59.46	6710.34	-8922.69	-8.36	-2397.32
820	53278.92	59.69	4326.95	-8831.17	-8.25	-2064.99
860	53446.53	59.89	1934.96	-8738.11	-8.14	-1737.16
900	53597.40	60.06	-464.44	-8643.68	-8.03	-1413.69
940	53732.21	60.21	-2870.20	-8548.07	-7.92	-1094.45
980	53851.40	60.33	-5281.37	-8451.14	-7.82	-779.30
1020	53955.79	60.44	-7697.10	-8353.96	-7.73	-468.11
1060	54045.93	60.53	-10116.65	-8255.89	-7.63	-160.76
1100	54122.44	60.60	-12539.35	-8157.20	-7.54	142.87
1140	54185.96	60.65	-14964.59	-8058.27	-7.45	442.91

Two methods were used in order to compute the values for the equilibrium constants. First method, I, uses the computational relations discussed before, (23) and (24), while the second one, II, uses Van't Hoff's equation, (25).

$$\ln K_p = -\frac{\Delta_R G_T^0}{R \cdot T} \quad (25)$$

Using the methods described before, we computed the values for the equilibrium constants as presented in Table 4. The values obtained by both methods, for both equilibrium constants, do not differ by more than 0.44%.

Table 4. The dependence of the equilibrium constants with temperature.

T [K]	K_{p1}		K_{p2}	
	I	II	I	II
780	0.0132	0.0132	4.6834	4.6984
820	0.0702	0.0705	3.5416	3.5531
860	0.3218	0.3234	2.7559	2.7651
900	1.2946	1.3009	2.1982	2.2057
940	4.4618	4.664	1.7915	1.7977
980	15.0374	15.1087	1.4877	1.4929
1020	44.5253	44.7339	1.2560	1.2605
1060	121.6893	122.2517	1.0760	1.0799
1100	309.5796	310.9887	0.9338	0.9373
1140	738.4565	741.7662	0.8197	0.8229

To prove that the steam methane reforming process is indeed described by the chemical equilibrium, Figure 2 reveal the correspondence between the

equilibrium constant for the first reaction, steam methane reforming, expressed as activity, and temperature for different constant pressure values. It can be seen that the value of the constant is somewhere around one.

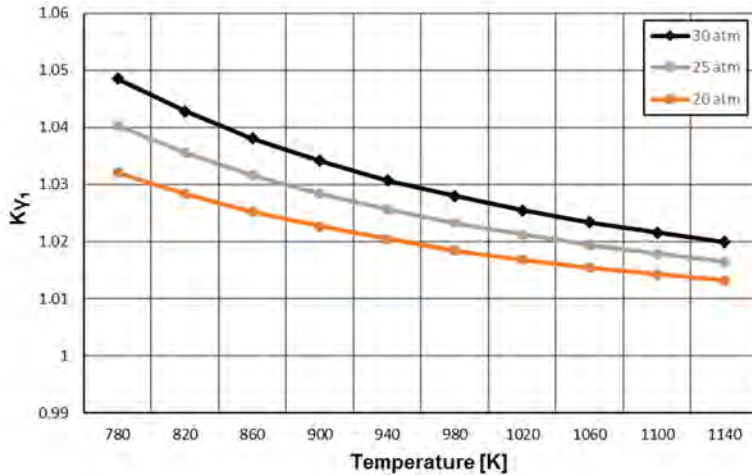


Figure 2. Variation of the first equilibrium constant with the temperature for different constant pressure values

The same is happening for the second reaction. Figure 3 shows that the equilibrium constant, for the water gas shift reaction, has values in the range of 1.01 – 1.04 which can be approximate to 1.

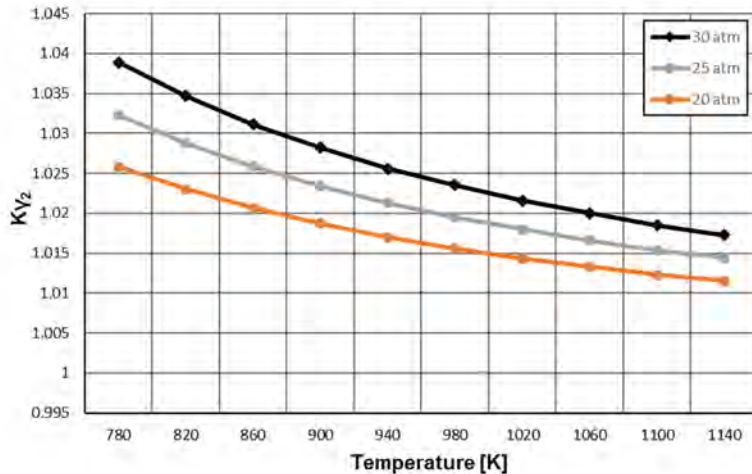


Figure 3. Variation of the second equilibrium constant with the temperature for different constant pressure values

The mathematical model was developed and solved using MatLab with the purpose of determining the values of α and β for different operating conditions: pressure, temperature and feed ratio. The pressures taken into consideration were 10, 20, 25, 30, 35, 40 and 50 atm, while the feed ratio has the following values: 3, 3.5, 4, 5 and 6. The temperature domain was set between 780 and 1140 K.

The results are represented by the graphics below and explained in the next paragraph.

Figure 4 shows that the conversion of methane is increasing with the increase in temperature and feed ratio. It can be noted that the temperature has a stronger influence than the feed ratio. Thereby, increasing the temperature from 810 up to 1110 K will cause an increase of about 4.5 times in methane conversion, while an increase in feed ratio determines an increase in methane conversion only of about 1.1 times.

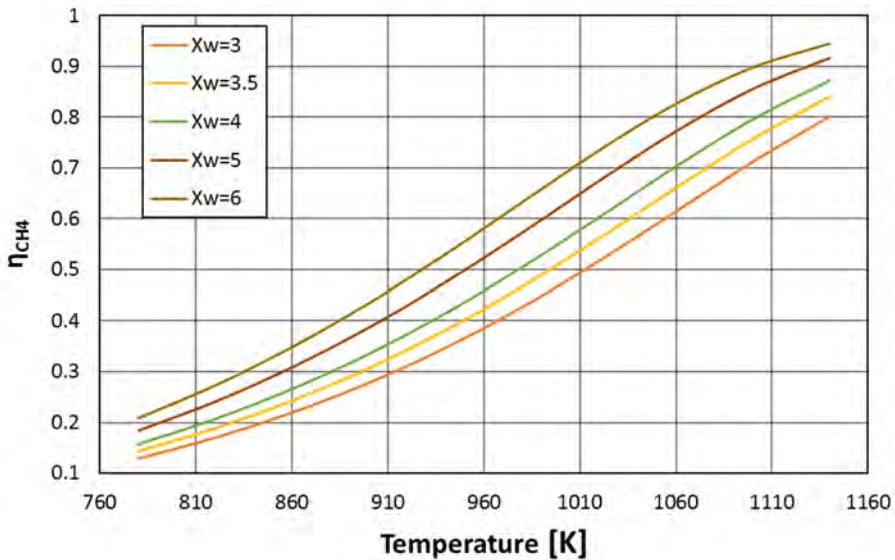


Figure 4. Variation of the conversion for methane with the temperature at constant pressure, $P=30$ atm

In the case of carbon monoxide, Figure 5, we can see exactly the opposite. The conversion of carbon monoxide decreases with the increase in both, feed ratio and temperature.

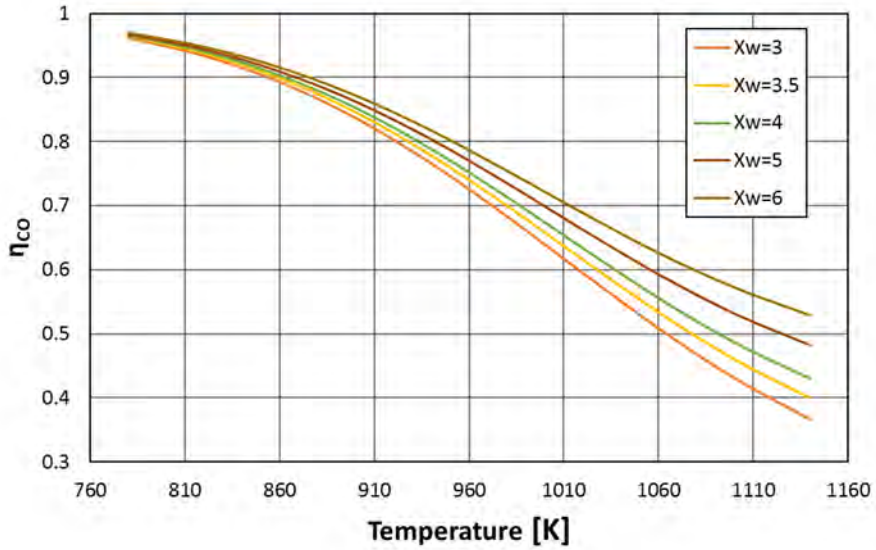


Figure 5. Variation of the conversion for carbon monoxide with respect to temperature at constant pressure, $P=30$ atm

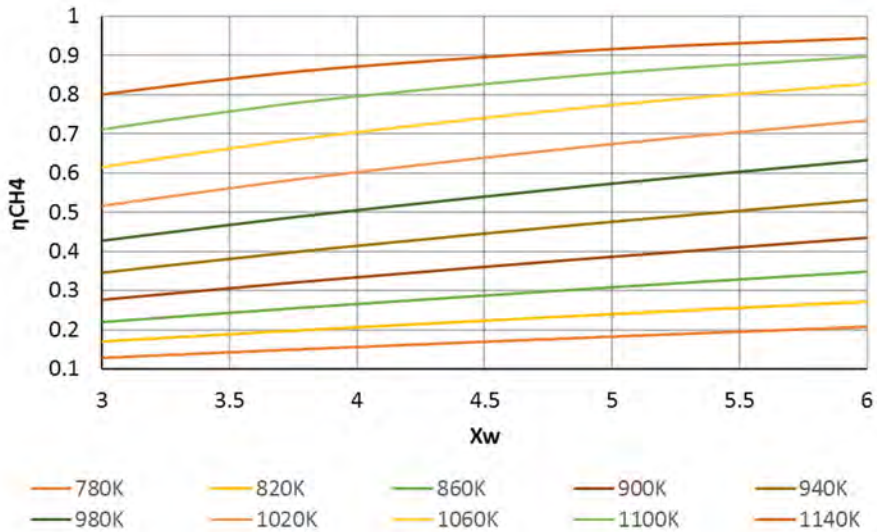


Figure 6. Variation of the conversion for methane with different feed ratios and temperatures, at constant pressure, $P=30$ atm

Figure 6 reveals that at 30 atmospheres, the conversion of methane is strongly increasing with the increase in temperature and slowly increases with an increase in the feed ratio.

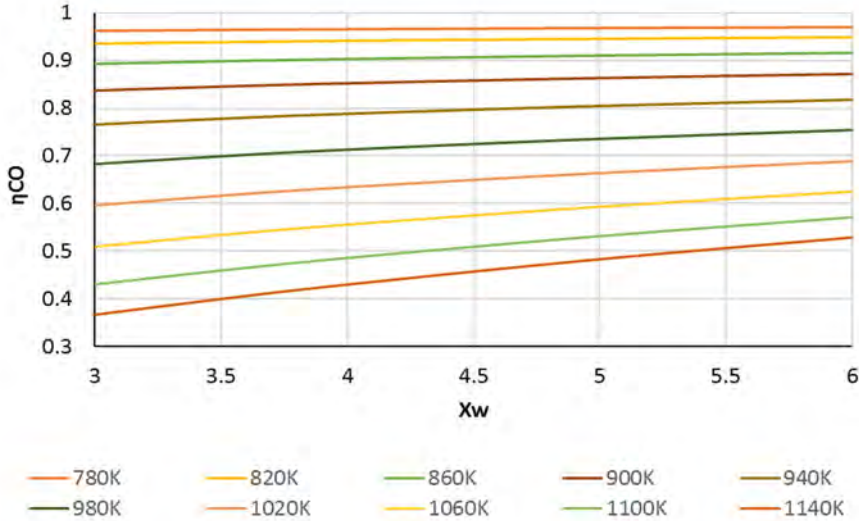


Figure 7. Variation of the conversion for carbon monoxide with different feed ratios and temperatures, at constant pressure, P=30 atm

On the other hand, from Figure 7 we can denote that at the same pressure, 30 atmospheres, the conversion of carbon monoxide is decreasing with an increase in temperature and it remains almost constant with an increase in the feed ratio.

CONCLUSIONS

In this paper there were established based on the characteristic equation the stoichiometric independent reactions for the steam methane reforming process using the algebraic Graham-Schmidt method and thermodynamic analysis.

It was elaborated the mathematical model of mass balance, both in primary form, and also the mathematical model of the equilibrium process.

Solving the equilibrium mathematical model for different operating conditions, temperature, pressures and feed ratios, we found the optimal working conditions. Based on the analysis of the model results, optimal pressure would be 30 atmospheres, feed ratio equal with 3 and the temperature range between 780 – 1140 K.

At a production capacity of 1200 tons of ammonia per day, for a pressure of 30 atm and a feed ratio equal with 3, the value obtained for the length of the reforming reactor, 10.00 m, is in good accordance with the length of the reforming reactor used by S.C. Ameropa AZOMURES, where for the same working conditions the reforming reactor is 10.33 m long.

The developed model can be used to simulate and study the reforming process of methane for many other different operating conditions.

REFERENCES

1. J. Jeenchary; K. Siemanond; *Comput.-Aided Chem. Eng.*, **2018**, 43, 385-390.
2. A. Sánchez; M. Martin; *J. Cleaner Prod.*, **2018**, 178, 325-342.
3. S. Giddey; S.P.S. Badwal; A. Kulkarni; *Int. J. Hydrogen Energy*, **2013**, 38, 14576-14594.
4. A. Soria; L. Szabo; P. Russ; W. Suwala; I. Hidalgo; A. Purwanto; World energy technology outlook 2050, European Commission, **2006**.
5. T.S. Uyar; D. Beşikci; *Int. J. Hydrogen Energy*, **2017**, 42, 2453-2456.
6. D. Pashchenko; *Fuel*, **2019**, 236, 686-694.
7. B.C.R. Ewan; R.W.K. Allen; *Int. J. Hydrogen Energy*, **2005**, 30, 809-819.
8. A. Calisan; C.G. Ogulgonen; A. Yilmaz; D. Uner; S. Kinkal; *Int. J. Hydrogen Energy*, **2019**: <https://doi.org/10.1016/j.ijhydene.2019.04.033>
9. J.R. Rostrup-Nielsen; T. Rostrup-Nielsen; *CATTECH*, **2002**, 6, 150-159.
10. C. Calistru; C. Leonte; I. Siminiceanu; C. Hagiu; O. Popa; Tehnologia îngrășămintelor minerale, Vol I; Ed. Tehnică București: România, **1984**; pp. 105-148.
11. S. Drăgan; Elemente de ingineria proceselor chimice; Ed. UBB Cluj-Napoca; România, **2004**, pp. 40-44.

MODELLING AND SIMULATION OF WATER GAS SHIFT REACTOR USING COMSOL MULTIPHYSICS

ADRIAN CATALIN SOIT^a, IONELA DUMBRAVA^a,
VLAD-CRISTIAN SANDU^a, ANA-MARIA CORMOS^{a*}

ABSTRACT. Hydrogen production from fossil fuels plays an important role in the global H₂ demand. In general, H₂ production from fossil sources implies syngas generation, typically by gasification or reforming, followed by the water gas shift process. The aim of this work is to determine the behaviour of the water gas shift process (in a packed bed reactor) through modelling and simulation using COMSOL Multiphysics software. In the developed model, diffusion is the main type of transport of the chemical substances. The challenges are to model the complex phenomena associated with a multiscale system: a macroscale level in the macropores between the dumped catalyst particles and a microscale level, inside of the pellets' micropores.

Keywords: *Hydrogen production, Water gas shift reactor, CFD modelling using COMSOL Multiphysics software.*

INTRODUCTION

Fossil fuels supply the majority of the world's energy demand. Carbon dioxide obtained from fossil fuels contributes to climate change, therefore the main focus is now to produce clean and renewable energy. H₂ is an important raw material for the chemical and petrochemical industries and could have an important part in alternative fuels [1]. To produce H₂, there are a wide variety of processes, which according to the sources used, can be divided in two major categories: conventional and renewable technologies [2]. The conventional methods use fossil fuels as raw materials and include methods such as hydrocarbon reforming and hydrocarbon pyrolysis to produce H₂. The reforming processes (steam reforming, partial oxidation and autothermal reforming) are the most developed at this moment to meet almost the entire

^a *Babeş-Bolyai University, Faculty of Chemistry and Chemical Engineering, 11 Arany Janos str., RO-400028, Cluj-Napoca, Romania*

* *Corresponding author e-mail: cani@chem.ubbcluj.ro*

hydrogen demand. The renewable methods use biomass and water in order to obtain hydrogen. In biomass processes there are two subtypes of methods: one implies thermochemical processes and the second one uses biological processes. The second renewable method, water splitting, uses only water as the source of H₂ through electrolysis, thermolysis and photo-electrolysis process [2]. In general, H₂ production from fossil sources implies syngas generation, typically by gasification or reforming followed by water gas shift (WGS) process. Carbon dioxide and other impurities, obtained after WGS conversion, are separated in a hydrogen purification unit (Figure 1).

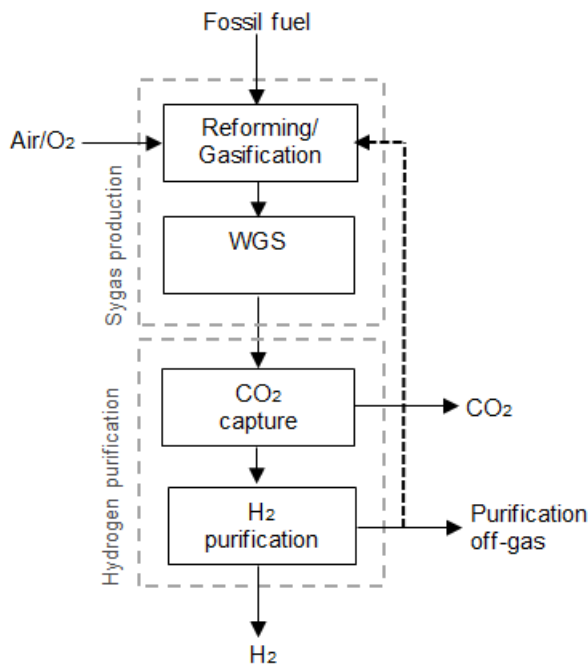


Figure 1. Steam reforming of natural gas [1]

Currently, steam reforming of natural gas produces 48% of the total hydrogen demand. Consequently, steam reforming with emphasis on water gas shift deserves special attention. Natural gas can be converted to syngas, followed by the WGS reaction to produce carbon dioxide and hydrogen from water vapors and carbon monoxide [1]:



In process industry, the water gas shift reaction takes place in 2 steps. In the first one, the carbon monoxide concentration decreases from 10-13% to 2-3% (molar %). The temperature for the first step is between 350-550 °C, depending on the inlet gas composition. The pressure is between 20-30 bar and the gas velocity can reach from 400 to 1200 m·h⁻¹, related to the dry quantity of the gas [2]. The high-temperature catalysts used for water gas shift conversion are presented in Table 1.

Table 1. High temperature catalysts [1]

Catalyst properties	Working conditions
CuO·CeO·8O ₂ -y(Cu-CeO ₂) Fe ₃ O ₄ /Cr ₂ O ₃ , 180-250 μm	473-623.15 K, CO/H ₂ O=1/3 1 bar, 6 bar, 27 bar, 623-713.15 K
Fe ₃ O ₄ /Cr ₂ O ₃ 89% Fe ₂ O ₃ , 9% Cr ₂ O ₃ 80-95% Fe ₂ O ₃ , 5-13% Cr ₂ O ₃ , 1-5% CuO	3-5 bar, 846-906.15 K 575-675.15 K 1 atm, 723.15 K,
CuO/ Fe ₃ O ₄ /Cr ₂ O ₃ , 180-250 μm 0.4 % Pt/Al ₂ O ₃ 1/4" x 3/8", 2.20 g/cm ³ 1/4" x 1/4", 1.25 g/cm ³ 11.3" x 8.5 mm, 1.35 g/cm ³	1 bar, 6 bar, 27 bar, 653-723.15 K 1 atm, 817.15 K Power Gas – pilot plant Girdler – pilot plant ICI – pilot plant

The second step of the WGS process takes place at low temperature, lower than 250 °C, and the carbon monoxide concentration is reduced to a 0.2-0.4% concentration. The low-temperature catalysts used for water gas shift conversion operate between 200 and 250 °C [3] (Table 2).

Table 2. Low temperature catalysts [1,3]

Catalyst properties	Working conditions
CuO-ZnO-Al ₂ O ₃ , 200-250 μm 1-2% Pt/ Al ₂ O ₃ 8-10% Cu-Al ₂ O ₃ Cu (111)	393-523.15 K 1 atm, 498-618.15 K 1 atm, 403-473.15 K 1 atm, 613.15 K

The most common reactors for the heterogeneous catalytic processes (in the case of WGS process) in the chemical industry are the packed bed reactors. The packed bed reactor is a column filled with porous catalyst particles (pellets) and can be packed in one compartment or can contain

supporting structures (channels or tubes). Depending on the way the gas is passing through the catalyst bed, there are 2 types of columns: with axial or radial flow of the gas.

MODEL DEVELOPMENT

Modelling and simulation of the water-gas shift process was made using COMSOL Multiphysics 5.2. A packed bed reactor filled with spherical catalyst pellets was chosen for this study (Figure 2). The packed bed reactor makes modelling of mass transfer and chemical reactions a challenge, rising from the fact that the transfer of species and the chemical reaction take place at different orders of magnitude, one at macroscale level in the macropores between the dumped catalyst particles and the second one at microscale level, inside of the micropores of the pellets [4]. The multiscale problem was solved with COMSOL Multiphysics software, using “Reactive Pellet Bed” feature, available in “Transport of Diluted Species” interface, specifically designed for this kind of problem [5].

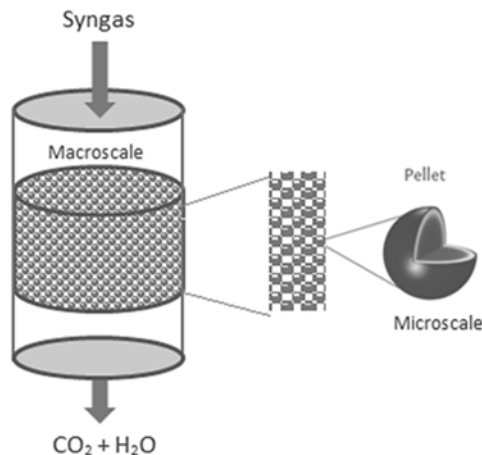


Figure 2. A macro and microscale of a packed bed reactor

The heterogeneous model is developed to account for the diffusional limitations. Certain assumptions have to be made for the overall reactor model:

- Mass transport inside the catalyst pellets, along the reactor length, takes place by diffusional and convective mechanisms;
- Catalyst pellets have a homogenous and porous structure;
- Mass transfer within the catalyst pellets occurs only in the radial direction;
- Reaction rate depends on the mass transfer inside the catalyst pellets.

Model equations at macroscale level [5]

The pressure drop along the reactor length is described by Ergun's equation:

$$-\frac{dP}{dx} = \frac{150\mu u}{D_p^2} \cdot \frac{(1-\varepsilon_b)^2}{\varepsilon_b^3} + \frac{1.75\rho u^2}{D_p} \cdot \frac{(1-\varepsilon_b)}{\varepsilon_b^3} \quad (2)$$

The mass transfer, which occurs by diffusional and convective mechanisms (for Transport of Diluted Species feature), is described by the following equation:

$$\nabla(-D_i \nabla c_i + c_i u) = R_i \quad (3)$$

The reaction rate source R depends on the transport inside the catalyst pellets.

$$R = (1 - \varepsilon_b) A_p (N \cdot n), \text{ at } r = r_p \quad (4)$$

Model equations at microscale level [5]

The reaction rate within the catalyst pellet is affected by the mass transfer inside the pellet (only diffusional mechanism is considered). The mass balance at microscale level is described by the following equation, using the normalized radius of the catalyst particle:

$$\nabla \cdot \left(- \left(\frac{r}{r_p} \right)^2 D_{cp} \nabla c_p \right) + \left(\frac{r}{r_p} \right)^2 \cdot R_p = 0, \text{ for } 0 < r < 1 \quad (5)$$

The distribution of the concentration in the pellet is represented by the following equation and describes the molar flux of the species according to the position in the reactor:

$$R = (1 - \varepsilon_b) A_p (-D_{cp} \nabla c_p \cdot n) \quad (6)$$

Reaction kinetics

The kinetic model developed by Germani et al., 2005 is used to describe the water-gas shift reaction. The WGS reaction can be considered at equilibrium and the rate of reaction is represented by Equation 7 (R_{WGS} unit is $[\text{mol} \cdot \text{m}^{-3} \cdot \text{s}^{-1}]$) for the temperature range 573-673 K and depends on the catalyst density, partial pressure of the components, equilibrium constant and Arrhenius equation [6].

$$R_{WGS} = \rho_{cat} k_{WGS} e^{\left(-\frac{E_{WGS}}{RT} \right)} p_{CO}^{0.13} p_{H_2O}^{0.49} p_{CO_2}^{-0.12} p_{H_2}^{-0.45} \left(1 - \frac{p_{CO_2} p_{H_2}}{p_{CO} p_{H_2O} K_{WGS}} \right) \quad (7)$$

The value of the pre-exponential factor is $k_{WGS} = 1.3 \cdot 10^6 \text{ mol}/(\text{kg cat} \cdot \text{s} \cdot \text{Pa}^{0.05})$ and the activation energy is $E_{WGS} = 86000 \text{ J/mol}$.

The equilibrium constant is obtained using the following equation [7]:

$$k_{WGS} = \exp(Z(Z(-0.1821Z + 0.563176) + 4.189249) + 0.341737) \quad (8)$$

where $Z = 1000/T - 1$.

RESULTS AND DISCUSSION

A summary of the packed bed reactor characteristics and operating data, used in this work, is presented in Table 3. The developed model was validated with data from an industrial plant, published in literature [8].

Table 3. Reactor parameters, case 1 [9]

Feed gas composition	%
CO	6.41
H ₂ O	38.53
H ₂	47.97
CO ₂	4.54
Ar	2.55
Reactor	
Height (m)	5.15
Diameter (m)	2.15
Catalyst pellets bed height (m)	3.65
Catalyst pellets diameter (m)	$4.4 \cdot 10^{-3}$
Catalyst pellets density (kg/m ³)	1260
Catalyst pellets porosity (-)	0.6
Steam/CO ratio	6
Feed Flowrate (kmol/s)	764.5
Gas velocity (m/s)	0.75
Pressure (atm)	23.53
Feed temperature (°C)	357

To verify the accuracy of the results for the developed model, the distribution of the carbon monoxide conversion along the reactor length (case 1) was determined (Figure 3).

In the developed model, the WGS equilibrium reaction is approximated by using an expression for fast WGS kinetics, derived for a platinum/ceria/alumina catalyst by Germani et al. [6]. The kinetics model was adapted to process conditions in order to achieve the output process parameters presented in literature [8]. The correlation coefficient, $R=0.9556$, indicates that there is a good correlation between the results of the simulation model in COMSOL and data presented in literature for water gas-shift process.

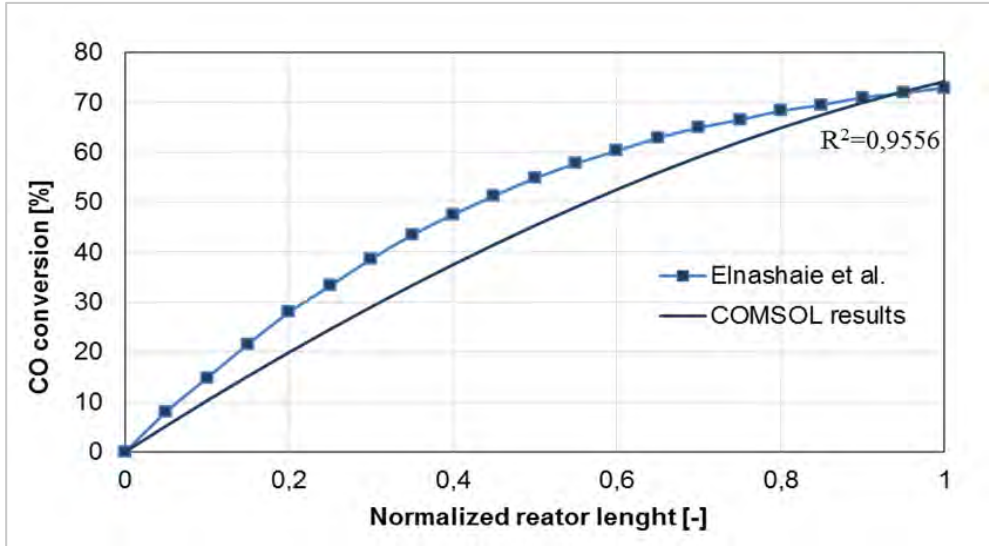


Figure 3. CO conversion along the normalized reactor length, case 1

In order to validate the developed mathematical model, a new simulation was done, using the adjusted model and different operating parameters presented in Table 4. The simulation results show a good correlation with data presented in literature ($R=0.9654$) (Figure 4).

Table 4. Reactor parameters, case 2 [8]

Feed gas composition	%
CO	5.22
H ₂ O	43.90
H ₂	47.40
CO ₂	2.47
Ar	1.01
Reactor	
Steam/CO ratio	8.4
Feed Flowrate (kmol/s)	776
Gas velocity (m/s)	0.75
Pressure (atm)	23.53
Feed temperature (°C)	355

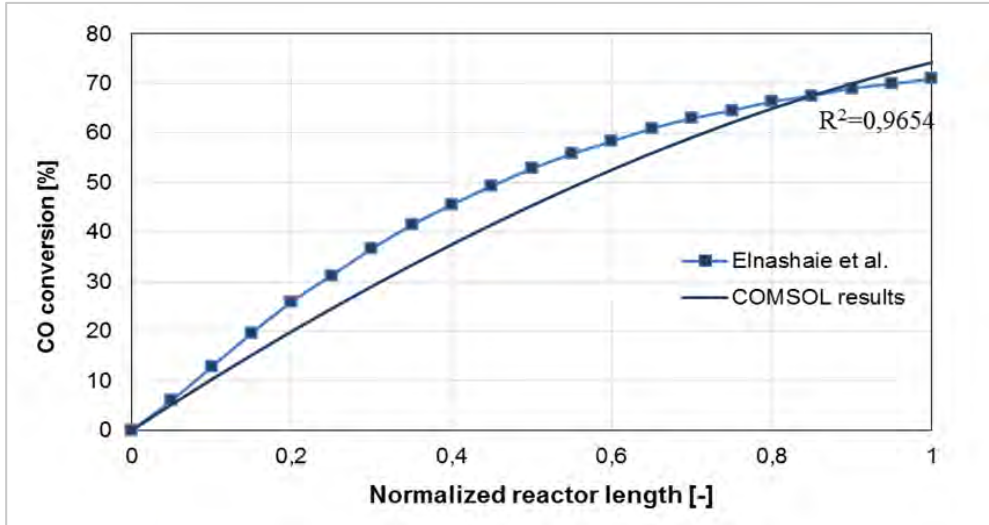


Figure 4. CO conversion along the normalized reactor length, case 2

Based on simulation of the developed model, the variation of the gaseous composition along the reactor length was determined (Figure 5), showing that carbon monoxide is almost fully converted and as result the hydrogen molar fraction is increasing along the reactor length.

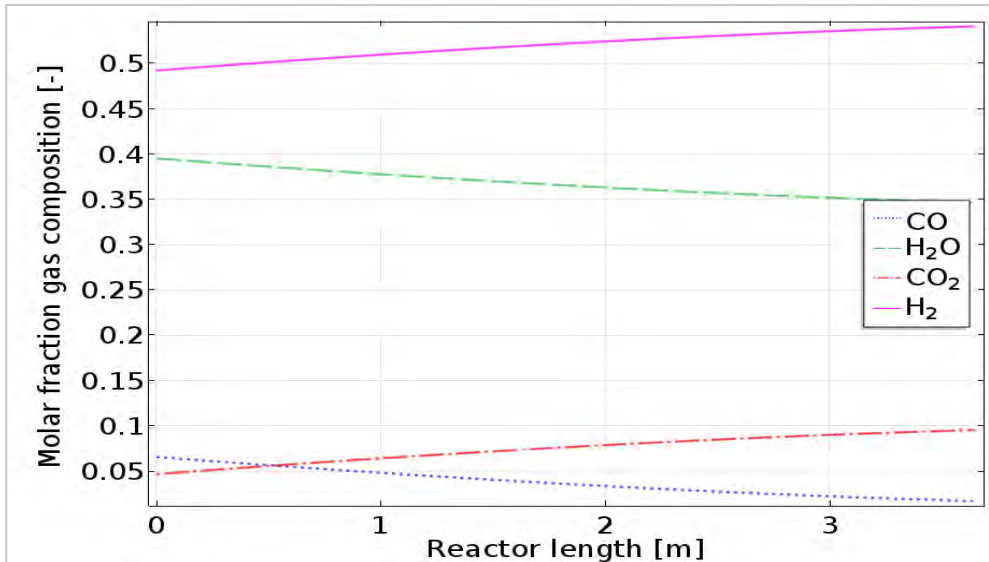


Figure 5. Gas composition distribution along the reactor length

In order to see the distribution inside the reactor bed a 3D model was built. Based on computational time constrains only a small section of the reactor was chosen for simulation. Figure 7 shows the variation of CO partial pressure in the reactor, how has expected the concentration decrease from the inlet to the exit of the reactor.

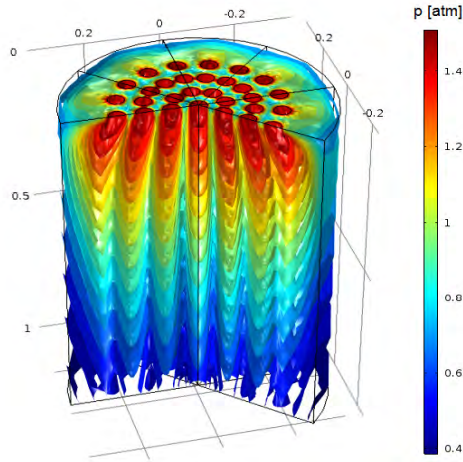


Figure 6. 3D partial pressure distribution of CO in the reactor

The highest partial pressure of hydrogen is at the catalyst pellet surface, where the chemical reaction occurs (Figure 7).

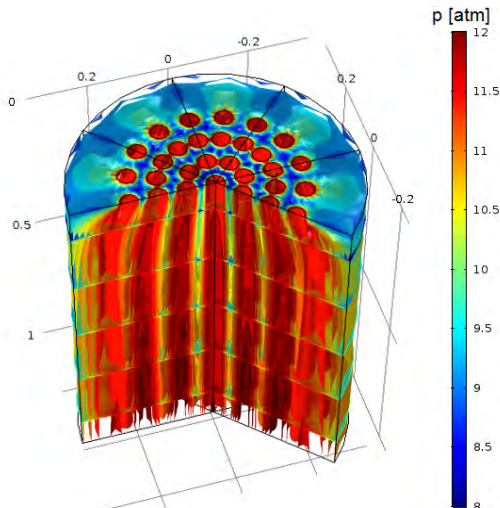


Figure 7. 3D partial pressure distribution of H₂ in the reactor

CONCLUSIONS

Hydrogen production from fossil fuels plays an important role in the global demand of H_2 , as a result, there is a significant interest in optimization and control of the process. A detailed mathematical model was developed for analysing hydrogen production through Water Gas Shift process in a packed bed reactor. The developed model of WGS is implemented and solved in COMSOL Multiphysics 5.2. Based on simulation of the developed model, the variation of the gaseous composition along the reactor length was determined. The developed model of water gas-shift process was validated with data collected from a pilot plant published in literature. The simulation results show a carbon monoxide conversion in range of 74.2 % in line with the published data (72.9 %). Based on computational time constrains, a reactor bed section was simulated to see the gas composition on longitudinal and radial section, using 3D models.

The developed model described the WGS process only in the case of using high-temperature stage of catalyst. As future work in order to find the optimal working conditions of WGS reaction and to achieve a higher conversion of carbon monoxide (implicitly a higher amount of hydrogen) a low-temperature stage catalyst model would have to be implemented in COMSOL Multiphysics. The developed mathematical model would be used for analysing the water gas-shift process efficiency and understanding the micro level interactions of various processes taking place inside a packed bed reactor. Furthermore, the model would be used in evaluation of various operating conditions for optimization of technical indicators of the water gas-shift process.

ACKNOWLEDGMENTS

This work was supported by a grant of the Romanian National Authority for Scientific Research and Innovation, CCCDI - UEFISCDI, project number COFUND-ACT ERANET-3D-CAPS (contract number: 87/2017): "3D Printed Capture Materials for Productivity Step-Change", within PNCDI III.

NOMENCLATURE

A_p	specific area for granule, m^2/m^3
c_i	bulk concentration of specie i , $mol\ m^{-3}$
c_p	bulk concentration of specie i catalyst granules, $mol\ m^{-3}$
D_i	molecular diffusion coefficient of specie i , $m^2\ s^{-1}$
D_{cp}	molecular diffusion coefficient inside of granule, m^2/s
D_p	particle diameter, m
n	surface normalized vectors for granules
N	gas molar flow to catalyst surface [$mol/(m^2 \cdot s)$]
p	pressure, Pa
R_i	reaction rate source, $mol/(m^3 \cdot s)$
R_p	reaction rate in micropore, $mol/(m^3 \cdot s)$
r	variable
r_p	particle radius, m
u	velocity, $m\ s^{-1}$
ε_b	bed porosity, -
μ	gas viscosity [$Pa \cdot s$]
ρ	fluid density, $kg\ m^{-3}$

REFERENCES

1. S. Saeidi, F. Fazlollahi, S. Najari, D. Iranshashi, J. Klemes, L. Baxter, *J. Ind. Eng. Chem.*, **2017**, *49*, 1-25.
2. P. Nikolaidis, A. Poullikkas, *Renewable Sustainable Energ. Rev.*, **2017**, *67*, 597-611.
3. C. Rhodes, G. Hutchings, A. Ward, *Catalysis Today*, **1995**, *23*, 43-58.
4. J. Rawlings, J. Ekerdt, "Chemical Reactor Analysis and Design Fundamentals", Nob Hill Publishing, Madison, **2002**.
5. ***, *COMSOL Multiphysics User's Guide*, version 5.2, COMSOL, Inc, www.comsol.com.
6. G. Germani, P. Alphonse, M. Courty, Y. Schuurman, C. Mirodatos, *Catalysis Today*, **2005**, *110*, 114-120.
7. H. Reijers, J. Boon, G. Elzinga, P. Cobden, W. Haije, R. van den Brink, *Industrial & Engineering Chemistry Research*, **2009**, *48*, 6975-6982.
8. S. Elnashaie, F. Alhabdan, *Mathematical Computer Modelling*, **1989**, *12*, 1017-1034.

SOYBEAN BIOESTER OBTAINED IN A BUBBLE COLUMN ESTERIFICATION REACTOR – A RHEOLOGICAL STUDY

SORINA BORAN^a, ANDRA TĂMĂȘ^{a*}, GIANNIN MOȘOARCĂ^a

ABSTRACT. The paper presents the rheological characterization of a bio-ester with possible lubricant properties, obtained from soybean oil fatty acids. The rheological characterization was carried out under thermostatic conditions, using a Brookfield CAP2000+L viscometer in the characteristic domain of these fluids. The variation of the apparent viscosity η_a as a function of shear rate $\dot{\gamma}$ and the variation of the two indices (K and n) as a function of temperature were determined, as well as the flow activation energy, E_a from Arrhenius type equations. A rheological model was proposed.

Keywords: *apparent viscosity, fatty acids, non-Newtonian behavior*

INTRODUCTION

At present time, environmental protection as well as concerns regarding future energetic security have become of prime importance. That is why the use of bio-based lubricants is important in the transport and industrial sectors, to the detriment of classic synthetic lubricants.

With proper formulation of the base oil and with proper use of additive packages, bio-based lubricants can work better than conventional lubricants [1].

It is important to study the rheological properties of lubricating products, with or without additions of various additives, in order to know their tribological behavior [2-8].

Environmental protection is at present a very important issue [9]. That is why eco-friendly technologies are to be used for protecting the environment. Esterification processes can be performed in bubble column reactors, which were also used in different technologies, such as polymerization processes, when the residual monomer did not appear in the final product [10-14] and the heat transfer may be monitored by the boiling heat transfer coefficients [15-18].

^a Politehnica University Timișoara, Faculty of Industrial Chemistry and Environmental Engineering, 6 Vasile Pârvan Bd., RO-300223, Timișoara, Romania

* Corresponding author: andra.tamas@upt.ro

As a continuation of research undertaken in previous years [19-24], at present we aim to obtain lubricating products that do not affect the environment, but which have superior lubricating properties, using bubble column reactors technologies.

For this purpose, it was obtaining a bio-ester with possible lubricating properties using as acid component the soybean oil fatty acids, *n*-propanol and *p*-toluene-sulphonic acid as catalyst, in a bubble column reactor. The rheological behavior of the bio-ester was studied.

RESULTS AND DISCUSSION

Some physico-chemical properties of the bio-ester are presented in Table 1.

Table 1. Some physico-chemical properties of the bio-ester

Property	Value
Appearance	viscous, opalescent
Color	orange
Acidity index, mg KOH g ⁻¹	< 1
Refractive index, (20°C)	1.4562
Density (25°C), g cm ⁻³	0.9981

The variation of the apparent viscosity η_a as a function of shear rate $\dot{\gamma}$, at different temperature values, is shown in Figure 1.

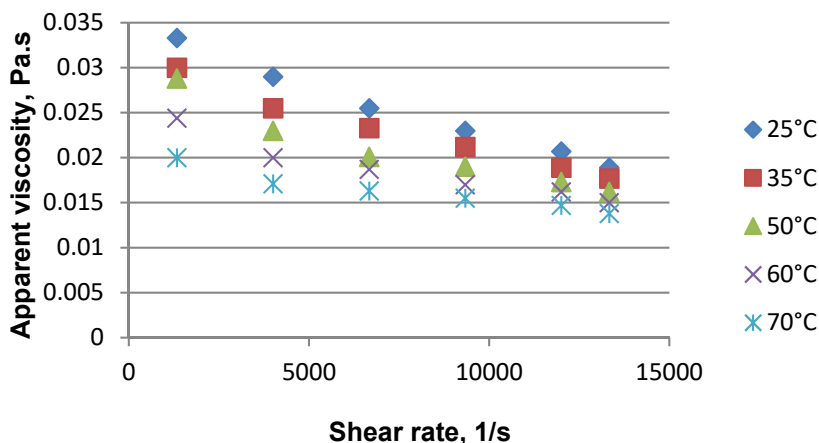


Figure 1. Apparent viscosity vs. shear rate for bio-ester at different temperature values

It is noticed that the values of the apparent viscosity decrease with the shear rate increasing, behavior that is characteristic of non-Newtonian fluids (shear-thinning behavior). The dependence $\eta_a = f(\dot{\gamma})$ can be described by the equation Ostwald de Waele, equation (1):

$$\eta_a = K \cdot \dot{\gamma}^{n-1} \tag{1}$$

where: K – the flow consistency index, $Pa \cdot s^n$; n – the flow behavior index [25,26].

The particular forms of equation (1), corresponding to the five temperature values, are shown in Table 2.

Table 2. Particular forms of equation (1)

Temperature, °C	$\eta_a = f(\dot{\gamma})$	R ²
25	$\eta_a = 0.19 \cdot \dot{\gamma}^{-0.234}$	0.9191
35	$\eta_a = 0.15 \cdot \dot{\gamma}^{-0.219}$	0.9343
50	$\eta_a = 0.164 \cdot \dot{\gamma}^{-0.24}$	0.9836
60	$\eta_a = 0.103 \cdot \dot{\gamma}^{-0.198}$	0.9740
70	$\eta_a = 0.058 \cdot \dot{\gamma}^{-0.147}$	0.9658

The pseudoplastic behavior is also demonstrated by the sub-unit values of the flow behavior index.

The variation of the two indices (K, n) as a function of temperature is shown in Figure 2, and in Figure 3 is presented the variation of the apparent viscosity with temperature, for three values of the shear rate.

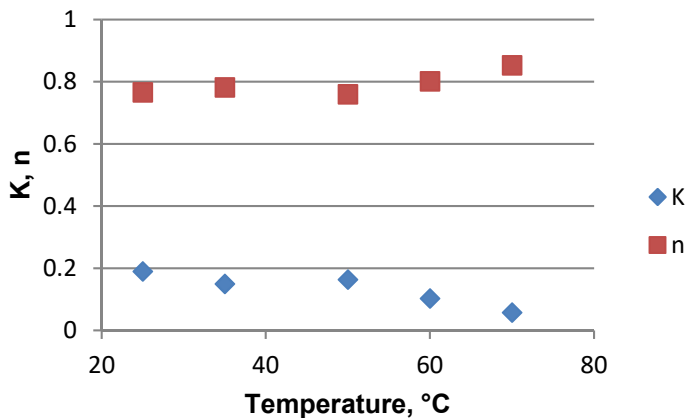


Figure 2. The material consistency and flow behavior index vs. temperature

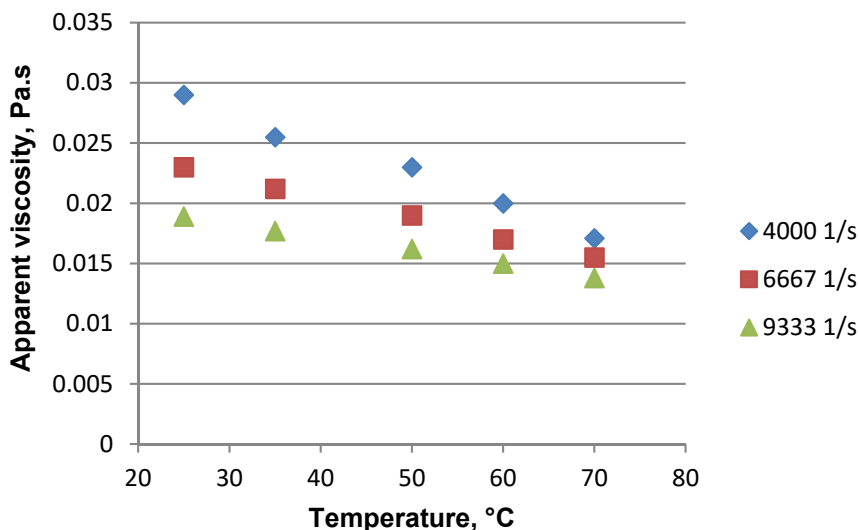


Figure 3. Apparent viscosity vs. temperature at different shear rate values

The temperature increase leads to microdrops mobility intensification which influences the activation energy of the system. The phenomenon can be explained by an Arrhenius type equation (equation (2)):

$$\eta_a = A' \cdot e^{\frac{E_a}{R \cdot T}} \quad (2)$$

where E_a is the activation energy of viscous flow, J mol^{-1} ; R is the gas general constant, $\text{J mol}^{-1} \text{K}^{-1}$; T is absolute temperature and A' represents the material constant, Pa s . The dependence $\ln \eta_a = f(1/T)$ was graphically represented, as obtained from the logarithmic form of equation (2), for apparent viscosity values corresponding to the three chosen values of the shear rate. Particular expressions of equation (2) as well as the values of the activation energy are presented in Table 3.

Table 3. Particular forms of equation (2)

$\dot{\gamma}, \text{s}^{-1}$	$\eta_a = A' \times 10^4 \cdot \exp(\frac{E_a}{R \cdot T})$	$E_a, \text{kJ} \cdot \text{mol}^{-1}$
4000	$\eta_a = 6.6 \cdot \exp(\frac{1130.7}{T})$	9.4
9333	$\eta_a = 11.9 \cdot \exp(\frac{886.2}{T})$	7.4
13333	$\eta_a = 18.4 \cdot \exp(\frac{696.6}{T})$	5.8

CONCLUSIONS

It was studied the rheological behavior of a bio-ester obtained from soybean oil fatty acids in the bubble column reactor at reflux.

The synthesized ester exhibits pseudoplastic behavior characterized by the decrease in apparent viscosity with the shear rate increasing and subunit values of the flow behavior index. These values increase with increasing temperature, without exceeding the value 1.

It is also observed that the activation energy of viscous flow decreases with the shear rate increasing.

EXPERIMENTAL SECTION

General procedure for ester preparation

Synthesis of the bio-ester was performed in the bubble column reactor at reflux. The ratio fatty acids from soybean oil: n-propanol was 1:2, using 0.4% catalyst [17-22].

The physico-chemical properties were determined by using standardized techniques: the pycnometer method for density determination and the Abbe refractometer for refractive indices.

The rheological characterization of the samples was carried out under thermostatic conditions (temperature range 25÷70°C), using a Brookfield CAP2000+L viscometer in the characteristic domain of these fluids.

REFERENCES

1. A.Z. Syahir et. al.; *J. Cleaner Prod.*, **2017**, 168, 997-1016
2. C.C. Chou; S.H. Lee; *J. Mater. Process. Technol.*, **2008**, 201, 542-547
3. J.E. Martín-Alfonso; C. Valencia; *Tribol. Int.*, **2015**, 90, 426-434
4. M.H. Esfe; H. Rostamian; M. Rejvani; M.R.S. Emami; *Physica E*, **2018**, 102, 160-170
5. M.H. Esfe; M. Afrand; W-M. Yan et. al.; *Int. Commun. Heat Mass Transfer*, **2016**, 76, 133-138
6. T. Sui; M. Ding; C. Ji et. al.; *Ceram. Int.*, **2018**, 44, 18438-18443
7. A.A. Nadooshan; M.H. Esfe; M. Afrand; *Physica E*, **2017**, 92, 47-54
8. M.J. Souza de Carvalho; P.R. Seidl; C.R.P. Belchior; J.R. Sodre; *Tribol. Int.*, **2010**, 43(12), 2298-2302
9. G. Mosoarca; C. Vancea; S. Popa; S. Boran; *Bull. Environ. Contam. Toxicol.*, **2018**, 100(5), 733-739

10. S. Popa; C. Csunderlik; S. Florea; V. Jâșcanu; D. Jurcău, N. Pleșu; *Rev.Chim.*, **2002**, 53(4), 259-263
11. S. Popa; V. Jâșcanu; D. Jurcău, N. Pleșu; *Rev.Chim.*, **2003**, 54(7), 595-598
12. S. Popa; C. Csunderlik; V. Jâșcanu; D. Jurcău, N. Pleșu; *Materiale plastice*, **2003**, 40(4), 177-181
13. S. Popa; C. Csunderlik; V. Jâșcanu; D. Jurcău, N. Pleșu; *Materiale plastice*, **2004**, 41(2), 62-65
14. S. Popa; S. Boran; *Materiale plastice*, **2016**, 53(3), 410-413
15. A. Tămaș; S. Boran; *Studia UBB Chemia*, **2019**, LXIV, 1, 93-102
16. S. Boran; S. Nițu; *Materiale Plastice*, **2017**, 54(2), 386-389
17. S. Popa; S. Boran; V. Simulescu; *Materiale Plastice*, **2017**, 54(2), 359-361
18. S. Boran; A. Tămaș; *Materiale Plastice*, **2016**, 53(3), 505-508
19. S. Popa; S. Boran; *Rev. Roum. Chim.*, **2016**, 61(11-12), 851-855
20. S. Popa; S. Boran; *Rev. Roum. Chim.*, **2015**, 60(10), 991-995
21. S. Boran; A. Tămaș; *J. Serb. Chem. Soc.*, **2014**, 79 (2), 241-251
22. S. Boran; A. Tămaș; *Studia UBB Chemia*, **2013**, LVIII, 1, 21-30
23. D. Kohn, S. Popa, *Exp. Heat Transfer*, **1999**, 12(3), 193-202
24. S. Popa, S. Boran, *Thermal Science*, **2015**, 21(5), 2031-2037
25. A. Miclăuș; V. Pode; *Cazuri particulare de curgere a fluidelor ideale si reale. Elemente de reologie*, Casa Cărții de Știință, Cluj-Napoca, **2018**, pp. 49
26. A. Ya. Malkin; A.I. Isayev; *Rheology: Concepts, Methods, and Applications*, 2nd ed., Chem Tec Publishing Toronto, **2012**, pp. 131.

TREATED DIATOMITE FOR TOLUIDINE BLUE REMOVAL FROM WASTEWATER. IS IT WORTH IT?

ANDRADA S. MĂICĂNEANU^{a*}, RALUCA PLEȘA CHICINAȘ^b,
HOREA BEDELEAN^c

ABSTRACT: The adsorption of Toluidine Blue (TB) cationic dye was performed using raw and treated (thermal, chemical, thermo-chemical, ultrasonic) diatomite. Solid samples were characterized using X-ray diffraction (XRD), scanning electron microscopy (SEM), X-ray photoelectron spectroscopy (EDX), and Fourier Transformed Infrared Spectroscopy (FTIR). Adsorption experiments were performed in batch conditions ($20 \pm 2^\circ\text{C}$, 100 mg TB/L, 100 mL, 0.1 g adsorbent). The best sample proved to be the one thermally treated at 250°C for 2 h with an adsorption capacity of 7.97 mg/L and 77% removal efficiency. The regeneration process of the used diatomite was also performed (calcination, HCl, water), the most efficient was the one using water. Kinetic models (pseudo-first-, pseudo-second-order, liquid film, and intra-particle diffusion) were considered to describe the experimental data. The calculated data showed that liquid film diffusion might be rate-determining step in this case.

Keywords: diatomite, adsorption, toluidine blue, regeneration, kinetics

INTRODUCTION

Industrial activities such as textile, cosmetics, pulp and paper, plastic, paints, printing, leather, pharmaceuticals, food, and mineral processing are all discharging wastewaters with a high content of dyes [1,2]. Wastewater treatment, based on physical, chemical, or biological processes, such as coagulation, flotation, adsorption, chemical oxidation, filtration, ozonation, ion-exchange, and aerobic and anaerobic microbial degradation, were all

^a Madia Department of Chemistry, Indiana University of Pennsylvania, Indiana, PA 15705, USA

^b Ana Aslan Technical College, 41 Decebal st., 400124, Cluj-Napoca, Romania

^c Department of Geology, Babes-Bolyai University, 1 M. Kogălniceanu st., 400048, Cluj-Napoca, Romania

* Corresponding author: sanda.maicaneanu@iup.edu

considered for dye removal from wastewater. Between the available methods, adsorption has proven to be effective and convenient and activated carbon the adsorbent used with the best results. Due to the high costs involved in its regeneration, low-cost substitute materials were considered [1,3,4].

There are many studies which have shown that numerous natural and inexpensive materials were successfully applied in the removal of dyes from wastewaters, such as coal, wood powder, lignin, shale oil ash, zeolite, perlite, clay minerals, diatomite, activated slag, activated carbon, fly ash, and agricultural wastes [3-5].

The most important property of an adsorbent is the surface area and structure. Any solid material with a microporous structure and a large surface area can be used as adsorbent. Diatomite is one of the materials which fulfils these conditions [6,7].

Diatomite is a fine, siliceous natural rock, composed mainly by microscopic frustules (skeletal remains) of silica microfossils of dead diatoms, radiolaria, and sponges. Most diatoms are elongated (pennate diatoms), while others are round (centric diatoms). The main component of diatomite is amorphous silica ($\text{SiO}_2 \cdot n\text{H}_2\text{O}$). Sometimes the siliceous deposits may be pure, sometimes they are mixed with clay, carbonates, or organic matter. It's a pale-colored, soft, light-weight sedimentary rock, with 80-90% voids in its structure [6-8].

Diatomite has numerous physical and chemical properties that are important for the adsorption process, which include high porosity, high permeability, small particle size, high surface area, and low thermal conductivity. All these properties make diatomite a low-cost alternative to activated carbon, suitable for many industrial applications such as filtering and adsorption of organics and heavy metals from wastewater [6,9,10]. Diatomite surface is terminated by OH groups (will form hydrogen bonds with the adsorbate) and oxygen bridges, which act as adsorption sites [11].

Not many studies considered the influence of various treatments on adsorptive (organic compounds) properties of diatomite. Aivalioti et al. [12,13] studied BTEX, MTBE, and TAME adsorption on raw, thermally, chemically (acid), and both chemically and thermally treated diatomite, with the sample treated with HCl being the most effective [13]. Dye and printing wastewaters were used to test adsorptive properties of diatomite treated with HCl 5% followed by calcination at 500°C [14]. HF etching (various concentrations, time of reaction, temperatures) was proved to drastically change the porous structure of diatomite and therefore adsorptive properties towards methylene blue [15]. Thermo-chemical treated diatomite (H_2SO_4 5-6M, 900°C) was used

to remove methylene blue from aqueous solutions, two studies indicating that this type of treatment improves its performances as adsorbent [16,17]. Diatomite subjected to a NaOH treatment proved to improve its adsorptive properties towards methylene blue adsorption [18].

The aim of this study was to explore the use of Romanian pennate frustules diatomite as adsorbent for toluidine blue (TB) dye removal from aqueous solution and to decide if the treatments applied to the raw diatomite are justified. Reutilization of the spent diatomite after regeneration was also considered. As treatment applied to diatomite are likely to modify its porous structure, kinetic models (pseudo-first-, pseudo-second-order, liquid film, and intra-particle diffusion) were considered to describe the experimental data.

RESULTS AND DISCUSSION

Adsorbent characterization

The diatomitic ore from Minișu de Sus, the most important one in Romania, is located in the western part of the country, in Arad County. It is of Sarmatian age and it is positioned within the lower tuffaceous diatomitic complex. Diatomite layers are usually interbedded with clays, limestone as thin intercalations, as well as with silts, sands, and pyroclastic material. The diatomite from Minișu de Sus may be characterized as clayey diatomites as it contains some amounts of smectitic clays, whereas the presence of calcite or other carbonate mineral is negligible. The white-yellowish diatomite consists mainly of a mixture of small elongate frustules of pennate diatoms, clay minerals, and amorphous silica. The pennate type of diatoms gives the material superior technical properties, compared to those constituted from centric forms [8].

X-ray diffraction analyses performed on random powders indicate the presence of silica minerals as the main component (Figure 1). The highly crystalline peaks of cristobalite and quartz could be observed. The presence of biogenic opal A (amorphous silica) is indicated by a slightly broad reflexion centered at $2\theta=20-25^\circ$ [19] and well crystallized quartz. The quartz crystals are even allogenic, of a volcanogenic origin, or formed from the devitrified glass. Smectitic clay minerals (montmorillonite) and feldspars are also present but in small amounts.

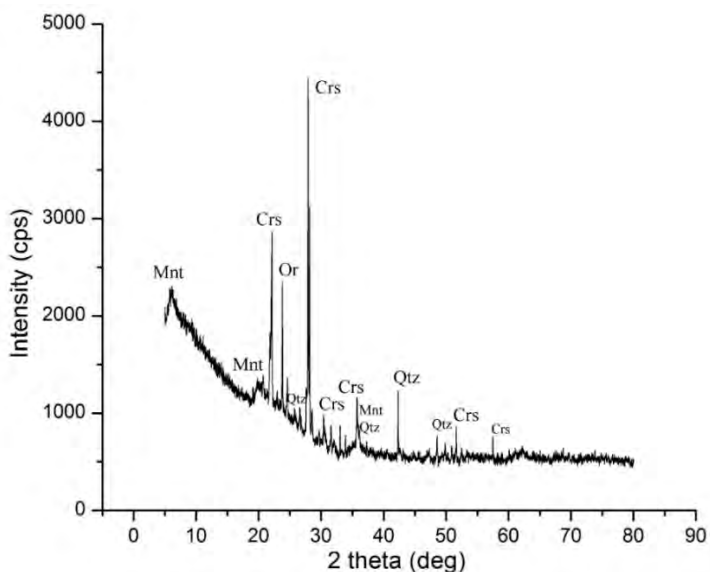


Figure 1. XRD pattern of raw diatomite (D) from Minișu de Sus (Arad County, Romania). Legend: Crs = cristobalite, Mnt = montmorillonite, Or = orthoclase, Qtz = quartz

SEM analysis provides data on the morphology of diatoms and on the porosity of the material. The images revealed the presence of the pennate frustules of diatoms with open-pores dispersed in clay matrix (Figure 2). The porous structure can be observed. Pores and open voids provide natural filtration and adsorption properties to the diatomaceous material.

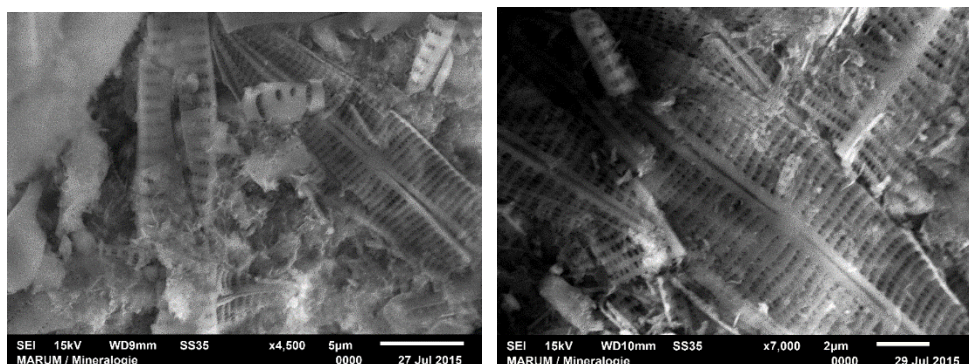


Figure 2. SEM images of raw diatomite (D) from Minișu de Sus (Arad County, Romania). Fragments of pennate diatoms frustules hosted in a clayey matrix.

The chemical composition of the diatomitic material varies, due to the lithological heterogeneity of the ore [8]. SiO_2 is the main oxide, between 65-76%, constituting the diatom frustules, opal-A is present in the cement, while detrital quartz and silicates (feldspar, clay minerals) are also present. Al_2O_3 has average values between 5-19 %, being found in feldspars and clay minerals. Fe_2O_3 is contained mainly by iron oxi-hydroxides and varies between 3-7%. CaO is in small amounts, between 2-6%. It is present in plagioclases, montmorillonite and probably in secondary carbonates. According to the $\text{SiO}_2:\text{Al}_2\text{O}_3$ ratio, the diatomites for Minișu de Sus belong to the clayey-type. From the EDX spectra of the considered diatomite sample (D) (Figure 3), the atomic elemental composition in wt. % was depicted as follows: 64.6 – O, 26.5 – Si, 5.69 – Al, 1.12 – Ca, 0.98 – Fe, 0.64 – Mg, 0.26 – Na and 0.15 – K (the difference up to 100% corresponds to gold used for sample preparation).

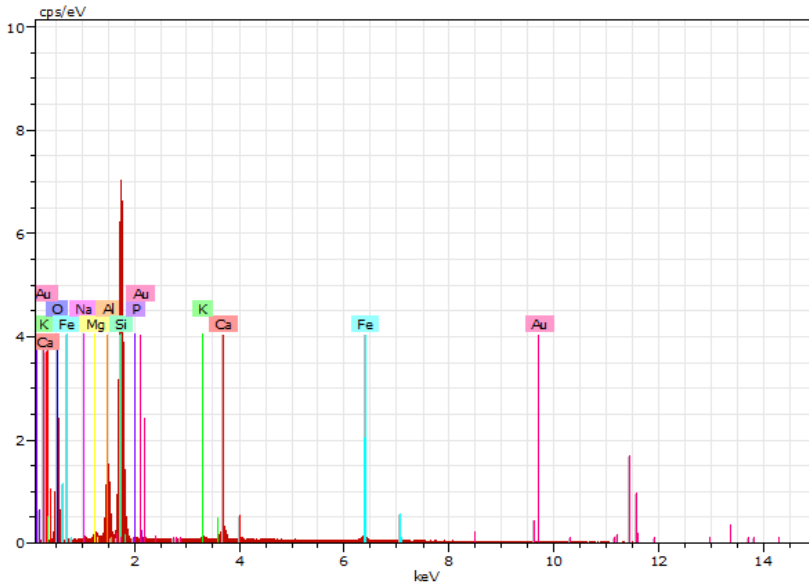


Figure 3. EDX spectra of raw diatomite (D) from Minișu de Sus (Arad County, Romania).

The FTIR spectra for raw diatomite and some of the treated samples (the ones which were giving the best results in terms of dye removal efficiencies) are presented in Figure 4. The main bands indicated the presence of diatomite specific peaks, Figure 4 and Table 1. All the samples present similar spectra with a slight increase in the intensity in case of thermal and thermo-chemical treated samples. The bands at $3625\text{-}3630\text{ cm}^{-1}$ are attributed

to Si-OH stretching. The bands in the 3440-3443 cm^{-1} range are characteristic to O-H stretching vibration, while the 1636 cm^{-1} band is characteristic to H-O-H bending of adsorbed water molecules. The 1093-1094, 795-797, and 467-468 cm^{-1} bands are characteristic to Si-O-Si asymmetric stretching, Si-O-Si symmetric stretching and Si-O-Si / Si-O-Al bending, respectively [20-23].

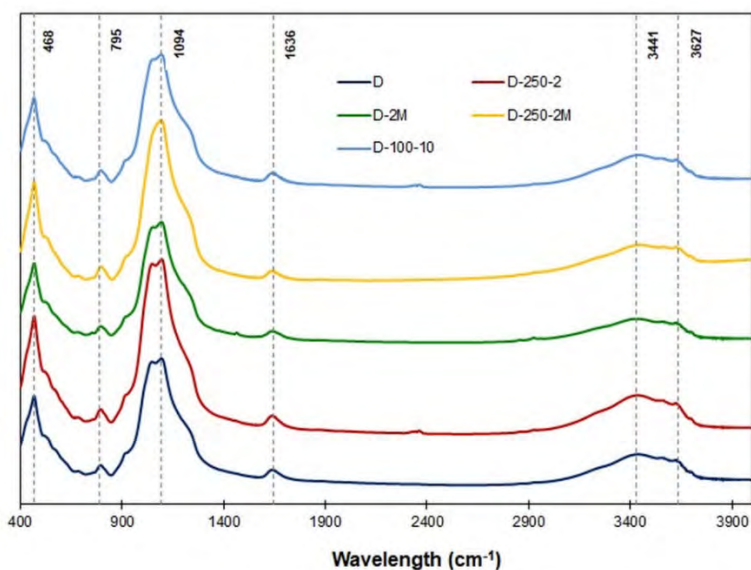


Figure 4. FTIR spectra of D, D-250-2, D-2M, D-250-2M, and D-100-10 diatomite samples.

Table 1. Most relevant infrared spectral bands of the D, D-250-2, D-2M, D-250-2M, and D-100-10 samples [20-23].

Sample	D	D-250-2	D-2M	D-250-2M	D-100-10	Assignment
Wavelength (cm^{-1})	468	467	468	467	467	Si-O-Si / Si-O-Al symmetric bending
	795	795	796	797	796	Si-O-Si symmetric stretching
	1094	1094	1094	1093	1094	Si-O-Si asymmetric stretching
	1636	1636	1636	1636	1636	H-O-H bending
	3441	3440	3440	3444	3443	O-H stretching
	3627	3626	3626	3625	3630	Si-OH stretching

Adsorption results

For each considered treatment applied to the raw diatomite sample, maximum removal efficiencies were considered and compared. In the case of thermally treated samples, Figure 5a, a small increase in removal efficiency, from 71 to 77%, was observed for D-250-2 sample. This fact might be attributed to the fact that as the temperature increases water is removed from the solid surface, making pores more accessible. Further increase of the temperature led to partial collapsing of the porous structure [24] and therefore to a decrease of the surface available for adsorption, hence a decrease of removal efficiency to 58% recorded for D-750-2 sample. When calcination time was increased from 1 to 4 hours at 500°C, the decrease in removal efficiency was constant irrespective to the calcination time (71 to 57%).

When chemical treatment was considered, Figure 5b, a slight increase in removal efficiency was observed for D-2M sample (from 71 to 76%), while with a further increase of the HCl concentration, D-4M sample, removal efficiency dropped to 67%. This decrease might be due to the reaction occurring between the acid and the metal oxides on the adsorbent surface, reaction products blocking the pores of the diatomite, thereby reducing adsorption efficiency [25].

Thermo-chemical treatment of the raw diatomite did not show a positive trend on improving its adsorption capacity, Figure 5c. The removal efficiency values decreased from 71 to 57% for D and D-750-2M, respectively.

In the case of ultrasonic treatment, increasing of power and treatment time led to the same trend in removal efficiency evolution, Figures 5d and 5e. The best results, with a removal efficiency of 76% were obtained in case of both D-100-10 and D-120-8 samples. Further increase of time (> 10 min) and power (> 120 W) could have as a result pores destruction and therefore a decrease in removal efficiency values. Between the best results obtained for various treatments, Figure 6, slight improvements in terms of removal efficiency by comparison with D sample were obtained just for D-250-2, D-2M, D-100-10, and D-120-8 samples.

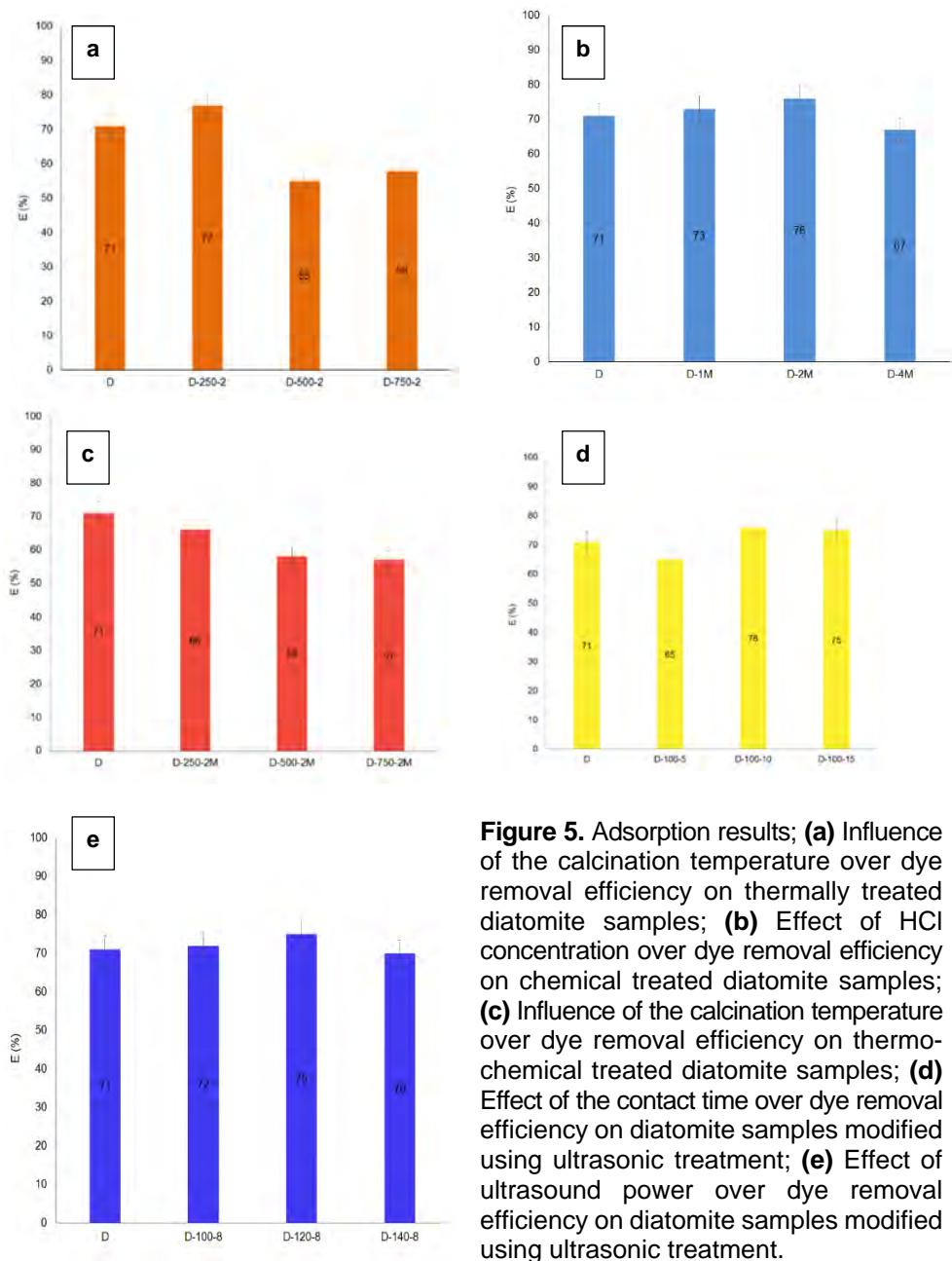


Figure 5. Adsorption results; **(a)** Influence of the calcination temperature over dye removal efficiency on thermally treated diatomite samples; **(b)** Effect of HCl concentration over dye removal efficiency on chemical treated diatomite samples; **(c)** Influence of the calcination temperature over dye removal efficiency on thermo-chemical treated diatomite samples; **(d)** Effect of the contact time over dye removal efficiency on diatomite samples modified using ultrasonic treatment; **(e)** Effect of ultrasound power over dye removal efficiency on diatomite samples modified using ultrasonic treatment.

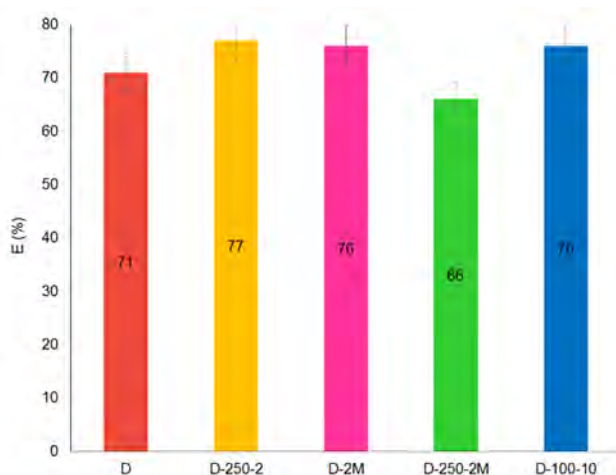


Figure 6. Comparison of the maximum removal efficiencies obtained for each considered treatment.

Adsorbent regeneration

The regeneration methods used on spent diatomite samples as described in the Experimental section, proved to have similar results when temperature and acid were used. Thermal treatment at 500°C and repeated contact with HCl led to a drastically decrease of removal efficiency (52%) after the third regeneration-adsorption cycle, Figure 7.

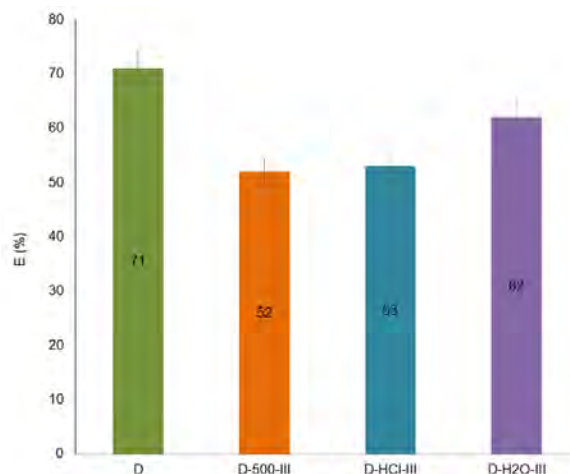


Figure 7. Effect of the regeneration method over dye removal efficiencies obtained after the third regeneration-adsorption cycle.

These two methods are quite expensive and have a high environmental impact. In the case of water, a slower decrease in removal efficiency was recorded, 69, 65, and 62% after the first, second, and third regeneration cycle, respectively. Depending on the dye concentration present in water and considering that diatomite is a low-cost material, usage up to 3-5 cycles with water as a regeneration agent could be a promising process for colored wastewater treatment. When studied only thermal regeneration (300-900°C), Auguedal et al. found that at 600°C, the adsorbed Red ETL dye was completely removed, and around 73% was restored after three regeneration cycles [26].

Adsorption kinetics

Several adsorption kinetic models, such as pseudo-first- (Lagergren), pseudo-second-order, liquid film, and intra-particle diffusion models, (equations are presented in Table 2), were used to test experimental data in order to investigate the adsorption mechanism and potential rate determining steps [27-30]. The pore diffusion coefficient, D (cm²/s) was also calculated (assuming a spherical geometry of the adsorbents – average size 0.1 cm) using the following equation [31,32]:

$$D = 0.003 \cdot \frac{r_0^2}{t_{0.5}} \quad (1)$$

Based on the pseudo-second-order model, $t_{0.5}$ was estimated using equation [32,33]:

$$t_{0.5} = \frac{1}{k_2 q_e} \quad (2)$$

Time evolution of TB concentration for D and D-250-2 samples, Figure 8, shows that the removal process takes place with a relatively small rate and the equilibrium was reached after about 300 min.

The results obtained for all considered models are presented in Table 2. The pore diffusion coefficients are 7.93×10^{-8} and 2.67×10^{-8} cm²/s for D and D-250-2, respectively, higher values than rate determining range (10^{-11} – 10^{-13} cm²/s) [33]. Taking into consideration all the calculated values, regression coefficient (R^2) values, the fact that in the case of liquid film model the intercepts have values very close to 0 [34], Table 2, and also the shape of the time evolution curve (Figure 8), we have concluded that in this particular case, liquid film diffusion could be rate-determining step.

Table 2. Pseudo-first-, pseudo-second-order, intra-particle, and liquid film diffusion parameters for TB adsorption onto D and D-250-2 samples.

Diatomite sample	Pseudo-first-order				Pseudo-second-order		
	$\ln(q_e - q_t) = \ln q_e - k_2 \cdot t$ [27]				$\frac{t}{q_t} = \frac{1}{k_2 \cdot q_e^2} + \frac{t}{q_e}$ [28]		
	$q_{e,exp}$	k_1	$q_{e,cal}$	R^2	k_2	$q_{e,cal}$	R^2
D	7.39	0.0112	9.394	0.9525	3.0790	13.45	0.9816
D-250-2	7.97	0.0124	10.29	0.9335	5.0937	12.24	0.9945
	Intra-particle diffusion				Liquid film diffusion		
	$q_t = k_{ip} \cdot t^{0.5}$ [29]				$\ln(1 - F) = -k_{fd} \cdot t$ [30]		
D	0.5086	-1.1903	0.9966	0.0112	-0.2403	0.9525	
D-250-2	0.0119	1.6859	0.9518	0.0124	-0.2558	0.9335	

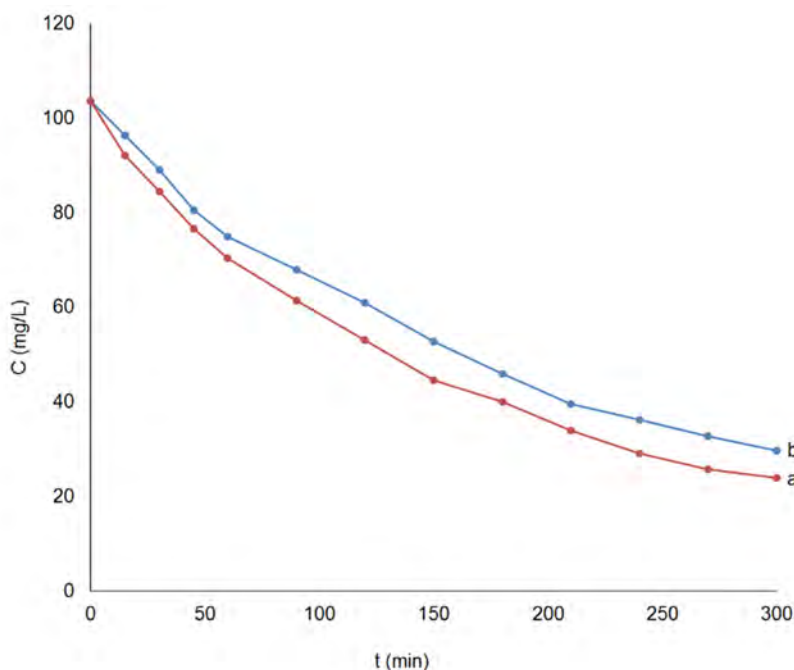


Figure 8. Time evolution of TB concentration for adsorption on (a) D and (b) D-250-2 diatomite samples.

CONCLUSIONS

A Romanian diatomite sample subjected to various treatments (thermal, chemical, thermo-chemical, and ultrasonic) was tested for the removal of toluidine blue cationic dye from aqueous solutions. XRD, FTIR, and SED-EDX analyses confirmed the siliceous nature of the diatomaceous material, presence of the pennate frustules of diatoms, and the small amount of impurities. Between the considered treatments applied to the raw diatomite, improvements in terms of adsorption capacity and removal efficiency were obtained in case of: D-250-s (7.97 mg/g and 77%), D-2M and D-120-8 (7.85 mg/g and 75%), and D-100-10 (7.93 mg/g and 76%) by comparison with D (7.39 mg/g and 71%). Regeneration of the diatomite samples was realized using thermal, acid, and water methods. The results showed that when the regeneration was realized with water, the smallest decrease in removal efficiency was obtained even after three regeneration-adsorption cycles (a drop of 13% by comparison with thermal regeneration where a 27% drop was recorded). The calculated data showed that liquid film diffusion might be rate-determining step in this case.

To answer the question from the title, besides the 2 h at 250°C treatment, the slight improvement in adsorption capacities and efficiency obtained for all the other treatments do not justify the costs of these treatments.

EXPERIMENTAL

Materials

Diatomite sample (raw diatomite) collected from Minișul de Sus deposit, Arad County, Romania was used as an adsorbent in this study. Characterization of diatomite was realized using X-ray diffraction (XRD), scanning electron microscopy (SEM), X-ray photoelectron spectroscopy (EDX), and Fourier Transformed Infrared Spectroscopy (FTIR).

Toluidine Blue, $C_{15}H_{16}ClN_3S \cdot 0.5 ZnCl_2$, 373.97 g/mol, TB (Sigma Aldrich) was used as model dye molecules for the adsorption processes. A stock solution of 1000 mg/L was used to prepare the desired concentration (100 mg/L) solution.

Adsorbent preparation

Thermal, chemical, thermo-chemical, and ultrasonic treatments were applied to the raw diatomite sample. A total of 17 samples have been prepared as described below.

Raw diatomite was first subjected to a grinding process, followed by size separation to obtain the 0.6-1.0 mm fraction, which was further used throughout the experiments. Raw diatomite was then washed a few times with distilled water in order to remove fine particles and dried at 105°C for 24h.

Thermal treatment was realized through calcination at different temperatures in 250-750°C interval for 1, 2, and 4 h, modified after Aivalioti et al. [12,13]. Five thermal modified samples were obtained, Table 3.

Chemical treatment was performed using HCl solution of different concentrations (1 M, 2 M, and 4 M), modified after Zhang et al. [25]. Raw diatomite and acid solution were contacted at room temperature under mechanical stirring (300 rpm) for 3 h at a solid:liquid ratio of 1:10. The obtained samples were separated from the acid solution, thoroughly washed with distilled water until no chlorine was detected (AgNO_3 0.01 N) and dried at 105°C for 24 h, Table 3.

Thermo-chemical treatment was achieved using a chemical treated sample (HCl 2M, as described above) subsequently calcined at 250, 500, and 750°C for 2 h, Table 3.

Ultrasonic treatment, modified after Zhang et al. [25], was realized using power settings in 100-180 W interval and contact time of 5 to 15 min as follows: 20 g of raw diatomite and 100 mL distilled water were added in a glass beaker, which was then placed in an ultrasonic bath at room temperature at an established power and time interval. The solid was recovered by settling, washed with distilled water and dried at 105°C for 24 h. Six samples were thus obtained, Table 3.

Adsorbent characterization

XRD analyses of diatomite samples were performed using a D8 ADVANCE Bruker diffractometer, $\text{CuK}\alpha$ anticathode. The diffractograms were recorded from 5° to 80°, 2 θ degree. The analytic conditions were 40 kV, 40 mA, and a step of 0.02 degrees/min.

SEM-EDX analyses were performed using a JEOL JSM-6510 and Bruker EDX equipment. Prior to scanning, the diatomite sample was mounted on a stainless-steel slab with double stick tape and coated with a thin layer of gold in high vacuum condition.

FTIR analyses were performed on dried samples prepared by encapsulating 1.2 mg of finely grounded particles in 300 mg of KBr. Infrared spectra were obtained using a JASCO 615 FTIR spectrometer 400-4000 cm^{-1} (resolution, 2 cm^{-1}).

Adsorption experiments

TB adsorption process was conducted in batch conditions, in a thermostated batch reactor placed on a shaker (50 rpm), using 1 g adsorbent (0.6-1.0 mm grain size), 100 mL dye solution (100 mg/L), at $20 \pm 2^\circ\text{C}$. Working conditions were selected based on preliminary experimental results. Dye concentration from solution was determined using a UV-Vis Jenway 6305 spectrophotometer (calibration curve 2-10 mg/L) at the maximum absorption wavelength of $\lambda_{\text{TB}} = 633 \text{ nm}$. Experiments were conducted in the same conditions for all diatomite samples considered. The evolution and effectiveness of the dye adsorption process were evaluated by means of the amount of dye adsorbed, q (mg/g) and removal efficiency, E (%) [35].

Adsorbent regeneration

Although diatomite is a low-cost material, there might be instances when regeneration and/or dye recovery will be required. Therefore, this study considered the potential reuse of the spent diatomite, proposing three regeneration methods for the raw diatomite, namely: thermal, acid, and water, Table 4. In case of acid (HCl) and water (distilled) regeneration, diatomite was contacted with the liquid using a solid:liquid ratio of 1:10, under continuous stirring (shaker) at 50 rpm for 5 h. Three regeneration-adsorption cycles were realized in each case.

Table 3. Diatomite treatments and samples labeling.

Treatment	Label	Parameter		
Raw	D	grinding / size separation / washing		
Thermal		Temperature ($^\circ\text{C}$)		Time (h)
	D-250-2	250		2
	D-500-1	500		1
	D-500-2	500		2
	D-500-4	500		4
Chemical		HCl concentration (M)		
	D-1M	1		
	D-2M	2		
	D-4M	4		
Thermo-chemical		Temperature ($^\circ\text{C}$)	Time (h)	HCl concentration (M)
	D-250-2M	250	2	2
	D-500-2M	500	2	2
	D-750-2M	750	2	2

Ultrasonic		Power (W)	Time (min)
	D-100-5	100	5
	D-100-10	100	10
	D-100-15	100	15
	D-100-8	100	8
	D-120-8	120	8
	D-140-8	140	8

Table 4. Spent diatomite regeneration; type, samples labeling, and removal efficiencies.

Regeneration	Label	Regeneration parameters	Regeneration-adsorption cycle	E (%)
Raw	D	-		71
Thermal	D-500-I	500°C, 2 h	I	58
	D-500-II		II	54
	D-500-III		III	52
Acid	D-HCl-I	HCl 2M, 5 h	I	65
	D-HCl-II		II	55
	D-HCl-III		III	53
Water	D-H ₂ O-I	H ₂ O, 50°C, 5 h	I	69
	D-H ₂ O-II		II	65
	D-H ₂ O-III		III	62

Abbreviations

C_e – concentration of dye at equilibrium (mg/L)

D – pore diffusion coefficient (cm^2/s)

E – removal efficiency (%)

F – fraction attainment at equilibrium ($=q_t/q_e$)

k_1 – pseudo-first-order rate constant (1/min)

k_2 – pseudo-second-order rate constant (g/mg·min)

k_{fd} – liquid film diffusion rate constant (1/min)

k_{ip} – intra-particle diffusion rate constant ($\text{mg/g}\cdot\text{min}^{0.5}$)

q – the amount of dye adsorbed (mg/g)

q_e – the amount of dye adsorbed at equilibrium – adsorption capacity (mg/g)

$q_{e,exp}$ – the experimental amount of dye adsorbed at equilibrium (mg/g)

$q_{e,cal}$ – the calculated amount of dye adsorbed at equilibrium (mg/g)

q_t – the amount of dye adsorbed at time t (mg/g)

r_0 – diatomite grain diameter (cm)

t – time (min)

$t_{0.5}$ – time for half adsorption (s)

REFERENCES

1. E. Erdem; G. Çölgeçen; R. Donat; *J. Colloid Interf. Sci.*, **2005**, 282, 314-319.
2. M. Toor; B. Jin; S. Dai; V. Vimonses; *J. Ind. Eng. Chem.*, **2015**, 21, 653-661.
3. J.X. Lin; S.L. Zhan; M.H. Fang; X.Q. Qian; *J. Porous Mat.* **2007**, 14, 449-455.
4. E. Bulut, M. Özacar; I. A. Şengil; *J. Hazard. Mater.*, **2008**, 154, 613-622.
5. L. Lian; L. Guo; C. Guo; *J. Hazard. Mater.*, **2009**, 161, 126-131.
6. P. Moslehi; P. Nahid; *Int. J. Eng., Transactions B: Applications*, **2007**, 20, 141-146.
7. M.A.M.M. Khraisheh; Y.S. Al-Degs; W.A.M. Mcminn; *Chem. Eng. J.*, **2004**, 99, 177-184.
8. V.C. Brana; C. Avramescu; I. Călugăru; *Substanțe minerale nemetalifere*, Editura Tehnică, București, **1986**, pp. 133-135.
9. A. Sari; D. Çitak; M. Tuzen; *Chem. Eng. J.*, **2010**, 162, 521-527.
10. M.A. Al-Ghouti; M.A.M. Khraisheh; S.J. Allen; M.N. Ahmad; *J. Environ. Manage.*, **2003**, 69, 229-238.
11. M.A.M.M. Khraisheh; M.A. Al-Ghouti; S.J. Allen; M.N. Ahmad; *Water Res.*, **2005**, 39, 922-932.
12. M. Aivalioti; I. Vamvasakis; E. Gidarako; *J. Hazard. Mater.*, **2010**, 178, 136-143.
13. M. Aivalioti; P. Papoulias; A. Kousaiti; E. Gidaracos; *J. Hazard. Mater.*, **2012** 207-208, 117-127.
14. W. Zhaolun; Y. Yuxiang; Q. Xuping; Z. Jianbo; C. Yaru; N. Linxi; *Environ. Chem. Lett.*, **2005**, 3, 33-37.
15. W.-T. Tsai; C.-W. Lai; K.-J. Hsien; *J. Colloid Interf. Sci.*, **2006**, 297, 749-754.
16. Z. Al-Qodah; W.K. Lafi; Z. Al-Anber; M. Al-Shannag; A. Harahsheh; *Desalination*, **2007**, 217, 212-224.
17. E.A. Mohamed; A.Q. Selim; A.M. Zayed; S. Komarneni; M. Mobarak; M.K. Seliem; *J. Colloid Interf. Sci.*, **2019**, 534, 408-419.
18. J. Zhang Jian; Q. Ping; M. Niu; H. Shi; N. Li; *Appl. Clay Sci*, **2013**, 83-84, 12-16.
19. S.D.J. Inglethorpe; *Industrial minerals, Laboratory manual: Diatomite*, BGS Technical Report WG/92/39, **1993**.
20. N. Inchaurredo; J. Font; C.P. Ramos; P. Haure; *Appl. Catal. B*, **2016**, 181, 481-494.
21. H. Liang; S. Zhou; Y. Chen; F. Zhou; C. Yan; *J. Taiwan Inst. Chem. Eng.*, **2015**, 49, 105-112.
22. W. Tang; K. Qiu; P. Zhang; X. Yuan; *Appl. Surf. Sci.*, **2016**, 362, 545-550.
23. T. Qian; J. Li; X. Min; Y. Deng; W. Guan; L. Ning; *Energ. Convers. Manage.*, **2015**, 98, 34-45.
24. S.S. Ibrahim; A.Q. Selim; *Physicochem. Probl. Mi.*, **2012**, 48(2), 413-424.
25. G.Zhang; D. Cai; M. Wang; C. Zhang; J. Zhang; Z. Wu; *Micropor. Mesopor. Mat.*, **2013**, 165, 106-112.
26. H. Aguedal; A. Iddou; A. Aziz; A. Shishkin; J. Ločs; T. Juhna; *Int. J. Environ. Sci. Technol.*, **2019**, 16, 113-124.
27. S. Lagergren; *Kungl. Svenska Vetenskapsakad. Handl.*, **1898**, 24, 1-39.

28. Y.S. Ho; G. McKay; *Process Saf. Environ.*, **1998**, 76, 332-340.
29. W.J. Weber; J.C. Morris; *J. Sanit. Eng. Div. ASCE*, **1963**, 89, 31-60.
30. G.E. Boyd; A.W. Adamson; L.S. Myers Jr.; *J. Am. Chem. Soc.*, **1947**, 69, 2836-2848.
31. V. Srihari; A. Das; *Desalination*, **2008**, 225, 220-234.
32. X.-Y. Pang; F. Gong; *E-J. Chem.*, **2008**, 5, 802-809.
33. L.C. Cotet; A. Măicăneanu; C.I. Fort; V. Danciu; *Sep. Sci. Technol.*, **2013**, 48, 2649-2658.
34. N. Caliskan; A.R. Kul; S. Alkan; E.G. Sogut; I. Alacabey, *J. Hazard. Mater.*, **2011**, 193, 27-.
35. D.M. Gligor; A. Măicăneanu, Applications of Clay Minerals in Electrochemistry and Wastewater Treatment, in *Clay: Types, Properties and Uses*, J. P. Humphrey, D.E. Boyd) Eds.; Nova Science Publishers Inc., New York, **2011**, Chapter 1, pp. 1-62.

REMEDICATION OF LEAD (II) AND MALACHITE GREEN FROM AQUEOUS SOLUTION USING PALM OIL FRUIT FIBRE

SHIN-LEEI OOI^a and SIEW-TENG ONG^{a,b*}

ABSTRACT. Oil palm fruit fibre (OPFF) was investigated for its potential and probability to remove heavy metal ion and dye from the aqueous solutions. Different operational parameters were studied under batch experiment. The effective pH to attain maximum adsorption of MG and Pb(II) by OPFF was around pH 4 to 5. The adsorption process was rapid at the beginning and slowly achieved equilibrium within 180 minutes and 120 minutes for MG and Pb(II), respectively. From the experimental result, the pseudo-second-order kinetic model provided better correlation compared to pseudo-first-order kinetic model with $R^2 > 0.999$. Various isotherm equations, such as Langmuir, Freundlich, and BET isotherm models were used to analyze the adsorption isotherm result. The experimental data fitted well into Langmuir and BET isotherm models with $R^2 = 0.996$ and 0.984 , respectively. The maximum adsorption capacity of OPFF from Langmuir equation was 41.67 and 10.10 mg/g for MG and Pb(II), respectively. Besides, characterization study of OPFF which include point of zero charge (pH_{zpc}), chemical modification on the functional group and surface morphology was also performed in this study.

Keywords: *Pb(II), Malachite Green, Oil palm fibre, Adsorption, Batch study, Characterization study*

INTRODUCTION

Industrial wastewater inevitably contains pollutants and if it is being discharged to the environment without a proper treatment, this can cause a serious environmental issue. The removal of dyes from industrial wastewater is one of the challenging environmental problems faced by many countries.

^a *Department of Chemical Science, Faculty of Science, Universiti Tunku Abdul Rahman, Jalan Universiti, Bandar Barat, 31900 Kampar, Perak, Malaysia.*

^b *Centre for Biodiversity Research, Universiti Tunku Abdul Rahman, Jalan Universiti, Bandar Barat, 31900 Kampar, Perak, Malaysia.*

* *Corresponding author: ongst@utar.edu.my; ongst_utar@yahoo.com*

At present, there are many industries such as textile, dye manufacturing, paints, paper, carpet, leather, food, and tannery which using various types of dyes to colour their products. The worldwide annual production of dyes is about 7×10^5 tons and these dyes are discharged into waste streams by the aforementioned industries that cause negative impact to the environment and human health [1,2]. Besides from being highly coloured, studies have also shown that some dyes, dye precursors and their biotransformation products could be health threatening as they are toxic, mutagenic and carcinogenic in nature [3,4]. For instance, cationic dyes, which are widely used in colouring acrylic fibre are considered to be more toxic than other classes of dyes [5,6]. Malachite Green (MG), which is a type of cationic dye, has been selected as the adsorbate in this study because from the available scientific evidence, MG poses a serious health concerning issue. MG is known to be a multi-organ toxin and its potential carcinogenic, teratogenic, mutagenic and genotoxic properties has been well documented [4, 7-11].

Apart from coloured pollutant, heavy metal contamination is also a worrying issue in the control of environmental pollution. There are various routes in which heavy metals may enter the human body which include food, water, air, or absorption through the skin. The accumulation of heavy metals in the soft tissue can cause severe and adverse health problem to the nervous system, liver, and bones. In fact, there are several tragedies that occurred due to heavy metal contamination, which include Minamata disease (due to methyl mercury contamination) and another example is the endemic of "Itai-Itai" disease due to cadmium toxicity in Jitsu river of Japan.

Lead, Pb (II) is a heavy metal that is commonly found in industrial effluents due to their widespread usage in various industries such as lead-acid batteries manufacturing, paints, ceramics, soldering, and electroplating. However, Pb(II) is a highly toxic heavy metal which will cause infertility, nervous system damage, anaemia, muscle and joint pains, diminishing IQ, kidney problem and high blood pressure to human [12]. The potential health hazard problems associated with lead has made it to be categorized as one of the top 20 hazardous substances under U.S. Environmental Protection Agency. According to Malaysia Environmental Quality (Sewage and Industrial Effluent) Regulation 1979, the lead content in effluent to be discharged is required to be not more than 0.1 mg/L [13].

Therefore, it is of utmost important to remove or at least reduce Malachite Green (MG) and Pb(II) content to the permitted level before discharging them into the open stream. As Malaysia is one of the world's largest producers and exporters of crude palm oil (CPO), there is about 3.0 million tons of oil palm empty fruit bunch (EFB) fibres being generated every year. Although these solid wastes have been used as solid fuel in boilers of

processing mills, organic fertilizer, and reinforcing fibres for composite making [14], the utilization is still not fully maximized. Therefore, in this research, the feasibility of using oil palm fruit fibre as an adsorbent for heavy metals and dyes removal from aqueous solution was explored. It is hoped that this can reduce the amount of these solid wastes and also protect the environment from being polluted.

RESULTS AND DISCUSSION

FTIR Analysis. Figure 1 shows the infrared spectra of OPFF before and after adsorption of Pb(II). Table 1 summarizes the IR analysis for OPFF and the types of vibrations involved. It was found that the absorption band in this study was quite similar to the reported values from the literature.

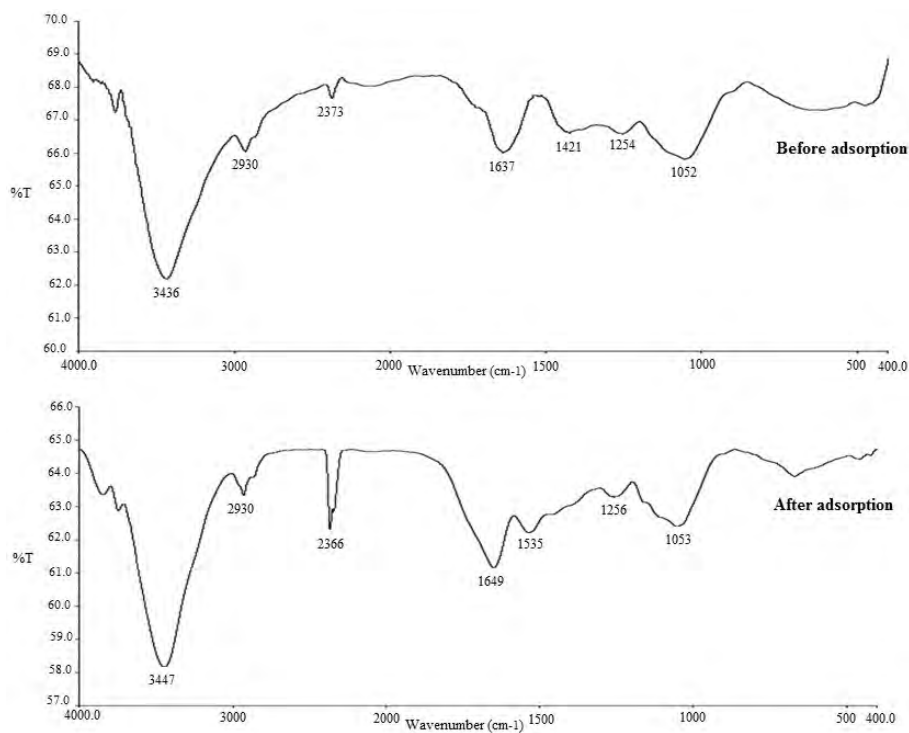


Figure 1. Infrared spectrum of OPFF before and after adsorption of Pb(II)

The absorption of the OH group was found in the region of 3600-3200 cm^{-1} . The peak around 2900 cm^{-1} is due to C-H stretching whereas the one around 1050 cm^{-1} indicated the presence of lignin structure in OPFF. It was noticed that FTIR spectra of the OPFF (before and after adsorption), regardless of MG or Pb(II) are very similar to each other. This could be due to the limitations in the sensitivity of the instrument. Besides, as it has been postulated that the removal process mainly involved adsorption, which is a surface chemistry process, therefore, it is generally acceptable that the FTIR spectra before and after adsorption would not show much difference [15]. In addition, the FTIR spectra analysis of OPFF after Pb(II) adsorption (Table 2) and E-OPFF are also very similar to that of the unesterified material.

Table 1. FTIR spectral of OPFF before and after adsorption of MG

Wave number (cm^{-1})		Type of vibration
Before adsorption	After MG adsorption	
3764	3753	-OH stretching vibrations
3436	3436	-OH stretching vibrations (aromatic and carboxylic acid)
2930	2930	-CH stretching(methylene/methyl/methoxy)
2373	2370	-OH stretch (carboxylic group)
1637	1734	C=O stretching
1421	1428	-CH stretching(methylene/methyl/methoxy)
1254	1259	C-O from phenolic groups
1052	1053	C-O from phenolic groups

Table 2. FTIR spectral of OPFF before and after adsorption of Pb(II)

Wave number (cm^{-1})		Type of vibration
Before adsorption	After adsorption Pb(II)	
3436	3447	-OH stretching vibrations (aromatic and carboxylic acid)
2930	2930	-CH stretching(methylene/methyl/methoxy)
2373	2366-2342	-OH stretch (carboxylic group)
1637	1649	C=O stretching
1421	1535	-CH stretching(methylene/methyl/methoxy)
1254	1256	C-O from phenolic groups
1052	1053	C-O from phenolic groups

Scanning Electron Microscopy (SEM). Scanning electron microscope was used to study the surface morphology of OPFF. Figures 2a and 2b show the SEM images of original OPFF and OPFF after adsorption. From the SEM micrographs, the present of the lignin structure was evident and this was still maintained after the adsorption process. It was also observed that OPFF belongs to a non-porous material, due to the absence of pores and cavities.

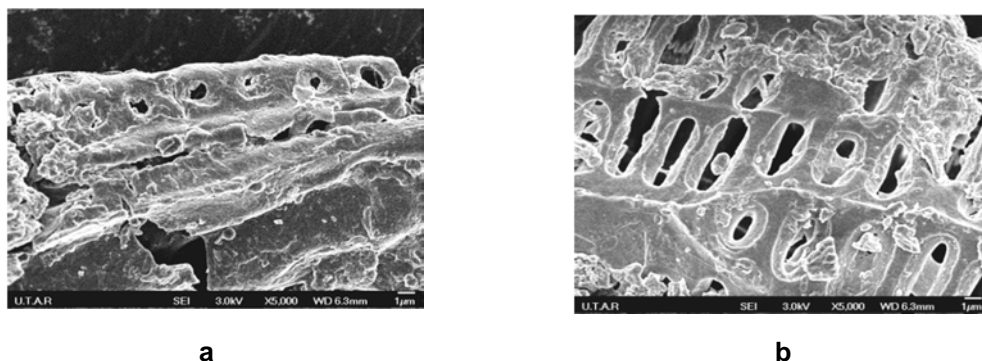


Figure 2. SEM micrograph of OPFF (a) before adsorption (b) after adsorption

Determination of pH point of zero charge (pH_{pzc}). The pH_{zpc} of the oil palm fruit fibre was measured by using the mass titration method [16]. The point of zero charge is the pH value where the net total particle charge is zero [17]. This parameter is very important to describe the variable-charge surface which is either positive or negative of adsorbent. Based on the result, the pH_{pzc} of OPFF was determined to be around pH 5. When the pH of the solution is above pH_{pzc} , the surface charge of the OPFF will become negative. Meanwhile, the surface charge of OPFF will become positive when the pH of the solution is below pH_{pzc} .

Effect of pH. Figure 3 shows the percentage uptake of MG and Pb(II) versus pH. The percentage uptake was the lowest at pH 2. As the pH was increased to pH 3, the percentage uptake of MG increased drastically to 99.02%. Thereafter, the adsorption uptake remains nearly constant in the pH range of 3-8. As for Pb(II) uptake, the effect of pH was studied in the range of 2-5 because Pb(II) form precipitate at pH above 5. Similar to the trend observed in MG uptake, the lowest uptake of Pb(II) was also recorded at pH 2. Thereafter, it increased sharply to 94.67% at pH 3. The maximum Pb(II) uptake is 97.11% and obtained at pH 5. Although the pH_{pzc} of OPFF was around pH 5, an appreciable amount of adsorbates can be removed below pH_{pzc} and this could be attributed by the simultaneous occurrence of different kinds of interactions such as entrapment, ion-exchange, hydrophobic attraction and physical adsorption [6]. Similar adsorption pattern has been reported in the uptake of cadmium ions by various fruit peel wastes [18].

It is suggested that at low pH, the carboxyl and hydroxyl groups on the surface of OPFF were predominantly protonated, thus inhibiting the uptake of MG and Pb(II). Besides, hydrogen ion, H^+ will also compete with MG and Pb(II) for the adsorption sites. The adsorption of MG and Pb(II) are not favourable in acidic medium because of the electrostatic repulsion. As the pH increased, the adsorption became favourable due to the deprotonation of hydroxyl ($Ar-O^-$) and carboxyl group ($-COO^-$) on the surface of OPFF. This will increase the electrostatic attraction between negative surface charge of OPFF and the cationic MG and Pb(II). The % uptake of MG and Pb(II) by using OPFF shows that it is highly dependent on solution pH. Because the maximum adsorption of the MG and Pb(II) occurs around pH 4-5, therefore, the following parameters were carried out at pH 4 for both MG and Pb(II).

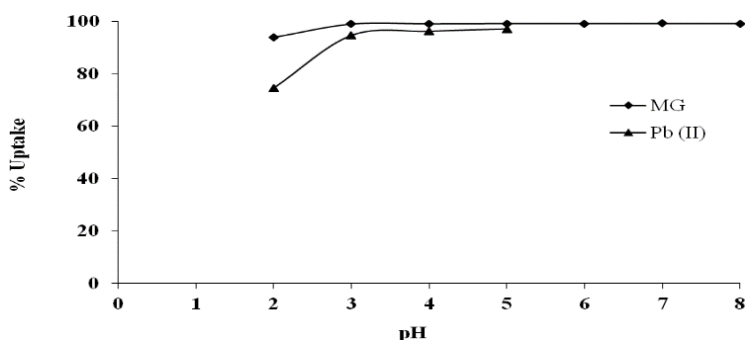


Figure 3. Effect of pH on the uptake of MG and Pb(II) by OPFF

The carboxyl groups in OPFF were esterified using acidic methanol method [19] to verify the importance role of carboxyl groups in the adsorption process of MG and Pb(II). The results on the percentage uptake of MG and Pb(II) showed that native OPFF has higher percentage uptake as compared to e-OPFF. This is because this type of modification will render the carboxyl groups unavailable for the binding and result in a reduction in the adsorption site for MG and Pb(II). The percentage uptake of Pb(II) and MG by using the native OPFF are 95.98 % and 99.10 %, respectively, whereas the uptake of Pb(II) and MG by using esterified OPFF are only 43.98 % and 95.62 %, respectively.

Effect of initial concentrations and contact time. The main purpose to study the effect of initial concentrations and contact time is to determine the equilibrium time for maximum adsorption. Figures 4 and 5 show the effect of initial concentrations and contact time on the uptake of MG and Pb(II), respectively by using OPFF. Different concentrations were used for MG and Pb(II) due to the different requirement set by local regulation.

Both results indicated that the percentage uptake of MG and Pb(II) decreased gradually with increasing concentrations. At the first 30 minutes, the uptake rate increased rapidly and thereafter the dye and metal uptake rate become slower and finally reached equilibrium at 120 minutes for both adsorbates.

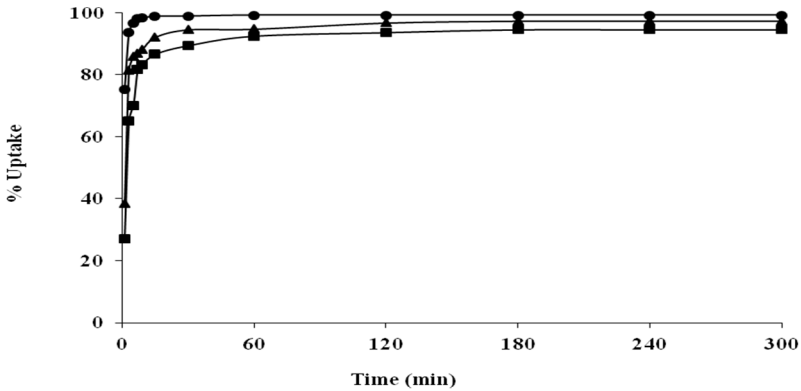


Figure 4. Effect of initial concentrations and contact time on the adsorption of MG by OPFF. ●, ▲, ■ – 100, 150 and 200 mg/L of MG

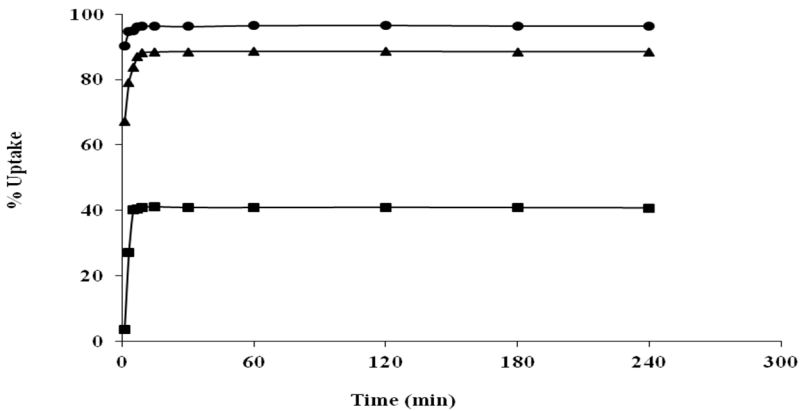


Figure 5. Effect of initial concentrations and contact time on the adsorption of Pb (II) by OPFF. ●, ▲, ■ – 20, 50 and 80 mg/L of Pb(II)

The fast uptake for initial stage is associated with the huge number of vacant sites on the OPFF at the beginning. After the adsorption takes place, the uptake rate becomes slower and required longer time to achieve equilibrium because the active site of OPFF was saturated with adsorbates.

The results showed that the time needed to achieve equilibrium was independent of the initial dye and heavy metal concentrations.

Kinetic studies. The experimental data were examined using different equations, pseudo-first-order [20] and pseudo-second-order kinetics [21] in order to identify which model will be more suitable to describe the system under study. Besides, this can also be used to explain the rate-controlling steps in the adsorption process.

The linear equation of pseudo-first-order (Eq. 1) [20] and pseudo-second-order (Eq. 2) [21] can be expressed as follows:

$$\log (q_e - q_t) = \log q_e - \frac{k_1}{2.303} t \quad (1)$$

and

$$\frac{t}{q_t} = \frac{1}{h} + \frac{1}{q_e} t \quad (2)$$

where q_e = the amount of MG/ Pb(II) adsorbed at equilibrium (mg/g), q_t = the amount of MG/ Pb(II) adsorbed at time t (mg/g), k_1 = the rate constant of pseudo-first-order adsorption (1/min), h ($k_2 q_e^2$) = the initial adsorption rate (mg/g min) and k_2 = the rate constant of pseudo-second-order kinetics (g/mg min).

Based on the results obtained, the theoretical q_e values generated by pseudo-first-order kinetic model equation gave unreasonable values compared to those determined experimentally (Table 3). Besides, the R^2 of the pseudo-first-order was relatively low as compared to pseudo-second-order model for MG and Pb(II). This result indicates that the adsorption process of both MG and Pb(II) onto OPFF is better explained via pseudo-second-order model which is based on the assumption that the rate-limiting step may be due to chemisorptions, which involve valency force through sharing and exchanging of electron between adsorbent and adsorbate [21]. The applicability of pseudo-second-order model in the adsorption of dyes or heavy metal ions have also been reported in other works involving H_2SO_4 activated *Salvadora persica* [2], alginate-coated perlite beads [4], AC prepared from *Amygdalus scoparia* [8], corn cob [15], rambutan peel [22], pigeon pea hulls [23] and chitin hydrogels [24].

Table 3. Pseudo-first-order and pseudo-second-order kinetic model parameters for different initial MG and Pb(II) concentrations

Initial MG concentration (mg/L)	$q_{e, \text{exp}}$ (mg/g)	Pseudo-first-order kinetic model			Pseudo-second-order kinetic model		
		$q_{e, \text{cal}}$ (mg/g)	k_1 (1/min)	R^2	$q_{e, \text{cal}}$ (mg/g)	k_2 (g/mg min)	R^2
100	19.916	0.5058	0.05067	0.677	20.000	0.41670	1
150	30.708	4.6666	0.02764	0.768	31.250	0.03103	1
200	39.740	9.1201	0.02994	0.795	40.000	0.01524	1
Initial Pb (II) concentration (mg/L)							
20	4.369	0.4875	0.4859	0.950	4.386	7.4260	1
50	8.935	2.6242	0.3823	0.943	9.009	0.7247	1
80	6.552	15.6675	0.8360	0.937	6.623	0.0857	0.998

In view of the suitability of the adsorption process to be described by pseudo-second-order kinetic model, the values of q_e , k_2 , and h against C_o in the corresponding linear plots of the pseudo- second-order equation were regressed to obtain expressions for these values in terms of the initial dye concentration. These parameters could be expressed as a function of C_o for MG and Pb(II) as follows [25]:

$$q_e = \frac{C_o}{A_q C_o + B_q} \quad (3)$$

$$k_2 = \frac{C_o}{A_k C_o + B_k} \quad (4)$$

$$h = \frac{C_o}{A_h C_o + B_h} \quad (5)$$

where A_q , B_q , A_k , B_k , A_h and B_h are constant for the respective equations and obtained through regression from the linear plots. The generalized predictive models for MG and Pb(II) adsorbed at any contact time and initial dye concentrations within the given range with relationship of q_t , C_o and t can be expressed as follow:

$$q_t = \frac{C_o t}{A_h C_o + B_h + (A_q C_o + B_q)t} \quad (6)$$

By substituting the calculated constant values, the theoretical model for MG-OPFF system could be expressed by the following equations:

$$q_t = \frac{C_o t}{0.074C_o - 6.852 + (0.001C_o + 4.833) t} \quad (7)$$

whereas for Pb(II)-OPFF system, it can be represented by Eq. 9.

$$q_t = \frac{C_o t}{0.255C_o - 6.225 + (0.086C_o + 3.023) t} \quad (8)$$

Figures 6 and 7 show the comparison of the predicted theoretical values and experimental data for MG and Pb(II) adsorption, respectively by OPFF. The result indicated that the pseudo-second-order provided a good prediction for the amounts of MG and Pb(II) adsorbed onto OPFF, but not at higher concentration. The deviation observed at higher concentration could be related with the poor R^2 of the linear graph k_2 , h , and q_e against C_o .

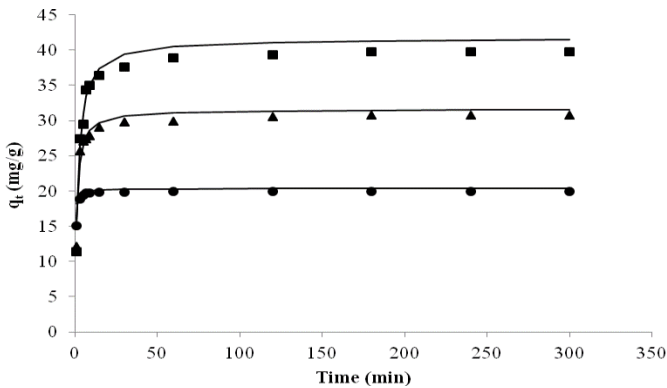


Figure 6. Comparison plots between the measured and pseudo second-order modeled time profiles for MG adsorption by OPFF. ●, ▲, ■ – 100, 150 and 200 mg/L of MG; symbol = experimental data, line = pseudo second order model.

Adsorption Isotherm. The adsorption isotherm is useful in providing the information about the adsorption properties, equilibrium data, and interaction between the adsorbate and adsorbent with a homogenous or heterogeneous surface. In order to obtain the equilibrium relationships between the adsorbent and adsorbate, Langmuir, Freundlich, and Brunauer-Emmett-Teller (BET) isotherm models [26-28] were being employed to determine and analyze the adsorption behaviour of MG and Pb(II) on OPFF.

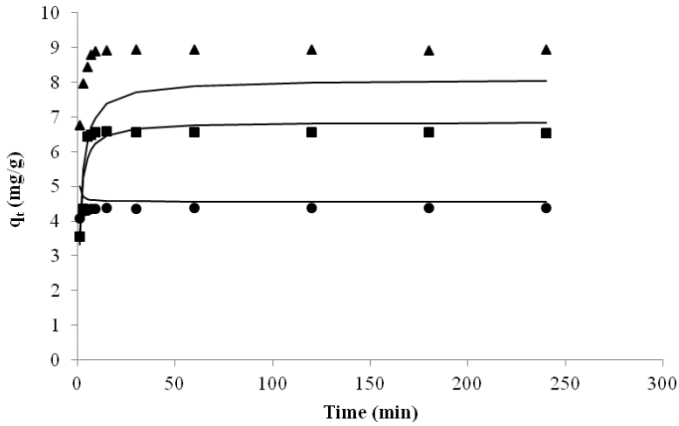


Figure 7. Comparison plots between the measured and pseudo second-order modeled time profiles for Pb(II) adsorption by OPFF. ●, ▲, ■ – 20, 50 and 80 mg/L of Pb(II); symbol = experimental data, line = pseudo second order model.

The Langmuir isotherm is based on the assumption that adsorbate is forming monolayer coverage on the adsorbent surface and the adsorbent surface consists of homogenous sites with constant adsorption energy. When the dye or heavy metal ions fill up the vacant site of adsorbent, the adsorption process will no longer be favourable. Besides that, there are no interactions between the neighbouring adsorbed molecules; each site can adsorb only one molecule and no phase transitions. The linear form of the Langmuir isotherm can be expressed by the following equation [26]:

$$\frac{C_e}{q_e} = \frac{1}{q_{\max}} C_e + \frac{1}{K_L q_{\max}} \quad (9)$$

where C_e = equilibrium concentration of the adsorbate (mg/l), q_e = amount of adsorbate adsorbed at equilibrium (mg/g), q_{\max} = maximum adsorption capacity (mg/g), K_L = constant related to the energy of the adsorbent (l/mg).

The coefficient of determination, R^2 is 0.996 and 0.984, respectively for the linear plot of MG and Pb(II) adsorbed on OPFF. This result indicates the applicability of Langmuir isotherm to the adsorption of MG and Pb(II) by OPFF. Therefore, it is assumed that a monolayer coverage of adsorbate occurs over the adsorbent's surface with constant adsorption energy. The constant values K_L and q_e could be obtained from the intercept and the slope of the plots, respectively. The value maximum adsorption capacity, q_e is 41.67 mg/g and the value of K_L is 0.73. The Langmuir isotherm values for the adsorption of MG and Pb(II) were shown in Table 4.

As for Freundlich isotherm, it involved physicochemical adsorption on the heterogeneous surface of the adsorbent. This isotherm can be used to describe the non-ideal adsorption that is more flexible and do not indicate an adsorption limit. The Freundlich isotherm can be expressed by the following equation [27]:

$$q_e = K_f C_e^{1/n} \quad (10)$$

The equation above can be linearized by taking logarithm of both sides. The linear equation of Freundlich isotherm is shown as follow:

$$\log q_e = \log K_f + \frac{1}{n} \log C_e \quad (11)$$

where K_f = Freundlich constant for adsorption capacity, n = Freundlich constant for intensity, q_e = Amount of dye and metal adsorbed at equilibrium (mg/g), C_e = Equilibrium concentration of the dye and metal (mg/L)

A linear plot of $\log q_e$ versus $\log C_e$ was obtained and the values of K_f and n can be determined from the intercept and slope of the linear plot, respectively. The Freundlich isotherm values for the adsorption of MG and Pb(II) were presented in Table 4. Based on the R^2 values, Langmuir isotherm was found to be a more suitable model to describe the adsorption of both MG and Pb(II) on OPFF compared to Freundlich isotherm.

Table 4. Langmuir, Freundlich, and BET constants for the adsorption of MG and Pb(II) by OPFF

Adsorbate	Langmuir			Freundlich			BET		
	q_{\max} (mg/g)	K_L (L/mg)	R^2	K_f	n	R^2	K_B	q_{\max} (mg/g)	R^2
MG	41.67	0.73	0.996	17.14	2.29	0.986	13320	41.66	0.996
Pb(II)	10.10	1.06	0.984	4.59	2.22	0.763	563782	10.10	0.984

BET isotherm is extended based on the Langmuir isotherm which assumes that the adsorbent surface is composed of fixed individual sites, and molecules can be adsorbed to a thickness of more than one layer, on the surface of the adsorbent. The linear form of BET equation can be written as follows [28]:

$$\frac{C_e}{(C_s - C_e)q} = \frac{1}{K_B q_{\max}} + \left(\frac{K_B - 1}{K_B q_{\max}} \right) \left(\frac{C_e}{C_s} \right) \quad (12)$$

where C_s = Saturation concentration of solute (mg/L), K_B = Constant describing the energy of interactions between the solute and the adsorbent surface, q_{\max} = Amount of solute in forming a complete monolayer (mg/g)

The BET isotherm values for the adsorption of MG and Pb(II) were presented in Table 4 and from the result, it is evident that the equilibrium adsorption also fitted well into the BET isotherm. The applicability of both Langmuir and BET isotherm suggest that the adsorbate forming a monolayer on the surface of adsorbent and the adsorption of the adsorbate was extended beyond monolayer coverage.

CONCLUSIONS

This study identified OPFF, which is an agricultural waste could be used as the potential low-cost adsorbent to remove the MG and Pb(II) from aqueous solution. According to the result obtained, the pH_{pzc} of OPFF is around pH 5. The percentage uptake of MG and Pb (II) decreased when using the esterified OPFF, suggesting the involvement of COOH group in the adsorption process. The effective pH to attain maximum adsorption of MG and Pb(II) were around pH 4 to 5. A rapid uptake was observed at the beginning of the process and the contact time needed for the attainment of equilibrium was 3 hours for MG and 2 hours for the Pb(II). It was found that the pseudo-second-order kinetic model provides a better R^2 as compared pseudo-first-order kinetic model, which suggested the chemisorption of MG and Pb(II) onto OPFF. Finally, Langmuir and BET isotherm appeared to be the most appropriate models to illustrate the adsorption process, with the high R^2 which are 0.996 and 0.984 for MG and Pb(II), respectively, for both isotherm. The maximum adsorption capacities of OPFF obtained from Langmuir isotherm are 41.67 mg/g and 10.10 mg/g for MG and Pb(II), respectively.

EXPERIMENTAL SECTION

Preparation of MG and Pb(II) stock solution

Synthetic dye solution of MG (Cl = 42,000, MW = 929.02 g/mol, chemical formula = $\text{C}_{46}\text{H}_{50}\text{N}_4 \cdot 3\text{C}_2\text{H}_2\text{O}_4$, $\lambda_{\text{max}} = 618 \text{ nm}$, Sigma-Aldrich Pte. Ltd) was used as adsorbate in this study. As for Pb(II), the synthetic heavy metal solution was prepared from A.R. grade $\text{Pb}(\text{NO}_3)_2$. All the chemicals were used as received without any further purification. A 1000 mg/L of stock solution was prepared for both adsorbates and subsequently diluted when necessary.

Preparation of adsorbent

The oil palm fruit fibre (OPFF) was used as adsorbent in this study and it was collected from a Batu Kawan palm oil plantation in Penang, Malaysia. It was washed several times with tap water and rinsed with distilled

water to remove the dust and dirt on the surface of fibre. Then, it was dried under the sunlight for a few days. The dried OPFF was ground by using the mortar and pestle and sieved to obtain the particle sizes ranging from 0.5 – 1 mm and stored in dry plastic container for further use.

Characterisation of adsorbent

Fourier Transform Infrared Spectrophotometer (FTIR)

The functional groups present on OPFF were determined using Perkin-Elmer System 2000 FT-IR Spectrometer. The OPFF sample disk was prepared by mixing the dried adsorbent with KBr. The spectra of oil palm fruit fibre before and after undergoing adsorption of MG and Pb(II) were recorded.

Scanning Electron Microscopy (SEM)

Scanning electron microscope (SEM) was used to examine the surface morphology of OPFF before and after adsorption process. The surface morphology was studied using FESEM JSM 6701F (JEOL). Before the sample was analyzed, the prepared pellet was coated with a thin layer of gold to prevent the occurrence of charging effect.

Batch experiments

Batch experiments were carried out at room temperature ($25 \pm 2^\circ\text{C}$). The batch adsorption experiments were performed in duplicate and the results given are the means with a relative standard deviation (RSD) of less than 5 %. Adsorption experiments were carried out by agitating 0.10 g of adsorbent in 20 mL of MG or Pb(II) solutions in a centrifuge tube at 150 rpm on an orbital shaker for 4 hours to allow the attainment of equilibrium. After that, the adsorbent-adsorbate mixture was centrifuged at 3000 rpm for 2 minutes for phase separation. For MG, the supernatant was used to analyze for its dye concentration by using the Perkin Elmer UV-Vis spectrophotometer. All the measurement was made at the wavelength corresponding to its maximum absorption, $\lambda_{max} = 618 \text{ nm}$. As for Pb(II), the final concentrations of the metal ions were analyzed by using the Perkin Elmer Atomic Absorption Spectrophotometer (AAS).

The percentage uptake and the amount of MG and Pb(II) adsorbed (q) was determined by using the following equations:

$$\% \text{ Uptake} = \frac{C_o - C_e}{C_o} \times 100 \% \quad (13)$$

$$q = C_o - C_e \times \frac{V}{M} \quad (14)$$

where C_o and C_i are the initial and equilibrium concentration of MG or Pb(II), respectively, V = the volume of the solution (L) and W = the mass of the adsorbent (g).

For the effect of pH, a series of 50 mg/L of MG solutions were prepared. The initial pH of the MG solutions was adjusted to the range of pH 2 -10 by adding a few drops of HCl or NaOH of different concentrations (0.1 M – 0.5 M) prior to the experiment. The step above was repeated by using the Pb(II) solutions with the pH range from 2 to 5 and the concentration is 10 mg/L. In order to study the role of carboxyl groups in the adsorption of MG and Pb(II), OPFF was subjected to esterification. The esterification of carboxyl groups on OPFF was carried out via acidic methanol method with slight modification [19].

The effect of initial concentrations and contact time experiments were studied by using MG and Pb(II) solutions with various concentrations. The samples were withdrawn and analyzed for their MG and Pb(II) concentrations at predetermined intervals (1, 3, 5, 7, 9, 15, 30, 60, 120, 180, 240 and 300 minutes). Adsorption isotherms were obtained by varying the Pb(II) concentration from 10 to 50 mg/L whereas for the MG is from 50 to 130 mg/L.

ACKNOWLEDGEMENTS

The financial support and research facilities by Universiti Tunku Abdul Rahman are acknowledged.

REFERENCES

1. J.W. Lee, S.P. Choi, R. Thiruvengkatachari, W.G. Shim, H. Moon, *Dyes and Pigments*, **2006**, 69, 196.
2. S.N. Jain, Z. Shaikh, V.S. Mane, S. Vishnoi, V.N. Mawal, O.R. Patel, P.S. Bhandari, M.S. Gaikwad, *Microchem. J.*, **2019**, 148, 605.
3. W.H. Cheung, Y.S. Szeto, G. McKay, *Bioresource Technol.*, **2008**, 100, 1143.
4. Ş. Parlayici, *J. Anal. Sci. Technol.*, **2019**, 10:4.
5. K. Hunger (ed.), "*Industrial Dyes: Chemistry, Properties, Applications*", Wiley-VCH, Weinheim, **2003**, chapter 2.
6. S.T. Ong, S.Y. Tan, E.C. Khoo, S.L. Lee, S.T. Ha, *Desalin. Water Treat. J.*, **2012**, 45, 161.

7. S. Bera, V.P. Sharma, S. Dutta, D. Dutta, *J. Taiwan Inst. Chem. Eng.*, **2016**, 67, 271.
8. R. Bagheri, M. Ghaedi, A. Asfaram, E.A. Dil, H. Javadian, *Polyhedron*, **2019**, 171, 464.
9. J. Yu, L. Zhang, B. Liu, *Int. J. Environ. Res. Public Health*, **2019**, 16, 3297.
10. S.T. Ong, S.T. Ong, Y.T. Hung, Y.P. Phung, *Desalin. Water Treat. J.*, **2015**, 55, 1359.
11. P.P. Kwan, S. Banerjee, M. Shariff, F. Md.Yusoff, *Food Control*, **2020**, 108, 106866.
12. P.S. Keng, S.L. Lee, S.T. Ha, Y.T. Hung, S.T. Ong, *Environ. Chem. Lett.*, **2014**, 12, 15.
13. S.T. Ong, Y.C. Foo, Y.T. Hung, *Res. J. Chem. Environ.*, **2013**, 17, 53.
14. M.S. Mohamad Amran, M. Dalia Khalid, E. A. Al-Maamary, *J. Adv. Sci. Eng. Res.*, **2011**, 1, 76.
15. H.Y. Gan, L.E. Leow, S.T. Ong, *Acta Chimica Slovenica*, **2017**, 64, 144.
16. J.S. Noh, J.A. Schwarz, *Great Britain*, **1990**, 28, 675.
17. F.I. Morais, A.L. Page, L.J. Lund, *Soil Sci. Soc. America J.*, **1976**, 40, 521.
18. W. Saikaew, P. Kaewsarn, *Songklanakarin J. Sci. Technology*, **2009**, 31, 547.
19. J.L. Gardea-Torresdey, *J. Hazard. Materials*, **1999**, B80, 175.
20. S. Lagergren, *Handlingar*, **1898**, 24, 1.
21. Y.S. Ho, G. McKay, *Process Biochemistry*, **1999**, 34, 451.
22. H.J. Lee, S.T. Ong, *Environ. Protect. Eng.*, **2017**, 43, 169.
23. D.K. Venkata Ramana, *Chem. Eng. J.*, **2012**, 197, 24.
24. H. Tang, W.J. Zhou, L. Zhang, *J. Hazard. Mat.*, **2012**, 209, 218.
25. Y.S. Ho, G. McKay, *Water Research*, **2000**, 34, 735.
26. I. Langmuir, *J. Am. Chem. Soc.*, **1916**, 38, 2221.
27. H.M.F. Freundlich, *J. Phys. Chem.*, **1906**, 57, 385.
28. S. Brunauer, P.H. Emmett, E. Teller, *J. Am. Chem. Soc.*, **1938**, 60, 309.

COMPUTATIONAL ASSESSMENT OF THE ADME-TOX PROFILES AND HARMFUL EFFECTS OF THE MOST COMMON USED PHTHALATES ON THE HUMAN HEALTH

DANA CRĂCIUN^a, DANIELA DASCĂLU^{b*}, ADRIANA ISVORAN^b

ABSTRACT. In this study we consider 25 of the most commonly used phthalates and summarize the available data that support their effects on humans. For 15 of the 25 investigated phthalates (60%) there are no human hazard assessment data, neither from experimental nor from computational studies, which underlines the necessity of their risk assessment. Consequently, we have used various computational tools to predict their ADME-Tox profiles and assess their harmful effects on humans. The outcomes of our study reveal that the investigated phthalates have good bioavailability and skin permeability which are associated with toxicity, especially when they are inhaled. They are able to interact with important molecular targets in the human organism such as membrane receptors, cytochromes, kinases, phosphatases, transcription factors, or transporters. These interactions may conduct to predicted harmful effects of phthalates, such as toxicity and irritations of the respiratory and gastrointestinal tracts, skin and eye irritations, endocrine disruption potential, or non-genotoxic carcinogenicity. The investigated phthalates are not predicted to produce genotoxic carcinogenicity, mutagenicity and cardiotoxicity. Beside the investigated phthalates, the di(2-ethylhexyl) phthalate reflects the highest number of toxic effects, and the dodecyl phthalate and the diisotridecyl phthalate illustrate the smallest number of possible toxicological effects, namely skin irritation, non-genotoxic carcinogenicity and endocrine disruption potential.

Keywords: *phthalates, ADME-Tox, pharmacokinetics, toxicological effects.*

^a West University of Timisoara, Teacher Training Department, 4 V. Parvan, RO-300223, Timisoara, Romania

^b West University of Timisoara, Department of Biology-Chemistry and Advanced Environmental Research Laboratories, 16 Pestalozzi, RO-300115, Timisoara, Romania

* Corresponding author: daniela.dascalu@e-uvv.ro

INTRODUCTION

The use of plasticized products has considerably increased in the last decades, exceeding 300 million tons in 2010 [1]. Plastics are synthetic organic polymers of high molecular mass and in order to enhance their physical properties they are often mixed with various additives. Some of these additives, such as phthalates, proved to be of particular concern for the human health. Phthalates are alkyl aryl esters of 1,2-benzenedicarboxylic acid used in the manufacture of plastic as plasticizer agents, *i.e.* to make hard plastic softer and more flexible. They are also used as solvents in paint and are found in ordinary plastics, common household products, toys, personal care and cosmetics products, medical devices, pharmaceutical products, automobile upholstery and so on. Monitoring data indicated that the general population may be exposed to phthalates via inhalation of outdoor and indoor air and dust, ingestion of food and drinks, by using some pharmaceutical products and by dermal contact with products and/or clothes containing these compounds, and that it is almost impossible to avoid them [2]. Consequently, they can leach in blood and enter the blood circulation [3], with numerous studies confirming the presence of phthalate metabolites in human urine, breast milk and some serum samples. The daily intake of phthalate in humans was estimated at 1.7–52.1 µg/kg/day [4], children exposure being 2-to 4-fold higher than for adults [5, 6]. Occupational exposure to phthalates may also occur through inhalation and dermal contact at workplaces where they are manufactured or used.

There are numerous *in vitro* and *in vivo* studies published concerning the harmful effects of the common phthalates on animals and humans, with most *in vivo* data being obtained from animal subjects, usually rodents. There are significant differences between animals and humans and, consequently, it is difficult to predict the biological effects of phthalates on humans by using animal subjects [7]. This is the reason why, in this study, we have reviewed only available data that have been obtained on human subjects concerning the biological effects of 25 of the most commonly used phthalates shown in Figure 1.

These data have been extracted from the following sources: specific literature, National Institute for Occupational Safety and Health (NIOSH), Pocket Guide to Chemical Hazards [8], Occupational Safety and Health Administration (OSHA) [9], Toxicology Data Network/ Hazardous Substances Data Bank (TOXNET/HSDB) [10], PubChem [11] databases and BIBRA working groups results [12], respectively. We considered the information available in these databases on the 15th of February 2019.

The target organs of phthalates in humans are: eyes, skin, respiratory system, central and peripheral nervous systems, reproductive system, breast,

liver, and pancreas [8, 9, 11, 13]. The possible effects of phthalates on the human health were also reviewed by Hauser and Calafat (2005) [14], Asghari et al (2015) [15], Katsikantami et al (2016) [16] and Rowdhwal and Chen (2018) [17]. These studies suggest that some of the phthalates produce eyes, nose, and skin irritations conducting to allergies, rhinitis or asthmatic reactions, they are endocrine disrupting compounds producing reproductive and developmental toxicity, cancer, obesity and type 2 diabetes, the harmful effects being usually higher in children [16, 18].

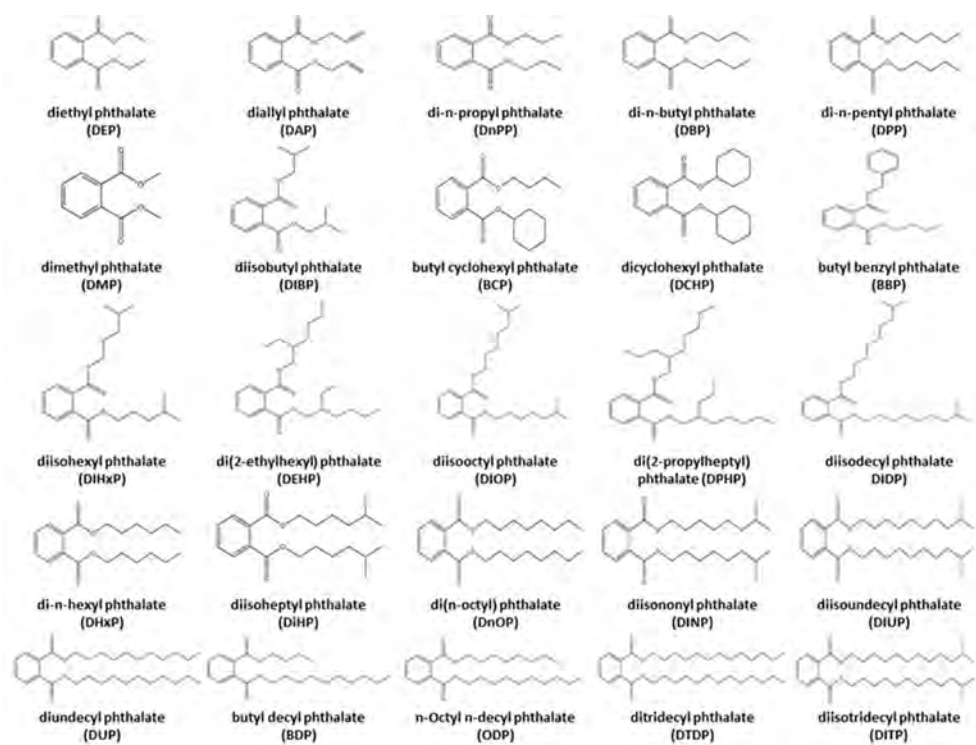


Figure 1. Phthalates considered in this study: formulas, names and abbreviations

Dimethyl phthalate (DMP) may cause irritation of the stomach, dizziness, and unconsciousness [10], the inhalation of its vapors irritates the nose and upper respiratory tract [8, 10, 12], and it produces skin and eye sensitization and irritation reactions [10, 12]. Diethyl phthalate (DEP) may produce abdominal pain and nausea [11], male reproductive effects [2, 19,

20, 21], changes in body weight and liver weight, respectively [2]. Prolonged inhalation of DEP causes irritation of the nose, throat and respiratory system, it may produce allergic reactions similar to asthma, and repeated exposure may cause nerve damage [10]. Lopez-Carrillo et al. (2010) suggested a possible connection between exposure to DEP through cosmetics and personal care products and an increased risk of breast cancer [22]. Di-n-butyl phthalate (DBP) may cause abdominal pain, nausea, diarrhea, vomiting, dizziness and headache [10, 12], may produce adverse respiratory outcomes [23], endometriosis, and has an anti-androgenic action [10]. DBP provokes skin and eye irritations, dermatitis [10], and prenatal exposure to DBP may cause adverse effects on the neurodevelopment and the behavior of young children [24]. Diisobutyl phthalate (DIBP) may cause male reproductive tract development problems [2]. Di-n-pentyl phthalate (DPP) may produce central nervous system depression and dermal irritations [10]. Butyl benzyl phthalate (BBP) is associated with rhinitis and eczema in children [25], may produce skin irritations [12] and endometriosis [10], and its presence is associated to airway inflammation in children [10]. Di(2-ethylhexyl) phthalate (DEHP) may cause irritation of eyes and mucous membranes, mild gastric disturbances and moderate diarrhea, it affects the reproductive system and the gestational age for newborns, and conducts to a decrease in the hemoglobin level [10]. Matsumoto et al. (2008) observed an association between higher DEHP serum levels and a shorter duration of pregnancy [26]. Literature also shows a positive correlation between phthalate metabolites in urine and symptoms of attention-deficit/hyperactivity disorder ADHD among school-age children [10]. Maternal exposure to DEHP may affect sex steroid hormones' status in the fetal and newborn stages [27, 28]. Prenatal and postnatal exposure was associated with the occurrence of asthma in children, particularly in boys [29], and has adverse effects on the neurodevelopment and the behavior of young children [23]. DEHP may produce changes to the male reproductive tract [2, 30, 31] and adversely affect the liver and thyroid [2, 10]. DEHP can cause endometriosis in reproductive-age women [32, 33], opacification of the lungs in pre-term infants [10], and is associated with allergic symptoms in children [34]. Di(n-octyl) phthalate (DnOP) may produce endometriosis, asthmatic reaction and skin irritation [10]. Diisodecyl phthalate (DIDP) may produce asthma and have an anti-androgenic action, and may affect the male reproductive system [10]. Two cases of allergic dermatitis as a result of occupational exposure to DIDP have been registered [10].

No human studies were available for 15 (60%) of the 25 phthalates under investigation. In humans, phthalates are metabolized to their monoesters that may also reflect different degrees of toxicity, but we underline that we have not considered these metabolites in our study.

Some studies suggest that the quantity and quality of the available data are not consistent [2, 35], and that there is no clear indication of the harmful effects of every phthalate in humans [2, 14, 36-38]. Also, as humans are continuously exposed to various combinations of chemical compounds, and phthalates are only one component of this mixture, some of the findings could not be exclusively associated to phthalates and it is difficult to obtain objective information concerning their exposure and epidemiologic data.

The concerns regarding the effects of phthalate exposure has led the U.S. Food and Drug Administration (FDA) and the European Medicines Agency (EMA) to establish guidelines on patient exposure to some phthalates if they are present in pharmaceutical products. Nevertheless, human contamination with phthalate may occur from a number of different other sources.

In our opinion, there are insufficient or missing data concerning the health risks of some phthalates, and further research on evaluating their effects in humans is needed. As it is not a simple task and humans are not volunteers for such experiments, computational analysis may be used to predict the biological effects of phthalates in humans. These predictions may be further investigated by experimental techniques. There is a great variety of computational tools available for the assessment of the biological effects of chemicals, most of them being designed for studying drugs, and the continuous development of such tools can be observed. A comprehensive overview can be found in the review of Raies and Bajic (2016) [39]. Furthermore, the specific literature shows promising results concerning the computational assessment of the toxicity of different chemicals other than drugs [39-47], reflecting the actuality of these research tools. Moreover, a recent study found that the existing models available for predicting various toxicity endpoints of drugs could be successfully used for industrial chemicals [48]. These tools also limit the amount of animal testing and the environmental effects, and reduce the costs of research and development activities. Consequently, in this study, we use various computational approaches for predicting the absorption, distribution, metabolism, excretion and toxicity (ADME-Tox) profiles, the pharmacokinetics, the molecular targets, the biological activity spectra and toxicological endpoints for the most commonly used phthalates (Figure 1). The predictions are further compared to each other and to the known effects of each considered phthalate in humans (when available). The correlations between computational results and *in vivo* experimental data are discussed.

RESULTS AND DISCUSSIONS

The use of the FAFDrugs4 tool to produce the ADME-Tox profiles of the phthalates considered in this study leads to the results presented in Table 1

with two filters corresponding respectively to the ingestion and inhalation as routes of exposure. Compounds not fulfilling the selected filters and/or presenting a high-risk structural alert do not reveal bioavailability and/or reflect high toxicity, and are considered not to be used by humans, their status being set to “rejected” in Table 1 [49].

The results obtained using the FAFDrugs4 computational tool reveal that all considered phthalates expose good oral bioavailability and at least reduced toxicity, regardless of the exposure modality. None of the phthalates pass the Pfizer 3/75 rule for toxicity and the high molecular weight phthalates also do not respect the GSK 4/400 rule.

Table 1. ADME-Tox profiles of phthalates: white boxes reveal that the rules are respected and grey boxes reflect that the rules are broken. Accepted compounds are those reflecting a good oral bioavailability and low toxicity when used by humans. Rejected compounds are those revealing medium to high toxicity.

Phthalate	route of exposure	Oral Bioavailability			Safety profile		status
		R05 violations	Veber Rule	Egan Rule	GSK Rule	Pfizer Rule	
DMP	ingestion	0	Good	good	good	warning	accepted
	inhalation	0	Good	good	good	warning	rejected
DEP	ingestion	0	Good	good	good	warning	accepted
	inhalation	0	Good	good	good	warning	rejected
DAP	ingestion	0	Good	good	good	warning	accepted
	inhalation	0	Good	good	good	warning	rejected
DnPP	ingestion	0	Good	good	good	bad	accepted
	inhalation	0	Good	good	good	bad	rejected
DBP	ingestion	0	Good	good	good	bad	accepted
	inhalation	0	Good	good	good	bad	rejected
DIBP	ingestion	0	Good	good	good	bad	accepted
	inhalation	0	Good	good	good	bad	rejected
BCP	ingestion	0	Good	good	good	bad	accepted
	inhalation	0	Good	good	good	bad	rejected
DPP	ingestion	1	Good	good	good	bad	rejected
	inhalation	1	Good	good	good	bad	rejected
BBP	ingestion	0	Good	good	good	bad	rejected
	inhalation	0	Good	good	good	bad	rejected
DCHP	ingestion	1	Good	good	good	bad	accepted
	inhalation	1	Good	good	good	bad	rejected
DHxP	ingestion	1	Good	good	good	bad	rejected
	inhalation	1	Good	good	good	bad	rejected

DIHxP	ingestion	1	Good	good	good	bad	accepted
	inhalation	1	Good	good	good	warning	rejected
DiHP	ingestion	1	Good	good	good	bad	rejected
	inhalation	1	Good	good	good	bad	rejected
BDP	ingestion	1	Good	good	good	bad	rejected
	inhalation	1	Good	good	good	bad	rejected
DEHP	ingestion	1	Good	good	good	bad	rejected
	inhalation	1	Good	good	good	bad	rejected
DnOP	ingestion	1	Good	good	good	bad	rejected
	inhalation	1	Good	good	good	bad	rejected
DIOP	ingestion	1	Good	good	good	bad	rejected
	inhalation	1	Good	good	good	bad	rejected
ODP	ingestion	1	Good	good	bad	bad	rejected
	inhalation	1	Good	good	bad	bad	rejected
DINP	ingestion	1	Good	good	bad	bad	rejected
	inhalation	1	Good	good	bad	bad	rejected
DPHP	ingestion	1	Good	good	bad	bad	rejected
	inhalation	1	Good	good	bad	bad	rejected
DIDP	ingestion	1	Good	good	bad	bad	rejected
	inhalation	1	Good	good	bad	bad	rejected
DIUP	ingestion	1	Good	good	bad	bad	rejected
	inhalation	1	Good	good	bad	bad	rejected
DUP	ingestion	1	Good	good	bad	bad	rejected
	inhalation	1	Good	good	bad	bad	rejected
DTDP	ingestion	2	Good	good	bad	bad	rejected
	inhalation	2	Good	good	bad	bad	rejected
DITP	ingestion	2	Good	good	bad	bad	rejected
	inhalation	2	Good	good	bad	bad	rejected

Most of the phthalates have the status set to rejected, especially when inhaled. The most frequent reasons for rejecting these phthalates are: too many rotatable bonds, high values of partition coefficient, too few hydrogen bonds donors and acceptors, and the presence of consecutive alkyl chains as high risk structural alerts. The good oral bioavailability is also predicted when using the admetSAR tool [50] (see Table 2 below). This tool has been also used to predict the pharmacokinetic profiles of the phthalates, presented in Table 2 together with predictions concerning the inhibition of the human CYPs that were obtained using the SwissADME computational tool [51].

The results presented in Table 2 reveal that, usually, low molecular weight phthalates expose high gastrointestinal absorption and blood-brain-barrier permeability. The predictions concerning the high gastrointestinal absorption and the blood-brain barrier permeability of the low molecular

weight phthalates are in accordance with the observed effects on humans for acute exposure: gastrointestinal disorders (DMP, DEP, DBP, DEHP) [10] and central nervous system disorders (DEP, DBP, DPP, DEHP) [10, 23]. These outcomes reveal that the investigated phthalates are not considered to be inhibitors of the renal organic cationic transporter. Some of the investigated phthalates are predicted to be able to inhibit the human CYPs, with smaller molecular weight phthalates usually affecting CYP1A2 and CYP2C9 and higher molecular weight phthalates affecting CYP3A4. These interactions are assessed further by molecular docking.

As dermal contact is one of the ways of exposure to phthalates, we have computed their skin permeation coefficients using the SwissADME tool [51] and predicted their skin sensitization potentials using the PredSkin tool [52, 53]. The values of the skin permeation coefficients are revealed in Figure 2. A larger negative value of logKp corresponds to a less skin permeant compound. It is known that logKp=-4.96 for diclofenac, an anti-inflammatory drug with a good skin permeability [51].

Table 2. SwissADME and admetSAR predictions concerning the pharmacokinetic profile of phthalates: BBB+ – permeation of the blood-brain barrier, GI+ – gastrointestinal absorption, P-gp – glycoprotein P, ROCT – renal organic cationic transporter, CYPs – human cytochromes.

Phthalate	Probability of				SwissADME predictions concerning the inhibition of the human CYPs				
	BBB	GI	P-gp substrate	ROCT non-inhibitor	CYP 1A2	CYP 2C19	CYP 2C9	CYP 2D6	CYP 3A4
DMP	0.958	0.960	-0.736	0.917	Yes	No	No	No	No
DEP	0.926	0.975	-0.691	0.889	Yes	No	No	No	No
DAP	-0.957	0.920	-0.724	0.837	Yes	Yes	No	No	No
DnPP	0.933	0.976	-0.618	0.868	Yes	Yes	No	No	No
DBP	0.939	0.979	-0.547	0.849	Yes	Yes	No	No	No
DIBP	0.930	0.974	-0.646	0.891	Yes	Yes	No	No	No
BCP	-0.902	0.994	0.544	0.730	Yes	Yes	Yes	No	No
DPP	0.955	0.972	0.522	0.847	Yes	No	Yes	No	No
BBP	0.934	0.986	-0.677	0.785	Yes	Yes	No	Yes	No
DCHP	-0.943	0.972	0.515	0.768	No	No	Yes	No	No
DHxP	0.945	0.977	0.500	0.826	Yes	No	Yes	No	No
DIHxP	0.945	0.943	0.558	0.832	No	No	No	No	No
DiHP	0.940	0.946	0.509	0.839	No	No	No	No	No
BDP	0.945	0.979	0.500	0.844	Yes	No	Yes	No	Yes
DEHP	0.938	0.977	0.500	0.826	No	No	Yes	No	Yes
DnOP	-0.945	0.954	-0.511	0.818	No	No	No	No	Yes
DIOP	0.927	0.954	-0.511	0.818	No	No	No	No	No
ODP	0.938	0.979	0.500	0.844	No	No	No	No	Yes

DINP	0.927	0.954	-0.511	0.818	No	No	No	No	Yes
DPHP	0.927	0.954	-0.511	0.818	No	No	Yes	No	Yes
DIDP	0.945	0.977	0.500	0.826	No	No	No	No	No
DIUP	0.945	0.977	0.500	0.826	No	No	No	Yes	No
DUP	0.945	0.977	0.500	0.826	No	No	No	Yes	No
DTDP	0.945	0.977	0.500	0.826	No	No	No	No	No
DITP	0.927	0.954	0.511	0.818	No	No	No	No	No

Figure 2 illustrates that most of the investigated phthalates, especially those with a higher molecular weight, are predicted as having good skin permeability. This outcome is in good correlation with the Pred-Skin predictions (Figure 3), revealing that numerous of the investigated phthalates have a skin sensitization potential a complex immunological disease having an essential impact on the quality of life and on the working abilities of people professionally exposed to them. Furthermore, these predictions correspond to known data reflecting the skin irritation potential of DEP, DAP, DBP, DPP, BBP, DNOP, DIDP [10].

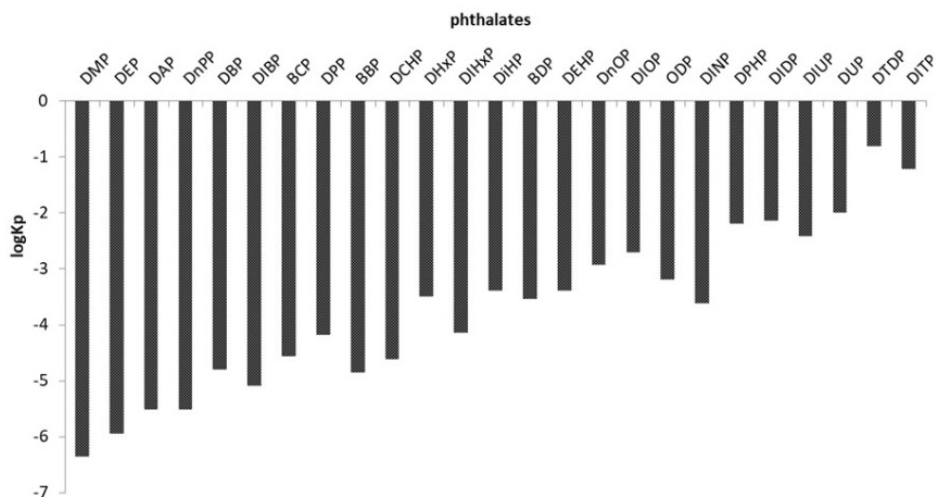


Figure 2. Skin permeation coefficients (logarithmic values) for the investigated phthalates.

The predictions concerning the possible endocrine disruption potential of investigated phthalates, computed using the ENDOCRINE DISRUPTOME tool [54], are shown in Table 3, and reflect that all investigated phthalates could have a low antagonistic effect on the androgen receptor. Anti-androgenic effects have been reported for DBP and DIDP in literature [10]. Other nuclear receptors affected by a large number of the studied phthalates are the glucocorticoid receptor (GR) and the thyroid receptors α (TR α) and β

(TR β). It is not surprising that the androgen and glucocorticoid receptors are quite similarly affected by the studied phthalates, as it is already known that the nuclear hormone receptors share highly conserved ligand binding domains [55]. DCHP is considered to have moderate agonistic and antagonistic effects on both androgen and estrogen receptors and it may also act on the glucocorticoid receptor and on the thyroid receptors. DCHP and DIOP are predicted to have the highest endocrine disruption potentials as they may affect numerous nuclear receptors.

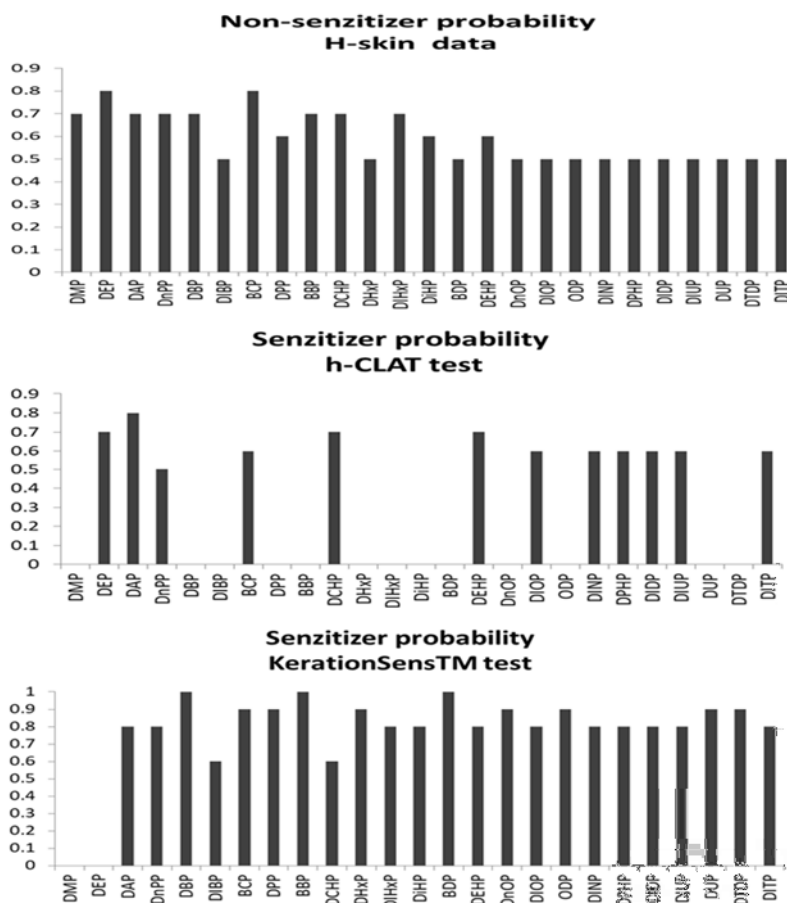


Figure 3. Predictions concerning skin sensitization potentials of the investigated phthalates. White boxes reflect a non-sensitizer potential, light grey boxes reflect a moderate sensitizer potential and dark grey boxes reflect a high sensitizer potential. There are predictions based on human data (H-skin), h-CLAT (human Cell Line Activation Test) and KeratinoSensTM tests.

The Pred-herg [56] computational tool has been used to obtain information concerning the ability of the investigated phthalates to inhibit the hERGK⁺ channels, the results being presented in Figure 4. Both binary and multiclass prediction models predict a non-inhibitory potential of the hERGK⁺ channel. Furthermore, specific literature does not mention cardiotoxicity among the toxicological endpoint of these phthalates.

The use of the Toxtree [57] computational facility to assess the harmful effects of the investigated phthalates illustrates that they belong to the chemical class of low toxicity (except DAP which reflects an intermediate toxicity), they do not reveal a genotoxic carcinogenicity and mutagenicity, and that all of the investigated phthalates present a structural alert (phthalate diesters as peroxisome proliferators) for non-genotoxic carcinogenicity (Table 4).

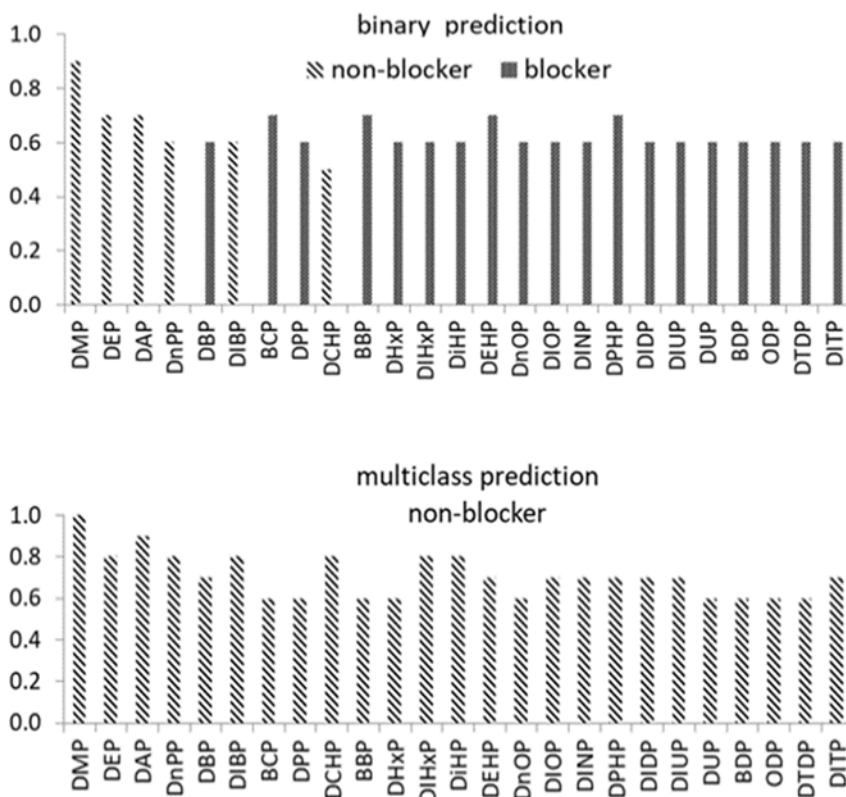


Figure 4. Reliability of the predictions concerning the inhibition of hERGK⁺ channel

Table 3. ENDOCRINE DISRUPTOME results concerning the interactions of the phthalates with the nuclear receptors. White boxes correspond to compounds predicted as non-affecting the nuclear receptors (SE>0.75), light blue boxes correspond to compounds with a low probability of disrupting the nuclear receptors (0.50<SE<0.75) and dark grey boxes correspond to compounds with a medium probability of disrupting the nuclear receptors (0.25<SE<0.50).

Phthalate	Docking scores															
	AR	AR an	ER α	ER α an	ER β	ER β an	GR	GR an	LXR α	LXR β	PPAR α	PPAR β	PPAR γ	RXR α	TR α	TR β
DMP	-6.1	-6.0	-5.7	-5.9	-6.1	-5.8	-5.8	-5.8	-6.2	-6.5	-5.6	-6.2	-6.0	-5.8	-6.5	-6.4
DEP	-6.3	-6.5	-6.0	-6.0	-6.4	-6.0	-5.7	-5.7	-6.5	-6.6	-5.7	-6.1	-6.1	-5.8	-6.7	-6.8
DAP	-6.4	-6.8	-6.5	-6.4	-6.8	-6.3	-6.2	-6.1	-7.0	-6.9	-6.3	-6.3	-6.7	-6.8	-7.0	-7.0
DnPP	-6.4	-6.8	-6.5	-6.4	-6.9	-6.6	-6.1	-6.1	-7.1	-7.0	-5.9	-6.2	-6.7	-6.6	-7.0	-6.9
DBP	-6.6	-6.5	-6.7	-6.7	-7.1	-6.4	-6.5	-6.2	-7.3	-7.3	-6.6	-6.5	-7.0	-6.9	-7.2	-7.3
DIBP	-6.7	-7.1	-7.3	-7.2	-7.4	-7.1	-6.4	-6.6	-7.6	-7.6	-6.7	-6.8	-7.3	7.6	-7.6	-7.7
BCP	-7.0	-7.4	-7.7	-7.8	-8.0	-7.9	-7.2	-7.1	-8.3	-8.5	-7.5	-8.0	-7.9	-8.7	-7.9	-8.1
DPP	-6.6	-6.3	-6.8	-6.9	-6.5	-6.4	-6.2	-6.1	-7.0	-7.3	-7.0	-7.0	-7.1	-7.2	-7.7	-7.7
DCHP	-7.6	-7.4	-8.8	-8.7	-8.9	-8.5	-8.5	-8.2	-9.4	-9.2	-7.8	-8.4	-8.5	-9.4	-7.3	-9.1
BBP	-7.6	-7.8	-8.3	-7.9	-7.9	-7.5	-7.7	-6.8	-8.2	-8.6	-8.0	-8.2	-8.1	-8.3	-8.8	-8.8
DHxP	-6.2	-6.4	-6.8	-7.2	-6.7	-6.7	-6.6	-5.9	-7.5	-7.6	-63.6	-7.3	-7.2	-7.5	-7.9	-8.0
DIHxP	-6.5	-6.7	-7.4	-7.4	-7.0	-7.1	-6.8	-6.8	-7.9	-8.0	-7.4	-7.7	-7.7	-8.5	-8.8	-8.4
DIHP	-5.7	-6.5	-7.6	-7.6	-6.7	-7.4	-7.2	-6.2	-8.1	-8.1	-6.6	-7.9	-7.1	-8.2	-8.0	-8.5
DEHP	-5.38	-6.3	-7.5	-7.7	-6.3	-7.5	-7.6	-7.4	-8.2	-8.2	-6.8	-7.9	-7.6	-8.3	-7.3	-8.0
DnOP	-4.8	-6.3	-7.4	-7.4	-6.3	-6.9	-7.0	-6.2	-9.3	-8.0	-7.1	-7.6	-7.3	-8.2	-7.3	-7.8
DIOP	-5.3	-6.0	-9.1	-9.3	-6.6	-7.8	-9.2	-7.8	-9.9	-9.7	-8.8	-9.2	-8.6	-10.2	-9.4	-9.5
DINP	-5.0	-5.4	-7.8	-7.3	-5.6	-7.2	-7.6	-6.6	-7.8	-8.1	-6.8	-7.8	-7.8	-8.8	-7.4	-8.2
DPHP	-3.8	-5.5	-6.8	-7.1	-4.5	-6.8	-7.7	-6.9	-7.9	-8.3	-7.0	-8.1	-7.3	-8.3	-5.7	-7.5
DIDP	-5.0	-4.4	-7.8	-7.7	-6.7	-7.1	-7.6	-7.9	-7.7	-8.6	-7.2	-7.9	-7.8	-8.6	-6.6	-7.9
DIUP	-4.9	-4.2	-7.8	-7.6	-5.7	-7.2	-8.0	-7.0	-7.9	-8.4	-7.5	-7.7	-7.9	-8.7	-6.2	-7.5
DUP	-4.6	-3.8	-7.4	-7.5	-5.7	-7.9	-7.1	-6.7	-7.7	-8.4	-6.9	-7.3	-7.3	-7.7	-5.9	-7.6
BDP	-6.4	-6.5	-6.9	-7.1	-6.6	-6.8	-6.8	-6.2	-7.2	-7.9	-7.4	-7.3	-7.4	-7.8	-8.0	-7.6
ODP	-4.4	-5.7	-7.3	-7.4	-5.7	-6.9	-7.5	-6.5	-7.5	-8.3	-7.0	-7.6	-7.3	-8.4	-6.9	-8.0
DTDP	-5.0	-4.1	-7.1	-7.3	-6.3	-6.8	-7.9	-6.5	-7.6	-8.2	-7.0	-7.6	-7.4	-7.7	-5.7	-6.3
DITP	-4.7	-4.0	-8.0	-7.3	-5.6	-7.2	-7.8	-6.9	-7.8	-8.5	-7.6	-7.6	-8.1	-8.5	-5.5	-6.4

Table 4. Predictions obtained using the Toxtree software concerning the harmful effects of the investigated phthalates.

Phthalate/ predicted biological effects	Skin irritation and corrosion	Eyes irritation	Genotoxic carcinogenicity	Non-genotoxic carcinogenicity	Mutagenicity (Ames test)	Toxicity class
DMP	Irritation	No	No	Yes	No	Low
DEP	Irritation	No	No	Yes	No	Low
DAP	Irritation	No	No	Yes	No	Intermediate
DnPP	Irritation	No	No	Yes	No	Low
DBP	Irritation	No	No	Yes	No	Low
DIBP	Irritation	No	No	Yes	No	Low
BCP	Irritation	No	No	Yes	No	Low
DPP	Irritation	No	No	Yes	No	Low
BBP	Irritation	No	No	Yes	No	Low
DCHP	Irritation	No	No	Yes	No	Low
DHxP	Irritation	No	No	Yes	No	Low
DIHxP	Irritation	No	No	Yes	No	Low
DiHP	Not corrosive	No	No	Yes	No	Low
BDP	Not corrosive	No	No	Yes	No	Low
DEHP	Not corrosive	No	No	Yes	No	Low
DnOP	Not corrosive	No	No	Yes	No	Low
DIOP	Not corrosive	No	No	Yes	No	Low
ODP	Not corrosive	No	No	Yes	No	Low
DINP	Not corrosive	No	No	Yes	No	Low
DPHP	Not corrosive	No	No	Yes	No	Low
DIDP	Not corrosive	No	No	Yes	No	Low
DIUP	Not corrosive	No	No	Yes	No	Low
DUP	Not corrosive	No	No	Yes	No	Low
DTDP	Not corrosive	No	No	Yes	No	Low
DITP	Not corrosive	No	No	Yes	No	Low

The assessment of the interactions of the phthalates with CYPs has been performed using the SwissDock software [58]. The illustrations concerning the results furnished by this computational tool are revealed in Figure 5 and all the free energies of the predicted interactions are exposed in Figure 6. Figure 5a illustrates the predicted binding modes (BMs) for the interaction of DHxP (presented as dark grey sticks) with CYP1A2 (presented as a light grey cartoon), none of them corresponding to the active site, the location of which is shown by the presence of the prosthetic group hem (dim grey sticks) and the inhibitor alpha-naphthoflavone (black sticks). Figure 5b reveals the BM with the highest free energy for the interaction of DEHP (shown in dark grey sticks) with the active site of CY3A4. The protein is shown as a light grey cartoon, the prosthetic group hem is revealed as a light grey wire, while

the inhibitor tert-butyl {6-oxo-6-[(pyridin-3-ylmethyl)amino]hexyl}carbamate is shown as black sticks. Figure 5b illustrates that the binding mode of DEHP corresponds to the position of the inhibitor tert-butyl {6-oxo-6-[(pyridin-3-ylmethyl)amino]hexyl}carbamate and underlines the inhibitory potential of DEHP on CYP3A4.

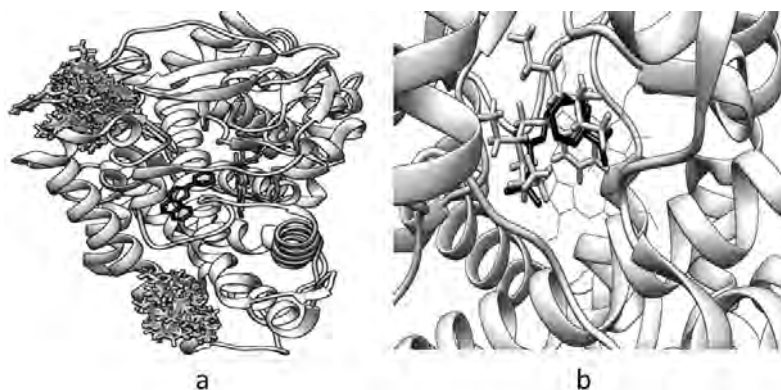


Figure 5. (a) Illustration of the binding modes of di-n-hexyl phthalate (dark grey sticks) to the CYP1A2 (light grey cartoon). The hem group is illustrated with dim grey sticks and the inhibitor alpha-naphthoflavone that is present in the crystallographic structure of the CYP1A2 is revealed using black sticks. (b) Illustration of the binding of di(2-ethylhexyl) phthalate (dark grey sticks) to the active site of CY3A4. The protein is shown as a light grey cartoon, the prosthetic group hem is revealed as a light grey wire and the inhibitor tert-butyl {6-oxo-6-[(pyridin-3-ylmethyl)amino]hexyl}carbamate is shown using black sticks

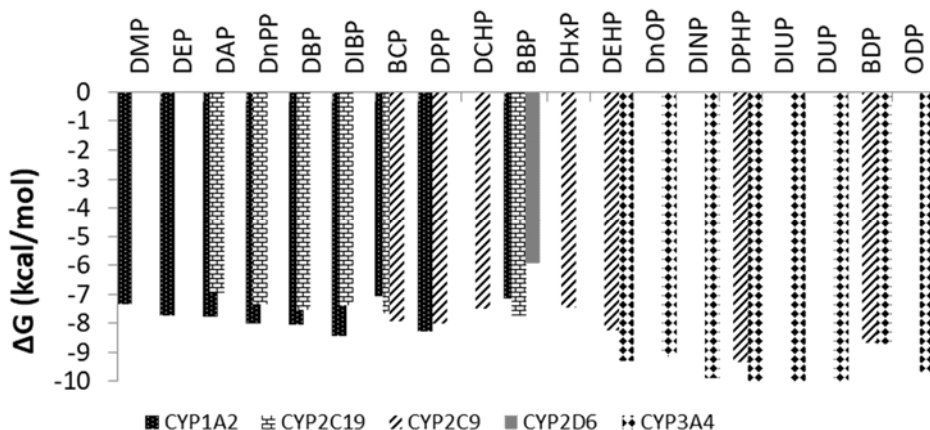


Figure 6. Computed free energies for the interactions of the phthalates with human cytochromes involved in the metabolism of xenobiotics

Figure 6 emphasizes that almost all predictions made by the SwissADME tool concerning the inhibition of cytochromes known to be involved in the metabolism of xenobiotics (including drugs) are confirmed by the molecular docking study. DHxP and BDP are predicted to bind to CYP1A2, although there are no binding modes corresponding to the active site of the enzyme (as it is illustrated in the Figure 5a for the interaction of DHxP with CYP1A2). These predictions do not exclude the inhibitory potential of DHxP and BDP on CYP1A2, as these interactions may have allosteric effects on the biological activity of the enzyme. Experimental data confirm the interaction of DEHP with CYP2C9, this cytochrome being responsible for the metabolism of DEHP [59]. The inhibitory potential of phthalates on the cytochromes is important to be considered because these enzymes are involved in the metabolism of numerous endogenous and exogenous compounds (drugs and other xenobiotics).

CONCLUSIONS

Considering the high development rate of the industries of food and drinks, furnishing and paint, cosmetics, hygiene, or of pharmaceutical and medical products, the potential exposure and accumulation of phthalates in the human body is increased which emphasizes the necessity of assessing the risks of these chemicals. A special attention is needed for people who are professionally exposed to a higher amount of phthalates. Within this study we have used various computational tools to investigate the toxicity of 25 of the most commonly used phthalates for humans. To the best of our knowledge, for 12 of the 25 investigated phthalates (48%), this is the first study providing data concerning their effects on humans. The predictions made by the various computational tools used in this study are in good agreement with each other and also with published data concerning the effects on human health observed for some of the investigated phthalates which increases the value of predictions concerning the toxicological effects for the phthalates that were not investigated. The obtained results reveal that phthalates are a class of compounds reflecting oral bioavailability, skin penetration and toxicity. When they are inhaled, their toxicity is increased. The investigated phthalates are predicted to be able to interact with important molecular targets in the human organism (membrane receptors, kinases, phosphatases, transcription factors and transporters) and these interactions may disrupt the physiological activity of the targets, conducting to predicted harmful effects such as skin irritation, antagonistic effect on some nuclear receptors, non-genotoxic carcinogenicity, or inhibition of cytochromes involved in the metabolism of

xenobiotics (especially CYP1A2 and CYP3A4). The investigated phthalates do not reveal a genotoxic carcinogenicity and mutagenicity. Ditridecyl phthalate and diisotrodecyl phthalate illustrate the smallest number of possible toxicological effects, namely skin irritation, non-genotoxic carcinogenicity and endocrine disruption potential. Our study reveals that lower molecular weight phthalates are predicted to be able to conduct to almost all investigated toxicological endpoints. Thus, we consider these phthalates to be the most dangerous ones and recommend that their use be avoided. Finally, we are of the opinion that this study highlights the necessity of further complex experimental investigations concerning the harmful effects of phthalates on humans.

EXPERIMENTAL SECTION

Our study concerns the application of the following computational tools to envisage the possible biological effects on humans of the most commonly used phthalates: (i) the FAFDrugs4 tool [49] for producing the ADME-Tox profiles; (ii) admetSAR [50] and SwissADME [51] for envisaging pharmacokinetic profiles [50]; (iii) Pred-Skin for predicting skin sensitization [52, 53]; (iv) ENDOCRINE DISRUPTOME for predicting endocrine disruption potential [54]; (v) Pred-hERG for predicting the inhibitory potential against hERGK+ channel [56]; (v) ToxTree for predicting toxicity class, carcinogenicity and mutagenicity [57]; and (vii) SwissDock [58] to assess the interactions of the cytochromes P450 (CYP) involved in xenobiotics metabolism (CYP1A2, CYP2C9, CYP2C19, CYP3A4, CYP2D6) with phthalates.

Absorption, Distribution, Metabolism, Excretion and Toxicity (ADME-Tox) profiles are commonly used to predict disposition of drugs within the human organism in the initial stage of their design. There are several *in silico* approaches used to predict the ADME-Tox profiles. These approaches are centered on a set of rules based on the physicochemical properties of the chemical compound that are used to predict its bioavailability and safety. The physicochemical properties are computed by the computational tools enumerated in the previous paragraph starting from the Simplified Molecular-Input Line-Entry System (SMILES) formulae of the investigated phthalates. The SMILES formulae are extracted from the ZINC [60] and PubChem [11] databases, respectively. The bioavailability designates the absorbed part of the ingested amount of a chemical compound. In order to predict the bioavailability, the physicochemical properties reflecting the hydrophilicity and solubility of a chemical compound are important and the following rules are commonly used: the rule-of-5 violations (RO5, also known as the Lipinski's rule) [61], Egan's Rule [62], and Veber's Rule [63]. The compounds

with more than one violation of the RO5 rule reflect poor absorption. The safety profile illustrates the adverse effects of a chemical compound and is based on a few other common rules, such as the GlaxoSmithKline rule [64] and the Pfizer 3/75 rule [65].

The human exposure to phthalates can take place by ingestion, inhalation, dermally and/or eye contact, or by intravenous injection through medical devices. When producing the ADME-Tox profiles for phthalates using the FAFDrugs4 computational tool, the routes of exposure through ingestion and inhalation are considered and specific filters for the physicochemical properties are applied [49]. The accuracy of the predictions obtained using the FAFDrugs4 computational tool is about 70%.

The physicochemical properties of small organic molecules may also be used for predicting their pharmacokinetics. The lipophilicity and polarity of a small molecule are useful molecular descriptors used to evaluate the passive human gastrointestinal absorption (GI) and the blood-brain barrier permeation (BBB), and they are considered when predicting the pharmacokinetics of phthalates using the SwissADME [51] and admetSAR [50] tools. SwissADME has been used to estimate the interactions of phthalates with cytochromes P450 (CYPs) that are known to be strongly involved in the metabolism of xenobiotics, namely CYP1A2, CYP2C9, CYP2C19, CYP2D6, and CYP3A4. This estimation is established using a support vector machine algorithm based on a large dataset of chemical compounds known to be substrates or inhibitors of the CYP enzymes. The estimation of the interactions of these chemicals with the CYPs enzymes informs about their pharmacokinetics associated xenobiotics-xenobiotics interactions. The SwissADME tool predicts pharmacokinetics profiles with an accuracy of 70%. The AdmetSAR tool has been also used for estimating the pharmacokinetic profiles of the phthalates, the predictive accuracy of this tool being 76.7% [50].

Pred-Skin is a web-based tool that uses QSAR method for determining the skin sensitization potential: the binary predictions of human skin sensitization potentials are based on human data (the prediction accuracy is between 73% and 76%), the binary and multiclass predictions of murine skin sensitization potentials are based on animal data (LLNA, the prediction accuracy is between 70% and 84%), and the binary predictions based on non-animal data, i.e. Direct Peptide Reactivity Assay (DPRA), KeratinoSens, and the human Cell Line Activation Test (h-CLAT) with an accuracy of prediction between 80% and 86% [52, 53]. Usually, one positive result in one of the KeratinoSens™ or h-CLAT tests designates a potential skin sensitizer compound, and two negative results point towards a non-sensitizer compound [66]. Within this study we only consider predictions based on human data, and on the KeratinoSens™ and h-CLAT tests.

ENDOCRINE DISRUPTOME is a web facility based on the molecular docking approach using the AutoDock Vina algorithm, and predicts interactions between the chemical compound with 14 distinct human nuclear receptors: androgen receptor (AR), estrogen receptors α (ER α) and β (ER β), glucocorticoid receptor (GR), liver X receptors α (LXR α) and β (LXR β), peroxisome proliferator activated receptors α (PPRA α), β/δ (PPRA β), and γ (PPRA γ), retinoid X receptor α (RXR α) and thyroid receptors α (TR α) and β (TR β). This tool predicts both agonistic and antagonistic (an) effects for the nuclear receptors AR, ER α , ER β and GR [54]. The predictions are quantitatively described by the sensitivity parameter (SE) based on the docking scores. Taking into account the values of this parameter, compounds are categorized in four classes: compounds with high probability of disrupting the nuclear receptors ($SE < 0.25$); compounds with a medium probability of disrupting the nuclear receptors ($0.25 < SE < 0.50$); compounds with a low probability of disrupting the nuclear receptors ($0.50 < SE < 0.75$) and compounds predicted as non-affecting the nuclear receptors ($SE > 0.75$). The accuracy of predictions made by this tool is about 72% [54].

Pred-hERG is another web facility based on the QSAR method that allows to obtain predictive models concerning the ability of a chemical compound to inhibit the human ether-à-go-go related gene (hERG)K⁺ channels. This inhibition may conduct to cardiac side-effects such as heart arrhythmia and even possibly death [56]. The predictions made by the Pred-hERG tool have an accuracy of up to 89%.

The Toxtree software has been used to obtain predictions concerning carcinogenicity and mutagenicity, which are two other important toxicological endpoints that must be assessed for the chemical compounds [57]. These predictions are based on applying the Crammer rules [67] for assessing the toxicity class, and the Benigni/Bossa rule for predicting the carcinogenicity and mutagenicity [68]. The accuracy of the Toxtree predictions is 70%.

Molecular docking is used to assess the interactions of the phthalates with CYP1A2, CYP2C9, CYP2C19, CYP2D6 and CYP3A4, and is implemented under the SwissDock tool [58]. We have considered both blind and rigid docking. As the Protein Data Bank [69] contains numerous structures for the considered CYPs, the structural files with the following PDB entry codes are used in our molecular docking studies: 2HI4 for CYP1A2, 4N2Z for CYP2C9, 4GQS for CYP2C19, 4XRZ for CYP2D6 and 4D6Z for CYP3A4. These structural files have been chosen so as to correspond to the complexes made by the enzymes with inhibitors and having the best resolution. The ligands, except HEM, have been removed from every spatial structure of the enzymes and the structures have been prepared for docking using the *DockPrep* utility within the Chimera software [70]. The Chimera software has been also used for obtaining the visualization and analysis results.

REFERENCES

1. R.U. Halden, *Annu Rev Public Health*, **2010**, *31*, 179-194.
2. C. Gennings, R. Hausser, H.M. Koch, A. Kortenkamp, P.J. Lioy, P.E. Mirkes, B.A. Schwetz, *Report to the U.S. Consumer Product Safety Commission by the Chronic hazard advisory panel on phthalates and phthalate alternatives*, **2014**. <https://www.cpsc.gov/chap>. Accessed 18 January 2019.
3. R.M. David, R.H. McKee, J.H. Butala, R.A. Barter, M. Kayser, *Esters of aromatic mono-, di-, and tricarboxylic acids, aromatic diacids, and di-, tri-, or polyalcohols*. In *Patty's toxicology*, E. Bingham, B. Cohrssen, C.H. Powell Eds, John Wiley & Sons, New York, USA, **2001**, Volume 6. pp. 635.
4. J. Doull, R. Cattley, C. Elcombe, B.G. Lake, J. Swenberg, C. Wilkinson, G. Williams, van M. Gemert, *Regul Toxicol Pharmacol*, **1999**, *29*, 327-357.
5. M. Wittassek, H.M. Koch, J. Angerer, T. Bruning, *Mol Nutr Food Res*, **2011**, *55*, 7-31.
6. W. Davidson-Urbain, P. Jouvét, M.P. Vélez, P. Ayotte, P. Monnier, *Biomed J Sci & Tech Res*, **2018**, *6*, 5124-5129.
7. National Research Council. *Intentional Human Dosing Studies for EPA Regulatory Purposes: Scientific and Ethical Issues, Committee on the Use of Third Party Toxicity Research with Human Research Participants Science, Technology, and Law Program*, **2004**, <http://www.nap.edu/catalog/10927.html>. Accessed 20 January 2019.
8. The National Institute for Occupational Safety and Health (NIOSH). <https://www.cdc.gov/niosh/>. Accessed between November 2017 – February 2019.
9. Occupational Safety and Health Administration (OSHA). <https://www.osha.gov/>. Accessed between November 2017 – June 2017.
10. Toxicology Data Network (TOXNET). <https://toxnet.nlm.nih.gov/newtoxnet/hsdb.htm>. Accessed between November 2017 – February 2019.
11. The PubChem database. <https://pubchem.ncbi.nlm.nih.gov/#>. Accessed between November 2017 – June 2017.
12. BIBRA Toxicology Advice & Consulting. <https://www.bibra-information.co.uk/toxicity-profiles-overview/>. Accessed between November 2017 – February 2019.
13. D. Oral, P. Erkekoglu, B.K. Gumusel, M.-W. Chao, *J Environ Pathol Toxicol Oncol*, **2016**, *35*, 43-58.
14. R. Hauser, A.M. Calafat, *Occup Environ Med*, **2005**, *62*, 806-818.
15. M.H. Asghari, S. Saeidnia, M. Abdollahi, *Int J Pharm*, **2015**, *11*, 95-105.
16. I. Katsikantami, S. Sifakis, M.N. Tzatzarakis, E. Vakonaki, O.I. Kalantzi, A.M. Tsatsakis, A.K. Rizos, *Environ Int*, **2016**, *97*, 212-236.

17. S.S.S. Rowdhwal, JX. Chen, *Hindawi BioMed Research International*, **2018**, Article ID 1750368.
18. J. Knez, *Reprod Biomed Online*, **2013**, 26, 440-448.
19. R. Rozati, P.P. Reddy, P. Reddanna, R. Mujtaba, *Fertil Steril*, **2002**, 78, 1187-1194.
20. N. Pant, M. Shukla, D. Kumar Patel, Y. Shukla, N. Mathur, Y. Kumar Gupta, D.K. Saxena, *Toxicol Appl Pharmacol*, **2008**, 231, 112-116.
21. R. Hauser, *Int J Androl*, **2008**, 31, 112-117.
22. L. López-Carrillo, R.U. Hernández-Ramírez, A.M. Calafat, L. Torres-Sánchez, M. Galván-Portillo, L.L. Needham, R. RuizRamos, M.E. Cebrián, *Environ Health Perspect*, **2010**, 118, 539-544.
23. J.A. Hoppin, R. Ulmer, S.J. London, *Environ Health Perspect*, **2004**, 112, 571-574.
24. Y.-J. Lien, H.-Y. Ku, P.-H. Su, S.J. Chen, H.Y. Chen, P.C. Liao, W.J. Chen, S.L. Wang, *Environ Health Perspect*, **2015**, 123, 95-100.
25. C.G. Bornehag, J. Sundell, C.J. Weschler, K.-G. Bornehag, J. Sundell, C.J. Weschler, T. Sigsgaard, B. Lundgren, M. Hasselgren, L. Hägerhed-Engman, *Environ Health Perspect*, **2004**, 112, 1393-1397.
26. M. Matsumoto, M. Hirata-Koizumi, M. Ema, *Regul Toxicol Pharmacol*, **2008**, 50, 37-49.
27. L.C. Li, S.L. Wang, Y.C. Chang, P.C. Huang, J.T. Cheng, P.H. Su, P.C. Liao, *Chemosphere*, **2011**, 83, 1192-1199.
28. A. Araki, T. Mitsui, C. Miyashita, T. Nakajima, H. Naito, S. Ito, S. Sasaki, K. Cho, T. Ikeno, K. Nonomura, R. Kishi, *PLoS One*, **2014**, 9, Article ID e109039.
29. H.-Y. Ku, P.-H. Su, H.-J. Wen, S.-L. Wang, *PLoS One*, **2015**, 10, e0123309.
30. R. Rozati, P.P. Reddy, P. Reddanna, R. Mujtaba, *Fertil Steril*, **2002**, 78, 1187-1194.
31. S.H. Swan, S. Sathyanarayana, E.S. Barrett, *Hum Reprod*, **2015**, 30, 963-972.
32. S.H. Kim, S. Chun, J.Y. Jang, H.D. Chae, C.-H. Kim, B.M. Kang, *Fertil Steril*, **2011**, 95, 357-359.
33. S.H. Kim, S. Cho, H.J. Ihm, Y.S. Oh, S.H. Heo, S. Chun, H. Im, H.D. Chae, C.H. Kim, B.M. Kang, *J Clin Endocr Metab*, **2015**, 100, E1502-E1511.
34. B. Kolarik, K. Naydenov, M. Larsson, C.G. Bornehag, J. Sundell, *Environ Health Perspect*, **2008**, 116, 98-103.
35. Y. Wang, S.H. Bryant, T. Cheng, J. Wang, A. Gindulyte, B.A. Shoemaker, P.A. Thiessen, S. He, J. Zhang, *Nucleic Acids Res*, **2017**, 45, D955-D963.
36. P. Wolkoff, *Int J Hyg Environ Health*, **2013**, 216, 371-394.
37. M. De Falco, M. Forte, V. Laforgia, *Front Environ Sci*, **2015**, 3, 1-12.
38. M.A. Kamrin, *J Toxicol Environ Health, Part B*, **2009**, 12, 157-174.
39. A.B. Raies, V.B. Bajic, *Wiley Interdiscip Rev Comput Mol Sci*, **2016**, 6, 147-172.
40. C. Lu, C.M. Holbrook, L.M. Andres, *Environ Health Perspect*, **2010**, 118, 125-130.
41. D. Craciun, D. Modra, A. Isvoran, *AIP Conf Proc*, **2015**, 1694, 040007-1-040007-6.
42. Y. Gao, T. An, Y. Ji, G. Li, C. Zhao, *Environ Pollu*, **2015**, 206, 510-517.

43. O.V. Tinkov, L.N. Ognichenko, V.E. Kuzmin, L.G. Gorb, A.P. Kosinskaya, N.N. Muratov, E.N. Muratov, F.C. Hill, J. Leszczynski, *Struct Chem*, **2016**, *27*, 191-198.
44. I.A. Sheikh, R.F. Turki, A.M. Abuzenadah, G.A. Damanhour, M.A. Beg, *PLoS ONE*, **2016**, *11*, Article ID e0151444.
45. A. Isvoran, A. Ciorsac, V. Ostafe, *ADMET & DMPK*, **2017**, *5*, 192-200.
46. M. Roman, D.L. Roman, V. Ostafe, A. Ciorsac, *Pharm Res*, **2018**, *35*, Article ID 41.
47. M. Roman, D.L. Roman, V. Ostafe, A. Isvoran, *J Bioinform Genomics Proteomics*, **2018**, *3*, 1029.
48. V.M. Alves, E.N. Muratov, A. Zakharov, N.N. Muratov, C.H. Andrade, T. Tropsha, *Food Chem Toxicol*, **2018**, *112*, 526-534.
49. D. Lagorce, L. Bouslama, J. Becot, M.A. Miteva, B.O. Villoutreix, *Bioinformatics*, **2017**, *33*, 3658-3660.
50. F. Cheng, W. Li, Y. Zhou, J. Shen, Z. Wu, G. Liu, P.W. Lee, Y. Tang, *J Chem Inf Model*, **2012**, *52*, 3099-3015.
51. A. Daina, O. Michielin, V. Zoete, *Sci Rep*, **2017**, *7*, Article ID 42717.
52. R.C. Braga, V.M. Alves, E.N. Muratov, J. Strickland, N. Kleinstreuer, A. Tropsha, C.H. Andrade, *Chem Inf Model*, **2017**, *57*, 1013-1017.
53. V.M. Alves, S.J. Capuzzi, R.C. Braga, J.V.B. Borba, A.C. Silva, T. Luechtefeld, T. Hartung, C.H. Andrade, E.N. Muratov, A. Tropsha, *ACS Sustainable Chem Eng*, **2018**, *6*, 2845-2858.
54. K. Kolsek, J. Mavri, M. Sollner Dolenc, S. Gobec, S. Turk, *J Chem Inf Model*, **2014**, *54*, 1254-1264.
55. W. Gao, C.E. Bohl, J.T. Dalton, *Chem Rev*, **2005**, *105*, 3352-3370.
56. R.C. Braga, V.M. Alves, M.F. Silva, E. Muratov, D. Fourches, L.M. Lião, A. Tropsha, C.H. Andrade, *Mol Inform*, **2015**, *34*, 698-701.
57. G. Patlewicz, N. Jeliakova, R.J. Safford, A.P. Worth, B. Aleksiev, *SAR QSAR Environ Res*, **2008**, *19*, 495-524.
58. A. Grosdidier, V. Zoete, O. Michielin, *Nucleic Acids Res*, **2011**, *39*, W270-W277.
59. S. Singh, S.S.-L. Li, *Genomics*, **2011**, *97*, 148-157.
60. J.J. Irwin, B.K. Shoichet, *J Chem Inf Model*, **2005**, *45*, 177-182.
61. C.A. Lipinski, F. Lombardo, B. Dominy, P.J. Feeney, *Adv Drug Deliv Rev*, **1997**, *23*, 3-25.
62. W.J. Egan, K.M. Merz, J.J. Baldwin, *J Med Chem*, **2000**, *43*, 3867-3877.
63. D.F. Veber, S.R. Johnson, H.Y. Cheng, B.R. Smith, K.W. Ward, K.D. Kopple, *J Med Chem*, **2002**, *45*, 2615-2623.
64. M.P. Gleeson, *J Med Chem*, **2008**, *51*, 817-834.
65. J.D. Hughes, J. Blagg, D.A. Price, S. Bailey, G.A. DeCrescenzo, R.V. Devraj, E. Ellsworth, Y.M. Fobian, M.E. Gibbs, R.W. Gilles, N. Greene, E. Huang, T. Krieger-Burke, J. Loesel, T. Wager, L. Whiteley, Y. Zhang, *Bioorg Med Chem Lett*, **2008**, *18*, 4872-4875.
66. Y. Otsubo, T. Nishijo, M. Miyazawa, K. Saito, H. Mizumachi, H. Sakaguchi, *Reg Tox Pharm*, **2017**, *88*, 118-124.
67. G.M. Cramer, R.A. Ford, R.L. Hall, *Food Cosmet Toxicol*, **1978**, *16*, 255-276.

68. R. Benigni, C. Bossa, *Toxicol Mech Methods*, **2008**, *18*, 137-147.
69. H.M. Berman, J. Westbrook, Z. Feng, G. Gilliland, T.N. Bhat, H. Weissig, I.N. Shindyalov, P.E. Bourne, *Nucleic Acids Res*, **2000**, *28*, 235-242.
70. E.F. Pettersen, T.D. Goddard, C.C. Huang, G.S. Couch, D.M. Greenblatt, E.C. Meng, T.E. Ferrin, *J Comput Chem*, **2004**, *25*, 1605-1612.

EFFECT OF AN EXPERIMENTAL GREEN TEA EXTRACT BLEACHING GEL ON THE COLOR CHANGES OF A COMPOSITE RESIN

CORINA VOINA^a, ADRIANA MURESAN^b, ADA DELEAN^a,
AMALIA IONELA MOLDOVAN^c, LAURA SILAGHI DUMITRESCU^{d*},
ANDRADA VOINA TONEA^e, MADALINA VALEANU^f

ABSTRACT. The effect of the color change of stained and then bleached composite resins blocks have been evaluated. 28 blocks, made from Admira fusion composite resin and divided in 3 groups, were included in the present study. They were stained in coffee for 3 days and then bleached with Opalescence gel (GO) and experimental bleaching gel based on green tea extract (GE). All color indices were measured in all situations (initially, after staining and after bleaching) with Vita Easy Shade spectrophotometer. It was used the CIE*L*a*b system for the color change parameters. The group bleached with Opalescence presented the most significant color changes. The bleaching effect of the experimental gel is lower that Opalescence bleaching gel.

Keywords: green tea, composite blocks, staining, bleaching, color change

^a Department of Odontology and Oral Pathology, Faculty of Dental Medicine, University of Medicine and Pharmacy "Iuliu Hațieganu", 33 Motilor Street, 400001, Cluj-Napoca, Romania

^b Department of Functional Sciences, Faculty of Medicine, University of Medicine and Pharmacy "Iuliu Hatieganu", 3 Clinicilor Street, 400006, Cluj-Napoca, Romania

^c Physics and Chemistry Department, Technical University of Cluj-Napoca, 28 Memorandumului Street, Cluj-Napoca 400114, Romania

^d Babes Bolyai University -"Raluca Ripan" Chemistry Research Institute, 30 Fântânele Street, 400294, Cluj-Napoca, Romania

^e Department of Dental Matherials, Faculty of Dental Medicine, University of Medicine and Pharmacy "Iuliu Hatieganu", 15 Babes Victor Street, 400012, Cluj-Napoca, Romania

^f Department of Medical Informatics and Biostatistics, Faculty of Medicine, University of Medicine and Pharmacy "Iuliu Hatieganu", 6 Pasteur Louis Street, 400349, Cluj-Napoca, Romania

* Corresponding author: lauraiulia2000@yahoo.com

INTRODUCTION

Since the introduction of the bleaching therapeutic procedures by Haywood and Heyman in 1989 [1], teeth whitening has gained significant acceptance among dental practitioners and patients, both through the simplicity of the procedure and its effectiveness [2].

In the treatment of lesions with loss of tooth substance, the light-curing composite resins are the most used materials for restoration, and therefore the requirements of patients include a better adaptation of the restoration color and a greater stability over time [3]. These two properties depend on the chemical composition of the resin and how it is finished after application in the tooth cavity. Intrinsic factors, such as changes in the structure of the filler, the matrix and the silane, but also the extrinsic ones can cause changes in the color of the composite restoration materials [4].

Due to the unlimited possibilities of combinations and the existence of an extensive range of shades and opacities to reproduce as accurately as possible the optical properties of the dental structures, the initial appearance of composite restorations can be excellent [5]. However, a major disadvantage of composite resins is their great color instability [5]. External factors that may induce color changes include food dyes, beverages, UV radiation, temperature differences and water absorption [5].

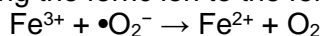
The most well-known method of treating tooth discolorations is dental bleaching, performed either by the patient at home under the guidance of the dentist, using prefabricated or customized trays, or in the dental office. The most used substances for tooth bleaching are based on hydrogen peroxide (HP) or carbamide peroxide (PC) [6].

Carbamide peroxide is an organic derivative that decomposes during bleaching treatment with hydrogen peroxide (H_2O_2) and urea (CH_4N_2O). Urea decomposes further into ammonia and water, which tends to increase the pH of the solution.

Hydrogen peroxide generates by decomposition (Fenton reaction, Haber-Weiss reaction with metal ions) the hydroxyl radical, a molecule with an even higher oxidative potential [7]. This reaction is catalyzed by metal ions such as Fe^{2+} or Cu^+ . Cell iron cannot mediate a Fenton reaction in vivo. The release of iron ions from cellular transport and storage proteins can mediate a Fenton reaction with hydroxyl ion formation and this reaction is favored by the chelating agents contained in the bleaching agent and acid pH [9].

The Haber-Weiss reaction steps are [8]:

- reducing the ferric ion to the ferrous ion:



- Fenton reaction:



Characteristic of these free radicals of oxygen, respectively hydroxyl ($\bullet\text{OH}^-$), superoxide ($\bullet\text{O}_2^-$), singlet oxygen ($\bullet\text{O}_2$) produced as a result of these reactions is their great chemical instability [7].

Also, the hydroxyl radical reacts very easily and can oxidize any organic substrate, as long as, it is close to it [9]. On the other hand, the oxidative reaction is nonspecific and the hydroxyl radical can also affect the organic matrix of the enamel, dentine [10, 11] and composite resins restorations. The present study aims to evaluate the color change of the composite resins restorations during teeth whitening with carbamide peroxide gels and experimental green tea extract bleaching gel.

RESULTS AND DISCUSSION

Twenty-eight blocks of nanohybrid composite resin, taken in this study, were randomly divided into three groups: GC, which served as control group and two experimental groups: GO bleached with commercial preparation based on 16% carbamide peroxide and GE subjected to bleaching treatment with experimental whitening gel based on 16% carbamide peroxide and green tea extract.

To the test groups were applied processes of staining and then of chemical bleaching. Also, to all composite resin blocks were registered the following color parameters: brightness, L, the color parameter in the red-green axis, a, the color parameter in the yellow-blue axis, b, as well as the total color change ΔE . These parameters were measured in the initial situation (before applying any treatment), after staining and after the bleaching process.

The values of the indices measured for the control group GC are presented in **Table 1**.

Table 1. The average values measured in the three situations for the GC.

Block	Initial evaluation	Evaluation after staining		Evaluation after bleaching	
	L	L	ΔE	L	ΔE
10	71.2(0.7)	65.7(0.4)	10.1	65.7(0.1)	0
12	74.2(0.1)	57.4(1)	5.39	57.4(0.1)	0
17	77.9(6.9)	58.7(0.1)	21.8	58.7(0.1)	0
19	81.3(0.7)	79.3(1.6)	3.61	79.3(0.1)	0
21	74.3(0.5)	72.4(0.3)	2.74		0
22	81.6(0.5)	76.3(0.3)	6.84	76.3(0.1)	0
23	73.9(0.1)	79.9(0.6)	6.5	79.9(0.1)	0
24	81.5(0.6)	74.2(0.2)	8.44	74.2(0.1)	0
25	80.7(2.1)	72.7(1.3)	9.64	72.7(0.1)	0

L, a and b were described using the mean (standard deviation).

The values of the indices measured for GO, group bleached with commercial whitening gel are presented in **Table 2**.

Table 2. The average values of the indices measured in the three situations for GO.

Block	Initial evaluation	Evaluation after staining		Evaluation after bleaching	
	L	L	ΔE	L	ΔE
1	79.3(3.8)	71.2(0.1)	8.78	82(0)	11.9
5	70.6(0.5)	65.3(0.2)	8.38	76.3(0.2)	17
6	70.9(0.9)	67.5(0)	7.04	82.2(0.1)	20.3
7	77(0.1)	72.8(0.3)	5.93	76.4(0.2)	11.2
8	68.2(1.8)	60.2(0)	11.35	74.1(0.1)	17.7
13	71.6(0.1)	63.9(0.6)	11.34	72.6(0.1)	12.5
16	74(1)	63.1(0.9)	11.44	76.5(0.3)	13.9
20	81(2.1)	74.6(3.2)	6.96	73.2(0)	1.86

The values of the indices measured for the group GE group bleached with experimental gel are presented in **Table 3**.

Table 3. Mean values of the indices measured in the three situations for GE.

Block	Initial evaluation	Evaluation after staining		Evaluation after bleaching	
	L	L	ΔE	L	ΔE
4	65.6(0.3)	64.9(3.7)	5.23	75.3(0.4)	16.52
2	79.5(4.2)	69.8(0.1)	10.31	71(1.3)	3.32
11	77.7(5.3)	59.8(0.5)	18.1	68.2(0.3)	14.12
15	74.4(0.3)	59.7(0.2)	16.87	68.1(0.1)	11.4
18	73.5(0.3)	62.3(0.1)	13.02	67.9(0.2)	8.43
3	73.8(0.1)	61.7(0.1)	15.53	63.3(1.5)	10.69
9	79.9(3.4)	57.5(1.1)	87.14	66.5(0.1)	10.37
14	79.1(4.8)	57.5(1.42)	24.21	68(0.2)	11.09

Regarding the brightness parameter L, after staining (L_2), this differs statistically and significantly between the three groups tested ($p < 0.001$, Kruskal-Wallis test). Continuing the post-hoc comparisons, we determined that between the GO and GC groups there were no significant differences in brightness ($p = 0.053$, Mann-Whitney U test), but between GE and GO and GE and GC the differences were significant ($p < 0.001$, Mann-Whitney U test).

The brightness parameter L, after whitening (L_3), it differed statistically between the three groups tested ($p < 0.001$, Kruskal-Wallis test). Continuing the post-hoc comparisons, we determined that between the GE and GC

groups there were no significant differences in brightness ($p = 0.193$, Mann-Whitney U test), but between GE and GO and GE and GC the differences were significant ($p < 0.05$, Mann-Whitney U test).

In the GO group there are statistically significant differences between L_1 - L_2 ($p < 0.001$), L_1 - L_3 ($p = 0.022$) and L_3 - L_2 ($p < 0.001$) pairs. In the GE group there are statistically significant differences between L_1 - L_2 ($p < 0.001$), L_1 - L_3 ($p = 0.002$) and L_3 - L_2 ($p < 0.001$) pairs.

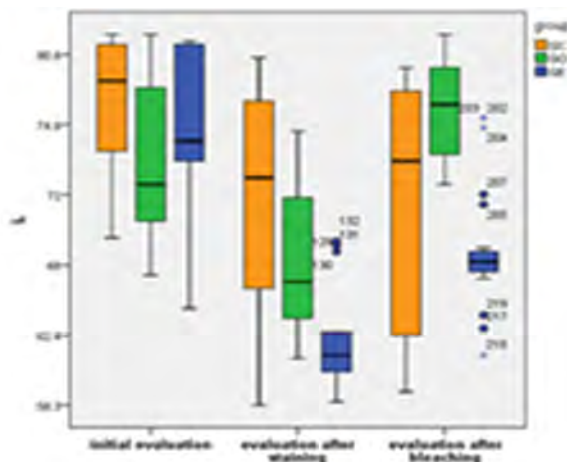


Figure 1. Modifications of the L parameter.

Regarding parameter Δa , after staining (a_2), it differs statistically significantly between the three groups tested ($p < 0.001$, Kruskal-Wallis test). Continuing the post-hoc comparisons, we determined that between GE and GO there were no significant differences ($p = 0.074$, Mann-Whitney U test), but between GE vs GC ($p < 0.001$) and GO vs GC ($p = 0.016$) the differences are significant.

Parameter Δa after bleaching (a_3) differed statistically between the three groups tested ($p < 0.001$, Kruskal-Wallis test). Continuing the post-hoc comparisons, we determined that between the GE and GO groups there were no significant differences in brightness ($p = 0.131$, Mann-Whitney U test), but between GE vs GC ($p = 0.004$) and GO vs GC ($p < 0.001$), the differences are significant.

In the GO group, there are statistically significant differences between a_1 - a_2 pairs ($p < 0.001$) and a_3 - a_2 pairs ($p < 0.001$), but between a_1 - a_3 there are no significant differences ($p = 0.1$).

In the GE group there are statistically significant differences between a_1 - a_2 pairs ($p < 0.001$), a_1 - a_3 ($p < 0.001$) and a_3 - a_2 pairs ($p < 0.001$).

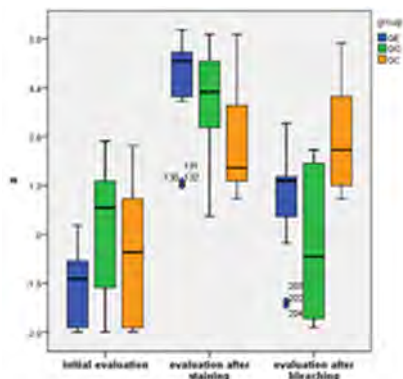


Figure 2. Modifications of Δa parameter.

Regarding the parameter Δb , after staining (b_2), it differs significantly between the three groups tested ($p < 0.001$, Kruskal-Wallis test). Continuing the post-hoc comparisons, we determined that between GE and GO there were no significant differences ($p = 0.19$, Mann-Whitney U test), but between GE vs GC ($p < 0.001$) and GO vs GC ($p < 0.001$), the differences are significant.

The parameter Δb after bleaching (b_3) did not differ statistically between the three groups tested ($p = 0.161$, Kruskal-Wallis test). Continuing the post-hoc comparisons, we determined that between the GE and GO groups there were significant differences in brightness ($p = 0.049$, Mann-Whitney U test), but between GE vs GC ($p = 0.193$) and GO vs GC ($p = 0.975$), the differences are not significant. In the GO group there are statistically significant differences between the pairs b_1 - b_2 ($p < 0.001$), b_3 - b_2 ($p < 0.001$), and b_1 - b_3 ($p < 0.001$). In the GE group there are statistically significant differences between the pairs b_1 - b_2 ($p < 0.001$), b_1 - b_3 ($p = 0.028$) and b_3 - b_2 ($p < 0.001$).

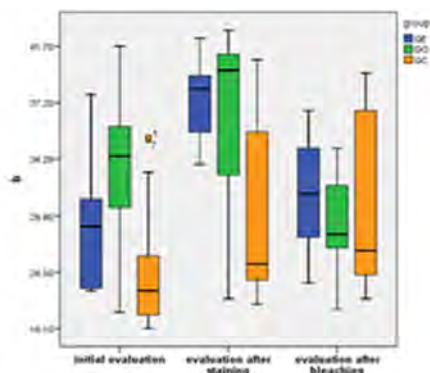


Figure 3. Modifications of Δb parameter.

Color change, ΔE , after staining (E_2) differs statistically significantly between the three groups tested ($p < 0.001$). Continuing the post-hoc comparisons, we found statistically significant differences between all groups of two groups taken: GE vs GO, GE vs GC and GO vs GC ($p < 0.001$). Regarding the parameter ΔE , after staining (E_2) between the groups GE and GO there are significant differences ($p < 0.001$). The ΔE parameter after bleaching (E_3) between the GE and GO groups did not show significant differences ($p < 0.001$).

In the GO group there are statistically significant differences between E_3-E_2 ($p = 0.001$). In the GE group there are statistically significant differences between E_3-E_2 ($p = 0.005$).

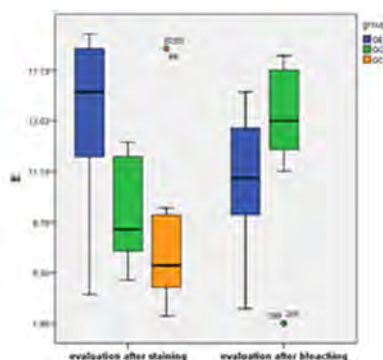


Figure 4. Modification of ΔE parameter.

It is well known that using CIEL^{*}a^{*}b system is the best option to measure the color change parameters [12]. Various research demonstrated that ΔE values between 1 and 3 are detectable to the eyes and values over 3,3 are clinically undesirable [13, 14]. At the end of the bleaching process, the most significant color change is represented by the lot bleached with 16% Opalescence, followed by the lot bleached with experimental green tea extract.

Tooth bleaching is a dynamic process, which involves diffusion of the bleaching material, which interacts with the chromophore molecules, but also acts on the surfaces on which they are applied, producing surface micromorphological changes and also changes in the depth of the tooth or restoration, modifying the optical properties [15].

Chromophore molecules fall into two categories: large organic compounds, which have conjugated double bonds in their structure and metal-containing compounds. The bleaching of the organic compounds with hydrogen peroxide implies the oxidation of the double bonds, after which they break. This causes the chromophore substance to become a lighter colored compound [16].

New studies have shown that during tooth bleaching process can result increased tooth sensitivity, changes in the microstructure of teeth and in the same time whitening gels can react chemically with composite restorations, glass ionomer cements, sealing materials and ceramic crowns, thus reducing their durability [16].

Other studies have shown that composite resin restorations are susceptible to unacceptable color changes, even when using OTC home systems [17].

Admira fusion is a nano-hybrid restoration material based on Ormocer technology (organically modified ceramics), which has been used instead of the classical matrix consisting of large and pre condensed molecules from an inorganic matrix with a high degree of crosslinking with the property of low shrinkage during light curing [18]. For this reason, the Admira fusion composite does not contain classical monomers, such as bisphenol A-glycidyl methacrylate, triethylene glycol dimethacrylate or hydroxyethyl methacrylate, thus eliminating the possibility of their release after polymerization and making the material more biocompatible. Recent study has proven that small dimensions of nano-filled composite resins may present low staining awareness [19, 20]. Also, Ayad has proven in a study that Ormocer based composite resins have undoubtedly a lower color sensitivity [21].

In literature, numerous studies [22],[13] have shown that the structure of the composite resin and its particle characteristics have a direct impact on the susceptibility to extrinsic staining. Furthermore, it has been shown that composite resins can undergo superficial and structural alterations, caused by mastication or various finishing and polishing processes [23-25]. The conclusion of the study was that carbamide peroxide was responsible for removing the dyes on the surfaces of the study specimens. It is known that during the tooth bleaching process, the active agents can penetrate the enamel and dentine, oxidizing the chromophore molecules. Some studies have indicated that surface bleaching of composite resins after bleaching was probably due to superficial cleaning of the samples, not necessarily to the intrinsic color change [26]. Therefore, after bleaching, the color of the composite resin restoration does not always match the color of the neighboring dental structures.

Recent research concerns raise the attention on the effects of natural herbal extracts. Numerous studies have indicated the anticancer, antibacterial and antioxidant effects of different plant extracts [27-29]. In addition, herbal products are non-cytotoxic, easily accessible, with a long shelf life [30].

It is known that the application of antioxidants after bleaching has beneficial effects on the adverse reactions following this therapeutic procedure. One such oxidant is green tea extract, due to its flavonoid content

[31, 32]. Thus a lot of studies have shown that green tea extract has the ability to neutralize free radicals and through this, it balance the oxidative stress from some diseases [31-33].

In a research, Khamverdi et al have proven that using green tea extract on teeth after bleaching with carbamide peroxide gels, might counterbalance the oxygen free radicals, responsible for altering the adhesion of composite resin restorations [30].

Some studies have demonstrated that alcoholic green tea extract has the most important antioxidant effect from some previously studied leafy herbal extracts [34,35].

Weber et al. have confirmed in analyze that due to their antioxidant power some herbal extracts can offer an innovative path to the prophylaxis of tooth erosions [36].

In another research, it was shown that noni juice can be a good alternative to sodium hypochlorite for endodontic irrigation and that it can successfully remove the root canal smear layer [37].

A recent study, regarding the bone loss in peri-implantitis, has demonstrated that this process can be the consequence of an oxidative stress and treating peri-implantitis with antioxidant herbal extract therapy can be a good choice [38].

Previous investigations have proven that triphala, a mix of equal proportion of three herbs has chelating action, removing the root canal smear layer [39 - 43].

Nowadays, it is a huge tendency of using plant extracts medicines due to their numerous, concomitant actions and very limited negative side effects and they can provide a good alternative to chemically synthetic therapy [44].

CONCLUSIONS

The results of the total color modification ΔE , after staining show values greater than 3 for all the groups studied, so the staining process was efficient in the whole study group.

After the bleaching process, the most significant color change was recorded by the group GO, bleached with Opalescence, while the GE experimental group recorded lower ΔE values, proving the antioxidant capacity of the green tea extract. However, in both cases $\Delta E_3 > 3$, so the color change was detectable with the naked eye.

EXPERIMENTAL SECTION

Specimen's preparation

The twenty-eight composite blocks with the size of 5mmx5mmx5mm were prepared from Admira fusion, a nano-hybrid composite resin (VocoGmbH, Cuxhaven, Germany). Silicone conformers (Elite HD putty, Zhemack SpA, Badia Polesine, Italy) were made, in which the composite blocks were constructed according to manufacturer's protocol.

Staining protocol

The entire group of composite blocks was subjected to a staining process, being immersed in coffee solution for 8 hours / day, for 3 consecutive days. The coffee solution was prepared in the Saeco Pico Baristo machine in espresso mode, using 5 grams of Lavazza coffee (Luigi Lavazza SpA, Turin, Italy) in 100 ml of water. Freshly prepared coffee solution was used at each session. During this procedure, the blocks were kept immersed in artificial saliva at 37°C.

Bleaching protocol

The bleaching protocol aimed to simulate a home-use bleaching treatment, using individualized trays. Thus, 16% carbamide peroxide bleaching gel (Opalescence, Ultradent Products, South Jordan, UT, USA) was applied to the GO group 6 hours/day for 7 consecutive days. Study group GE was bleached with the experimental gel for 6 hours / day for 7 consecutive days. At the end of each bleaching step, the blocks were rinsed for 60 seconds in water and then stored in artificial saliva at 37°C.

Experimental bleaching gel preparation

The green tea based experimental extract was prepared at the "Raluca Ripan" Chemistry Institute of Babes-Bolyai University, Cluj-Napoca as follows: 20 g of green tea leaves were added to 200 ml of boiled distilled water (R.Twining and Company Limited, London, UK). The extract solution was left to infuse for 10 minutes. The obtained product was filtered to remove possible impurities and was stored in sterile containers at 4°C for later use. To obtain the experimental bleaching gel, the extract solution was used, to which carbamide peroxide, polyethylene glycol and silicon dioxide were added according to the formula: 100 g experimental bleaching gel contains: 22.2 g polyethylene glycol, 7.7 g silicon dioxide, 16 g carbamide peroxide and 54,1 g green tea extract.

Color measurement

Measurement of color parameters was performed using the Vita EasyShade Advance 4.0 spectrophotometer (Vita zahnfabrik, Bad Säckingen, Germany). The measurements were made in the CIE $L^*a^*b^*$ global mode and aimed to determine the color parameters L_1 (brightness), a_1 (the chromatic parameter in the red-green axis) and b_1 (the chromatic parameter in the yellow-blue axis) for the initial situation, L_2 , a_2 , b_2 and ΔE_1 after the staining process and parameters L_3 , a_3 , b_3 and ΔE_2 after bleaching procedure. For each unit and each situation, three measurements were made, among which an arithmetic mean was calculated.

The measurements were used to calculate the color difference, according to the formula:

$$\Delta E_{ab}^* = \sqrt{(L_2^* - L_1^*)^2 + (a_2^* - a_1^*)^2 + (b_2^* - b_1^*)^2}$$

The SPSS software package version 21.0 (SPSS Inc., Chicago, USA) was used for statistical analysis and graphical representations. The acceptable error threshold was $\alpha=0.05$. In order to describe the continuous quantitative data with, we used the arithmetic mean and the standard deviation (SD). The Kruskal-Wallis ANOVA was used to test the differences in the investigated independent groups. The Mann-Whitney test was used in post-hoc analysis when significant differences were identified by Kruskal-Wallis ANOVA test. The Wilcoxon Signed Rank test was used to test the differences in the paired groups.

ACKNOWLEDGMENTS

We thank our contributors from Composite Materials Laboratory, part of Babes- Bolyai University - Raluca Ripan Chemistry Research Institute, who provided insight and expertise that greatly assisted the research.

REFERENCES

1. V.B. Haywood, H.O. Heymann, "Nightguard vital bleaching", *Quintessence Int.* **1989**, *20*,173-176.
2. D.C. Mada, C. Gasparik, M. Moldovan, C.S. Miron-Borzan, A.I. Irimie, D. Cornea, D.I. Dudea, R.S. Campian. *Stud. UBB Chem.*, **2016**, *1*, 43-52.
3. E.J. Jr Swift, J. Perdigão, H.O. Heymann, A.. Jr Wilder, S.C. Bayne, K.N. Jr May, J.R. Sturdevant, T.M. Roberson. *J. Dent.*, **2001**, *29*,1-6.

4. A.F. Reis, M. Giannini, J.R. Lovadino, G.M. Ambrosano, *Dent. Mater.*, **2003**, 19,12-18.
5. D.A. Prodan, C. Gasparik, D.C. Mada, V. Miclaus, M. Baciut, D. Dudea, *Clin. Oral Invest.*, **2015**, 1, 867-875.
6. D.C. Mada, C. Gasparik, A.I. Irimie, M.D. Mada, D. Dudea, R.S. Campian. *Clujul Med.*, **2018**, 91(2), 222-228.
7. M. Valko, C. Rhodes, J. Moncol, M.M. Izakovic, M. Mazur, *Chem.-Biol. Interact.* **2006**, 160(1),1-40.
8. W.H. Koppenol. *Redox Report.* **2001**,6(4), 229-234.
9. NP82 CO. SCIENTIFIC COMMITTEE ON CONSUMER PRODUCTS SCCP.
10. J.A. Rodrigues, G.P.F. Oliveira, C.M. Amaral, *Braz. Oral. Res.*, **2007**, 21, 170-175.
11. G. Kugel, S. Ferreira, J. Mass. *Dent. Soc.*, **2005**, 53, 34.
12. R. Beltrami, M. Ceci, G. De Pani, L. Vialba, R. Federico, C. Poggio, M. Colombo, *Eur. J. Dent.* **2018**, 12, 49.
13. C. Poggio, R. Beltrami, A. Scribante, M. Colombo, M. Chiesa, *Dent. Res. J. (Isfahan)* **2012**, 9, 567-573.
14. A.H. Brook, R.N. Smith, D.J. Lath. *Int. Dent. J.* **2007**, 57, 324-330.
15. S.R. Kwon, P.W. Wertz. *J. Esthet. Restor. Dent.* **2015**, 27, 240-257.
16. C.M. Carey, *J. Evid.-Based Dent. Pr.* **2014**, 14, 70-76.
17. S. Kurtulmus-Yilmaz, E. Cengiz, N. Ulusoy, S.T. Ozak, E. Yuksel, *J. Dent.* **2013**, 41, e70-75.
18. S. Kalra, A. Singh, M. Gupta, V. Chadha, *Cont. Clin. Dent.* **2012**, 3, 48-53.
19. I. Nasim, P. Neelakantan, R. Sujeer, C. V. Subbarao et al. *J Dent.* **2010**, 38, 137-143.
20. C. Poggio, M. Ceci, R. Beltrami, M. Mirando, J. Wassim, M. Colombo, *Acta Biomater. Odontol. Scand.* **2016**, 2, 95-101.
21. N.M. Ayad. *Eur. J. Esthet. Dent.* **2007**, 2, 236-247.
22. C. Poggio, L. Vialba, A. Berardengo, R. Federico, M. Colombo, R. Beltrami, A. Scribante, *J. Funct. Biomater.* **2017**, 26, 1-8.
23. P.P. Garcia, N.E. Rodrigues, P.A. Santos, J.Á. Campos, R. G.Dibb, *Mater. Research.* **2008**, 11, 193-197.
24. R.P. Ramos, D.T. Chimello, M.A. Chinelatti, R.G. Dibb, J. Mondelli, *Oper. Dent.* **2000**, 25, 448-453.
25. I. Nasim, P. Neelakantan, R. Sujeer, C. V. Subbarao. *J. Dent.*, **2010**, 38, e137-142.
26. P. Villalta, H. Lu, Z. Okte, F. Garcia-Godoy, J. M. Powers, *J. Prosthet. Dent.*, **2006**, 95, 137-142.
27. S. Vidhya, S. Srinivasulu, M. Sujatha, S. Mahalaxmi, *Oper. Ddent.*, **2011**, 36, 433-438.
28. M. Türkün, A.D. Kaya, *J. Oral Rehabil.*, **2004**, 31, 1184-1191.
29. Z. Khamverdi, L. Rezaei-Soufi, S. Kasraei, N. Ronasi, S. Rostami, *Restor. Dent. Endod.*, **2013**, 38, 241-247.
30. Z. Khamverdi, P. Khadem, A. Soltanian, M. Azizi, *J. Dent.(Tehran, Iran).* **2016**, 13, 244-251.

31. J. Bornhoeft, D. Castaneda, T. Nemoseck, P. Wang, S.M. Henning, M.Y. Hong, *J. Med. Food.*, **2012**, *15*, 726-732.
32. A.M. Van Nederkassel, M. Daszykowski, D.L. Massart, Y. Vander Heyden, *J. Chromatogr. A*, **2005**, *1096*, 177-186.
33. T. Yokozawa, J.S. Noh, C.H. Park, *Evid.-Based Complementary Altern. Med.*, **2012**, *2012*, 845917.
34. J. Patil, A. Reddy, B.S. Venigalla, K. Shekar, C. Ravichandra, D. Binoy, *Endodontol.*, **2015**, *27*, 129.
35. J. Oh, H. Jo, A.R. Cho, S.J. Kim, J. Han, *Food control*. **2013**, *31*, 403-409.
36. M.T. Weber, M. Hannig, S. Pötschke, F. Höhne, C. Hannig, *Caries Res.*, **2015**, *49*, 477-487.
37. N. Jain, Y.C. Rajwar, M. Batra, H.P. Singh, R. Bhandari, P. Agarwal, *Sch. J. Appl. Med. Sci.*, **2014**, *2*, 253-257.
38. S. Aksakalli, *Dent.*, **2013**, *4*, 1-3.
39. M. Seal, R. Rishi, G. Satish, K.T. Divya, P. Talukdar, R. Maniyar, *J. Int. Soc. Prev. Community Dent*. **2016**, *6*, 105-109.
40. M. Pujar, S.D. Makandar, *Int. J. Contemp. Dent. Med*. **2011**, *2*, 34-37.
41. S. Prakash, A.U. Shelke, *J. Indian Soc. Periodont.*, **2014**, *18*, 132-135.
42. S. Kamat, K. Rajeev, P. Saraf, *Endodontol.*, **2011**, *23*, 98-101.
43. V. Agrawal, S. Kapoor, I. Agrawal, *J. Diet. Suppl.*, **2017**, *14*, 229-240.

REMINERALIZATION PRODUCTS EFFECT ON HUMAN ENAMEL IN VITRO STUDY

LAURA SILAGHI-DUMITRESCU^a, ANA MARIA MIHĂILESCU^c,
ALEXANDRINA MUNTEAN^{b*}, CODRUTA SAROSI^a,
DOINA PRODAN^a, MEDA ROMANA SIMU^b, MARIOARA MOLDOVAN^a,
ANDREA KUI^d, MIHAELA PASTRAV^b

ABSTRACT. The aim of this in vitro study was to assess the remineralization process of human enamel, using two commercial pastes (containing calcium, phosphates, hydroxyl-apatite and sodium fluoride) and an experimental gel (obtained from fruit extract). 40 caries free extracted human teeth were divided into 4 groups: 3 study groups (n=12), and 1 control group (n=4). For the study groups, the remineralization agent differed: GC Tooth Mousse, Recaldent, Remin Pro (Voco) and an experimental gel made by “Raluca Ripan” Chemistry Institute (Cluj Napoca, Romania). ATR-FTIR (Jasco-610, Japan) was employed to verify the protective effect of the remineralizing products on enamel. UV-Vis spectra were used to determine mineral loss and gain during demineralization-remineralization process. No significant statistic difference emerged between specimens in study groups and the specimens in control group. Under the limitations of the in vitro study, the application of the tested product proved to be effective on enamel remineralization.

Keywords: *remineralization, enamel, mineral deficiency*

^a Babes Bolyai University, “Raluca Ripan” Institute for Research in Chemistry 30 Fântânele street, RO-400294

^b Iuliu Hațieganu University of Medicine and Pharmacy, Paediatric Dentistry Department, 31 A. Iancu street, RO-400083

^c Iuliu Hațieganu University of Medicine and Pharmacy, Department of Oral Rehabilitation, Health and Management, 15 V. Babes street, RO-400012

^d Iuliu Hațieganu University of Medicine and Pharmacy, Department of Dental Prosthetics, 31 Clinicilor street, RO-400006.

* Corresponding author: andaorto@yahoo.com

INTRODUCTION

Dental enamel is composed of 96% inorganic material and 4% organic material and water. The inorganic component, morphologically, arranged in the form of densely packed rods or prisms consist on millions of hydroxyapatite crystals. Enamel's organic matrix contains 35-40% insoluble fractions - like aminoacids, organized in polypeptides chains. The characteristics of these proteins resemble in some directions with collagen and keratin. The rest of 60-65% of the organic martix consists on soluble proteins (15%), other peptides (25%), citric acid (20%) and glycoproteins (5%) [1].

The enamel's water (about 97% of it) is attached to the protein molecules; extremely low quantity of water can be found inside the inter-prismatic spaces of hydroxyl-apatite's, especially near the enamel-dentine junction [2].

The biomineralization of enamel is a complex process through which the extracellular matrix proteins (like amelogenin) mediate the production of hydroxyapatite crystals (starting from calcium and phosphates). This process of biomineralization induced and controlled by intracellular and extracellular matrix, allowed the inorganic ions to attach to a biological structure. The biological structure (made from anionic macromolecules represented by phospholipids, glycoproteins and phosphoproteins) acts like a frame of extracellular and intracellular matrix on which inorganic elements will deposit [3,4].

A prolonged exposure of the dental enamel to acids derived from juices (citric acid, phosphoric acid, carbonic acid) can lead to dental erosion and demineralization of the hard tissues. On the other hand, according to the literature, the biomineralization of dental enamel with different materials - like bio-active glasses, collagen, different phosphate and calcium resin-based cements or calcium silicate cements - may be used to achieve mineral gain of hard dental tissues [5,6,7]

The current study was designed to compare the remineralization process of human enamel, using two commercial pastes (containing calcium, phosphates, hydroxyl-apatite and sodium fluoride) and an experimental gel (obtained from fruit extract).

RESULTS AND DISCUSSION

For the human teeth from control group (stored in artificial saliva – AS), evaluated at 7 and 20 days, no modification regarding dental enamel structure emerge. (Fig.1)

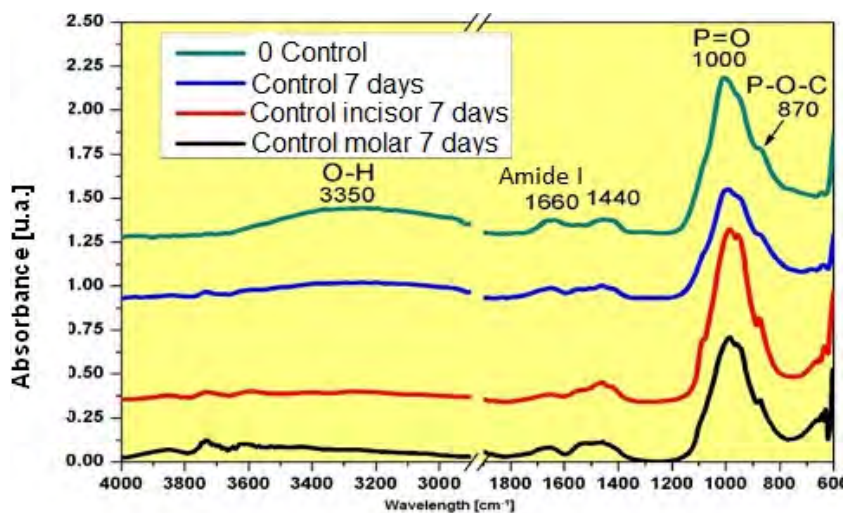


Figure 1. The absorption spectra in ATR-FTIR for human teeth immersed in AS for 7 days

GC Tooth Mousse© (Recaldent) was the agent to remineralize the teeth included in the first study group. Teeth demineralized with citric acid did not reveal statistically significant differences after demineralization-remineralization protocol. (Fig. 2-a)

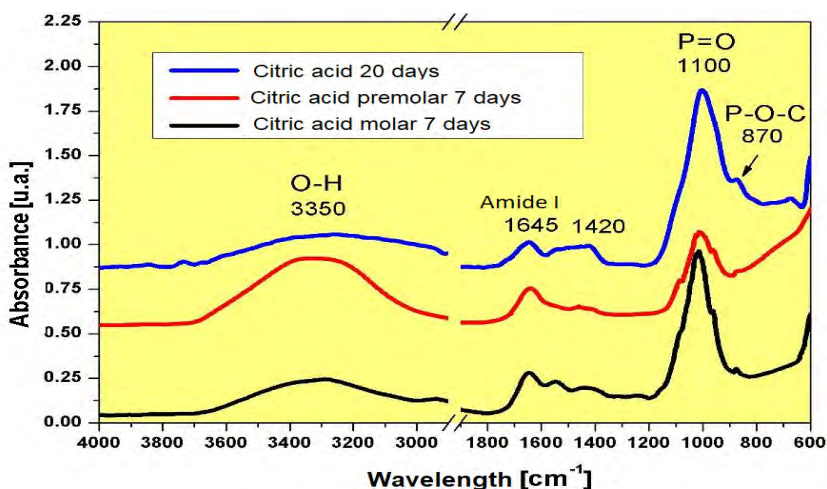


Figure 2-a. The absorption ATR-FTIR spectra for human teeth in first study group (after demineralization and remineralization with GC Tooth Mousse© (Recaldent))

No significant statistic difference emerged between specimens in study group 1 demineralized with Coca Cola solution and remineralized with GC Tooth Mousse© (Recaldent) and the specimens in control group. (Fig. 2-b)

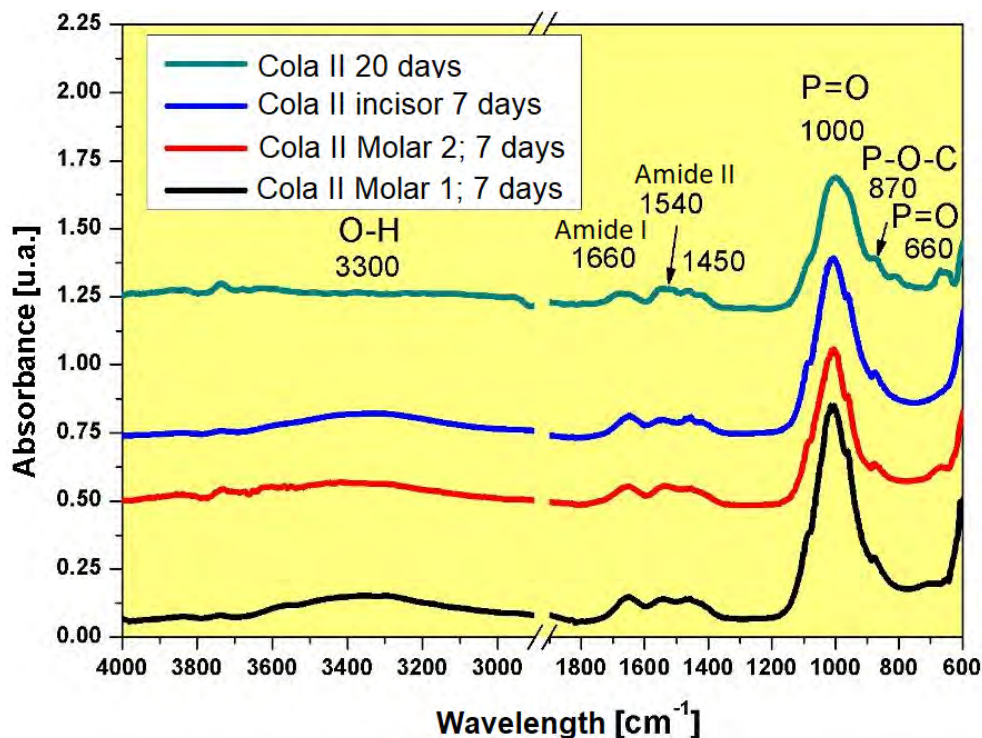


Figure 2-b. The absorption spectra in ATR-FTIR of human teeth de-mineralized in Coca Cola solution and remineralized with commercial tooth paste GC Tooth Mousse© (Recaldent)

For the study group 2, for the remineralization processes another commercial available paste with hydroxyapatite and sodium fluoride has been used (Remin Pro© - Voco). The differences were not statistically significant when compared with the teeth in control group. (Fig. 3a, 3b)

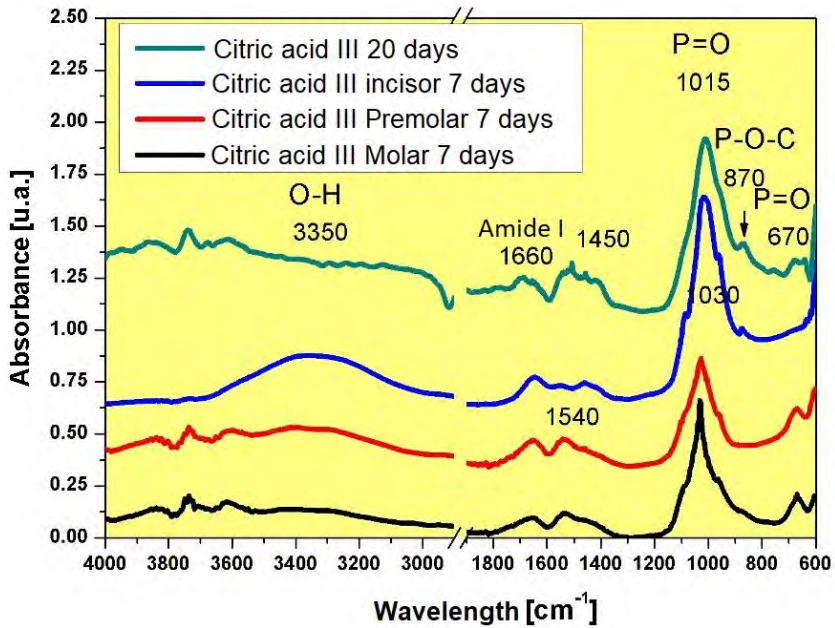


Figure 3-a. Absorption spectra in ATR-FTIR for human teeth demineralized with citric acid solution and remineralized with Remin Pro© (Voco)

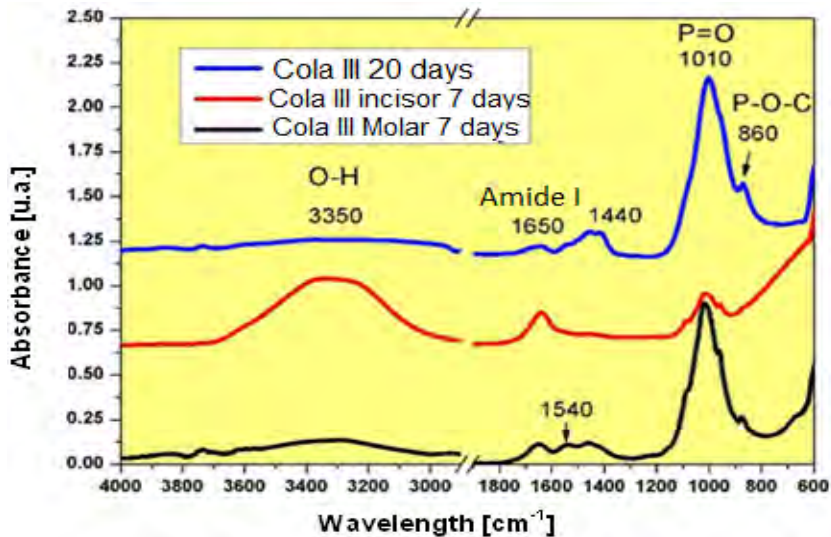


Figure 3-b. The absorption spectra in ATR-FTIR of human teeth demineralized in Coca Cola solution and remineralized with Remin Pro – Voco paste

For the study group 3, teeth were demineralized using the same protocol other than the remineralization process was performed with an experimental gel made by the “Raluca Ripan” Chemistry Institute, Cluj Napoca (Fig. 4-a and 4-b). The experimental gel (G29), incorporate: colloidal silica/ hydroxyapatite/ hydroxyapatite with zinc oxide = 1:2:3; lyophilized concentrate from pineapple and quince; vegetal pectin = 4-6 g; at pH = 7.5-8.

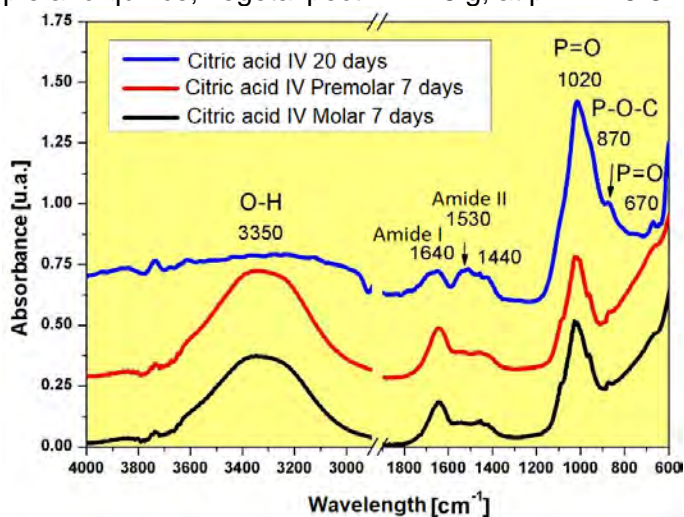


Figure 4-a. The absorption spectra in ATR-FTIR of human teeth demineralized in citric acid and remineralized with experimental gel G29

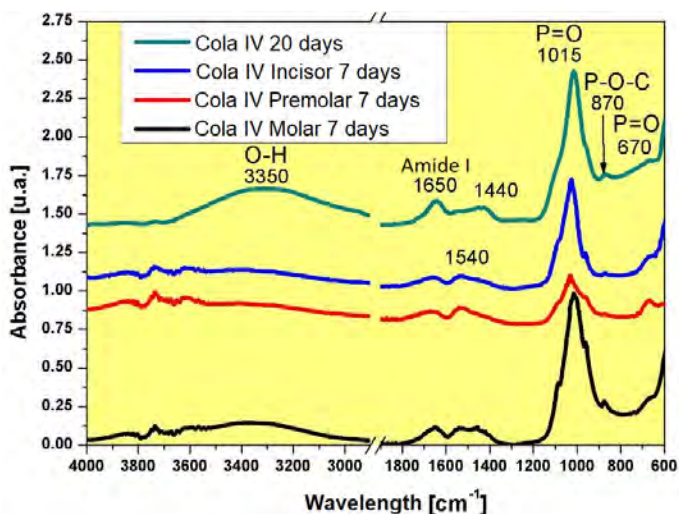


Figure 4-b. The absorption spectra ATR-FTIR of the human teeth demineralized with Coca Cola solution and remineralized with the experimental gel G29.

UV-Vis recordings were made in the 400-900 nm range, on human enamel samples, before / after demineralization and after remineralization. The spectra were used to determine mineral loss and gain during demineralization – remineralization process. (Fig. 5, 6).

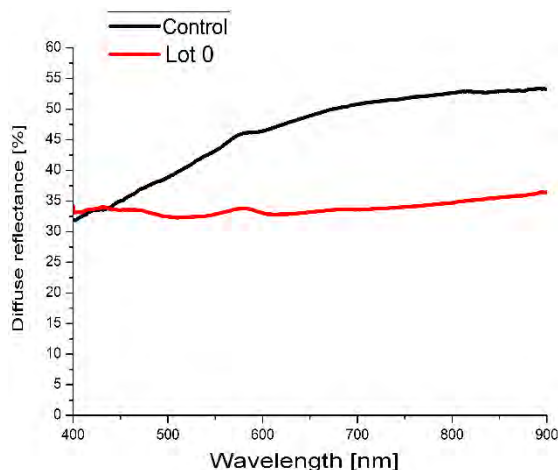


Figure 5. UV-VIS reflexion spectra for control group (enamel untreated) and Lot 0 (enamel demineralized)

In figure 5 is showed a decrease of diffuse reflectance after tooth demineralization (group 0), compared with the control of the sample.

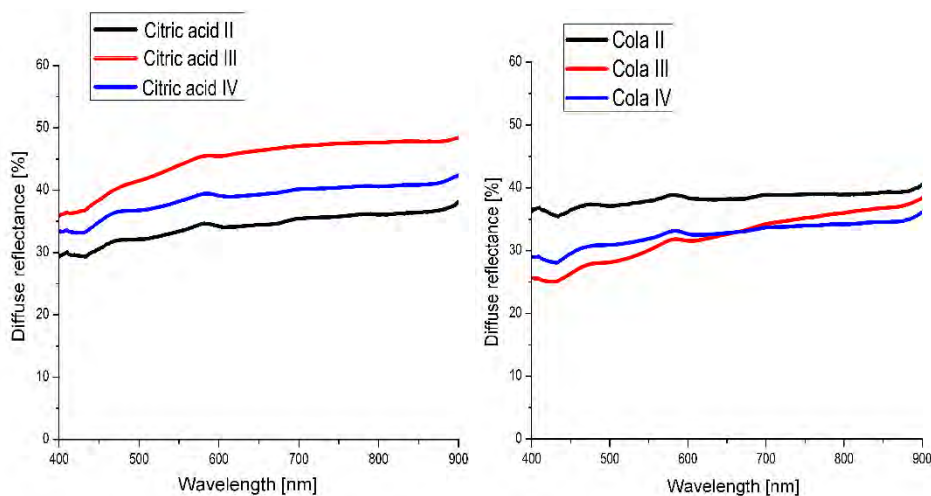


Figure 6. UV-VIS reflexion spectra for teeth demineralized in citric acid and Cola, remineralized with GC Tooth Mousse© (II), Remin Pro© (III) and experimental gel (IV)

Figures 6 show the diffused reflectance of the teeth from group 0, after the remineralization with commercial toothpaste, respectively the experimental gel. The decrease of the reflectance during the demineralization and its increase after the remineralization is the result of continuous changes of the crystals on the enamel surface during these processes.

According to the specialized literature, based on the optical diffusion properties, the demineralization processes of the teeth can be analyzed quantitatively and qualitatively, the color parameters and the translucency can be determined. The possible advantages of using optical methods of analysis in the field of dental medicine are related to the simplicity of the method of analysis in view of the fact that it is a non-destructive method, which involves relatively low costs, and the analysis can be performed without the need for direct contact with the dental tissue. Based on these optical analyzes, the demineralization processes of the teeth can be detected in early stages

The demineralization process can be discontinued by providing a suitable environment for remineralization by means of different remineralizing agents. If demineralization exceeds the self-regulated remineralization, excessive loss of mineral content may take place, endangering the integrity of the tooth [8, 9].

The early stages of demineralisation involve a softening of the enamel surface to a depth of the order of 1-10 microns. Many studies were developed to understand the process of enamel demineralization at the very beginning, in order to appreciate if these early stages are reversible [10]. Saliva provides protective effects by neutralizing and cleaning the acids; it is a source of inorganic ions necessary for the remineralization process. Enamel has no spontaneous capability to repair when affected by specific dental pathologies such as caries, abrasions or fractures because it contains no cells [11, 12].

The results of previous studies have suggested that an IR peak near 1015 cm^{-1} is indicative of acid-induced alteration of the atomic bonding in superficial enamel apatite [13, 14, 15].

The mineral in dental enamel is a calcium-deficient carbonated HAP containing fluoride. A simplified formula for tooth mineral composition is $\text{Ca}_{10-x}\text{Na}_x(\text{PO}_4)_6 - y(\text{CO}_3)z(\text{OH})_2 - u\text{Fu}$; thus, enamel differs from 'stoichiometric' HAP, which has the formula $(\text{Ca}_{10}(\text{PO}_4)_6(\text{OH})_2)$ [12,14]. The ATR-FTIR spectrum of the enamel surface (Figure 1a) was consistent with the results obtained in previous studies. A very strong peak was observed at $\sim 1015\text{ cm}^{-1}$, which was attributed to the phosphate (PO_4) anti-symmetric stretching mode (ν_3). The phosphate symmetric stretching mode ($\nu_1\text{ PO}_4$) appeared at $\sim 962\text{ cm}^{-1}$. Strong peaks assigned to B-type carbonate substitution (carbonate substitution for the phosphate ion) were observed at 872 cm^{-1} ($\nu_2\text{ CO}_3$) and at

1405 and 1450 cm^{-1} , respectively ($\nu_3 \text{CO}_3$).²⁹ Substitutions (especially by carbonate) in the mineral crystal lattice weaken enamel structure, rendering the mineral more acid-soluble than HAp [16, 17, 18].

In Figure 1, ATR-FTIR spectra for the teeth in control group, all representative spectra recorded in the region of 800 – 1180 cm^{-1} presented the specific hydroxyapatite bands, respectively the vibration bands P=O assigned to the phosphate (PO_4^{3-}) at 1100-1000 cm^{-1} , accompanied by a secondary vibration band at 870 cm^{-1} specific also for P-O-C of hydroxyapatites. Maximum absorption rates at 1650 cm^{-1} , 1540 cm^{-1} and 1450 cm^{-1} can be assigned to amide I and amide II bands from the proteins found the enamel structure, with C=O and N-H vibrations. In addition, another large absorption band detected at 3700-3000 cm^{-1} was assigned to hydroxyl group (O-H) with a secondary band at 1640 cm^{-1} , which may overlap over amine I bands [19, 20].

For the specimens in control group, analysed at 7 and 20 days, we did not notice modification regarding dental structure, in accordance with the data found in literature [13, 16].

When compared the specimens spectra from study group 1 (teeth remineralized with GC Tooth Mousse®), with the specimens in control group, we notice at 7 and 20 days, increased values for hydroxyl bands at 3350 cm^{-1} and 1630 cm^{-1} while for the amide I bands from 1440 cm^{-1} the absorption has the tendency to decrease. A possible explanation of the phenomena resides in water content of hydroxyapatite.

The casein phosphopeptide-amorphous calcium phosphate technology developed based on the alleviating properties of milk and salivary proteins. The casein phosphopeptides allow high concentrations of calcium, phosphate, and fluoride ions that stabilized in solution, in a bioavailable form for the promotion of remineralization [19, 21].

In our study, we noticed a displacement through wider vibration bands of the maximum absorption values, due to the interactions between calcium and phosphate (contained in enamel and the remineralization paste).

No significant statistical difference emerged between specimens in first study group, unconcerned demineralizing solutions and the specimens in control group.

For the second study group, the demineralization protocol respects the algorithm presented for study group 1, but for remineralization we used Remin Pro®, a commercial paste having hydroxyapatites and sodium fluoride in composition.

When compared demineralization (with citric acid solution) spectra and remineralization (with Remin Pro®) spectra, phosphate bands were detected increased for the study group specimens. This aspect is in accordance with

data found in the literature, because it indicates an increasing degree of mineralization of the hydroxyapatites groups from enamel structure. No significant statistic difference between specimens in second study group and the specimens in control group was notice [10, 22].

For the third study group, teeth were de-mineralized applying the same protocol as for the first two study groups, but in the remineralization process we used an experimental gel made by the Institute of Chemistry "Raluca Ripan" Cluj Napoca. The vibration observed was characteristic for hydroxyapatites and amelogenin proteins from the enamel, but with no significant statistical difference compared with the specimens from the control group.

The basic principle of remineralization is by advocating a biological or non-invasive approach rather than the surgical approach for early enamel lesions. The demineralization – remineralization cycles occur throughout the lifetime, which attributes to the limited reparability of the enamel by mineral gain [23].

As the study is limited to *in vitro* conditions, further clinical trials are required to assess the remineralization potential of various products. The influence of saliva and plaque/pellicle on enamel was not addressed in this study [24]. In addition, dental plaque/pellicle may provide a significant level of enamel protection against demineralization generated by acidic beverages.

CONCLUSIONS

Under the limitations of the present *in vitro* study, the application of the tested product proved to be effective on initiated/ preventing enamel demineralization. Enamel softened by acidic beverages can re-harden following exposure to selected products by simple application of tested gels.

EXPERIMENTAL SECTION

40 caries free extracted human teeth, obtained under a protocol approved by the University's Ethics Committee (decision nr.221/17.05.2017), were divided into 4 groups. Study groups included teeth from anterior and lateral sector of dental arch, extracted for orthodontic or periodontal purposes.

Exclusion criteria for teeth were as follows:

- Teeth with cracks or discoloration;
- Teeth with enamel hypoplasia or any other developmental anomalies;
- Teeth procured from a patient suffering from transmissible or systemic conditions affecting hard tissues.

After the extraction, teeth were cleansed of soft tissue and debris inspected for cracks, hypoplasia and white spot lesions; they were disinfected in 5.25% sodium hypochlorite solution for one hour and stored in artificial saliva until used.

Teeth were randomly divided into 3 study groups (n=12), and 1 control group (n=4). Teeth from each study group were prepared for the demineralization - remineralization process. For demineralization, teeth were immersed in 10 ml 0.1% citric acid solution (n=6) and in Coca-Cola solution (n=6). Demineralization procedure: 20 minutes in demineralizing solution, 3 times a day, for 20 days.

After demineralizing, a remineralization product was applied on every tooth. Between demineralization/remineralization procedures, teeth were kept in artificial saliva (AS) at 37°C until next day.

For the study groups (3), the remineralization agent differed, as follows:

Group II - a commercial remineralization tooth-paste GC Tooth Mousse© (Recaldent);

Group III - Remin Pro© (Voco),

Group IV - an experimental gel (G29) made by the “Raluca Ripan” Chemistry Institute, Cluj Napoca, Romania, based on natural ingredients. The experimental gel G29 contains: colloidal silica/ hydroxyapatite/ hydroxyapatite with zinc oxide = 1:2:3, lyophilized concentrate from pineapple and quince, vegetal pectin = 4-6 g, pH = 7.5-8.

The remineralizing products were applied neat onto the surface of the teeth, without brushing, for 3 min, and then washed with distilled water and store in artificial saliva (AS).

Teeth from control group were immersed in AS at 37°C for 20 days. AS, with a pH of 7.4, contained 1.5 mmol/l CaCl₂, 50 mmol/l KCl, and 20 mmol/l Tris - tris(hydroxymethyl)aminomethane.

ATR-FTIR spectroscopy

In the present in vitro study, ATR-FTIR (Attenuated Total Reflection Fourier Transform Infrared Spectroscopy) (Jasco-610, Japan) was used to verify the protective effect of the remineralizing products on enamel exposed to the demineralizing solutions. The specimens were analysed at 7 days and 20 days of demineralization-remineralization process.

All the representative spectra recorded in the region of 800-1800 cm⁻¹ (at 4 cm) showed phosphate bands representative of mineral components. The phosphate bands increased during the seven-day period in the BG group. Increased phosphate peaks were also observed in the BG group after 14 and 21 days.

UV-Vis spectroscopy

Spectra were collected in the range of 400–900 nm, using UV-Vis Lambda 35 spectrometer, equipment with integrated sphere and 0° geometric configuration, was measured diffuse reflectance. Each specimen was analysed in 3 different positions before and after treatment.

REFERENCES

1. L. Chen, K. Liang, J. Li, D. Wu, X. Zhou, J. Li, *Arch Oral Biol*, **2013**, *58*, 975-980.
2. T. Leventouri, A. Antonakos, A. Kyriacou, *Int J Biomater*, **2009**, *2009*, 698547.
3. Z. Wang, T. Jiang, S. Sauro, Y. Wang, I. Thompson, T.F. Watson, Y. Sa, W. Xing, Y. Shen, M. Haapasalo, *J Dent*, **2011**, *39*, 746-756.
4. L. Gu, J. Kim, Y.K. Kim, Y. Liu, S.H. Dickens, D.H. Pashley, L. Jun-qi, R.T. Franklin, *Dent. Mater.*, **2010**, *26*, 1077-1089.
5. I.C. Fort, G. Turdean, R. Barabas, D. Popa, A. Ispas, M. Constantiniuc, *Stud UBB Chem*, **2019**, *1*, 125-133.
6. D. Skrtic, J.M. Antonucci, E.D. Eanes, *J Res Natl Inst Stand Technol*, **2003**, *108*, 167-182.
7. M.G. Gandolfi, P. Taddei, F. Siboni, E. Modena, E. Dorigo De Stefano, C. Prati, *Dent Mater*, **2011**, *27*, 1055-1069.
8. T. Narongdej, R. Sakolnamarka, T. Boonroung, *J Am Dent Assoc*, **2010**, *141*, 995-999.
9. A.P. Forsback, S. Areva, J.I. Salonen, *Acta Odontol Scand*, **2004**, *62*, 14-20.
10. Y. Fan, J.R. Nelson, J.R. Alvarez, J. Hagan, A. Berrier, X. Xu, *Acta Biomater*, **2011**, *7*, 2293-2302.
11. A. Lussi, E. Hellwig, D. Zero, T. Jaeggi, *Am J Dent*, **2006**, *19*, 319-325.
12. M. Oshiro, K. Yamaguchi, T. Takamizawa, H. Inage, T. Watanabe, A. Irokawa, S. Andro, M. Miyazaki, *J Oral Sci*, **2007**, *49*, 115-120.
13. X. Wang, A. Klocke, B. Mihailova, L. Tosheva, U. Bismayer, *J. Phys. Chem. B*, **2008**, *112*, 8840.
14. X. Hu, Y. Peng, C.P. Sum, J. Ling, *J Endod*, **2010**, *36*, 2008-2011.
15. X. Wang, B. Mihailova, A. Klocke, U. E. Fittschen, S. Heidrich, M. Hill, R. Stosch, B. Guttler, J.A. Broekaert, U. Bismayer, *J Biomed Mater Res A*, **2009**, *88*, 195-204.
16. H. Eimar, E. Ghadimi, B. Marelli, H. Vali, S.N. Nazhat, W.M. Amin, J. Torres, O. Ciobanu, R.F. Albuquerque Junior, F. Tamimi, *Acta Biomater*, **2012**, *8*, 3400-3410.
17. J. Reyes-Gasga, E.L. Martínez-Piñeiro, G. Rodríguez-Álvarez, G.E. Tiznado-Orozco, R. Garcia-Garcia, E.F. Bre, *Mater Sci Eng C*, **2013**, *33*, 4568-4574.
18. C. Xu, R. Reed, J.P. Gorski, Y. Wang, M.P. Walker, *J Mater Sci*, **2012**, *47*, 8035-8043.

19. M. Selimovic-Dragas, L. Hasic-Brankovic, F. Korac, N. Đapo, A. Huseinbegovic, S. Kobaslija, M. Lekic, S. Hatibovic-Kofman, *Bosn J Basic Med Sci*, **2013**, *13*, 197-202.
20. D. Sucala, C. Sarosi, Catalin Popa, I. Cojocaru, M. Moldovan, G.A. Mohan, *Stud UBB Chem*, **2018**, *2*, 71-81.
21. G.M. Hassan, E. Aboelezz, A. El-Khodary, H.M. Eissa, *Nucl Instrum Methods Phys Res*, **2010**, *268*, 2329-2336.
22. J.A. Cury, L.M.A. Tenuta, *Braz Oral Res*, **2009**, *23*, 23-30.
23. B. Culic, C. Gasparik, M. Varvara, C. Culic, C. Dragos, L. Silaghi-Dumitrescu, D. Dudea, *Stud UBB Chem*, **2017**, *1*, 61-71.
24. S.S. Narayana, V.K. Deepa, S. Ahamed, E.S. Sathish, R. Meyappan, K.S. Satheesh Kumar, *J Indian Soc Pedod Prev Dent*, 2014, *32*, 19-25.

MULTIVARIATE CALIBRATION METHOD FOR SIMULTANEOUS ESTIMATION OF FLUOCORTOLONE CAPROATE, FLUOCORTOLONE PIVALATE AND CINCHOCAINE HCL IN SUPPOSITORY

ÖZLEM AKSU DÖNMEZ^a

ABSTRACT. In this paper, the simultaneous quantitative assay of Fluocortolone caproate (FCC), Fluocortolone pivalate (FCP) and Cinchocaine HCl (CIN) in suppository has been reported as a simple alternative analytical method. A partial least squares (PLS-2) regression was used for resolution of the overlapped spectrophotometric signals from mixtures of the three drugs. A calibration set containing FCC, FCP and CIN was constructed by using 3³ full factorial design in the concentration range of 4.5-8.5, 5-7 and 8-12 µg/mL, respectively. Absorption spectra were recorded in the range 240-350 nm. To check the quality of the proposed method, it was applied to the determination of these compounds in synthetic mixtures and pharmaceutical formulation, suppository. The PLS-2 method yielded recoveries ranging from 91 to 106%. The results compared well with those from the reported HPLC method.

Keywords: *fluocortolone caproate, fluocortolone pivalate, cinchocaine HCl, PLS*

INTRODUCTION

Fluocortolone caproate (FCC) and fluocortolone pivalate (FCP) are glucocorticoids with anti-inflammatory activity used topically for various skin disorders [1]. Cinchocaine HCl (CIN) is a long-acting amide anaesthetic used for surface anaesthesia for relief of pain [2]. The combination of these active compounds are used mostly to reduce the common symptoms caused by haemorrhoids.

^a *Yildiz Technical University, Faculty of Science and Arts, Department of Chemistry, Davutpasa, 34220 Istanbul, Turkey, oziaksu@yahoo.com*

There are a few studies in the literature describing the determination of fluocortolone and its esters FCC and FCP using thin layer chromatography [3] (TLC), high performance liquid chromatography [4-5] (HPLC), raman spectroscopy [6-7], and spectrophotometry [8]. Unlike fluocortolone, many studies including the use of spectrophotometry [2,9], fluorimetry [10], TLC [11], liquid chromatography-mass spectrometry [12], sequential injection chromatography [13], HPLC [2,14-16], gas chromatography [17], chemometry [18] and electroanalytical methods [19-21] have been used for the determination of CIN. A HPLC method has been reported for the simultaneous determination of the three drugs [22].

In spite of widely use of chromatographic techniques, spectrophotometric analysis, being simple, inexpensive and fast, constitutes a highly convenient alternative approach for the determination of drugs in pharmaceutical formulations. However, the greatest difficulties with the conventional spectrophotometric methods arise when the analytes to be determined give partial or fully overlapped spectra.

In recent years, multivariate calibration methods such as principal component regression (PCR) and partial least squares (PLS) have been applied to overlapped spectra or chromatograms successfully [23-30]. All these techniques have the advantageous of using the full spectral information and not only a characteristic peak value. Moreover, they allow for a rapid determination of the components, and usually there is no need of a prior separation. However, the literature survey reveals that no chemometric methods have been reported for the analysis of these three drugs in combination.

In this study, PLS-2 calibration model was described for the spectrophotometric multicomponent analysis of synthetic ternary mixtures consisting of FCC, FCP and CIN and pharmaceutical formulation, suppository. In order to appraise the results obtained by proposed method, reported HPLC method was used [22]. The scientific novelty of the present work is that the PLS-2 method is simple, rapid and cheap compared with chromatographic method.

RESULTS AND DISCUSSION

In the last years, the chemometric methods such as classical least-squares (CLS), PCR and PLS have become routine methods in multicomponent quantitative analysis [31-36]. The PLS calibration technique based on factor analysis can be performed in two different ways, PLS-1 and PLS-2. PLS-1 performs the optimization of the number of factors for only one component at a time. PLS-2 calculates the number of factors on all the components

simultaneously and one weighed number of factors is optimized. Here, the PLS-2 version that is optimized for the simultaneous determination of FCC, FCP and CIN was implemented. This multivariate method involves a calibration step in which relation between spectra and component concentrations is estimated from a set of reference samples, and a prediction step in which the results of the calibration are used to estimate the component concentration in an unknown sample spectrum [25,34]. The theory and applications of this method were documented in detail in the literature [37-38].

The electronic absorption spectra of FCC, FCP and CIN in methanol (Figure 1) show that they overlap significantly. Thus, these compounds can not be analyzed in the presence of each other by a simple calibration procedure without prior separation. Therefore, PLS-2 was used to resolve the spectra and to determine each component in the ternary mixture of FCC, FCP and CIN.

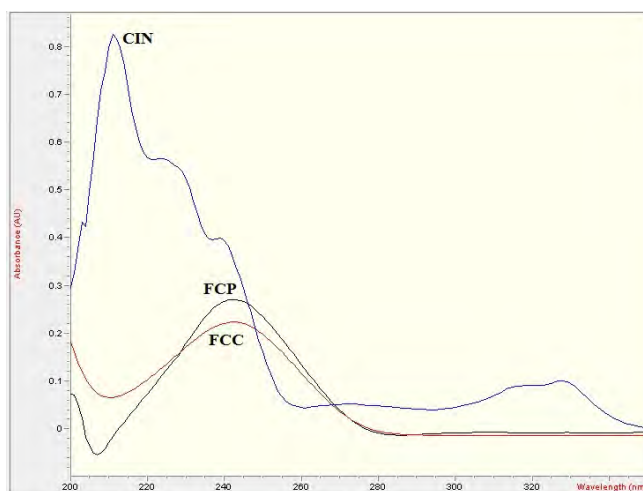


Figure 1. Absorption spectra of FCC (6.3 $\mu\text{g/mL}$), FCP (6.1 $\mu\text{g/mL}$) and CIN (10 $\mu\text{g/mL}$) in methanol.

For the PLS-2 calibration stage, 27 training samples were employed, conforming to 3^3 full factorial design [39]. The composition data of solutions is listed Table 1. The spectra of this calibration set were recorded in the spectral region between 240 and 350 nm with 1 nm intervals. The optimum number of factors and important statistical parameters: The root-mean square deviation (RMSD), relative error of prediction (REP%) and square of the correlation coefficient (R^2) are summarized in Table 2.

Table 1. Composition of the calibration sample

Sample	FCC($\mu\text{g/mL}$)	FCP($\mu\text{g/mL}$)	CIN($\mu\text{g/mL}$)
1	4.5	5	8
2	6.5	5	8
3	8.5	5	8
4	4.5	6	8
5	6.5	6	8
6	8.5	6	8
7	4.5	7	8
8	6.5	7	8
9	8.5	7	8
10	4.5	5	10
11	6.5	5	10
12	8.5	5	10
13	4.5	6	10
14	6.5	6	10
15	8.5	6	10
16	4.5	7	10
17	6.5	7	10
18	8.5	7	10
19	4.5	5	12
20	6.5	5	12
21	8.5	5	12
22	4.5	6	12
23	6.5	6	12
24	8.5	6	12
25	4.5	7	12
26	6.5	7	12
27	8.5	7	12

Table 2. Statistical parameters for the calibration using PLS-2

Parameters [*]	FCC	FCP	CIN
Factors	3	3	3
RMSD	0.186	0.081	0.073
REP%	2.86	1.35	0.73
R^2	0.987	0.990	0.998
LOD($\mu\text{g/mL}$)	0.31	0.22	0.13
LOQ($\mu\text{g/mL}$)	1.05	0.74	0.43

$$* \text{RMSD} = \left[\frac{1}{m} \sum_1^m (c_{act} - c_{pred})^2 \right]^{1/2} ; \% \text{REP} = \frac{100}{\bar{c}} \left[\frac{1}{m} \sum_1^m (c_{act} - c_{pred})^2 \right]^{1/2} \text{ and}$$

$$R^2 = 1 - \frac{\left(\sum_1^m (c_{act} - c_{pred})^2 \right)}{\left(\sum_1^m (c_{act} - \bar{c})^2 \right)}$$

where \bar{c} is the average component concentration in the m mixtures.

Application to synthetic mixtures

In order test to the quality of the proposed method, it was applied to the resolution of ternary synthetic mixtures containing different concentrations of three drugs. The composition of mixtures and the predictions of these synthetic samples are shown in Table 3. As regards the results provided by PLS-2 on the synthetic sample set, good recoveries were obtained for FCC, FCP and CIN (Relative error of prediction (REP%) values not exceed 15%).

Table 3. Results obtained by applying PLS-2 to synthetic samples

Analyte	Mixture 1			Mixture 2			Mixture 3		
	FCC	FCP	CIN	FCC	FCP	CIN	FCC	FCP	CIN
Added ($\mu\text{g/mL}$)	4.5	5.0	8.0	6.5	6.0	10.0	8.5	7.0	12.0
Found ($\mu\text{g/mL}$)	4.1	5.4	8.3	6.6	6.2	10.1	8.7	6.5	12.1
	4.7	4.9	8.2	6.8	5.9	10.0	9.2	6.3	12.1
	4.3	5.2	8.2	6.9	5.9	9.9	9.0	6.5	12.2
Mean	4.4	5.2	8.2	6.8	6.0	10.0	9.0	6.4	12.1
Recovery%	98	104	103	105	100	100	106	91	101
RMSD	0.4	0.4	0.2						
REP%	6.2	6.7	2.0						

Application to real samples

The PLS-2 method was used in the simultaneous determination of FCC, FCP and CIN in commercially available suppository formulation. Satisfactory results were obtained for all drugs and were good agreement with the label claims (The recoveries are within the range 98.36 – 104.76%).

The results obtained by proposed method was statistically compared with the literature method based on HPLC [22] by applying Student's *t*-test for accuracy and *F*-test for precision. The statistical results were summarized in Table 4. The results revealed that there is no significant difference between the proposed and reported method at the 95% confidence level with respect to accuracy and precision. Consequently, the above results show that the proposed method can be successfully applied for simultaneous determination of FCC, FCP and CIN in real samples.

Table 4. Determination of FCC, FCP and CIN in suppository^a using of PLS-2 and reference HPLC methods

n1=n2=5 Analyte (mg/suppository)	PLS-2			HPLC		
	FCC	FCP	CIN	FCC	FCP	CIN
mean ± SD ^b	0.66±0.02	0.60±0.01	1.04±0.03	0.64±0.01	0.61±0.01	1.01±0.02
Recovery%	104.76	98.36	104.00	101.58	100.00	101.84
<i>t</i> test of significance	2.01	1.57	1.90			
<i>F</i> test of Significance	4.00	1.00	2.25			
$t_{8}^{0,05}=2.31$ $F_{4,4}^{0,05}=6.39$						

^aUltraproct Suppository®(FCC 0.63 mg, FCP 0.61 mg, CIN 1.00 mg)

^bStandard deviation

CONCLUSIONS

The proposed method was applied to the simultaneous spectrophotometric analysis of FCC, FCP and CIN, in spite of a strong overlapping absorption spectra of these components in the wavelength range of 210-280 nm. The overlapping was successfully resolved using the PLS-2 algorithm. According to the results obtained in this work, application of the proposed method was found to be adequately accurate, simple, fast and inexpensive for the simultaneous determination of FCC, FCP and CIN in ternary mixtures of synthetic and pharmaceutical samples. In addition, the proposed calibration method do not require any prior treatment, and optimization of conditions such as pH, temperature, and flow rate in comparison with HPLC.

In conclusion, PLS-2 multivariate calibration method can be recommended as a very suitable choice to resolve severe overlapped absorption spectra of drug mixtures and used as cheap and accessible alternative for routine quality control testing of common pharmaceutical formulations of FCC, FCP and CIN.

EXPERIMENTAL SECTION

Chemicals and reagents

FCC, FCP and CIN were obtained from Zeytaş Ltd., Istanbul, Turkey. Analytical grade methanol and acetic acid were purchased from Merck Company (Darmstadt, Germany). Ultra-pure water was obtained in the laboratory using a Milli-Q purification system from Millipore (Milford, MA, USA)

The "Ultraproct Suppository[®]" commercial samples were acquired from Turkey pharmacies. Each suppository was labeled to contain 0.63 mg of FCC, 0.61 mg of FCP and 1 mg of CIN. The chemical structures of the drugs are shown in Figure 2.

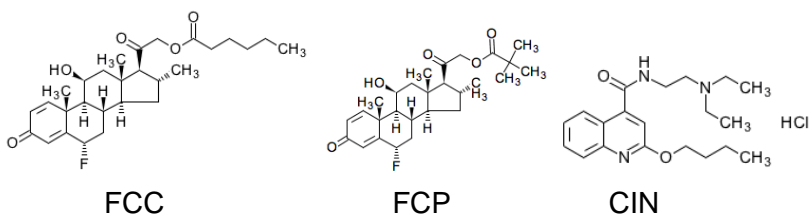


Figure 2. Molecular structures of the drugs analyzed

Instrumentation and software

Spectrophotometric measurements were performed with Agilent 8453 UV-Vis Spectrophotometer. PLS-2 was implemented using PLS-Toolbox software version 5.2 for use with MATLAB 11.

HPLC measurements were carried out on a Shimadzu HPLC system equipped with a model LC20 AT pump unit, SPD-20A UV-Vis detector and C18 (300 mm × 3.9 mm) RP column.

Preparation of standard solutions and calibration set

Stock standard solutions of the drugs (100 µg/mL) were prepared in methanol. Working solutions for calibration set were prepared by appropriate dilution of stock solutions with methanol. The calibration set for PLS-2 was generated by 3³- full factorial design. The levels correspond to values in the

range of 4.5-8.5 µg/mL for FCC, 5-7 µg/mL for FCP and 8-12 µg/mL for CIN. The absorbances were recorded in 1.00 cm cuvettes between 240 and 350 at every 1 nm.

Test samples for PLS-2

For evaluation of proposed method, three concentration levels were used. These levels have been selected by considering the amounts of the analytes in the calibration range. Three group of test solutions were analysed applying the studied method three times.

Sample preparation

Ten suppositories accurately weighed, melted by stirring on a water bath to homogenize and than cooled. A portion of the homogenized suppositories equivalent to one suppository was transferred into a beaker, 30 mL methanol was added and melting was performed on a water bath. The solution was cooled, filtered into 100 mL volumetric flask and then diluted to volume with methanol.

HPLC method

The determination of the contents of FCC, FCP and CIN in suppository was also verified by reported HPLC method [22]. The mobile phase was methanol-water-acetic acid (72:26:2). The analysis was done under isocratic conditions at a flow rate of 1.3 mL/min and the effluent was monitored by UV measurements at 240 nm.

REFERENCES

1. M. Kerscher; S. William; P. Lehmann; Topical Treatment with Glucocorticoids, in *Handbook of atopic eczema*, 2nd. ed; J. Ring; B. Przybilla; T. Ruzicka; Newyork: Springer-Verlag, Berlin Heidelberg, **2006**, pp.477-491.
2. A. El-Gindy; M. A. Korany; M. F. Bedair; *J. Pharm. Biomed. Anal.*, **1998**, 17, 1357-1370.
3. M. Amin; *Anal. Chem.*, **1987**, 328, 114-116.
4. S. Rohatagi; U. Tauber; K. Richter; H. Derendorf; *J. Clin. Pharmacol.*, **1996**, 36, 311-314.
5. O. Cudina; J. Brboric; Z. Vujic; D. Radulovic; S. Vladimirov; *Farmaco*, **2000**, 55, 125-127.
6. A.P. Gamot; G. Vergoten; M. Saudemon; G. Fleury; *Talanta*, **1985**, 32, 373-382.

7. A.P. Gamot; G. Vergoten; M. Saudemon; G. Fleury; J. Barbillat; *Talanta*, **1986**, 33, 295-298.
8. H.M. Lottfy; S.M. Tawakkol; N.M. Fahmy; M.A. Shehata; *Spectrochim. Acta A*, **2015**, 136, 937-952.
9. N.T. Abdel-Ghani; F.A. Ahmed; A.A. Mohamed; *Il Farmaco*, **2005**, 60, 419-424.
10. S. Essig; K.A. Kovar; *Chromatographia*, **2001**, 53, 321-322.
11. M.M. Mohammad; N.H. Zawilla; F.M. El-Anwar; S.M. Aly; *J. AOAC Int.*, **2007**, 90, 405-413.
12. T. Saito; S. Morita; I. Kishiyama; S. Miyazaki; A. Nakamoto; M. Nishida; A. Namera; M. Nagao; *J. Chromatogr. B Analyt. Technol. Biomed. Life Sci.*, **2008**, 872, 186-190.
13. D. Satinsky; P. Chocholous; O. Valova; L. Hanusov; P. Solich; *Talanta*, **2013**, 114, 311-317.
14. S. Izumoto; Y. Machida; H. Nishi; K. Nakamura; H. Nakai; T. Sato; *J. Pharm. Biomed. Anal.*, **1997**, 15, 1457-1466.
15. M.A. El-Sayed; *Biomed. Chromatogr.*, **2007**, 21, 491-496.
16. R.D. Barbosa; A. Klassen; P.D. Marcato; M. Franz-Montan; R. Grillo; L.F. Fraceto; E. Paula; *Lat. Am. J. Pharm.*, **2013**, 32, 1362-1369.
17. T. Ohshima; T. Takayasu; *J. Chromatogr. B Biomed. Sci. Appl.*, **1999**, 726, 185-194.
18. C. Soto; D. Contreras; M.I. Toral; L. Basaez; J. Freer; *J. Chil. Chem. Soc.*, **2009**, 54, 113-118.
19. H. Satake; T. Miyata; S. Kaneshina; *Bulletin Chem. Soc. Japan*, **1991**, 64, 3029-3034.
20. S. Komorsky-Lovric; N. Vukasinovic; R. Penovski; *Electroanalysis*, **2003**, 15, 544-547.
21. A.A. Ensafi; A.R. Allafchian; *Bull. Korean Chem. Soc.*, **2011**, 32, 2722-2726.
22. B. Aşçı; M. Koç; *Current Pharm. Anal.*, **2019**, 15, 32-38.
23. M.S. Collado; V.E. Mantovani; C.H. Goicoechea; A.C. Olivieri; *Talanta*, **2000**, 52, 909-920.
24. A. El-Gindy; A.A. Ashour; L. Abdel-Fattah; M.M. Shabana; *J. Pharm. Biomed. Anal.*, **2001**, 25, 923-931.
25. M.J. Culzoni, M.M. De Zan, J.C. Robles, V.E. Mantovani, H.C. Goicoechea, *J. Pharm. Biomed. Anal.*, **2005**, 39, 1068.
26. S. Şahin; C. Demir; Ş. Güçer; *Dyes and Pigments*, **2006**, 73, 368-376.
27. R.M. Maggio; P.M. Castellano; T.S. Kaufman; *Anal. Bioanal. Chem.*, **2008**, 391, 2949-2955.
28. N. Yongnian; Y. Wang; S. Kokot; *Spectrochim. Acta A*, **2008**, 70, 1049-1059.
29. E. Dinç; D. Balenau; G. Ioele; M. De Luca; G. Ragno; *J. Pharm. Biomed. Anal.*, **2008**, 48, 1471-1475.
30. C. Zapata-Urdua; M. Perez-Ortiz; M. Bravo; A.C. Olivieri; A. Alvarez; *Talanta*, **2010**, 82, 962-968.
31. S. Riahi; F. Hadiloo; S.M. Milani; N. Davarkhah; M.R. Ganjali; P. Norouzi; P.A. Seyfie; *Drug Test Anal.*, **2011**, 3, 319-324.
32. Ö.A. Dönmez; B. Aşçı; A. Bozdoğan; S. Sungur; *Talanta*, **2011**, 83, 1601-1605.

33. Ş. Dinç; Ö.A. Dönmez; B. Aşçı; A. Bozdoğan; *J. Liq. Chromatogr. Relat. Technol.*, **2014**, *37*, 560-571.
34. A.M. El-Kosasy; O. Abdel-Aziz; N. Magdy; N.M. El Zahar; *Spectrochim. Acta A*, **2016**, *157*, 26-33.
35. M.F. Abdel-Ghany; L.A. Hussein; M.F. Ayad; M.M. Youssef; *Spectrochim. Acta A.*, **2017**, *171*, 236-245.
36. H. Khajehsharifi; Z. Eskandari; N. Sareban; *Arabian J. Chem.*, **2017**, *10*, 141-147.
37. H. Martens; T. Naes; *Multivariate Calibration*, Wiley, Chichester, U.K, **1989**.
38. P. Geladi; B.R. Kowalski; *Anal. Chim. Acta*, **1986**, *185*, 1-17.
39. D.C. Montgomery; *Design and Analysis of Experiments*, Wiley, Newyork, **1997**.

RADIOCARBON INVESTIGATION OF A SUPERLATIVE GRANDIDIER BAOBAB, THE BIG RENIALA OF ISOSA

ROXANA T. PATRUT^{a,b*}, ADRIAN PATRUT^a,
JEAN-MICHEL LEONG POCK-TSY^c, STEPHAN WOODBORNE^d,
LASZLO RAKOSY^b, PASCAL DANTHU^e, ILEANA-ANDREEA RATIU^a,
JENÖ BODIS^a, KARL VON REDEN^f

ABSTRACT. The article discloses the accelerator mass spectrometry (AMS) radiocarbon dating results of the Big Reniala of Isosa, which is a massive Grandidier baobab (*Adansonia grandidieri* Baill.) of Madagascar. The investigation of this baobab shows that it consists of 5 perfectly fused stems and exhibits a cluster structure. The calculated wood volume of the tree is 540 m³, which makes the Big Reniala of Isosa the largest individual of all *Adansonia* species and also the biggest known angiosperm in terms of volume. Several samples were collected from the outer part of the stems. The oldest dated sample had a radiocarbon date of 934 ± 24 BP, which corresponds to a calibrated age of 845 ± 25 years. This value indicates an age of 1000 ± 100 years for the big Reniala of Isosa.

Keywords: AMS radiocarbon dating, *Adansonia grandidieri*, tropical trees, multiple stems.

INTRODUCTION

The *Adansonia* genus, which belongs to the Bombacoideae subfamily of Malvaceae, consists of eight or nine species. One or two species originate from the tropical (semi-)arid savanna of the African continent, six species are endemic to Madagascar and one species can be found only in Australia [1-5].

^a Babeş-Bolyai University, Faculty of Chemistry and Chemical Engineering, 11 Arany Janos, RO-400028, Cluj-Napoca, Romania

^b Babeş-Bolyai University, Faculty of Biology and Geology, 44 Republicii, RO-400015, Cluj-Napoca, Romania

^c DP Forêt et Biodiversité, Antananarivo, Madagascar

^d iThemba LABS, Private Bag 11, WITS 2050, South Africa

^e CIRAD, Unité HortSys, Université de Montpellier, Montpellier, France

^f NOSAMS Facility, Dept. of Geology & Geophysics, Woods Hole Oceanographic Institution, Woods Hole, MA 02543, U.S.A.

* Corresponding author: roxanapatrut@yahoo.com

In 2005, we started an extensive research program to elucidate several controversial or poorly understood aspects of the architecture, development and age of the African baobab (*Adansonia digitata* L.). The research is based on our novel methodology, which is not limited to demised specimens, but also allows to investigate and date live individuals. This original approach is based on AMS (accelerator mass spectrometry) radiocarbon dating of tiny wood samples collected from inner cavities, deep incisions/entrances in the trunk, fractured stems and from the outer part/exterior of the trunk/stems of large baobabs [6-13]. We found that typically, all large African baobabs are multi-stemmed and preferentially exhibit ring-shaped structures. The oldest African baobabs were found to have ages of over 2,000 years. Thus, the African baobab becomes the longest living angiosperm [9,11,13-15].

In 2013, we extended our research on the *Adansonia* genus by starting to investigate large individuals of the most representative three species of Madagascar, i.e., *Adansonia rubrostipa* Jum. & H. Perrier (Fony baobab), *Adansonia za* Baill. (Za baobab) and *Adansonia grandidieri* Baill. (Grandidier baobab), which grow in the west and south [5,16-19].

The Grandidier baobab, which is called Reniala by natives (in Masikoro, i.e., “Mother of the Forest”), is certainly the biggest and most famous of the six Malagasy *Adansonia* species. *A. grandidieri* is represented by large trees with massive cylindrical trunks and flat-topped crowns with almost horizontal, large branches [1,2,5].

Until 1998, it was believed that the distribution of *A. grandidieri* is restricted to only 5 locations in southwestern Madagascar. Thus, according to the IUCN Red List, *A. grandidieri* was classified as endangered [20]. However, new investigations based on photo-interpretation of very high resolution satellite images, which were subsequently validated by field investigations, showed that *A. grandidieri* is present in a much wider area and its population is much larger than previous estimates. According to this recent study, the total population of *A. grandidieri*, which covers an area of 26,232 km² along the Mangoky river and in the western part of the Menabe region, is around 1.2-1.3 million mature individuals [16,20].

The largest *A. grandidieri* are located in the Morombe area, especially in the so-called Andombiry Forest, which is surrounded by four villages: Belitsaka, Andombiry, Ankoabe and Isosa. In a previous article, we presented the AMS radiocarbon dating results of three famous *A. grandidieri* specimens, namely Tsitakakoike, the Pregnant baobab and the House baobab [18].

Here we disclose the investigation and AMS radiocarbon dating results of another very large specimen, the Big Reniala of Isosa.

RESULTS AND DISCUSSION

The Big Reniala of Isosa and its area. The very large baobab is located in a dry deciduous forest at only 100 m from the Morombe-Toliara road (at km 28.3 from Morombe) and at 1.5 km SW from the village Isosa, in the Morombe district, Atsimo-Andrefana region of southwestern Madagascar. Its GPS coordinates are 21°37.976' N, 043°34.474' E and the altitude is 21 m. Mean annual rainfall in the area is 458 mm (Morombe station).



Figure 1. General view of the Big Reniala of Isosa taken from the east (October 2018).

The baobab has a maximum height of 21.6 m and the circumference at breast height (cbh; at 1.30 m above ground level) is 23.22 m (**Figure 1**). The huge trunk forks at heights between 12.2 and 14.5 m into several large branches with diametres up to 2 m. The columnar trunk is almost cylindrical, having a circumference of 24.20 m at the base and 21 m at the height of 12 m.

According to a careful visual inspection and to the analysis of photographs, the trunk consists of 5 perfectly fused stems. The horizontal dimensions of the very impressive canopy are 45.2 (NS) x 37.2 (WE) m (**Figure 2**).

The calculated overall wood volume of the tree is 540 m³, out of which 485 m³ belongs to the trunk and 55 m³ to the canopy. By this value, the Big Reniala of Isosa becomes not only the largest *Adansonia grandidieri* in terms of volume (larger than the famous Tsitakakoike and Tsitakakantsa from the same forest), but also the largest individual of all *Adansonia* species and the largest known angiosperm.

The baobab of Isosa flushes leaves only in December, two months later than the other *Grandidier* baobabs of the area. It does no longer produce pods, which suggests an old age for all stems.



Figure 2. The image shows the impressive canopy of the baobab of Isosa (April 2019).

Wood samples. Several wood samples were extracted from 3 stems, by using two increment borers of different lengths (0.90 and 1.50m). Three samples (labelled 1, 2 and 3) were considered to be sufficiently long, namely 0.844, 0.785 and 1.117 m, for investigation. These samples were collected at convenient heights, between 1.38 and 1.52 m. A number of three tiny pieces/segments, each of the length of 10⁻³ m (marked as a, b, c), were extracted from determined positions of each sample.

AMS results and calibrated ages. Radiocarbon dates of the 9 sample segments are listed in Table 1. The radiocarbon dates are expressed in ¹⁴C yr BP (radiocarbon years before present, i.e., before the reference year 1950). Radiocarbon dates and errors were rounded to the nearest year.

Calibrated (cal) ages, expressed in calendar years CE (CE, i.e., common era), are also shown in Table 1. The 1-σ probability distribution (68.2%) was selected to derive calibrated age ranges. For one sample segment (2a), the 1-σ distribution is consistent with one range of calendar years. For the other eight segments, the 1-σ distribution is consistent with two or three ranges of calendar years. In these cases, the confidence interval of one range is considerably greater than that of the other(s); therefore, it was selected as the cal CE range of the segment for the purpose of this discussion. For obtaining single calendar age values of sample segments, we derived a mean calendar age of each segment from the selected range (marked in bold). Sample/segment ages represent the difference between the year 2019 CE and the mean value of the selected range, with the corresponding error. Sample ages and errors were rounded to the nearest 5 yr. This approach was used for selecting calibrated age ranges and single values for sample ages in all our previous articles on AMS radiocarbon dating of large and old angiosperm trees, especially of baobabs [6-15,17-19].

Table 1. AMS Radiocarbon dating results and calibrated calendar ages of samples/segments collected from the Big Reniala of Isosa.

Sample (Segment)	Depth ¹ [height ²] (10 ⁻² m)	Radiocarbon date [error] (¹⁴ C yr BP)	Cal CE range 1-σ [confidence interval]	Sample age [error] (cal yr CE)
1a	30 [138]	254 [± 19]	1650-1670 [41.8%] 1748-1754 [7.8%] 1783-1795 [18.6%]	360 [± 10]
1b	55 [138]	420 [± 20]	1458-1497 [63.6%] 1602-1606 [4.6%]	540 [± 20]
1c	84 [138]	629 [± 16]	1324-1342 [44.1%] 1390-1398 [24.1%]	685 [± 10]
2a	30 [143]	270 [± 18]	1644-1667 [68.2%]	365 [± 10]
2b	55 [143]	410 [± 17]	1461-1500 [52.9%] 1598-1610 [15.3%]	540 [± 20]
2c	78 [143]	618 [± 18]	1326-1341 [28.9%] 1390-1404 [39.3%]	620 [± 10]
3a	40 [152]	339 [± 21]	1510-1575 [54.7%] 1622-1636 [13.5%]	475 [± 30]
3b	75 [152]	604 [± 22]	1328-1338 [11.6%] 1390-1414 [56.6%]	620 [± 10]
3c	114 [152]	934 [± 24]	1070-1076 [4.6%] 1148-1203 [63.6%]	845 [± 25]

¹ Depth in the wood from the sampling point.

² Height above ground level.

Dating results of samples (segments). The oldest segments of the two samples collected with the shorter increment borer, namely 1c and 2c, which represent sample ends both, exhibit close ages. Their radiocarbon dates of 629 ± 16 BP and 618 ± 18 BP correspond to calibrated ages of 685 ± 10 and 620 ± 10 calendar yr. The oldest segment of the sample collected with the longer increment borer, i.e. 3c, which is also the sample end, has a radiocarbon date of 934 ± 24 BP. This value corresponds to a calibrated age of 845 ± 25 calendar yr. The lower ages of the other segments extracted from the three samples are in accordance with their positions in the stems.

Architecture of the baobab of Isosa. Our long-term research has revealed that large African baobabs are always multi-stemmed [9,13]. This statement is also valid for the large Malagasy baobabs, including the Grandidier baobabs [18]. As mentioned, the Big Reniala of Isosa consists of 5 perfectly fused stems.

Our research has also identified a new type of architecture that enables African baobabs to reach old ages and large sizes. In this novel architecture, the multiple stems define at ground level a circle or an ellipse, with an empty space between them; we named it ring-shaped structure (RSS). The most frequent is the closed RSS, in which the fused stems are disposed in a ring with a natural empty space inside, that we termed false cavity. For baobabs with a closed RSS, the age sequence of long samples collected from the false cavity walls toward the exterior of the trunk, as well as of samples collected from the exterior toward the false cavity, shows a continuous increase from the sampling point up to a certain distance into the wood, after which it decreases toward the opposite part [9,12]. The large Grandidier baobabs that we have previously dated have/had such a closed RSS [13].

In the case of the Big Reniala of Isosa, the age sequence of the samples, which were collected from the exterior of 3 different stems, shows a continuous increase with the depth in the wood, see Table 1. This fact demonstrates that the multi-stemmed Grandidier baobab of Isosa exhibit a cluster structure.

Age of the Big Reniala of Isosa. The age sequences of the samples collected from 3 different stems demonstrate that these stems and probably all 5 stems of the baobab belong to the same generation and have comparable ages. The age of the baobab can be estimated by extrapolating the age of the oldest dated sample segment, i.e., 3c, to the presumptive pith of the corresponding stem. Sample segment 3c, which has an age of 845 ± 25 yr, originates from a depth of 1.13 m in the wood. The corresponding stem has a diameter of around 3.50 m. Consequently, the presumptive pith is located at a distance of 1.75 m from the sampling point. In a conservative estimate, the age of the Big Reniala of Isosa is of 1000 ± 100 years.

CONCLUSIONS

The research presents the AMS radiocarbon investigation results of a very large Grandidier baobab, namely the Big Reniala of Isosa, Madagascar. The baobab consists of 5 fused stems and has a cluster structure. The wood volume of the Grandidier baobab of Isosa is 540 m³, which makes it the largest individual of all baobab species and also the biggest known angiosperm in terms of volume. Several wood samples were collected from the outer part of different stems. The oldest dated sample has a radiocarbon date of 934 ± 24 BP, which corresponds to a calibrated age of 845 ± 25 years. This value indicates that the Big Reniala of Isosa is 1000 ± 100 years old. It can be stated that the impressive baobab of Isosa started growing around the year 1000 CE.

EXPERIMENTAL SECTION

Sample collection. Samples 1 and 2 were collected with a Haglöf CH 900 increment borer (0.90 m long, 0.0108 m inner diameter). Sample 3 was collected with a modified Haglöf increment borer (1.50 m long, 0.0108 m inner diameter). A number of three tiny pieces/segments, of the length of 10⁻³ m, were extracted from predetermined positions along each wood sample. The segments were processed and investigated by AMS radiocarbon dating.

Sample preparation. The modified α -cellulose pretreatment method was employed for removing soluble and mobile organic components [21]. The resulting samples were combusted to CO₂, which was next reduced to graphite on iron catalyst [22,23]. The resulting graphite samples were analysed by AMS.

AMS measurements. The AMS radiocarbon measurements of samples 1 and 2 were performed at the NOSAMS Facility of the Woods Hole Oceanographic Institution (Woods Hole, MA, U.S.A.) by using the Pelletron® Tandem 500 kV AMS system [24]. The measurements of sample 3 were done at the AMS Facility of iThemba LABS, Johannesburg, Gauteng, South Africa, using the 6 MV Tandem AMS system [25]. In all cases, the obtained fraction modern values were finally converted to a radiocarbon date. The radiocarbon dates and errors were rounded to the nearest year.

Calibration. Radiocarbon dates were calibrated and converted into calendar ages with the OxCal v4.3 for Windows [26], by using the SHCal13 atmospheric data set [27].

ACKNOWLEDGMENTS

The investigation and sampling of the baobab was authorised by the Forestry Direction of the Ministry of Environment, Ecology and Forestry of Madagascar and by the Madagascar National Parks. The research was funded by the Romanian Ministry of National Education CNCS-UEFISCDI under grant PN-III-P4-ID-PCE-2016-0776, No. 90/2017.

REFERENCES

1. D.A. Baum, *Annals of the Missouri Botanical Garden*, **1995**, *82*, 440-471. doi: 10.2307/2399893.
2. G.E. Wickens, P. Lowe, "The Baobabs: Pachycauls of Africa, Madagascar and Australia", Springer, Dordrecht, **2008**, pp. 232-234, 256-257, 295-296. doi: 10.1007/978-1-4020-6431-9.
3. J.D. Pettigrew, L.K. Bell, A. Bhagwandin, E. Grinan, N. Jillani, J. Meyer, E. Wabuyele, C.E. Vickers, *Taxon*, **2013**, *61*, 1240-1250. doi: 10.1002/tax.616006.
4. G.V. Cron, N. Karimi, K.L. Glennon, C.A. Udeh, E.T.F. Witkowski, S.M. Venter, A.E. Assobadjo, D.H. Mayne, D.A. Baum, *Taxon*, **2016**, *65*, 1037-1049. doi: 10.12705/tax.65637.
5. A. Petignat, L. Jasper, "Baobabs of the world: The upside down trees of Madagascar, Africa and Australia", Struik Nature, Cape Town, **2015**, pp. 16-86.
6. A. Patrut, K.F. von Reden, D.A. Lowy, A.H. Alberts, J.W. Pohlman, R. Wittmann, D. Gerlach, L. Xu, C.S. Mitchell, *Tree Physiology*, **2007**, *27*, 1569-1574. doi: 10.1093/treephys/27.11.1569.
7. A. Patrut, D.H. Mayne, K.F. von Reden, D.A. Lowy, R. Van Pelt, A.P. McNichol, M.L. Roberts, D. Margineanu, *Radiocarbon*, **2010**, *52(2-3)*, 717-726. doi: 10.1017/S0033822200045732.
8. A. Patrut, K.F. von Reden, R. Van Pelt, D.H. Mayne, D.A. Lowy, D. Margineanu, *Annals of Forest Science*, **2011**, *68*, 93-103. doi: 10.1007/s13595-011-0107-x.
9. A. Patrut, S. Woodborne, R.T. Patrut, L. Rakosy, D.A. Lowy, G. Hall, K.F. von Reden, *Nature Plants*, **2018**, *4(7)*, 423-426. doi: 10.1038/s41477-018-0170-5.
10. A. Patrut, D.H. Mayne, K.F. von Reden, D.A. Lowy, R. Van Pelt, A.P. McNichol, M.L. Roberts, D. Margineanu, *Radiocarbon*, **2010**, *52(2-3)*, 717-726. doi: 10.1017/S0033822200045732.
11. A. Patrut, K.F. von Reden, D.H. Mayne, D.A. Lowy, R.T. Patrut, *Nuclear Instruments and Methods in Physics Research Section B*, **2013**, *294*, 622-626. doi: 10.1016/j.nimb.2012.04.025.
12. A. Patrut, S. Woodborne, K.F. von Reden, G. Hall, M. Hofmeyr, D.A. Lowy, R.T. Patrut, *PLOS One*, **2015**, *10(1)*: e0117193. doi: 10.1371/journal.pone.0117193.

13. A. Patrut, S. Woodborne, K.F. von Reden, G. Hall, R.T. Patrut, L. Rakosy, J-M. Leong Pock Tsy, D.A. Lowy, D. Margineanu, *Radiocarbon*, **2017**, 59(2), 435-448. doi: 10.1017/RDC.2016.92.
14. A. Patrut, L. Rakosy, R.T. Patrut, I.A. Ratiu, E. Forizs, D.A. Lowy, D. Margineanu, K.F. von Reden, *Studia UBB Chemia*, **2016**, LXI, 4, 7-20. doi:10.24193/subbchem.2016.4.103.
15. A. Patrut, R.T. Patrut, L. Rakosy, D.A. Lowy, D. Margineanu, K.F. von Reden, *Studia UBB Chemia*, **2019**, LXIV, 2 (II), 411-419. doi:10.24193/subbchem.2019.2.35.
16. G. Vieilledent, C. Cornu, A. Cuni Sanchez, J-M. Leong Pock-Tsy, P. Danthu, *Biological Conservation*, **2013**, 166, 11-22. doi.org/10.1016/j.biocon.2013.06.007.
17. A. Patrut, K.F. von Reden, P. Danthu, J-M. Leong Pock-Tsy, R.T. Patrut, D.A. Lowy, *PLOS One*, **2015**, 10(3): e0121170. doi:10.1371/journal.pone.0121170.
18. A. Patrut, K.F. von Reden, P. Danthu, J-M. Leong Pock-Tsy, L. Rakosy, R.T. Patrut, D.A. Lowy, D. Margineanu, *Nuclear Instruments and Methods in Physics Research Section B*, **2015**, 361, 591-598. doi:10.1016/j.nimb.2015.04.044.
19. A. Patrut, R.T. Patrut, P. Danthu, J-M. Leong Pock-Tsy, L. Rakosy, D.A. Lowy, K.F. von Reden, *PLOS One*, **2016**, 11(1): e146977. doi:10.1371/journal.pone.0146977.
20. H. Ravaomanalina, J. Razafimanahaka, "2016. *Adansonia grandidieri*." *The IUCN Red List of Threatened Species 2016*: e.T30388A64007143. dx.doi.org/10.2305/IUCN.UK.2016-2.RLTS.T30388A64007143.en.
21. N.J. Loader, I. Robertson, A.C. Barker, V.R. Switsur, J.S. Waterhouse, *Chemical Geology*, **1997**, 136(3), 313–317. doi: 10.1016/S0009-2541(96)00133-7.
22. Z. Sofer Z, *Anaytical Chemistry*, **1980**, 52(8), 1389-1391. doi: 10.1021/ac50058a063.
23. J.S. Vogel, J.R. Southon, D.E. Nelson, T.A. Brown, *Nuclear Instruments and Methods in Physics Research Section B*, **1984**, 5, 289-293. doi: 10.1016/ 0168-583X(84)90529-9.
24. M.L. Roberts, J.R. Burton, K.L. Elder, B.E. Longworth, C.P. McIntyre, K.F. von Reden, B.X. Han, B.E. Rosenheim, W.J. Jenkins, E. Galutschek, A.P. McNichol, *Radiocarbon*, **2010**, 52(1), 228-235. doi:10.1017/ S0033822200045252.
25. V.L. Mbele, S.M. Mullins, S.R. Winkler, S. Woodborne, *Physics Procedia*, **2017**, 90, 10-16. doi: 10.1016/j.phpro.2017.09.009.
26. C. Bronk Ramsey, *Radiocarbon*, **2009**, 51, 337-360. doi: 10.1017/ S0033822200033865.
27. A.G. Hogg, Q. Hua, P.G. Blackwell, M. Niu, C.E. Buck, T.P. Guilderson, T. J. Heaton, J. G. Palmer, P. J. Reimer, R. W. Reimer, C. S. M. Turney, R. H. Zimmerman, *Radiocarbon*, **2013**, 55(4), 1889-1903. doi:10.2458/azu_js_rc.55.16783.

GAS-CHROMATOGRAPHY ASSESSMENTS OF THE MAJOR VOLATILE COMPOUNDS IN TRADITIONAL FRUIT BRANDIES THROUGHOUT FRUIT AND WOOD MATURATION

THOMAS DIPPONG^a, ALEXANDRA AVRAM^{b,*},
CRISTINA MIHALI^a

ABSTRACT. Traditional home-made plum and apple brandies were analysed aiming to assess the main physico-chemical characteristics including density, ethanol content, total acidity, total extract, total sulphur dioxide (SO₂) and refractive indices. The major volatile compounds, such as, methanol, linear superior alcohols (propan-1-ol, butan-1-ol, butan-2-ol), branched superior alcohols (2-methylpropan-1-ol and 3-methylbutan-1-ol) and also ethyl acetate, acetaldehyde and acetal compounds, were assessed using gas chromatography coupled with flame ionization detector (GC-FID). The technology of incorporating fruit (cherries and pears) or wood (mulberry and poplar) in the brandy was presented along with the influence of their addition on the composition of the plum and apple brandies and on their physico-chemical characteristics. The changes in the composition of plum and apple brandies throughout 4 weeks of maturation process in the presence of wood or fruit, showed an increase in density, acidity and total extract and decrease in the concentration of ethanol, total sulphur dioxide (SO₂) and acetaldehydes. The addition of mulberry and poplar wood in the brandies decreased the concentration of acetaldehyde. The addition of both fruits significantly increased the concentration of ethyl acetate.

Keywords: *volatile substances, gas chromatography, wood embedding, fruit embedding*

^a Department of Chemistry and Biology, Faculty of Sciences, Technical University of Cluj-Napoca, Victoriei Street 76, 430122 Baia Mare, Romania

^b Faculty of Chemistry and Chemical Engineering, Babeş-Bolyai University, Arany Janos Street, 11, RO-400028, Cluj-Napoca, Romania

* Corresponding author: aavram@chem.ubbcluj.ro

INTRODUCTION

Plum brandy (“tuica, palinka”) is an alcoholic beverage obtained by the fermentation followed by distillation of plum marc without kernels, following a special technological process. Quality plum brandy has the specific taste and perfume of the fruit, flavours, obtained from the correct application of the crushing and fermentation processes, plus the features gained from maturing and aging [1]. The quality of brandy is influenced by several factors: soil and climate characteristics, plum varieties and the technological aspects of the manufacturing process [2,3]. Plum distillates are highly complex mixtures (higher alcohols, acids, esters, carbonyl compounds), contained in an ethanol-water mixture [4,5,6]. Plum brandy may also contain methyl alcohol resulting from the decomposition of pectin [2] similar to several other alcoholic beverages derived from fermented fruit [7,8]. The presence of this toxic substance in distillates is carefully monitored and supervised by the concerned authorities [1, 9]. The intake may become higher in the presence of ethyl alcohol, which is the antidote of methanol poisoning [7]. The methanol content of the alcoholic beverages derived from fermented fruit may be used to evaluate their authenticity and natural fruit origin [6].

Acetaldehyde is the most volatile substance in distilled alcoholic beverages, formed during fermentation and is considered the main compound resulting from the biochemical reaction of yeast acetic acid bacteria coupled with the self-oxidation of ethanol and phenolic compounds [10, 11, 12]. The acetal is formed during distillation, at elevated temperatures, and at high ethanol levels. Concentrations of acetaldehyde are dependent on fermentation conditions, temperature, pH, O₂ and SO₂ levels and the availability of nutrients from yeast [11, 12]. Formation of acetaldehyde is favoured by the storage of raw materials under anaerobic conditions [13]. Low concentrations of acetaldehyde give pleasant fruit flavours, while high concentrations can lead to irritating odours. Higher alcohols have a significant impact on the flavour of the brandy range, but also on the toxicity [14]. Also called fusel oils, they have a higher boiling point than ethanol, present a strong aroma and can be recovered depending on the raw materials and yeasts used for fermentation [10].

Apple brandy is an alcoholic beverage obtained through the distillation of fermented mashes of ripe apples. Fruit brandies are often stored for maturation in wood barrels (oak, mulberry, poplar or chesnut). During the maturation period, the beverage acquires interesting sensorial characteristics, as a result of extraction and degradation of many compounds from the wood matrix [15].

The analysis of fruit brandy (spirit) manufactured by traditional methods in European countries was the subject of several papers [4,5,16]. The analysis of these types of beverages has a significant importance in the authentication, control and prevention of fraud [16]. However, the details regarding the

manufacturing stages are less described. A thorough documentation on the home-made traditional fruit brandy in the Maramures area was performed. The distillate contains 3 parts: "forehead", "middle" and "tail". The forehead represents 1.5-2% of the distillate, with 70-72% alcohol with a large amount of methyl alcohol. The tail has a very low alcoholic content and sour taste. The middle (main distillate) represents 40-50% of the total distillate. Distillation stops when the tail has an alcohol content of below 15%. The forehead and tail are collected separately and added to the next decoction for distillation. First distillation produces brandy (30-35% alcohol) with an ambiguous taste. During the second distillation, the content of the most volatile component is reduced. Aging is usually completed in wood barrels, in which the brandy turns dark, yellow-brown and of harmonious taste.

The wood embedding technique consists in the insertion of handcraft objects made of poplar or mulberry wood, into the brandy bottles. In regards to the fruit embedding technique, the fruit is not only decorative; it imparts to the drink its color, aroma and special properties. It contains vitamins and minerals that get transmitted into the beverage. Once sealed, the bottle can be kept for decades.

The aims of the study were: (i) to present the traditional manufacturing process of fruit brandy production which is part of the gastronomic heritage from Maramures County (NW of Romania) (ii) to investigate the composition of different fruit brandies, (iii) to depict the changes that took place as a consequence of embedding wood or fruit in the fruit brandy. Physicochemical analysis of the brandy samples, including the gas chromatography analysis of volatile compounds were performed. The changes in physicochemical characteristics of brandies throughout 4 weeks maturation, when the product was kept in contact with wood or fruit, were investigated.

RESULTS AND DISCUSSIONS

Physico-chemical analysis of brandy assortments

Table 1 presents the physico-chemical determinations of four samples of fruit brandy: plum brandy (PB1), plum brandy with mulberry wood (PBM), AB (apple brandy), ABP (apple brandy with poplar wood).

The results shown in Table 1 indicate that the addition of wood to brandy have a significant influence on the following parameters: density, ethanol concentration, total acidity, total SO₂ and aldehyde content of the brandies and a less significant influence on the total extract of the beverages. The refractive index of the beverages showed only a slight variation. In the case of most of parameters, the influence was significant after 2 or 3 weeks.

Table 1. Physico-chemical properties of PB1, PBM, AB, ABP fruit brandy samples and their evolution during four weeks of preservation in contact with wood

Sample	Density (mg/mL)	Ethanol (%vol.)	Total extract (g/L)	Total acidity* (mg/L)	Total SO ₂ (mg/L)	Aldehydes** (mg/L)	Refractive index	
PB1	917.2 (0.27) ab	57.1 (0.04) h	0.0670 (0.004) a	115 (0.75) a	1.96 (0.03) g	12.2 (0.27) de	1.361 (5x10 ⁻⁴) a	
PBM	After 1 week	917.3 (0.15) ab	57.01 (0.04) gh	0.0680 (0.003) a	120 (0.50) b	1.84 (0.03) f	11.9 (0.36) bcde	1.361 (3x10 ⁻⁴) a
	After 2 weeks	917.4 (0.26) a	56.92 (0.09) gh	0.0685 (0.001) a	124 (0.61) c	1.72 (0.03) d	11.6 (0.27) abc	1.361 (3x10 ⁻⁴) a
	After 3 weeks	917.5 (0.15) b	56.87 (0.11) fg	0.0690 (0.003) a	126 (0.66) d	1.68 (0.02) cd	11.3 (0.35) a	1.362 (5x10 ⁻⁴) a
	After 4 weeks	917.6 (0.15) b	56.85 (0.04) f	0.0695 (0.001) a	131 (0.65) e	1.65 (0.02) c	11.2 (0.36) a	1.362 (3x10 ⁻⁴) a
AB	922.1 (0.2) c	54.73 (0.05) e	0.0690 (0.002) a	164 (0.66) f	1.78 (0.03) e	12.4 (0.27) e	1.363 (5x10 ⁻⁴) a	
ABP	After 1 week	922.5 (0.32) c	54.59 (0.06) d	0.0695 (0.001) a	186 (0.98) g	1.66 (0.04) c	12.0 (0.46) cde	1.363 (5x10 ⁻⁴) a
	After 2 weeks	923.1 (0.25) c	54.31 (0.05) c	0.0700 (0.001) a	198 (0.78) h	1.59 (0.02) b	11.7 (0.17) ab	1.363 (3x10 ⁻⁴) a
	After 3 weeks	923.7 (0.36) d	54.02 (0.09) b	0.0705 (0.001) a	205 (0.44) i	1.54 (0.04) a	11.4 (0.27) a	1.364 (5x10 ⁻⁴) a
	After 4 weeks	924.3 (0.27) d	53.73 (0.04) a	0.0710 (0.004) a	212 (0.66) j	1.52 (0.04) a	11.3 (0.17) a	1.364 (3x10 ⁻⁴) a

SD are shown in the brackets

* expressed as acetic acid; ** expressed as acetaldehyde

The values with different letters in a column (a, b, c etc.) are significantly different at P<0.05

It was found that the plum brandy density, acidity and total extract increased after the addition of mulberry wood, after the first week. Regarding the ethanol content, total SO₂ and aldehydes, they decreased over time. The density, acidity and extract of apple brandy increased even after one week of adding poplar wood. The alcohol losses of samples were due to both evaporation and changes that alcohol suffered over time. Part of the ethanol forms chemical combinations with acids and oxygen in air to form acetaldehydes, ethers. The

increase in total extract was recorded due to the transformations suffered by distillates over time. The increase in acidity was due to the presence of soluble acids in the composition of the two types of wood, and, especially the very slow oxidation of alcohol in acetic acid. After comparing the refractive indices, a slight increase was observed both for PB1 and PBM due to the dissolving and evaporation processes that occurred during storage.

Table 2 presents the physico-chemical properties in order to trace the fruit effect on the quality of the brandy: plum brandy (PB2), plum brandy matured with cherry (PBC) and plum brandy matured with pear (PBP). The fruit to brandy additions have a significant influence on the all the investigated parameters. The influence was significant after the first week of treatment except ethanol concentration of PBC brandy that showed a decrease after four weeks of maturation.

Table 2. Physico-chemical properties of PB2, PBC, PBP fruit brandy samples and their evolution during four weeks of preservation in contact with fruit

Sample	Density (mg/mL)	Ethanol (%vol.)	Total extract (g/L)	Total acidity* (mg/L)	Total SO ₂ (mg/L)	Aldehydes** (mg/L)	Refractive index	
PB2	932.0 (0.46) a	55.45 (0.09) c	0.0670 (0.001) a	117 (0.50) a	1.96 (0.01) e	4.40 (0.1) h	1.363 (3x10 ⁻⁴) a	
PBC	After 1 week	932.9 (0.61) b	55.41 (0.08) c	0.0677 (0.0015) ab	124 (0.87) b	1.90 (0.06) cde	4.07 (0.05) g	1.363 (5x10 ⁻⁴) a
	After 2 weeks	933.8 (0.32) cd	55.37 (0.14) c	0.0684 (0.0003) bc	136 (0.82) d	1.84 (0.03) abc	3.72 (0.08) e	1.363 (5x10 ⁻⁴) a
	After 3 weeks	934.5 (0.53) d	55.32 (0.07) cd	0.0693 (0.0004) bc	155 (1.27) e	1.80 (0.04) ab	3.56 (0.05) d	1.364 (5x10 ⁻⁴) a
	After 4 weeks	945.7 (0.47) h	55.28 (0.04) bcd	0.0705 (0.001) c	176 (1.01) g	1.78 (0.06) a	3.46 (0.03) cd	1.364 (3x10 ⁻⁴) a
PBP	After 1 week	933.4 (0.57)) bc	55.36 (0.09) bc	0.0696 (0.0006) bc	134 (1.13) c	1.91 (0.05) de	3.92 (0.06) f	1.364 (5x10 ⁻⁴) a
	After 2 weeks	935.9 (0.25) e	55.12 (0.09) abc	0.0724 (0.0006) d	161 (0.56) f	1.86 (0.03) bcd	3.42 (0.06) c	1.365 (3x10 ⁻⁴) b
	After 3 weeks	937.2 (0.27) f	55.06 (0.08) ab	0.0745 (0.0006) e	188 (0.87) h	1.83 (0.03) ab	3.04 (0.06) b	1.366 (5x10 ⁻⁴) c
	After 4 weeks	938.9 (0.44) g	55.01 (0.04) a	0.0760 (0.001) f	205 (0.44) i	1.82 (0.03) ab	2.80 (0.07) a	1.367 (3x10 ⁻⁴) d

* expressed as acetic acid; ** expressed as acetaldehyde

The values with different letters in a column (a, b, c) are significantly different at P<0.05

The ethanol, total SO₂, and aldehyde decreased under the influence of fruit, much more intensely than in the case of simple brandy. Alcoholic concentration decreases slowly after the introduction of cherries into plum brandy, probably due to the small size of the fruit, that, can absorb ethanol through a large contact surface. The alcohol losses of the samples are due to both evaporation and changes that alcohol suffers over time. Part of the alcohol forms chemical combinations with acids and oxygen in air, forming aldehydes, ethers. The plum brandy density increases after the addition of the fruit. The increase in total acidity in acetic acid has risen significantly, the samples falling within the limits that must be respected by the consumer. The increase in acidity is due to the soluble acids in the composition of the two types of fruit and to the very slow oxidation of alcohol in acetic acid. The value of acid extract increases significantly with the use of pears and less so when using cherries. No sulphates, chlorides or impurities were identified in any of the samples. By fruit addition to brandies, the refractive index showed a slight but significant increase, more evident in the case of pears.

Chromatographic analysis

The volatile compounds responsible for the specific aroma of the alcoholic beverages were separated by gas chromatography and presented in Table 3.

Table 3. The mean values of retention times (RT) and concentrations in mg / 100 mL absolute alcohol with SDs for all components identified in PB1 and PBM

No.	CG separated components	Plum brandy (PB1)		Plum brandy and mulberry (PBM)	
		Retention times (RT(min) ± SD)	Concentration (mg/100mL± SD)	Retention times (RT (min) ± SD)	Concentration (mg/100mL± SD)
1	Methanol	13.725 ± 0.012	201.22 ± 4.04a*	13.727 ± 0.012	205.56 ± 3.96a
2	Propan-1-ol	12.127 ± 0.010	39.93 ± 0.98a	12.127 ± 0.010	41.35 ± 0.99a
3	2-methylpropan-1-ol	15.408 ± 0.014	103.31 ± 2.82a	15.410 ± 0.014	99.92 ± 2.65a
4	3-methylbutan-1-ol	20.015 ± 0.017	269.67 ± 8.09a	20.017 ± 0.017	261.04 ± 7.94a
5	Ethyl acetate	5.076 ± 0.007	1355.04 ± 37.94a	5.075 ± 0.007	1348.84 ± 35.44a
6	Butan-1-ol	17.041 ± 0.015	2.12 ± 0.06a	17.044 ± 0.015	2.56 ± 0.08b
7	Butan-2-ol	13.928 ± 0.012	0.98 ± 0.02b	13.906 ± 0.012	0.72 ± 0.01a
8	Acetaldehyde	4.852 ± 0.005	12.41 ± 0.37b	4.852 ± 0.005	11.10 ± 0.32a
9	Acetal	17.634 ± 0.015	17.54 ± 0.45a	17.636 ± 0.015	17.10 ± 0.42a

* Means followed by the same letter in a row are not statistically different at P<0.05 significance level

Figure 1a presents the chromatogram of plum brandy 1 (PB1) while Figure 1b, the chromatogram of PBM with a quite similar pattern.

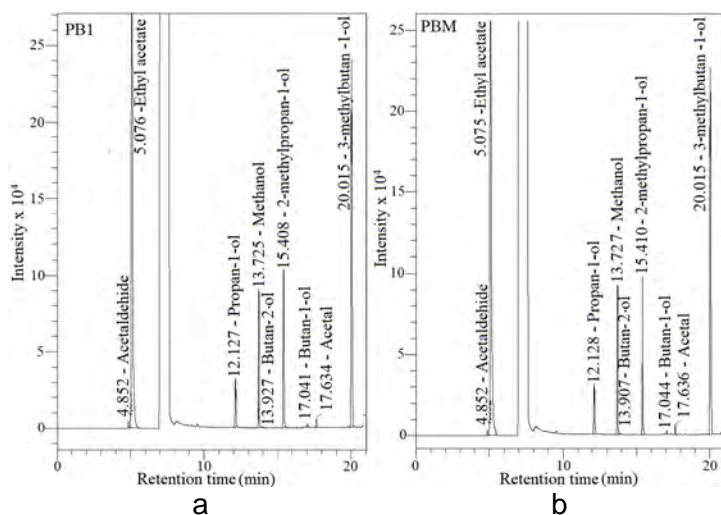


Figure 1. Chromatogram of plum brandy 1 (PB1, a), and plum brandy with mulberry wood (PBM, b)

In plum brandy methanol concentration is higher, when compared to other brandy alcoholic drinks due to the higher content of pectin in plums [14]. The effect of the addition of mulberry wood in the plum brandy was a slight increase in the concentration of methanol, propanol and 1-butanol, respectively, and a decrease of the concentration of 2-methylpropanol, ethyl acetate, 2-butanol, acetaldehyde and acetal.

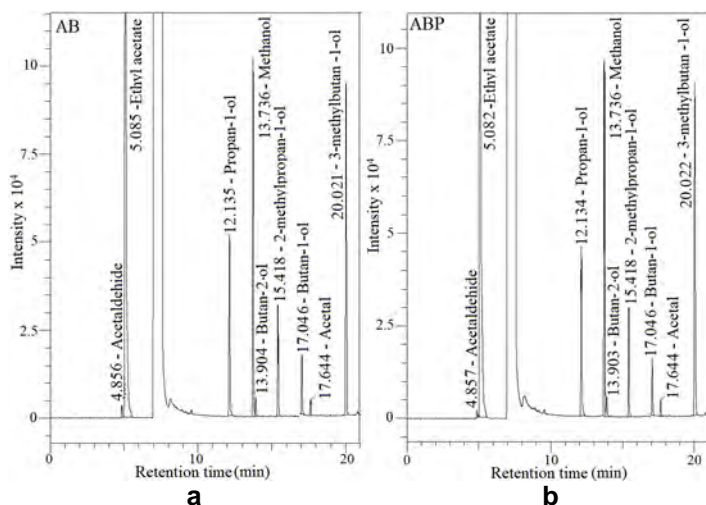


Figure 2. Chromatogram of apple brandy, AB (a) and apple brandy with poplar wood ABP (b)

The chromatograms of apple brandy and apple brandy matured in the presence of poplar wood are shown in Figure 2 a and b while the main volatile compounds present in apple brandies are shown in Table 4.

Table 4. Mean retention times (RT) and concentrations in mg / 100 mL absolute alcohol with SDs for all components identified in the AB and ABP titers

No.	GC Separated components	Apple brandy (AB)		Apple brandy with poplar wood	
		Retention times (RT (min) \pm SD)	Concentration (mg/100mL \pm SD)	Retention times (RT (min) \pm SD)	Concentration (mg/100mL \pm SD)
1	Methanol	13.736 \pm 0.012	235.04 \pm 3.66a*	13.736 \pm 0.012	234.02 \pm 3.65a
2	Propan-1-ol	12.135 \pm 0.011	68.31 \pm 1.58a	12.127 \pm 0.010	66.82 \pm 1.57a
3	2-methylpropan-1-ol	15.418 \pm 0.014	33.34 \pm 0.86a	15.418 \pm 0.014	34.26 \pm 0.89a
4	3-methylbutan-1-ol	20.021 \pm 0.016	107.64 \pm 2.94a	20.022 \pm 0.016	107.46 \pm 2.93a
5	Ethyl acetate	5.085 \pm 0.006	992.25 \pm 26.28a	5.082 \pm 0.006	993.48 \pm 26.32a
6	Butan-1-ol	17.046 \pm 0.015	17.45 \pm 0.09 b	17.046 \pm 0.015	17.03 \pm 0.09a
7	Butan-2-ol	13.904 \pm 0.011	7.54 \pm 0.04a	13.903 \pm 0.011	8.37 \pm 0.05b
8	Acetaldehyde	4.856 \pm 0.005	10.83 \pm 0.29a	4.857 \pm 0.005	9.99 \pm 0.24a
9	Acetal	17.644 \pm 0.014	12.75 \pm 0.31a	17.644 \pm 0.014	13.00 \pm 0.33a

* Means followed by the same letter in a row are not statistically different at P<0.05 significance level

Poplar wood added in apple brandy has the effect of increasing 2-methylbutanol, ethyl acetate, 2-butanol, acetal and decreasing methanol, propanol, 3-methyl-1-butanol, 1-butanol and acetaldehyde. Ethyl acetate occurred in high concentration, but still a lower value than in the case of plum brandy (PB1) or plum mulberry brandy. There is a slight increase in the propanol concentration in apple brandy when compared to the plum one. Similarly, an increase in butanol concentration is observed in the case of apple brandy. The concentration of methanol in apple brandy was higher than in the plum one due to the high content of pectin in the apple and by galacturonic acid methylation during fruit fermentation. The ethyl acetate concentrations in apple brandy are not significantly influenced by the poplar wood addition. Ester, due to the lowest organoleptic threshold, are very important in the contribution to spirit flavour, [14]. Butan-2-ol concentration in apple brandy increased by maturation in the presence of poplar wood probably under the influence of wood components.

The chromatograms of plum brandy 2, matured in the presence of fruit (pear and cherries) are shown in Figure 3.

The main volatile compounds present in brandy samples (PBP, PBC) in comparison to plum brandy 2 subjected to maturation in the presence of fruit, are shown in Table 5.

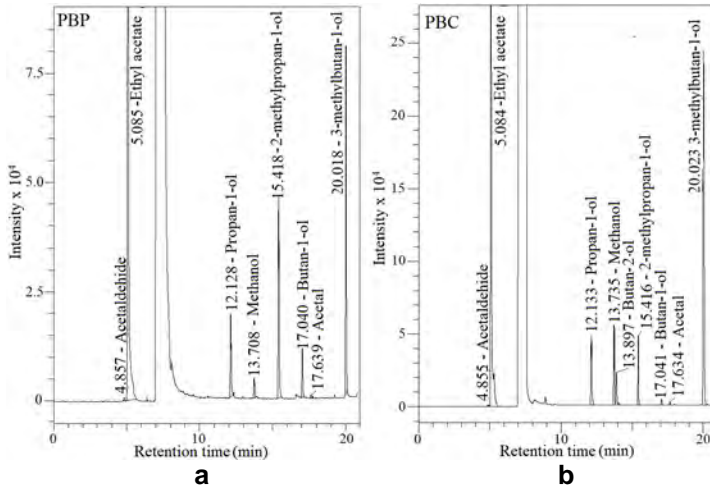


Figure 3. Chromatogram of plum brandy with pear PBP (a) and plum brandy with cherries PBC (b)

Table 5. Mean retention times (RT) and concentrations in mg / 100 mL absolute alcohol with SDs for all components identified in the PB 2 and PBP and PBC titers

No	CG separated components	Retention times (RT(min) \pm SD)	PB 2 (mg/100mL \pm SD)	PBP (mg/100mL \pm SD)	PBC (mg/100mL \pm SD)
1	Methanol	13.727 \pm 0.006	86.62 \pm 2.12 b*	13.18 \pm 0.37 a	131.32 \pm 4.03 c
2	Propan-1-ol	12.128 \pm 0.005	20.86 \pm 0.45a	32.06 \pm 0.58b	70.21 \pm 1.92c
3	2-methylpropan-1-ol	15.410 \pm 0.004	34.26 \pm 0.62a	62.81 \pm 1.c	53.47 \pm 1.42b
4	3-methylbutan-1-ol	20.017 \pm 0.005	144.18 \pm 5.24b	113.48 \pm 2.99a	294.15 \pm 6.52c
5	Ethyl acetate	5.081 \pm 0.004	118.26 \pm 3.07a	763.48 \pm 21.05b	1282.91 \pm 32.13c
6	Butan-1-ol	17.041 \pm 0.015	0.79 \pm 0.02a	15.18 \pm 0.45c	5.22 \pm 0.15b
7	Butan-2-ol	13.893 \pm 0.006	0.00 \pm 0.00a	0.00 \pm 0.00a	32.09 \pm 0.59b
8	Acetaldehyde	4.855 \pm 0.003	4.34 \pm 0.34c	2.81 \pm 0.08a	3.46 \pm 0.14b
9	Acetal	17.637 \pm 0.005	14.06 \pm 0.39c	2.60 \pm 0.07a	6.82 \pm 0.19b

* Means followed by the same letter in a raw are not statistically different at P<0.05 significance level

The amount of methanol decreases in the brandy containing pears and grows in cherry plum brandy because of the higher content of pectin in cherries, especially during fruit fermentation. By adding pears and cherries to plum brandy, a considerable increase of propanol and 3-methylbutanol is observed. The concentration of 2-methylpropanol and 1-butanol increases much more in the pear-containing brandy, than in that containing cherries. 3- methylbutanol and 2-methylpropanol may have both positive and negative

effects on the flavor, increasing their concentrations giving a strong, spicy aroma and specific taste, while low concentrations can give a fruity character [17]. Non-existing 2-butanol in plum brandy and that with pear increases greatly in cherry plum brandy. In literature, it has been shown that 1-butanol and 2-butanol are highly discriminating parameters of alcoholic beverages [18].

Acetal is present in very low concentrations in cherry or pear brandy, but its presence is relevant due to its contribution to the spirit flavour with unpleasant notes [19]. The acetal concentration decreases with the addition of fruit (pear and cherry) to the brandy. The content of acetaldehyde and higher alcohols are related to the ethanol content. Acetaldehyde content increases during aging due to chemical oxidation of ethanol and it may cause the formation of a larger quantity of acetal during maturation of distillates. Table 5 shows that the content of acetaldehyde decreases greatly under the influence of pears and cherries.

Ethyl acetate in plum brandy has a relatively low value, and due to the influence of the pears, it increases greatly, even more in cherry brandy [14]. Increasing the amount of ethyl acetate was due to the formation of chemical combinations of alcohol with the acids in the composition of wood, with oxygen in the air. The consequence is that ethyl acetate, due to the low organoleptic threshold, greatly influences the aroma of spirits, due to its decomposition to acetic acid and ethanol [14]. Other causes of the high levels of ethyl acetate may be the prolonged aerobic deposition of cherries or pears before introduction into the brandy, where rapid fermentation occurs, the destruction of acetic bacteria, or the corresponding separation of the fractions of the heads during distillation [14, 19].

Cluster analysis

Cluster analysis established the similarities between the brandy assortments and between the volatile components of the brandies. Figure 4 shows the formation of 2 major clusters, C1 and C2. Cluster C1 comprises 5 elements: the subcluster composed by brandies PB and PBM, another subcluster composed by AB and ABP, and, at a higher Euclidean distance, PBC. Cluster C2 comprises 2 elements: PB2 and PBP. The addition of fruit (cherry or pears) significantly influences the composition of volatile compounds while the addition of mulberry wood to plum brandy or of poplar wood to apple brandy do not, taking into account that PB1 and PBM, respectively AM and ABM, showed a high similarity considering the volatile compounds (Euclidean distance lower than 1).

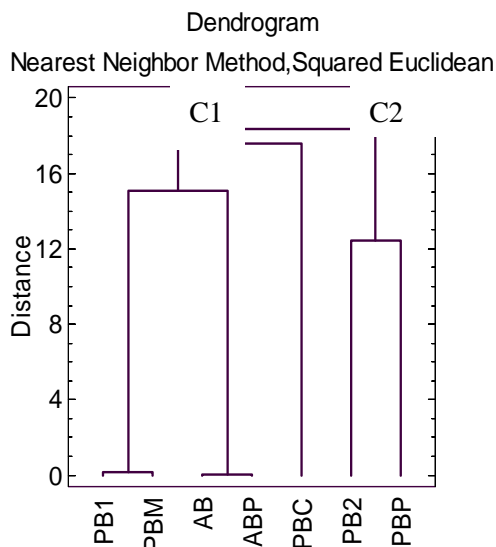


Figure 4. Cluster analysis of fruit brandies

CONCLUSION

The influence of wood and fruit addition to the plum and apple brandies on the composition of brandies during the maturation over 4 weeks was studied. Poplar and mulberry wood have a significant influence on the plum and apple distillates, the concentrations of ethanol and aldehydes decreasing in both distillates. Due to the evaporation of the volatile substances in the brandies in which mulberry and poplar wood were added, the amount of extract increased over time. The total acidity of the samples increased due to the decrease in alcoholic strength. The alcoholic concentration of the brandy with cherries and pears decreases when compared to that without fruit, due to the evaporation, absorption into fruit mass and esterification with acids derived from fruit. The aldehydes concentrations of the brandy with cherries and pears also decrease compared to that without fruit due to their high chemical reactivity. The refractive indices of plum brandies with cherries and pears showed a slight increase. Chromatographic analysis showed volatile compounds with large differences in their concentrations, depending on the range of brandy, but also on the maturation conditions. The superior quality of the brandy is given by a much lower content in higher alcohols, in methyl alcohol and in aldehydes, as well as a lower acidity. Large differences in volatile compounds were found, depending on the type of brandy (plum), but also on the fruit used.

EXPERIMENTAL SECTION

Provenance of fruit brandy samples

The fruit brandies (plum and apple) were purchased from local producers that used traditional manufacturing methods. Two fruit growing areas in Maramureş County were considered: the area around Baia Mare city and the northeastern part of the county where the tradition of fruit brandy manufacturing is well-preserved. Plum brandy 1 (PB1) and apple brandy originate from the fruit growing area around Baia Mare, while plum brandy 2 was produced in Poienile de sub Munte located in the northeastern part of Maramureş County.

Influence of wood and fruit on the fruit brandy physico-chemical properties

To simulate the aging process, pieces of mulberry or poplar wood were added to the plum or apple brandy. In other experiments, fruit (pear and cherry) were added to brandy samples to assess the influence of maturation in the presence of fruit.

Mulberry wood was added to PB1: plum brandy was poured into a glass bottle containing a mulberry piece of wood, at a ratio of about 5:100 (m/V). The same procedure was carried out for apple brandy but a piece of poplar was used instead. The influence of mulberry or poplar wood on the physico-chemical properties of fruit brandy was assessed by the weekly determination of density, ethanol concentration, total extract, total acidity, aldehyde content, refractive index, during a period of four weeks. The fruit influence on plum brandy was established the same way. The ratio fruit: brandy was 10:100 (m/V). We studied the changes in the physico-chemical composition of fruit brandies during the maturation process. After 4 weeks of maturation, the composition in major volatile compounds was comparatively analyzed in regards to control brandies without wood or fruit addition.

Physico-chemical analysis of distillates

The determination of the relative density of the product to be analyzed was carried out by the pycnometer method [20]. A 100 mL pycnometer was used and the relative density was calculated as a ratio of pycnometer mass filled with the alcoholic beverage and pycnometer mass filled with distilled water at 20°C.

The determination of the total dry extract is carried out following the established method [20-21] by putting a certain volume (25 mL) of brandy into a metallic flat-bottomed cylindrical capsule of known and constant mass. The brandy was evaporated on a water bath, dried in a laboratory oven at 105°C for 2 h and cooled in a desiccator for 30 minutes. The capsule containing the dry extract was weighed on the analytical balance and the result was expressed in g/L.

The determination of total acidity was performed following the established procedure [20]: a sample of 25 mL fruit brandy from which CO₂ was removed was diluted with 200 mL of cooled boiled distilled water and titrated against 0.05 N hydroxide solution in the presence of phenolphthalein [20-21].

The total SO₂ was measured according to the SR6182/13-2009 standard by converting the sulfites into volatile SO₂ that was steam distilled into a standard solution of I₂. A redox process takes place reducing partially I₂. The residual I₂ was determined by a redox titration with a standard solution of sodium thiosulphate in the presence of a starch indicator (1% aqueous solution).

The total SO₂ was measured according to the SR6182/13-2009 standard by converting the sulfites into volatile SO₂ that was steam distilled into a standard solution of I₂. A redox process takes place reducing partially I₂. The residual I₂ was determined by a redox titration with a standard solution of sodium thiosulphate in the presence of a starch indicator (1% aqueous solution). The aldehyde content was measured according to a standardized titrimetric method [22] based on the reaction of aldehydes contained in a 50 mL sample with 10 mL of a sodium bisulphite solution of known concentration (0.05 N). The mixture was stirred and kept in a dark environment for 30 minutes. Then an iodine standard solution of the same concentration was added and the excess of iodine was titrated with a sodium thiosulphate solution in the presence of a starch indicator. A blank sample of 50 mL distilled water was treated in a similar manner and the differences in the volumes of sodium thiosulphate solution used for blank sample and brandy sample was used to calculate the aldehyde concentration in mg/L, expressed as acetaldehyde, reported to the absolute ethanol. The qualitative test for the presence or the absence of sulphates was realized with hydrochloric acid and barium chloride. Determining the refractive index was done with a Zeiss Abbe refractometer Model G.

The volatile components in fruit brandies were analyzed by gas chromatography (GC) with a flame-ionization detector (FID) by direct injection into the gas chromatograph column using the method adapted from European Union reference method for volatile compounds [23] considering the recommendations and conclusions of similar studies [16, 24-25].

The used gas chromatograph is a Shimadzu 2025 model equipped with an automatic liquid sampler and a flame ionization detector. Separation of the analytes was performed on a capillary chromatographic column of polar silica coated with polyethylene glycol (characteristics: 30 m length x 0.32 mm x 0.25 µm thickness of polyethylene glycol film). The carrier gas was nitrogen with a flow rate of 1.5 mL/minute. The qualitative identification of the separated compounds was based on the retention time in the column compared to values of standards. The major identified and quantified volatile compounds, besides ethanol, were: acetaldehyde, ethyl acetate, propan-1-ol, methanol, butan-2-ol, 2-methylpropan-1-ol, butan-1-ol, acetal and 3-methylbutan-1-ol. All the reagents were of analytical grade. Ultrapure water

(Millipore system) was also used throughout all experiments. Due to a slow variation during the maturation process, the analysis by gas chromatography was performed only at the end of the study for the brandies with fruit and wood and for the control brandies unmodified by the addition of fruit or wood.

Statistical analysis

All the experimental measurements were performed in triplicate and were expressed as mean \pm SD (standard deviation). Statistical analysis of data was conducted with the software programs Excel and Statgraphic. To compare the values of the volatile compounds, the least significant difference was calculated by using the Statgraphic program. The same program was used to perform the analysis of data variance (ANOVA) for multiple sample comparison to determine which means are significantly different from which others. Cluster analysis was used to establish the similarity or dissimilarity between the fruit brandies by using their mean volatile composition as classification variables. Statgraphic was used to perform the cluster analyses and generate the dendrogram plot. The fruit brandies were clustered by using their mean volatile composition as classification variables. The data was standardized before clustering, to allow all characteristics contribute to a comparable extent to the discrimination process [19]. The distance measure was the Euclidean distance and the picked linkage method was average linkage. The clusters were generated with the nearest neighbor method.

REFERENCES

1. N. Pomohaci, I. Cioltean, L. Vişan, F. Rădoi, "Ţuica și rachiurile naturale", Editura Ceres, Bucureşti, **2002**.
2. M. Balcerek, K. Pielech-Przybylska, U. Dziekońska-Kubczak, P. Patelski, E. Strąk, *Food Technol Biotechnol*, **2017**, 55 (3), 333.
3. J. Mrvcic, S. Posavec, S. Karazic, D. Stanzer, A. Peša, V. Stehlik-Tomas, *Croatian J Food Sci Technol*, **2012**, 4 (2), 102.
4. J. Tóthová, L. Žiak, J. Sádecká, *Acta Chimica Slovenica*, **2008**, 1, 265.
5. N. Spaho, P. Dürr, S. Grba, E. Velagić-Habul, M. Blesić, *J-Institute of Brewing*, **2013**, 119, 48.
6. V. Tesevic, N. Nikicevic, A. Jovanovic, D. Djokovic, L. Vujisic, I. Vuckov, M. Bonic, *Food Technol Biotechnol*, **2005**, 43, 367.
7. M.D. Croitoru, E. Topor, I. Fülöp, E. Fogarasi, *Acta Medica Marisiensis*, **2013**, 59(4), 206.
8. D. Dimitrov, T. Yoncheva, V. Haygarov, *Ukrainian Food J*, **2016**, 5, 237.

9. Ordin nr. 368/**2008** pentru aprobarea Normelor privind definirea, descrierea, prezentarea si etichetarea bauturilor traditionale romanesti, Monitorul Oficial, Partea I nr. 496 din 02/07/2008 in Romanian (Order no 368/2008 for the approval of the Norms regarding the definition, description, presentation and labeling of traditional Romanian drinks, the Official Monitor, Part I, no 496, 02/07/2008)
10. M.J. Claus, K.A. Berglund, *Journal of Food Process Engineering*, 2005, 28, 53.
11. D.W. Lachenmeier, E.-M. Sohnius, *Food Chem Toxicol*, **2008**, 46, 2903.
12. P. Paiano, G. Bianchi, E. Davoli, E. Negri, R. Fanelli, E. Fattore, *Food Chem*, **2014**, 154, 26.
13. S. Cortés, R. Rodríguez, J.M. Salgado, J.M. Domínguez, *Food Control*, **2011**, 22, 673.
14. V. Kostik, B. Gjorgeska, B. Angelovska, I. Kovacevska, *Sci J. Anal Chem.*, **2014**, 2(4), 41.
15. I. Caldeira, M.C. Climaco, R.B. de Sousa, A.P. Belchior, *J. Food Eng.*, **2006**, 76, 202.
16. T.E. Coldea, C. Socaciu, Z. Moldovan, E. Mudura, *Notulae Botanicae Horti Agrobotanici*, **2014**, 42 (2), 530.
17. F. Rodrigues, M. Caldeira, J.S. Camara, *Anal Chim Acta.*, **2008**, 609, 82.
18. D. Wencker, M. Louis, G. Nomura, M. Hasselmann, *Annales des falsifications et de l'expertise chimique et toxicologique*, **1981**, 74, 487.
19. S. Cortés, R. Rodríguez, J.M. Salgado, J.M. Domínguez, *Food Control*, **2011**, 22, 673.
20. OIV (International Organisation of Vine and Wine), **2014**, *Compendium of international methods of analysis of spirituous beverages of vitivicultural origin, Alcoholic strength by volume – Type I methods*, <http://www.oiv.int/public/medias/2629/oiv-ma-bs-01.pdf>, accessed 10.03.2018
21. H. Heymann, S.E. Ebeler, *Rapid methods to analyze alcoholic beverages, In Sensory and Instrumental Evaluation of Alcoholic Beverages*, 1st ed.; H. Heymann, S.E. Ebeler, Academic Press, Elsevier, Amsterdam, Holland, **2017**, Chapter 5, pp. 84-104.
22. Food Safety and Standards Authority of India, Ministry of Health and Family Welfare Government of India, New Delhi, **2015**, *Manual of Methods for Analysis of Alcoholic Beverages*; pp.15-17
23. Commission Regulation (EC) No 2870/2000 of 19 Decembrie 2000 laying down Community reference methods for the analysis of spirits drinks, **2000**, *Official J. European Commun.*, L333/20.
24. R.R. Madrera, B.S. Valles, *J. Chromatogr Sci*, **2007**, 45, 428.
25. R.E. Anli, N. Vural, Y. Gucer, *J-Institute of Brewing*, **2007**, 113, 302.

TRACE METAL CONCENTRATION AND HUMAN HEALTH RISK ASSESSMENT IN DISTILLED ALCOHOLIC BEVERAGES IN ROMANIA

FLORIN DUMITRU BORA^{a*}, ANAMARIA CĂLUGĂR^b,
CLAUDIU IOAN BUNEA^b, VALENTIN PETRESCU MAG^c,
CLAUDIA CIMPOIU^d, VASILE RĂZVAN FILIMON^e

ABSTRACT. The concentration of 12 metals (Mg, Ca, K, Mn, Fe, Co, Ni, Cr, Cu, Pb, Cd, and Zn) in 14 classes of alcoholic beverages were determined by ICP-MS after HNO₃/H₂O₂ digestion. The mean concentration of metals (µg/mL) in these alcoholic beverages varied in the ranges 0.26-15.43, 0.94-234.43, 0.56-278.02, 0.02-2.69, 0.18-2.64, 0.03-0.13, 0.03-0.13, 0.02-0.29, 0.04-2.51, 0.03-0.30, 0.02-0.04, and 0.13-0.88 for Mg, Ca, K, Mn, Fe, Co, Ni, Cr, Cu, Pb, Cd, and Zn respectively. The concentration of metals found in these particular alcoholic beverages was below the International Statutory Limits for metals in alcoholic beverages. The estimated daily intake of the metals based on a per capita consumption of 14.4 L per annum pure alcohol was lower than the tolerable daily intake of each metal. The individual and combined target hazard quotients of the metals were <1, indicating no long-term health concerns from the consumption of these alcoholic beverages based on their metal content alone.

Keywords: alcoholic beverages, daily intake, target hazard quotients, Romania.

^a Research Station for Viticulture and Enology Targu Bujor, 65 G-ral Eremia Grigorescu, RO-805200, Galați Country Romania

^b University of Agricultural Sciences and Veterinary Medicine, Department of Horticulture and Landscaping, 3-5 Mănăştur Street, RO-400372 Cluj-Napoca, Romania

^c University of Agricultural Sciences and Veterinary Medicine, Department of Agriculture, 3-5 Mănăştur Street, RO-400372 Cluj-Napoca, Romania

^d Babeş-Bolyai University, Faculty of Chemistry and Chemical Engineering, 11 Arany Janos str., RO-400028, Cluj-Napoca, Romania

^e Research Station for Viticulture and Enology Iași, 48 Aleea Mihail Sadoveanu, RO-700489, Iași Country Romania;

* Corresponding author: borafiorindumitru@gmail.com

INTRODUCTION

The concentration of metals in many alcoholic beverages can be a significant parameter affecting their consumption and conservation. This derives from the negative and positive effects caused directly or indirectly by the presence of metals. Negative effects include beverage spoilage and hazing, as well as sensorial and health consequences [1]. Positive effects include the removal of bad odors and tasters [2], participation in fermentative processes [3], provision of pathways for dietary intake of some essential mineral [4], and usefulness for authentication purpose [5].

Metals find their way into alcoholic beverages at different stages and through various sources including raw materials, brewing, process type and equipment, bottling, aging/storage, and adulteration.

Several metal ions can be taken up from the surrounding soil by plants from which an alcoholic beverage is prepared. For instance, type of soil (i.e., it's geogenic), it's agrochemical treatments (e.g., the use of pesticides and fungicides), and the surrounding environmental pollution implies the mineral content of many beverages [6]. In this way, wines from vineyards in coastal areas are richer in Na [7]. Fungicides, pesticides, and fertilizers containing Cd, Cu, Mn, Zn and Pb, compounds can derive in increased contents of these metals in the alcoholic beverage [7]. Most of the Mg found in beer comes mainly from raw materials [1]. Cu in beer comes mainly from raw materials [4]; on the contrary, only a small percentage of the final Cu content in whiskey comes from the barely from which the spirit is distilled [8].

Hops, acids, silica gel, bases, flavoring agents, dilution water, additives, and stabilizers are potential sources of metal ions in the brewing process [4]. For example, the main source of Cu in wine is the CuSO_2 added to remove sulfidic odors [2]. The acidity of the liquor to be distilled may be important in this regard (e.g., in whiskeys), since more acidic beverage tend to contain more Cu [8]. The addition of fining and clarifying substances (e.g., flocculants) to reduce turbidity can bring about an increase in Al, Ca, Na in wine [7].

Major differences in metal content (e.g., Ni) have been found among alcoholic beverages depending on their processing. In this way, certain fermented beverages (e.g., beer and wine) contain several times more Ni than distilled beverages (e.g., brandy, vodka, and whiskey) [9].

Process equipment is frequently a key source of metal ions in the final products. Several examples follow: (1) the concentration of Cu comes from process equipment in vodka is twice as much that coming from raw materials [10]; in whiskey the main source of Cu is the copper still used for distillation process [8]; corrosion of tequila distillation equipment (made also from Cu),

provokes the presence of this in the final product [11]; storage of vodka in metal containers (e.g., Cu alloys or low-quality steel) results in their corrosion with the concomitant introduction of metals into the liquors [1], this is also the case with acidic wine vinegar [12]; the Cu, Fe, and Zn contained in home-produced alcoholic drinks can be essentially unrelated to the material fermented as it primarily depends on the several materials [13]; degree of still and the temperature in the distillate affect the Cu content in whiskey [1]; extremely high concentration of Fe, Zn, and Cu in home-produced beers and spirits can be largely traced to use of galvanized metal fermentation drums, when these replace old clay and wooden vessels [14]; the Fe content from musts and pulps increases due to the Fe concrete tanks used for the storage of raw materials [1]; contact of wine with process equipment, barrels, casks, and pipes is the usual source of Al, Cd, Cu, Cr, Fe, and Zn [7]; Pb plumbing can add Pb to beverages [2].

Metal addition from process equipment (e.g., stills) can be prevented by the use of high-quality steel or glass, although some organoleptic properties may be altered by the absence of certain metal ions added during distillation (e.g., the lack of minute amounts of Cu in tequila affects negatively its flavor).

Bottling equipment may also introduce metals in beverages. The content of Ca, Mg and Na brandies depends on the quality of water used for dilution after distillation [1]. The modification of certain imported alcoholic beverages „to bottle and sale by the addition of distilled or otherwise purified water to adjust the beverage to a required strength” is sometimes allowed. It is noteworthy that when metallic capsules seal alcoholic beverage bottles, some Pb may be carried over [15].

Possible effects caused by metals during these stages are multiple. Fe (III) and Mn (II) affect the stability of old wines and modify their sensorial quality after bottling since they are believed to activate molecular oxygen by forming reactive oxygen species (e.g., hydroxyl radicals) this is possible due to their electronic configurations involving unpaired electrons that may interact quantum mechanically with the dioxygen triplet [7]. Likewise, Fe catalyzes the oxidation of polyphenolic substances and Mn facilitates acetaldehyde formation, the products of these reactions yield undesirable precipitates. Cu and Zn can be introduced into beer by welded cans [4].

In the case of adulteration process, Pb and other metallic impurities can enter beverages during adulteration practices, e.g., adulterated vodka has been found to contain an excess of Ca and Mn ions [1]. The objective of the present study was to determine the concentration of 12 metals (Mg, Ca, K, Fe, Co, Ni, Cr, Cu, Pb, Cd, and Zn) in some alcoholic beverages, with a view to providing information on the metal profiles and risks associated with the consumption of these products.

RESULTS AND DISCUSSION

Wine Mineral Content

The mean concentration of Mg in the studied samples ranged from 0.26 to 15.43 µg/mL with an average of 3.84 µg/mL. The highest concentration of Mg was observed in cream liquors (15.43±1.57 µg/mL). The cream liquors, aperitif, local brandy, and local cider samples showed significantly higher mean concentrations ($p \leq 0.005$). The lowest mean level of Mg in the drinks samples was observed in rum (0.26±0.04 µg/mL). Iwegbue et al. [16] and Cameán et al. [17] reported Mg concentrations in the range of 0.26-25.45 µg/mL [16] and 0.24-11.20 µg/mL [17]. The levels of Mg recorded in the present study were lower than the levels reported in the wine literature 98.20 mg/L [18], 95-73 mg/L [19], 75.20 mg/L [20] however, the concentration of Mg in these samples was comparable to the levels found in spirits, liquor and whiskey [21].

The mean concentration of Ca in the alcoholic beverages varied from 0.94 to 234.43 µg/mL with an average of 23.77 µg/mL. Again, the highest concentration of Ca was observed in cream liquors (234.43±10.58 µg/mL). Cameán et al. [17] reported Ca levels ranging from 'not detected' to 14.80 µg/mL, while Iwegbue et al. [16] reported Ca levels from 1.43 µg/mL to 162.86 µg/mL. The high Ca concentration in the cream liquors could be due to enrichment of this type of drink with milk, which is known to contain substantial amounts of minerals [16]. The lowest mean level of Ca in the drinks samples was observed in dry gin (0.94±0.05 µg/mL). Lower level of Ca has been reported in the scientific literature in distilled products, 'not detected' to 14.80 mg/L (brandy) and from 6.00 to 11.00 mg/L (cognac) [22], 1.00 mg/L (gin) [23], 4.00 mg/L (rum) [23], 3.00 mg/L (rum) [22]. The concentration of Ca recorded in the present study was lower than the levels reported in the wine literature 83.50 mg/L [18], average values of 37.00 mg/L [19] and 65.90 mg/L [20]. In the coconut/orange liquor, showed significantly higher levels ($p \leq 0.005$) of Ca than the other brands analysed in this group. Apart from a few brands of coconut/orange liquor, the concentration of Ca in other classes of drinks was comparable to the concentration of reported in Brazilian cachaça and spirits [24].

The mean concentration of K in the alcoholic drinks ranged between 0.02 µg/mL to 278.02 µg/mL. The highest mean concentration of K was observed in cream liquors. The highest mean concentration of K varied significantly ($p \leq 0.005$) within the same class, as well as in other classes. The lowest mean level of Mg in the drinks samples was observed in aromatic schnapps. Cameán et al. [17] reported a K concentration ranging from 0.11 µg/mL to 70.06 µg/ml and Iwegbue et al. [16] reported K levels from

'not detected' to 322.58 µg/mL. Except for cream liquors, the K concentration in these alcoholic drinks was similar to the levels of K reported in Brazilian sugar cane spirit [24]. The concentration of K recorded was lower than the levels reported in the wine literature from 491.12 mg/L to 633.74 mg/L for red wines and from 148.66 mg/L to 327.64 mg/L for white wines [25] and 819.61 mg/L average value [26].

It was observed that the cream liquors contained a higher concentration of Mg, Ca and K compared with the other classes of alcoholic beverages. This suggests that persons who drink cream liquors in preference to spirits and other types of alcoholic drinks studied in this research would be likely to be exposed to more metals.

The highest mean level of Mn was observed in cognac (0.39 µg/mL) and the lowest in aromatic schnapps (0.02 µg/mL). The maximum permissible limit of Mn in drinking water is 0.40 µg/ml Iwegbue et al. [16]. The concentrations of Mn in the alcoholic beverages were lower than the permissible level in drinking water. Iwegbue et al. [16] reported Mn levels from 'not detected' to 0.33 µg/mL. Lower levels of Mn were observed in this study in comparison with the levels reported in wines 0.83 mg/L [25], 1.89 mg/L [18] and 2.04 mg/L [26], but were comparable to the levels reported from Brazilian cachaça and other international spirits [16].

The Fe concentration in the alcoholic beverages varied from 0.18 µg/mL to 2.64 µg/mL with an average of 1.03 µg/mL. The highest concentration of Mn was observed in spirit, while the lowest mean level was observed in aromatic schnapps. The guide provides a concentration of Fe in drinking water of 0.30 µg/mL [16]. The concentrations of Fe were higher than the permissible level in drinking water. Cameán et al. [17] reported Fe levels varying from 'not detected' to 2.03 µg/mL in Spanish brandy and Iwegbue et al. [16] reported Fe levels varying from 0.28 µg/mL to 1.48 µg/mL. The concentration of Fe found in the alcoholic drinks was comparable to the levels in Fe reported in the literature for other alcoholic beverages in beer and wine 0-25 mg/L [26; 15], in brandy 'not detected' to 2.30 mg/L [28; 15; 22], cognac 0.1 mg/L [28], gin 'not detected' [28] rum 1.00 mg/L [28], vodka 'not detected' [28], whiskey 'not detected' [28], 1.48 mg/L spirits [16], 0.29 mg/L brandy [16], 0.29 mg/L aromatic schnapps [16].

Co concentration in the beverages varied from 0.03 µg/mL to 0.16 µg/mL, with whiskey and aromatic schnapps having the maximum and minimum mean levels, respectively. The highest mean concentration of Co varied significantly ($p \leq 0.005$) within the same class, as well as in other classes. Xuebo et al. [29] reported a Co concentration ranging from 0.37 mg/L to 0.89 mg/L in baijiu (Chinese liquors) and Iwegbue et al. [16] reported Co levels varying from 'not detected' to 0.12 µg/mL. Lower levels of Co were

observed in this study in comparison with the levels reported in wines from 2.60 mg/L to 7.63 mg/L [25].

The mean concentration of Ni in the drinks varied between 0.02 µg/mL and 0.13 µg/mL. The highest mean concentration of Ni was observed in brandy and the lowest mean concentration was observed in aromatic schnapps. The maximum permissible limit of Ni in drinking water is 0.02 µg/mL Iwegbue et al. [16]. The mean concentration of Ni in most classes of these alcoholic beverages exceeded the maximum prescribed limit for Ni in drinking water. Iwegbue et al. [16], Xuebo et al. [29] and Ibanez et al. [1], also reported Ni mean concentration in alcoholic beverages which exceeded the maximum prescribed limit for Ni in drinking water. Ni concentration reported in this research were higher than the 0.0812-0.115 µg/mL reported in Brazilian cachaça and were comparable to levels reported for other alcoholic beverages 0.13 µg/mL in aromatic schnapps and 0.05 cognac [16]. Lower levels of Ni were observed in alcoholic beverages (this study) in comparison with the levels reported in wines from 0.073 mg/L to 19.40 mg/L [1].

The highest mean concentration of Cr was observed in cream liquor (0.29 µg/mL) and the lowest mean concentration was observed in spirit (0.02 µg/mL). The highest mean concentration of Cr varied significantly ($p \leq 0.001$) within the same class, as well as in other classes. Similar level of Cr has been reported in the literature [16] for alcoholic beverages, namely 0.28 µg/mL in cream liquor, 0.03 µg/mL in cognac and 0.05 µg/mL in punch, while level of Cr concentration in wine was higher (872.42 µg/L) than in the studied alcoholic beverages.

The mean concentration of Cu in the samples ranged from 0.04 µg/mL to 2.51 µg/mL, with an average of 0.43 µg/mL. The highest mean concentration of Cu was observed in cream liquor, while the lowest mean level was observed in the punch. The permissible limit of Cu in alcoholic beverages is set at 5.0 µg/mL [16]. The mean concentration of Cu in these alcoholic beverages was below the permissible limit. Cu concentration in the range of 1.64 to 4.40 µg/mL [16] has been reported for Brazilian cachaça and other international spirits [1].

Similar, in Spain the Cu concentration was in the range of 0.10 µg/mL to 8.01 µg/mL for brandy, gin, rum, liquor, and whiskey, in Denmark, Cu levels were in the range of 'not detected' to 0.12 µg/mL, were reported in for gin, rum, brandy and liquor [16]. The concentration of Cu found in the alcoholic drinks was comparable to the levels in Cu reported in the literature for other alcoholic beverages in spirits 0.40 mg/L [15], sherry brandy 0.22 to 5.31 mg/L [17], and in wine, fruit wine, cocktails from 'not detected' to 7.62 mg/L [1].

Table 1. Metal concentration (µg/mL) in distilled alcoholic beverages and liquors purchases in Romania (the values in parentheses represent the range)

Beverage type	Mg	Ca	K	Mn	Fe	Co	Ni	Cr	Cu	Pb	Cd	Zn
Whiskey	2.48±0.12 ^a (1.19-2.99)	6.99±0.55 ^{ad} (3.65-8.96)	6.18±0.68 ^d (4.08-8.54)	0.03±0.01 ^{cd} (<0.0001-0.07)	1.38±0.01 ^c (0.57-2.87)	0.16±0.06 ^a (0.05-0.45)	0.06±0.02 ^{cd} (0.03-0.21)	0.05±0.02 ^c (0.02-0.11)	0.19±0.06 ^{cd} (0.11-0.34)	0.28±0.06 ^a (0.14-0.52)	0.03±0.01 ^{ab} (0.01-0.10)	0.21±0.04 ^{cd} (0.13-0.38)
	3.07±0.47 ^a (0.79-11.21)	8.19±2.25 ^{cd} (4.67-20.09)	27.99±0.56 ^d (0.89-68.89)	0.07±0.02 ^{bc} (0.02-0.31)	0.87±0.12 ^{bc} (0.35-2.01)	0.05±0.02 ^{bc} (0.01-0.06)	0.03±0.01 ^d (0.01-0.05)	0.03±0.01 ^d (0.01-0.09)	0.24±0.09 ^a (0.08-0.78)	0.14±0.02 ^b (0.10-0.17)	0.03±0.01 ^{ab} (0.007-0.05)	0.45±0.11 ^b (0.09-0.76)
Local Brandy	6.48±0.78 ^c (4.53-18.32)	7.99±0.86 ^{cd} (3.87-12.05)	32.59±1.75 ^c (18.23-54.98)	0.07±0.02 ^{bc} (0.01-0.09)	1.22±0.13 ^{cd} (0.76-3.24)	0.08±0.04 ^b (0.03-0.10)	0.05±0.01 ^{cd} (0.02-0.08)	0.13±0.02 ^{cd} (0.09-0.21)	0.67±0.11 ^c (0.15±0.84)	0.15±0.06 ^b (0.11-0.18)	0.02±0.01 ^b (0.01-0.03)	0.28±0.09 ^c (0.16-0.38)
	15.43±1.57 ^a (6.55-23.42)	234.43±10.58 ^a (135.67-354.09)	278.02±9.91 ^a (79.56-632.11)	0.16±0.03 ^b (0.09-0.32)	2.10±0.21 ^b (0.89-5.61)	0.05±0.02 ^{bc} (0.03-0.07)	0.07±0.02 ^{cd} (0.04-0.10)	0.29±0.10 ^c (0.09-0.39)	0.15±0.04 ^{cd} (0.01-0.25)	0.18±0.09 ^b (0.13-0.24)	0.03±0.02 ^{ab} (0.001-0.04)	0.88±0.10 ^b (0.59-1.13)
Cream liquor	0.59±0.14 ^c (0.21-0.72)	3.07±0.66 ^{cd} (2.18-4.08)	5.41±0.90 ^{cd} (3.44-7.89)	0.39±0.06 ^a (0.12-0.43)	1.48±0.25 ^c (0.56-1.89)	0.03±0.02 ^{bc} (<0.0001-0.06)	0.11±0.04 ^{cd} (0.02-0.26)	0.06±0.02 ^c (0.04-0.18)	2.51±0.31 ^a (1.17-3.21)	0.30±0.13 ^a (0.04-0.76)	0.03±0.02 ^{ab} (0.02-0.08)	0.19±0.02 ^{cd} (0.15-0.34)
	0.50±0.05 ^c (0.28-1.76)	0.94±0.05 ^c (0.57-4.21)	4.33±0.09 ^{cd} (3.97-6.28)	0.03±0.01 ^{cd} (0.067-0.06)	0.39±0.06 ^a (0.06-0.98)	0.04±0.01 ^{bc} (0.01-0.08)	0.12±0.06 ^c (0.03-0.19)	0.02±0.02 ^c (0.01-0.08)	0.06±0.02 ^{cd} (0.01-0.24)	0.06±0.02 ^{cd} (0.08-0.22)	0.14±0.03 ^b (0.08-0.22)	0.03±0.01 ^{ab} (0.02-0.11)
Rum	0.08±0.36 ^c (0.08-0.10 ^a)	2.90±0.07 ^{cd} (0.78-4.57)	1.51±0.24 ^c (0.19-2.44)	0.02±0.02 ^{cd} (0.001-0.06)	0.85±0.06 ^{cd} (0.32-1.45)	0.03±0.02 ^{bc} (0.02-0.12)	0.06±0.02 ^{cd} (0.05-0.23)	0.26±0.06 ^c (0.08-0.30)	0.20±0.01 ^{cd} (0.12-0.34)	0.11±0.01 ^{cd} (0.06-0.17)	0.02±0.01 ^{ab} (0.01-0.18)	0.18±0.01 ^{cd} (0.10-0.21)
	0.55±0.10 ^c (0.23-1.89)	1.96±0.06 ^{cd} (0.23-7.32)	2.29±0.27 ^{cd} (1.09-5.76)	0.03±0.02 ^{cd} (0.01-0.04)	0.59±0.12 ^{cd} (0.19-1.88)	0.14±0.05 ^a (0.05-0.16)	0.09±0.02 ^{cd} (0.04-0.13)	0.03±0.02 ^c (0.01-0.08)	0.50±0.05 ^a (0.43-1.01)	0.18±0.08 ^b (0.09-0.28)	0.03±0.01 ^{ab} (0.02-0.08)	0.20±0.03 ^{cd} (0.13-0.28)
Vodka	0.28±0.05 ^c (0.13-0.49)	2.50±0.30 ^{cd} (0.68-3.07)	0.56±0.09 ^{cd} (0.36-3.08)	0.02±0.01 ^{cd} (0.001-0.06)	0.18±0.06 ^a (0.12-2.76)	0.03±0.01 ^c (0.02-0.04)	0.13±0.01 ^a (0.07-0.35)	0.03±0.02 ^c (0.02-0.05)	0.11±0.02 ^{cd} (0.06-0.25)	0.16±0.08 ^b (0.05-0.27)	0.02±0.01 ^{ab} (0.01-0.04)	0.13±0.01 ^d (0.09-0.21)
	0.69±0.05 ^c (0.47-4.80)	9.32±0.57 ^{cd} (7.04-26.97)	7.48±0.87 ^c (4.76-13.54)	0.05±0.01 ^{cd} (0.04-0.09)	0.36±0.06 ^{cd} (0.09-1.09)	0.05±0.02 ^{bc} (0.03-0.08)	0.07±0.02 ^{cd} (0.04-0.11)	0.06±0.01 ^c (0.05-0.14)	0.04±0.01 ^c (0.01-0.09)	0.03±0.02 ^c (0.01-0.03)	0.03±0.01 ^{ab} (0.01-0.03)	0.52±0.08 ^b (0.24-0.79)
Local Cider	4.82±1.18 ^d (3.68-9.13)	12.77±1.56 ^c (10.00-29.95)	7.19±0.63 ^c (2.12-16.89)	0.04±0.02 ^{cd} (0.01-0.05)	0.74±0.06 ^{cd} (0.53-2.01)	0.14±0.02 ^a (0.11-0.26)	0.05±0.02 ^{cd} (0.03-0.15)	0.06±0.01 ^c (0.03-0.09)	0.23±0.11 ^{cd} (0.20-0.57)	0.09±0.05 ^{bc} (0.06-0.16)	0.02±0.02 ^c (0.01-0.03)	0.29±0.05 ^c (0.14-0.35)
	2.56±0.19 ^c (0.11-6.23)	5.74±0.28 ^{cd} (0.78-18.66)	25.09±1.46 ^d (5.87-86.67)	0.03±0.02 ^{cd} (0.01-0.12)	2.64±0.71 ^c (0.45-7.34)	0.03±0.01 ^c (0.001-0.08)	0.03±0.01 ^c (0.01-0.09)	0.02±0.01 ^c (0.01-0.05)	0.95±0.05 ^a (0.56-1.89)	0.13±0.02 ^b (0.09-0.24)	0.02±0.02 ^c (0.01-0.07)	0.16±0.05 ^d (0.09-0.22)
Coconut/Orange liquor	3.25±0.24 ^c (0.87-11.09)	26.34±2.95 ^b (5.35-102.45)	23.74±2.12 ^c (10.12-135.54)	0.03±0.02 ^{cd} (0.01-0.07)	0.28±0.05 ^c (0.12-3.88)	0.12±0.01 ^a (0.05-0.23)	0.08±0.04 ^{cd} (0.07-0.12)	0.03±0.01 ^c (0.02-0.10)	0.05±0.03 ^c (0.04-0.13)	0.03±0.02 ^c (0.02-0.07)	0.04±0.01 ^a (0.03-0.05)	0.28±0.05 ^c (0.21-0.29)
	12.74±1.63 ^b (4.34-47.76)	9.33±0.50 ^{cd} (8.09-32.98)	49.18±2.26 ^b (32.87-66.52)	0.06±0.01 ^{cd} (0.008-0.009)	1.40±0.12 ^c (0.87-5.32)	0.05±0.01 ^{bc} (0.03-0.12)	0.05±0.01 ^{cd} (0.08-0.13)	0.02±0.01 ^c (0.01-0.05)	0.13±0.01 ^{cd} (0.03-0.19)	0.16±0.03 ^b (0.13-0.32)	0.02±0.01 ^b (0.01-0.04)	0.45±0.11 ^b (0.16-0.57)

Average value ± standard deviation (n = 3). Romans letters represent the significance of the variety difference (p ≤ 0.05). The difference between any two values, followed by at least one common letter, is insignificant

The mean levels of Pb in alcoholic beverages ranged from 0.03 µg/mL to 0.30 µg/mL. The highest mean concentration was observed in cognac, while the lowest mean value is in a punch, a home-made drink made from alcohol and fruits or fruit juice. These values are in accordance with Iwegbue et al. [16]. The acceptable limits for Pb in alcoholic beverages in some European countries are in the range of 0.20 µg/mL to 0.50 µg/mL. The mean concentration of Pb in these alcoholic beverages are below the permissible limit. The concentration of Pb found in the alcoholic drinks was comparable to the levels of Pb reported in the literature for other alcoholic beverages, which are from 'not detected' to 0.46 mg/L in beer [14], 'not detected' to 0.22 mg/L in spirits [15], 0.008 to 0.420 mg/L in cognac [22], 'not detected' to 0.035 mg/L in gin [15], and 'not detected' to 1.125 mg/L in wine, fruit wine, cocktails [1].

The mean concentration of Cd in these alcoholic beverages were similar except for local brandy, which had a mean level that was twice the level found in the other classes. The mean concentration of Cd ranged from 0.02 µg/mL to 0.04 µg/mL. The guideline value for Cd in drinking water is 0.05 µg/mL according to Iwegbue et al. [16]. The mean concentration of Cd in these alcoholic beverages was below the upper boundary these limits. The results of these studies indicate that persons who consume local brandy, in preference to other alcoholic beverages, are likely to be exposed to more Cd. Iwegbue et al. [16] came to the same conclusion in terms of coconut liquor consumption. The levels of Cd observed in these drinks were comparable to the levels of Cd reported for other alcoholic beverages in the scientific literature <0.005 mg/L in berry liquors [1], sherry brandy from 5.31-0.30 mg/L [17] and from 'not detected' to 0.052 mg/L in wine, fruit wines, cocktails. Iwegbue et al. [16] reported Cd levels from 'not detected' to 0.04 µg/mL in alcoholic beverages.

The mean concentration of Zn ranged from 0.13 µg/mL to 0.88 µg/mL with 0.31 µg/mL average value. The highest mean level of Zn was observed in cream liquor, while the lowest mean level was observed in aromatic schnapps. The permissible limit for Zn in alcoholic beverages is 5 µg/mL according to Iwegbue et al. [16]. The mean concentration of Zn in these alcoholic beverages was below the upper boundary these limits. Zn level concentration of 44 µg/mL to 69 µg/mL in rum and from 0.124 µg/mL to 0.151 µg/mL in cachaça and international spirits from Brazil have been reported by Iwegbue et al. [16]. The concentration of Zn found in the alcoholic drinks was comparable to the levels in Zn reported in the literature for other alcoholic beverages, like beer 0.1 mg/L - 68 mg/L [14; 15], brandy 3.0 mg/L [15; 22;

28], cognac 0.016 mg/L to 3.00 mg/L [28], gin 0.5 mg/L [28], rum 3.00 mg/L [28], vodka 'not detected' [28], whiskey 0.50 mg/L [28], spirits 3.0 mg/L [16], brandy 3.00 mg/L [16] and 0.12 mg/L aromatic schnapps [16].

Dietary intake of metals and target hazard quotients (THQs)

The estimated daily intake of metals based on a per capita consumption of 14.4 L per annum of pure alcohol is displayed in Table 2. The estimated THQs of the metals are displayed in Table 3. The intake values of Mg in this study were in the range of 0.14-8.60 $\mu\text{g}/\text{kg}$ b.w. per day. Higher intakes of Mg are likely for consumers of whiskey, brandy, local brandy, cream liquor, local cider, spirit, coconut/orange liquors, and aperitif. The recommended dietary allowance (RDA) values for male and female healthy adults are 400-420 mg/day and 310-320 mg/day, respectively [16]. Based on the results obtained, the dietary intake of Ca from the consumption of these drinks is in the range of 0.27-130.61 $\mu\text{g}/\text{kg}$ b.w. per day. Higher intakes of Ca are likely for consumers of whiskey, brandy, local brandy, cream liquor, cognac, rum, vodka, aromatic schnapps, punch, local cider, spirit, coconut/orange liquors, and aperitif. The RDA value of Ca is set at 1000 mg per day [16]. The dietary intake of K from the consumption of these alcoholic beverages ranged from 0.31-154.90 $\mu\text{g}/\text{kg}$ b.w. per day. Persons who drink cream liquor in preference to other types of the drink have higher K intake. Iwegbue et al. [16] reported dietary intake of Mg, Ca and K from consumption of distilled alcoholic beverages and liquors for international origin as 0.07-4.24, 0.23-27.14 and 0.08-53.76 $\mu\text{g}/\text{kg}$ b.w. per day based on 3.6 L per annum per capita consumption. The estimated intake of Mn and Fe were 0.01-0.09 and 0.10-117.00 $\mu\text{g}/\text{kg}$ b.w. per day, respectively. Higher intakes of Mn and Fe are likely for consumers of cream liquors and spirits. The recommended dietary allowances value for Fe and Mn are 2-5 and 10-18 mg per day, respectively, according to Iwegbue et al. [16].

The RDA value for Co is 100 μg per day according to Iwegbue et al. [16]. The estimated dietary intake of Co from these types of alcoholic beverages was lower than the RDA for Co. The recommended dietary allowance value for Ni is in the range of 35-700 $\mu\text{g}/\text{kg}$ b.w. per day. The estimated intake values for Ni varied from 0.02-0.07 $\mu\text{g}/\text{kg}$ b.w. per day. The recommended dietary allowances value for Ni is 5 $\mu\text{g}/\text{kg}$ b.w. per day.

The estimated dietary intake of Cu and Cr was 0.02-1.40 and 0.01-0.16 $\mu\text{g}/\text{kg}$ b.w. per day. The highest intake values of Cr and Cu was observed in cream liquor and cognac. The RDA values for Cu and Cr per person are 900-30 mg per day (15-500 $\mu\text{g}/\text{kg}$ b.w. per day) and 130 $\mu\text{g}/\text{kg}$ b.w. per day, respectively according to Iwegbue et al. [16].

The estimated daily intake of Pb from consumption of any type of these alcoholic beverages ranged between 0.02-0.16 $\mu\text{g}/\text{kg}$ b.w. per day. The Joint Food and Agriculture Organization/World Health Organization Expert Committee on Food Additives (JECFA) established a limit for Pb (3.6 $\mu\text{g}/\text{kg}$ b.w. per day). The dietary intake of Cd from the consumption of these classes of alcoholic beverages is in the range of 0.01-0.02 $\mu\text{g}/\text{kg}$ b.w. per day. The tolerable dietary intake of Cd is set at 1 $\mu\text{g}/\text{kg}$ b.w. per day according to Iwegbue et al. [16]. The intakes of Zn from the consumption of these alcoholic drinks were 0.07-0.49 $\mu\text{g}/\text{kg}$ b.w. per day. Higher intakes of Zn are likely for consumers of cream liquor, punch, and aperitif. The JECFA provisional maximal tolerable daily intake of Zn is 1000 $\mu\text{g}/\text{kg}$ b.w. per day [16].

Table 2 presents the results of the estimated THQ from the consumption of these alcoholic drinks. The interpretation of the THQ values is binary: THQ is either ≥ 1 or < 1 , where THQ > 1 indicates a health concern [30; 31; 32; 33; 16]. It must be noted that THQ is not a measured risk [30; 16; 34], but rather indicates a level of concern, and while THQ values are additive, they are not multiplicative, for example, the level of concern at THQ=20 is larger than, but not 10-fold, that at THQ=2 according to Iwegbue et al. [16]. The estimated THQ values for the individual and combined metals from consumption of these drinks were < 1 (Table 3). The THQ values reveal no significant concern to health for people with a 14.4 L per annum per capita consumption rate.

Risk assessment for a specific contaminant intake comprehensive consideration of all intake mechanisms, and alcoholic beverages consumption was just one such path, the amount of wine consumption was, therefore, more important for health risk assessment of wine in the daily diet of drinkers.

Table 2. Estimated dietary intake of metals ($\mu\text{g}/\text{kg}$ b.w. per day) based on a 14.4 L per annum per capita consumption

beverage type	Mg	Ca	K	Mn	Fe	Co	Ni	Cr	Cu	Pb	Cd	Zn
Whiskey	1.38	3.89	3.44	0.02	0.77	0.09	0.03	0.03	0.11	0.16	0.02	0.12
Brandy	1.71	4.56	15.59	0.04	0.48	0.03	0.02	0.02	0.13	0.08	0.02	0.25
Local Brandy	3.61	4.45	18.16	0.04	0.68	0.04	0.03	0.07	0.37	0.08	0.01	0.16
Cream liquor	8.60	130.61	154.90	0.09	117.00	0.03	0.04	0.16	0.08	0.10	0.02	0.49
Cognac	0.33	1.71	3.01	0.03	0.82	0.02	0.06	0.03	1.40	0.17	0.02	0.11
Dry Gin	0.28	0.27	2.41	0.02	0.22	0.02	0.07	0.01	0.03	0.08	0.02	0.09
Rum	0.14	1.62	0.84	0.01	0.47	0.02	0.03	0.14	0.11	0.06	0.01	0.10
Vodka	0.31	1.09	1.28	0.02	0.33	0.08	0.05	0.02	0.28	0.10	0.02	0.11
Aromatic schnapps	0.16	1.39	0.31	0.01	0.10	0.02	0.07	0.02	0.06	0.09	0.01	0.07
Punch	0.38	5.19	4.17	0.03	0.20	0.03	0.04	0.03	0.02	0.02	0.01	0.29
Local Cider	2.69	7.11	4.01	0.02	0.41	0.08	0.03	0.03	0.13	0.05	0.01	0.16
Spirit	1.43	3.20	13.98	0.02	1.47	0.02	0.02	0.01	0.53	0.07	0.01	0.09
Coconut/Orange liquor	1.81	14.68	13.23	0.02	0.16	0.07	0.04	0.02	0.03	0.02	0.02	0.16
Aperitif	7.10	5.20	27.40	0.22	0.78	0.03	0.03	0.01	0.07	0.09	0.01	0.25

Table 3. Estimated target hazard quotients (THQ) from the consumption of these alcoholic drinks

beverage type	Mg	Ca	K	Mn	Fe	Co	Ni	Cr	Cu	Pb	Cd	Zn
Whiskey	N/A	N/A	N/A	0.01	0.01	0.001	0.30	0.002	0.00002	0.003	0.0001	0.02
Brandy	N/A	N/A	N/A	0.01	0.01	0.001	0.09	0.001	0.00001	0.002	0.0001	0.02
Local Brandy	N/A	N/A	N/A	0.03	0.03	0.001	0.15	0.002	0.00005	0.009	0.0001	0.01
Cream liquor	N/A	N/A	N/A	0.06	0.06	0.002	0.09	0.001	0.00010	0.002	0.0001	0.02
Cognac	N/A	N/A	N/A	0.002	0.002	0.001	0.06	0.0003	0.00002	0.030	0.0001	0.02
Dry Gin	N/A	N/A	N/A	0.02	0.02	0.000	0.07	0.0004	0.00001	0.001	0.0001	0.02
Rum	N/A	N/A	N/A	0.001	0.001	0.001	0.06	0.0003	0.00010	0.003	0.00004	0.01
Vodka	N/A	N/A	N/A	0.002	0.002	0.001	0.26	0.002	0.00001	0.007	0.0001	0.02
Aromatic schnapps	N/A	N/A	N/A	0.001	0.001	0.0001	0.06	0.0003	0.00001	0.002	0.0001	0.01
Punch	N/A	N/A	N/A	0.003	0.003	0.0003	0.09	0.001	0.00002	0.001	0.00001	0.01
Local Cider	N/A	N/A	N/A	0.02	0.02	0.001	0.26	0.002	0.00002	0.003	0.00003	0.01
Spirit	N/A	N/A	N/A	0.01	0.01	0.002	0.06	0.0003	0.00001	0.010	0.0001	0.01
Coconut/Orange liquor	N/A	N/A	N/A	0.01	0.01	0.0002	0.22	0.001	0.00000	0.001	0.00001	0.02
Aperitif	N/A	N/A	N/A	0.05	0.05	0.001	0.09	0.001	0.00004	0.002	0.00006	0.01

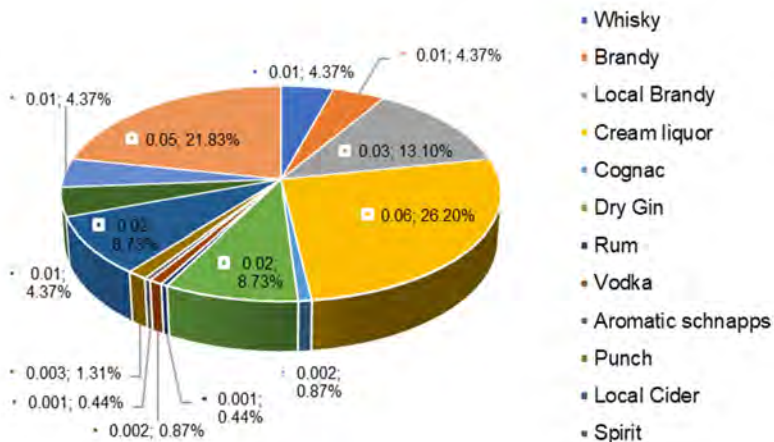


Figure 1. The average proportion of the total THQ for all the alcoholic beverages

In this research the THQ also represented the contribution of alcoholic beverages to contaminants in the acceptable range for daily diet, the average THQ of cream liquor was 26.20% (Figure 1) and Co 89.15% (Figure 2) which meant that the contribution of cream liquors consumption to the tolerable daily intake of Co was 89.15%.

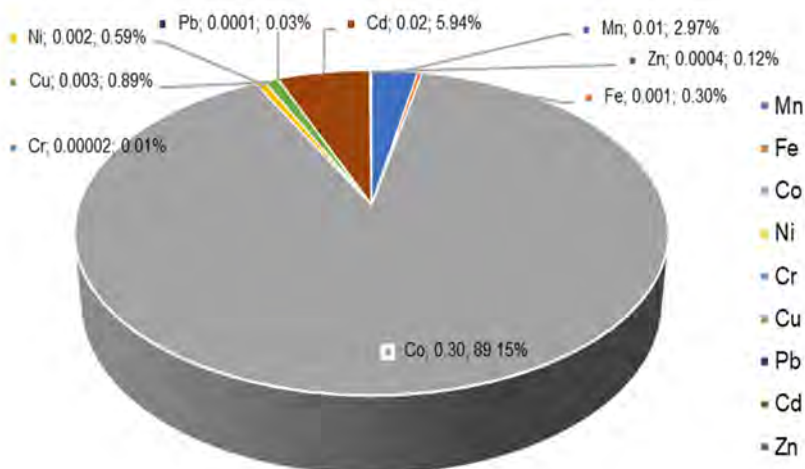


Figure 2. The average proportion of the total THQ for all the metals

CONCLUSIONS

Relatively low levels of both essential and potential hazardous metal ions were found in these types of alcoholic beverages. Based on a 14.4 L per capita consumption of pure alcohol, the local and international drinks instigated gave low dietary intakes of the essential and potentially toxic metals. It was observed that the cream liquors and cognac contained a higher concentration of Mg, Ca, K, Fe, and Cu compared with the other classes of alcoholic beverages. This suggests that persons who drink cream liquors in preference to spirits and other types of alcoholic drinks studied in this research would be likely to be exposed to more metals.

The THQ values may not present any detrimental health concerns for a lifetime based on the metal content alone. However, the hazardous and harmful use of alcohol is a major global contributing factor, such as liver cirrhosis, cancers, alcohol dependences, injuries, and others through the dangerous actions of intoxicated people.

EXPERIMENTAL SECTION

Sampling

Samples of different brands of alcoholic beverages with different batch numbers and manufacturing dates were collected from retail operations in Bucharest, Cluj, Maramureş, Constanţa, Galaţi, Braila, Satu-Mare, Salaj, Vâlcea, Alba, Covasna, Hargita and Mureş. The choice of brands was carefully made to reflect popular brands consumed by different income classes and influenced by availability at the time of purchase. The categorization and other information on the bottles of the alcoholic drinks are displayed in Table 4. The samples were stored at 3-5 °C until the analysis was made.

Table 4. Information on the samples studied

Alcoholic beverage	Percentage (v/v) alcohol	Class	Country of origin
Johnnie Walker	40	Whisky	UK
Small Batch	46.85	Whisky	America
Ardreg Ulgeadail	46	Whisky	Scotland
Arran Lochranza	43	Whisky	Scotland
Ballantine's	40	Whisky	Italy
Balvenie	40	Whisky	Scotland
Benriach	40	Whisky	Scotland

Alcoholic beverage	Percentage (v/v) alcohol	Class	Country of origin
Big Peat	46	Whisky	Scotland
Blanton's	51.5%	Whisky	America
Braeval	48.4	Whisky	Scotland
Baffalo Trace	40%	Whisky	America
Bulleit Bourbon	45.6	Whisky	America
Dalmore	40	Whisky	Scotland
Dramsylvania	40	Whisky	Scotland
Afinată	40	Brandy	Romania
Caisată	40	Brandy	Romania
Căpșunată	40	Brandy	Romania
Vișinată	40	Brandy	Romania
Plums brandy	40	Brandy	Romania
Pears brandy	40	Brandy	Romania
Quince brandy	40	Brandy	Romania
Apricots brandy	40	Brandy	Romania
Nuts liqueur	35	Cream liquor	Romania
Black blueberry liqueur	31	Cream liquor	Romania
Jägermeister	35	Cream liquor	Germany
Amaretto Disaronno	28	Cream liquor	Italy
Aperol	11	Cream liquor	Italy
Unicum	40	Cream liquor	Hungary
De kuyper	40	Cream liquor	Netherlands
Courvoisier Cognac	40	Cognac	France
Hennessy	40	Cognac	France
Martel	40	Cognac	France
Remy Martin	40	Cognac	France
Wembley London	40	Dry Gin	England
Beefeater London	40	Dry Gin	England
Gordons	37.5	Dry Gin	UK
Finsbury	40	Dry Gin	UK
London Hill	43	Dry Gin	UK
Havana Club	40	Rum	Cuba
Matusalem	40	Rum	Dominican Republic
Stroh 80	80	Rum	Austria
Bacardi	40	Rum	Cuba
Captain Morgan	35	Rum	Jamaica
Absolut Vodka	40	Vodka	Sweden
Finlandia Vodka	40	Vodka	Finland
Rasputin Vodka	40	Vodka	Germany

Alcoholic beverage	Percentage (v/v) alcohol	Class	Country of origin
Stolichnaya	40	Vodka	Russia
Zubrowka	40	Vodka	Poland
Wyborowa	40	Vodka	Poland
Eagles	42	Aromatic schnapps	Nigeria
Seamans	40	Aromatic schnapps	Nigeria
Kp	42	Aromatic schnapps	Nigeria
Crown	40	Aromatic schnapps	Nigeria
Garvey	30	Punch	Spain
Freihof Jagertee	40	Punch	Austria
Stroh Jagertee	40	Punch	Austria
Local cider	4.5	Cider	Romania
Tequila Blanco	38	Spirit	Mexico
Absolute Citron	40	Sprit	Sweden
Gordons Spark	5.5	Sprit	Nigeria
Malibu	21	Coconut liquor	UK
Calypso	28	Coconut liquor	Nigeria
Blue Curaçao	33.8	Coconut liquor	USA
Sweet „n” sour mix	32	Coconut liquor	USA
Cointreau	40	Orange liquor	France
Campari	20	Aperitif	Italy
Bacardi	40	Aperitif	Germany
Vino din tavola	10.5	Aperitif	Italy
Ricard	45	Aperitif	France

Reagents and solutions

Twelve elements (Mg, Ca, K, Mn, Fe, Co, Ni, Cr, Cu, Pb, Cd, and Zn) were determined in 14 classes of alcoholic beverages. The analysis was made using multielement analysis and ICP-MS technique, after appropriate dilution, using the external standard calibration method (Table 5). The calibration was performed using XXICertiPUR multielement standard and from an individual standard solution of Cr and Hg. The working standards and the control sample were prepared daily from the intermediate standards that were prepared from the stock solution. The intermediate solutions stored in polyethylene bottles and glassware was cleaned by soaking in 10% v/v HNO₃ for 24 hours and rinsing at least ten times with ultrapure water (18.2 MΩ cm⁻¹ ultrapure water-Types 1). The accuracy of the methods was evaluated by replicate analyses of fortified samples (10 µL-10 mL concentrations) and the obtained values ranged between 0.8-13.1 percent, depending on the element. The global recovery for each element was estimated and the obtained values were between 84.6-100.9% [35].

Table 5. Instrumental conditions for the determination of each element (ICP-MS technique)

Element	Correlation coefficient	LoD* (µg/L)	LoQ*** (µg/L)	BEC** (µg/L)
Mg	0.9999	2.7320	9.0990	9.0990
Ca	0.9999	5.6640	18.8640	20.8200
K	0.9999	2.1860	7.2790	31.7281
Mn	0.9999	0.0100	0.0340	0.0850
Fe	0.9999	5.2100	17.3501	71.3990
Co	0.9999	0.0365	0.1215	0.152
Ni	0.9999	0.0591	0.1968	0.091
Cr	0.9999	1.6630	5.5378	0.636
Cu	0.9999	0.0402	0.1339	0.237
Pb	0.9999	0.0003	0.0010	0.002
Cd	0.9999	0.0202	0.0673	0.027
Zn	0.9999	0.3780	1.2580	5.401

*Detection limit; **Background equivalent concentration; ***Quantification limit.

For quality control purposes, blanks and triplicates samples ($n = 3$) were analysed during the procedure. The variation coefficient was under 5% and detection limits (ppb) were determined by the calibration curve method. Limit of detection (LoD) and Limit of quantification (LoQ) limits was calculated according to the next mathematical formulas: $LoD = 3SD/s$ and $LoQ = 10 SD/s$ ($SD =$ estimation of the standard deviation of the regression line; $s =$ slope of the calibration curve).

Sample preparation for determination of metals using ICP-MS

For the determination of elements from wine samples 0.5 mL wine were mixed with 7 mL of HNO_3 65% and 1 mL of H_2O_2 and were mineralized in a clean Teflon digestion vessel using a microwave system Milestone START D Microwave Digestion System. Mineralization was done in three steps: step I (time 10 min., temperature 200°C), step II (time 15 min., temperature 200°C) and step III (time 40 min., ventilation - temperature 32°C). After mineralization, samples were filtered through a 0.45 mm filter paper and the volume was adjusted to a volume of 50 mL.

To confirm the best-chosen conditions for wine digestion standard additions for checking the accuracy of the microwave digestion and recoveries were calculated (Table 6). The digestion seemed visually completed in all of the combinations, but the spiked recoveries showed significant differences for total elements content ($p = 0.005$).

Table 6. Accuracy of the ICP-MS determination of metals in reference materials (NIST SRM 1572) (n=7)

Element	Certified Concentration (mg/L)	Measured Concentration (mg/L)
Mg	5.80±0.30	5.74±0.01
Ca	31.10±1.10	31.05±2.11
K	1.82±0.06	1.79±0.05
Mn	23.00±2.00	23.05±0.09
Fe	90.00±10.00	89.08±6.78
Co	20.00±0.01	21.45±2.33
Ni	600.00±300.00	612.34±27.98
Cr	0.80±0.20	0.79±3.22
Cu	16.50±1.00	16.49±1.22
Pb	13.30±2.40	13.30±2.56
Cd	36.00±0.10	36.67±1.05
Zn	29.00±2.00	29.34±0.99

Instrumentation

The elements were determined by using ICP-MS (iCAP Q Thermo scientific mode). The sample solution was pumped by a peristaltic pump from tubes arranged on autosampler (CETAC ASX-520), which was combined with a quartz cyclonic spray chamber (water-cooled 2°C). The instrumental setting and operative conditions are reported in Table 7.

Table 7. ICP-MS instrumental parameters

Parameter	Setting
RF-Power	1550
Reflected power	<5
Carrier gas flow (mL/min.)	1.0
Plasma gas flow (L/min.)	15
Auxiliary gas flow (mL/min.)	1.0
Spray chamber	Water cooled double pass
Spray-Chamber temperature (°C)	2
Lens voltage (V)	6.25
Mass range (AMU)	3-209
Mass resolution	0.7
Integration time points/ms.	3
Points per peak	3
Replicates	3

The instrument was daily optimized to give maximum sensitivity for M^+ ions and the double ionization and oxides monitored by the means of the ratios between Ba^{2+}/Ba^+ and Ce^{2+}/CeO^+ , respectively, these always being less than 2%.

Estimation of dietary intake (EDI) and THQ

The adult per capita consumption rate of pure alcohol in Romania is 14.4 L per annum. This value is from the calculation based on the Food and Agriculture Organization of the United Nations data, which includes fermented beverages and estimates of beer produced locally from sorghum, millet, and other agricultural products [36]. In this study, an adult per capita consumption rate of 14.4 L per annum of spirits, which is equivalent to 39 mL per day, and an average weight of 70 Kg per adult was adopted. EDI is measured in $\mu\text{g}/\text{kg}$ b.w. [37].

$$EDI = (FIR \times C) / Bwa$$

where EDI is estimated daily intake (μg analysed element/kg body weight/day), FIR is average daily consumption of alcohol (mL/kg), C is average concentration of the heavy metals in the samples ($\mu\text{g}/\text{mL}$) and Bwa is average body weight (Kg) [37, 16].

To assess the human risk from consumption of alcoholic beverages with metals, the target Hazard Quotient (THQ) was calculated as per the US EPA Region III Risk-Based Concentration Table [USEPA] (United States Environmental Protection Agency) 2011] [37]. The THQ is an estimate of the non-carcinogenic risk level due to pollutant exposure and calculated by the following equation:

$$THQ = 10^{-3} \times (Efr \times ED_{tot} \times Fir \times C) / (RfDo \times Bwa \times ATn)$$

where, THQ is target hazard quotient, Efr – exposure frequency (365 days/year), ED_{tot} – exposure duration (70 years), FIR – average daily consumption of alcohol (mL/kg), C – average concentration of the metals in samples ($\mu\text{g}/\text{mL}$), RfDo – oral reference dose (mg/kg/day), Bwa – average body weight (kg) and ATn – average exposure for non-carcinogens in year (365 days/year \times 70 years). THQ value below 1 indicant no adverse effect on human health.

Statistical analysis

The statistical interpretation of the results was performed using the Duncan test, SPSS Version 24 (SPSS Inc., Chicago, IL., USA). The statistical processing of the results was primarily performed to calculate the following statistical parameters: average and standard deviation. This data was interpreted with the analysis of variance (ANOVA) and the average separation was performed with the DUNCAN test at $p \leq 0.05$.

ACKNOWLEDGMENTS

This project is funded by the Ministry of Research and Innovation through Program 1 - Development of the National Research and Development System, Subprogram 1.2 – Institutional Performance - Projects for Financing the Excellence in CDI, Contract no. 37PFE/06.11.2018. Title of the project: "Increasing the institutional performance through consolidation and development of research directions within the USAMVCN".

REFERENCES

1. J.G. Ibanez; A. Carreon-Alvarez; M. Barcena-Soto; N. Casillas; *J. Food Compos. Anal.*, **2008**, 21, 672-683.
2. A.M. Green; A.C. Clark; G.R. Scollary; *Fresenius J. Anal. Chem.*, **1997**, 358, 711-717.
3. K. Akrida-Demertzi; A.A. Koutinas; *Dev. Food Sci.*, **1992**, 29, 475-489.
4. H. Mayer, O. Marconi; S. Floridi; L. Montanari; P. Fantozzi; *J. Inst. Brew.*, **2003**, 109(4), 332-336.
5. R. Kokkinofa; P. V. Petrakis; T. Mavromoustakos; C.R. Theocharis; *J. Agric. Food Chem.*, **2003**, 6233-6239.
6. F. Salvo; L.L. Bella; G.D. Nicotina; M. Dugo; *J. Agric. Food Chem.*, **2003**, 51, 1090-1094.
7. P. Pohl; *Trends Anal. Chem.*, **2007**, 26(9), 941-949.
8. T. Adam; E. Duthie; E.J. Feldmann; *J. Inst. Brew.*, **2002**, 108(4), 459-464.
9. G. Dugo; L.L. Pera; V.L. Bella; G.D. Salvo; *J. Agric. Food Chem.*, **2005**, 52, 1829-1834.
10. M. Navarro-Alarcon; *Food Addit. Contam.*, **2007**, 24(7): 685-694.
11. A. Carreon; N. Casillas; V. Gonzalez-Alvarez; R. Prado-Ramirez; *Mater. Performance*, **2001**, 50-52.
12. M.I. Guerrero; C. Herce-Paglia; A.G. Gonzalez; F.J. Heredia; A.M. Troncoso; A. M. Camean; *Sci. Aliment*, **1996**, 16: 143-149.
13. C. Reilly; *J. Sci. Food Agric.*, **1972**, 23(9): 1143-1144.
14. C. Reilly; *Ecol. Food Nutr.*, **1973**, 2(1): 43-47.

15. C.M. Mena; C. Cabrera; M.L. Lorenzo; M.C. Lopez; *J. Agric. Food Chem.*, **1997**, 45: 1812-1815.
16. C.M.A. Iwegbue; L.O. Overah; F.I. Bassey; B.S. Martincigh; *J. Inst. Brew.*, **2013**, 120: 521-528.
17. A.M. Cameán; I. Moreno; M. López-Artíguez; M. Repetto; A.G. González; *Talanta*, **2001**, 54: 53-59.
18. V. Ivanova-Petropulos; H. Wiltsche; T. Stafilov; M. Stafilov; H. Lankmayr; *Maced. J. Chem. Chem. Eng.*, **2013**, 32(2): 265-281.
19. S. Ražić; A. Onjia; *Am. J. Enol. Viticult.*, **2010**, 61(4): 506-511.
20. P. Kment; M. Mihaljević; M. Ettler; O. Šebek; L. Strand; L. Rohlová; *Food Chem.*, **2005**, 91(1): 157-165.
21. S.R. Gibbson; *Principles of nutritional assessment*, Oxford University Press, Oxford, **2005**, pp. 341-352.
22. E.H. Soufleros, A.S. Mygdalia; P. Natskoulis; *Food Chem.*, **2004**, 86: 625-636.
23. C. Macca; M. Bradshaw; A. Merkoci; C. Scollary; *Anal. Lett.*, **1997**, 30(6), 1223-1234.
24. R.F. Nascimento; C.WB. Bezerra; S. M.B. Furuya; M.S. Schultz; L.R. Polastro; B.S. Lima Neto; D.W. Franco; *J. Food Compos. Anal.*, **1999**, 12: 17-25.
25. F.D. Bora; A. Donici; T. Rusu; A. Bunea; D. Popescu; C.I. Bunea; *Not. Bot. Horti. Agrobo.*, **2018**, 46(1): 223-239.
26. M. Iglesias; E. Besalú; E. Anticó; *J. Agric. Food Chem.*, **2007**, 55(2): 219-225.
27. C. Reilly; *Ecol. Food Nutr.*, **1973**, 2(1): 43-47.
28. F.A. Cyro; *An. Farm. Quim. S. Paulo*, **1976**, 16(1): 61-67.
29. S. Xuebo; H. Min; Z. Li; L. Zhu; F. Zheng; M. Huang; X. Sun; H. Li; F. Chen; B. Sun; *J. Food, Saf.*, **2018**, 2: 43-49.
30. T. Hague; A. Petroczi; P.L.R. Andrews; J. Barker; D. Naughton; *Chem. Central J.*, **2008**, 4(1): 1-3.
31. D.P. Naughton; A. Petroczi; *Immun. Ageing*, **2008**, 5(1): 3. DOI: 10.1186/1742-4933-5-3.
32. D.P. Naughton; A. Petroczi; *Chem. Central J.*, **2008**, 2(22). DOI: 10.1186/1752-153X-2-22.
33. R.K., Sharma; M. Agrawal; *J. Environ. Biol.*, **2005**, 26: 301-313.
34. L.C. Chien; T.C. Hung; Y.K. Choang; C.Y. Yeh; P.J. Meng; M.J. Skieh; B.C. Han; **2002**, *Sci. Total Environ.*, 285: 177-185.
35. E.I. Geana, C. Sandru, V. Stanciu, et al., *Food Anal. Method*, **2017**, 10(1), 63-73.
36. World Health Organization, *Department of Mental Health and Substance Abuse, Geneva*, **2004**.
37. B. Song; M. Lei; T. Chen; Y.M. Zheng; Y.F. Xie; X.Y. Li; D. Gao; *J. Environ. Sci.*, **2009**, 21: 1702-1709.

PREPARATION AND STUDY OF GROWTH STIMULATING ACTIVITY OF 1-PROPYL-4-(3'-AMINO-1', 2', 4'-TRIAZOLO-3'- THIOPROPINYL) PIPERIDIN-4-OL

KANAGAT KAZHMUKHANOVICH KISHIBAYEV^{a*}, ZHANIBEK SERIKOVICH ASSYLHANOV^b, DARIA BAZARBEKOVNA MARKINA^c, SERGEY VITALIEVICH NECHIPURENKO^a, AZHAR AIDAROVNA ATCHABAROVA^a, RUSTAM RISHATOVICH TOKPAYEV^a, SERGEY ANATOLIEVICH YEFREMOV^a, SERGEY NIKOLAEVICH KALUGIN^b, VLADIMIR LEONIDOVICH RUSSINOV^d, KAZHMUKHAN ORAZOVICH KISHIBAYEV^e

ABSTRACT. Results on the obtaining and the study of a plant growth stimulator based on 1-propyl-4-(3'-amino-1',2',4'-triazolo-3'-thiopropinyl) piperidin-4-ol are presented in the article. 1-propylpiperidin-4-on and 3-mercaptopropinyl-5-amin-1,2,4- triazolo were obtained with the basic parameters of the synthesis for synthesizing of 1-propyl-4-(3'-amino-1', 2', 4'-triazolo-3'-thiopropinyl) piperidin-4-ol. The structures of the obtained organic compounds were proved using IR spectroscopy and ¹H and ¹³C NMR spectrometry. The obtained 1-propyl-4-(3'-amino-1'2'4'-triazolo-3'-thiopropynyl)-piperidine-4-ol was tested for growth-stimulating activity on spring wheat grains compared with control (water) and has proved to be a domestic growth regulator «Akpinol-alpha» (KN-2).

Keywords: growth stimulators, organic compounds, IR spectroscopy, NMR spectrometry, growth stimulating activity, piperidine.

^a Center of Physico - Chemical Methods of Research and Analysis of al-Farabi Kazakh National University (CPCMRA), 96A Tole bi St., 050012, Almaty, Kazakhstan

^b Scientific Research Institute of New Chemical Technologies and Materials (SRINCTM) of al-Farabi Kazakh National University, 96A Tole bi st., 050012, Almaty, Kazakhstan

^c Department of Chemistry and Chemical Technology of al-Farabi Kazakh National University, 71 Al-Farabi Ave., 050040, Almaty, Kazakhstan

^d Institute of Chemical Engineering of Ural Federal University named after the first President of Russia B.N. Yeltsin, 28 Mira St., 620002, Ekaterinburg, Russia

^e Faculty of Natural Science of Kazakh National Women's Teacher Training University, 99 Aiteke bi St., 050000, Almaty, Kazakhstan

* Corresponding author: kanagat_kishibaev@mail.ru

INTRODUCTION

Increasing severe abiotic stresses, such as drought, salinity and extreme temperature changes, are part of the major impacts of climate change. These stresses led to the loss of soil organic matter and other forms of soil degradation, which adversely affects agricultural productivity [1]. Another important consequence of climate change and abiotic stress is an increase of plant infection with pathogens and pests [2]. Currently, intensive research is being undertaken to improve plant growth and tolerance to various abiotic stresses, as well as to protect plants from pathogens using growth stimulants that promote the growth of rhizobacteria, which have great potential for sustainable cultivation of crops [3-7].

Indigenous microbes, including endophytes, closely cooperate with each other and can serve as a link of important physiological processes, especially the production of nutrients and the suitability of plants to abiotic stresses [8-9]. Plants sown with growth stimulators modified with rhizobacteria produce more root hairs and take mineral and microelements more efficiently from the soil. The growth of several plants is enhanced by the treatment of growth promoter modified rhizobacteria, such as lentils (*Lens esculenta*) [10], peas (*Pisum sativum* L.) [11], cucumber (*Cucumis sativus*) [12], rice (*Oryza sativa*) [13] and soy (*Glycine max*) [6]. Growth stimulators modified with rhizobacteria also cause systemic tolerance to various abiotic stresses in plants, such as salinity, drought and heavy metals by changing plant physiology [14].

The beneficial properties of bacteria promoting plant growth include the ability to synthesize biologically active compounds such as plant growth stimulators [15-16], osmolites [8], antifungal compounds [17], and 1-aminocyclopropane-1-carboxylate enzyme deaminase [18]. The *Pseudomonas* strain was able to suppress soybean root disease caused by fungal pathogens [19] and showed counteracting activity against several fungal pathogens such as *Fusarium oxysporum* and *Rhizoctonia solani*. Induced systemic resistance of deciduous plants to pathogens caused by plant growth stimulating rhizobacteria was reported too [20]. In addition, some reports suggest that some plant growth promoting rhizobacteria cause systemic tolerance in plants through increased antioxidant reactions at the level of enzyme activity and metabolite accumulation [21-23]. The antioxidant defense system plays an important role in the adaptation of plants to saline stress, which makes it possible to purify reactive oxygen species (ROS) [24].

Variability in the efficacy of biological drugs is a concern when used under different conditions. Hostile environmental conditions are harmful for the microbiome associated with the root and for the effective functioning of

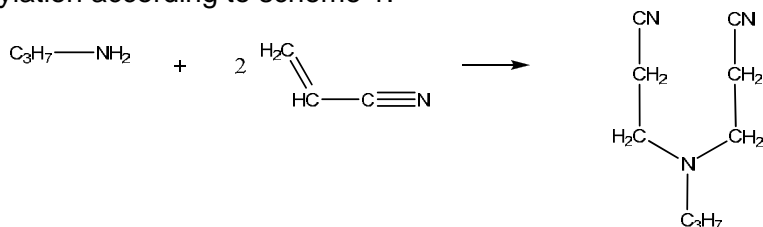
the injected rhizobacteria, that stimulate the growth of plant inoculants [17]. The effect of temperature on plant growth and on the ability of biological control of *Pseudomonas fluorescens* plant's growth stimulating rhizobacteria was observed in earlier studies [25]. In their study, these rhizobacteria suppressed *Fusarium* chickpea wilt at 30 °C, but not at 25 °C, in which the potential of the disease was high. It's interesting, that this suppression was associated with the production of extracellular metabolites that inhibit *F. oxysporum*, and the ability of rhizobacteria to stimulate plant growth, which was higher at 30 °C [17]. In this study, we obtained growth stimulator 1-propyl-4-(3'-amino-1',2',4'-triazolo-3'-thiopropinyl)piperidine-4-ol, studied their structural characteristics and evaluated the effect on the growth of stimulating activity of crops, namely grains of spring wheat.

The aim of this work is to obtain the growth stimulator 1-propyl-4-(3'-amino-1',2',4'-triazolo-3'-thiopropinyl)piperidine-4-ol and the study its growth-stimulating activity in relation to crops, namely grains of spring wheat.

RESULTS AND DISCUSSION

In the course of this work, acetylene alcohol 1-propyl-4-(3'-amino-1',2',4'-triazolo-3'-thiopropinyl)piperidine-4-ol was obtained in 4 stages and the optimal technological parameters of the reaction were selected to increase the yield of the target product.

Di-(2-cyanoethyl) propylamine was obtained by propyl amin cyanethylation according to scheme 1:



Scheme 1

To increase product yield of Di-(2-cyanoethyl)propylamine, optimal conditions were selected for carrying out reaction by changing such parameters as temperature and reaction time. As a result it was found that with increasing temperature product yield noticeably decreases and diminution in temperature till 10 °C also led to the yield decreases till 49%. The highest yield (54%) was achieved at room temperature (20 °C). As for reaction time, it was found that increasing of hours' number led to increase

of product yield too. When reaction continuance was 10 hours, the best yield was achieved and it was equal to 70%. The optimum parameters of reaction are presented in table 1. The structure and composition of the resulting compound were proved with a help of IR-spectroscopy.

Table 1. Parameters for obtaining of di-(2-cyanoethyl) propylamine

№	t, [°C]	Time,[h]	Yield,[%]	t, [°C]	Time,[h]	Yield, %
1	10	4	49	20	4	54
2	20	4	54	20	6	59
3	30	4	46	20	8	64
4	40	4	43	20	10	70

The presence of the characteristic functional groups of di-(2-cyanoethyl)propylamine was proved by IR-spectroscopy (Figure 1). There are absorption bands at 2248 cm^{-1} , which is characteristic for nitrile group, and adsorption bands at 2963 , 2874 , 2828 cm^{-1} , which is characteristic for the stretching vibrations of methyl, methylene groups were showed in the di-(2-cyanoethyl) propylamine IR-spectra.

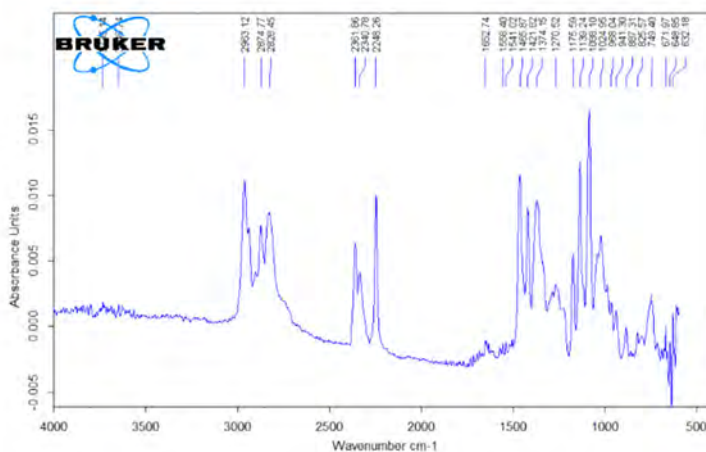
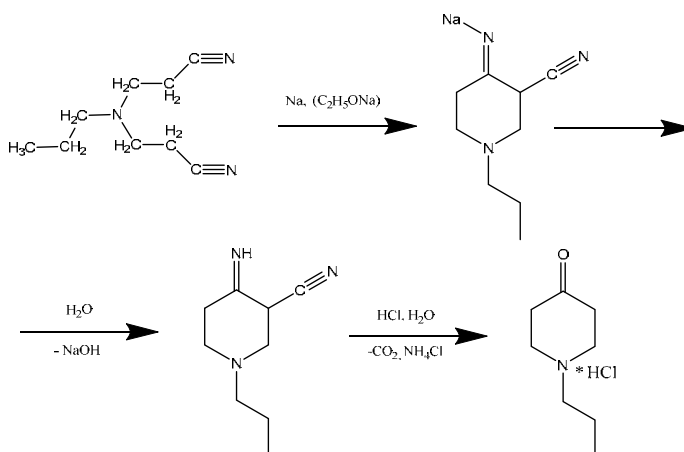


Figure 1. di-(2-cyanoethyl) propylamine IR-spectrum

Di-(2-cyanoethyl)propylamine obtained in the first stage was cyclized to 1-propylpiperidin-4-one (scheme 2) using a method similar to the one reported for the preparation of 1-methylpiperidine-4-one [27]:



The cyclization reaction took place at 105 °C in the medium of anhydrous toluene with an excess of metallic sodium. The reaction mixture was kept for 10 hours. The cyclization product was obtained in 41% yield.

In figure 2 is presented the IR spectrum of 1-propylpiperidin-4-one, which displays absorption bands, that were observed at 1638 cm^{-1} , corresponding to the stretching vibration of the ketone group, and absorption bands observed at 2959, 2934, 2873 cm^{-1} , which are characteristic for the stretching vibrations of methyl, methylene groups.

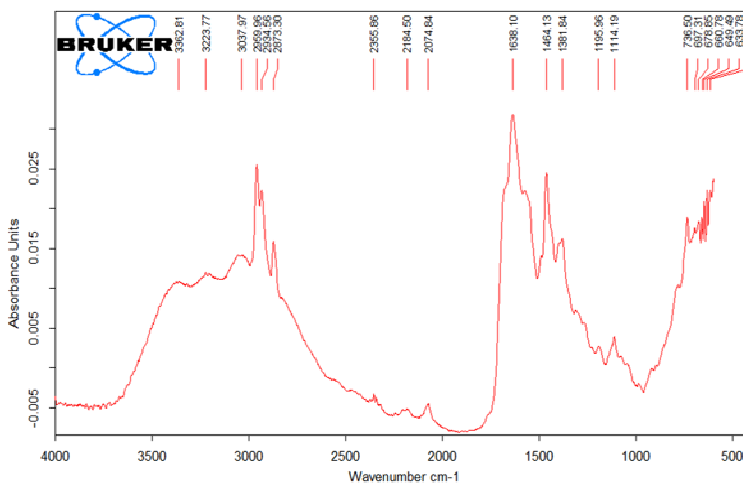
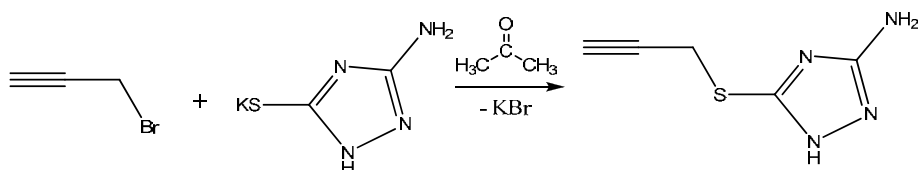


Figure 2. 1-propylpiperidin-4-one IR-spectrum

3-Mercaptopropinyl-5-amino-1,2,4-triazole was obtained by propargylation of potassium 1,2,4-triazolo-3-amino-5-sulfide with propargyl bromide in benzene as shown in scheme 3.



Scheme 3

Series of syntheses was carried out to optimize and increase the yield of the target propynylated triazole.

The reaction of propargylation with propargyl bromide of 1,2,4-triazolo-3-amino-5-potassium sulfide in ethanol was carried out for 8 hours at 75 °C, the product yield was 56%.

When interacting of 1,2,4-triazolo-3-amino-5-potassium sulfide with propargyl alcohol under similar conditions, the yield was 28% of the theoretical.

During the propargylation reaction with propargyl bromide of 1,2,4-triazolo-3-amino-5-potassium sulfide in benzene at 9-hour exposure to a temperature in range of 74 – 77 °C, a yield of 61% was achieved. And the interaction with propargyl alcohol, under the same conditions, led to a yield of 34% of the theoretical. The propargylation with propargyl bromide of 1,2,4-triazolo-3-amino-5-potassium sulfide in acetone with heating for 10 hours at 50 – 53 °C, yielded the product in 72%. When combining 1,2,4-triazolo-3-amino-5-potassium sulfide with propargyl alcohol for 10 hours in acetone at 50 – 53 °C the yield was 41%. In diethyl ether at 29 – 34 °C propargylation with propargyl bromide of 1,2,4-triazolo-3-amino-5-potassium sulfide within 11 hours of conversion of the target product, yield was 58 %. And during the interaction of 1,2,4-triazolo-3-amino-5-potassium sulfide with propargyl alcohol in diethyl ether under the same conditions 3-mercaptopropinyl-5-amino-1,2,4-triazolo was formed, and its yield was 37%. The main parameters of these methods are summarized in table 2.

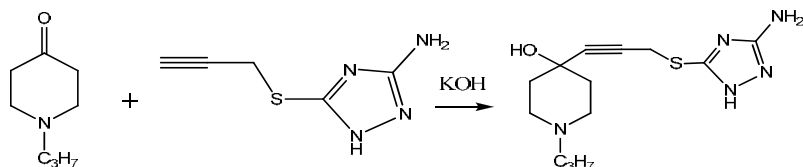
The structure of 3-mercaptopropinyl-5-amino-1,2,4-triazolo was confirmed by NMR spectroscopy (¹H and ¹³C). The ¹³C NMR spectrum is characterized by the presence of signals at 19.71 ppm, corresponding to the carbon of the methylene group of the propargyl substituent, signals at 73.89, 81.16 ppm are correlated with the acetylene carbon signals, and the signal at 154.91 ppm is correlated with the carbon in the fifth position of the triazole ring and a signal situated at 158.18 ppm is correlated with the carbon situated in the third position of the triazole ring.

Table 2. Reaction conditions applied in the preparation of 3-amino-5-thiopropinyl-1,2,4-triazole

No	Propargylating agent	Solvent	Temperature, °C	Time, h	Yield %
1	Bromide propargyl	Ethanol	75	8	56
	Propargyl alcohol		78	9	28
2	Bromide propargyl	Benzene	76	9	61
	Propargyl alcohol		80	8	34
3	Bromide propargyl	Acetone	52	10	72
	Propargyl alcohol		53	9	41
4	Bromide propargyl	Diethyl ether	29	11	58
	Propargyl alcohol		30	12	37

The ^1H NMR spectrum contains signal in the region at 0.1 ppm, corresponding to the hydrogen atom at the C-9 acetylene group. Signal at 3.73 ppm corresponds to the hydrogens of methylene group of the propargyl substituent. Hydrogen atoms under the amine substituent N-10 are prescribed as a broad signal at 6.09 ppm. Hydrogen at N-1 in the ^1H NMR spectrum is not prescribed according to substitution on D of the solvent.

1-Propyl-4-(3'-amino-1'2'4'-triazolo-3'-thiopropinyl)-piperidin-4-ol was obtained by the reaction between 1-propylpiperidin-4-one and 3-mercaptopropinyl-5-amino-1,2,4-triazole (scheme 4):



Scheme 4

Series of reactions was carried out in different solvents and different ratio caustic potassium for selection of optimal conditions of the addition 3-amino-5-thiopropinyl-1,2,4-triazole to the 1-propylpiperidin-4-one (Table 3).

Table 3. Parameters of obtaining of 1-propyl-4-(3'-amino-1'2'4'-triazolo-3'-thiopropinyl) - piperidin-4-ol

No	Solvent	Ppm : KOH	Yield, %
1	Diethyl ether	1:3	59
		1:5	70
		1:10	76
2	Ethanol	1:3	48
		1:5	59
		1:10	68

At fivefold excess of caustic potassium in diethyl ether similar yields were obtained as at the interaction in the medium of diethyl ether with a tenfold excess (yield is 70% and 76%, respectively). With a decrease in amount of caustic potassium till threefold excess, the yield decreased till 59%. The replacement of the solvent to the ethanol, at the other equal conditions, adducted to the yield decrease on the average of 10%, from which was drawn a conclusion, that the optimal conditions were achieved when carrying out the reaction in diethyl ether with a tenfold excess of caustic potassium (Table 3).

The structure 1-propyl-4-(3'-amino-1'2'4'-triazolo-3'-thiopropinyl) - piperidin-4-ol was confirmed by NMR-spectroscopy (H^1 and C^{13}). 1H NMR spectrum of compound of is characterized by the presence of three multiplet signals situated at 0.84-0.86, 1.65-1.67 and 2.91-2.93 ppm, corresponding to protons of the N-propyl substituent of piperidine ring H-9, H-8 and H-7, respectively. H-3,4 and H-2,6 Piperidine protons were resonated with the multiplets at 2.01-2.01 and 2.42-2.50 ppm., respectively. H-13 proton, which is located between sulfur atom and acetylenic fragment, was resonated with the singlet at 4.31 ppm. Amino group protons H-20 of the heterocyclic fragment were manifested by broad singlet at 5.11 ppm.

In the ^{13}C NMR spectrum there is a signal at 14.16 ppm, appropriate to the methyl carbon C-9 of the piperidine ring's propyl substituent. The peaks will correspond to the methylene substituent C-8, C-7 of propyl radical in area 22.75 and 24.55 ppm. Signal at 23.45 ppm. corresponds to the methylene group C-13 of the propyl radical. Methylene carbons C-2, C-6 of the piperidin ring prescribes in area 26.47 ppm., and C-3, C-5 at 29.76 ppm. Quaternary carbon C-10 prescribes at 29.42 ppm. Signals at 31.99 and 32.28 ppm. correlate with acetylene carbons C-11 and C-12. Signal at 125.16 ppm. corresponds to the C-15 carbon atom of triazol ring, respectively carbon's atom C-18 prescribes at 135.29 ppm.

The obtained 1-propyl-4-(3'-amino-1'2'4'-triazolo-3'-thiopropinyl)-piperidin-4-ol was tested for growth-stimulating activity on spring wheat grains compared with control (water) and has proved to be a domestic growth regulator «Akpinol-alpha» (KN-2).

For exploring growth-stimulating activity of obtained compound there were prepared hydrochloride solutions of 1-propyl-4-(3'-amino-1'2'4'-triazolo-3'-thiopropinyl)-piperidin-4-ol at the following concentrations: 0.01%, 0.001%, 0.0001% and model solutions of KN-2 in similar concentration.

Also, samples were selected for 100 wheat grains, which preliminary were soaked during 2 hours in obtained solutions. Then grains were placed into Petri dishes for intergrowth (Figure 3). The experiment was conducted for 5 days, during which the length of the roots and shoots of germinated grains was measured.

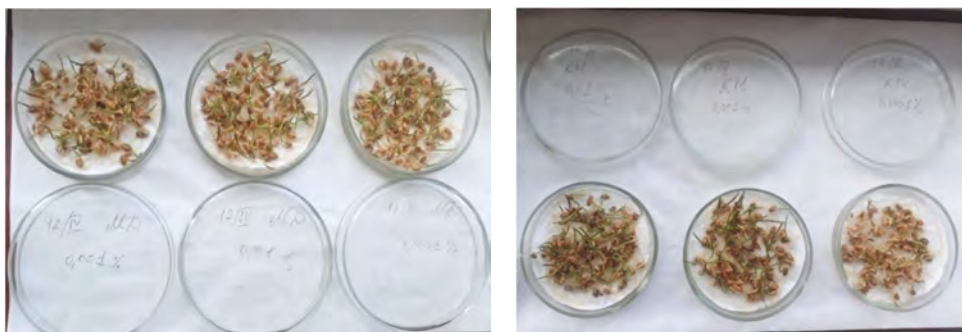


Figure 3. Germination of spring wheat grains in the presence of 1-propyl-4-(3'-amino-1'2'4'-triazolo-3'-thiopropinyl)- piperidin-4-ol (left) and KN-2 (right) in solution concentrations: 0.01%, 0.001%, 0.0001%

Results of growth-stimulating activity of 1-propyl-4-(3'-amino-1'2'4'-triazolo-3'-thiopropinyl) - piperidin-4-ol are presented in table 4.

Table 4. The effect of the 1-propyl-4-(3'-amino-1'2'4'-triazolo-3'-thiopropinyl) - piperidin-4-ol plant growth regulators on wheat germination

Growth-stimulator	Conc., %	Root length, mm	Shoot length, mm
Control (water)	-	43, 36, 25	36
1-propyl-4-(3'-amino-1'2'4'-triazolo-3'-thiopropinyl)-piperidin-4-ol	0.01	22, 26, 15	21
	0.001	43, 34, 23	36
	0.0001	46, 30, 28	29
Ethanol (KN-2)	0.001	36, 28, 27	27

The results showed that 1-propyl-4-(3'-amino-1'2'4'-triazolo-3'-thiopropinyl)-piperidin-4-ol have growth-stimulating activity and the parameters exceed the model drug. The dependence of activity on the concentration of the drugs was also observed. At the concentration increase (0,01%) there appears inhibitory effect of the drug and deceleration of wheat growth is observed. Decrease of the concentration till 0,0001% markedly leads to increase wheat's growth and accordingly, growth stimulating activity.

In this way, it is found out, that the maximum germination of wheat is observed at the 0,0001% concentration of 1-propyl-4-(3'-amino-1'2'4'-triazolo-3'-thiopropinyl) - piperidin-4-ol.

CONCLUSIONS

1-propyl-4-(3'-amino-1',2',4'-triazolo-3'-thiopropinyl)-piperidin-4-ol, which shows the properties of plant growth regulator was obtained. 1-propylpiperidine-4-on and 3-mercaptopropyl-5-amino-1,2,4-triazolo were synthesized to obtain this compound in compliance with the basic parameters of the synthesis.

The structures of the obtained organic compounds were confirmed by IR spectroscopy, ¹H and ¹³C NMR spectrometry.

The obtained compound is 1-propyl-4-(3'-amino-1',2',4'-triazolo-3'-thiopropinyl)-piperidin-4-ol and it was tested for growth-stimulating activity on spring wheat seeds by seed germination method. From the obtained preliminary results, it was concluded that the maximum germination of wheat was observed when the concentration of a solution of 1-propyl-4-(3'-amino-1',2',4'-triazolo-3'-thiopropinyl)-piperidin-4-ol is equal to 0.0001%.

EXPERIMENTAL

The ¹H and ¹³C NMR spectra were recorded on the JNM-ECA Jeol400 spectrometer (frequency is equal to 399.78 and 100.53 MHz, respectively) using CDCl₃ solvent. Chemical shifts are measured toward to the signals of residual protons or carbon atoms of deuterated chloroform.

IR spectra of the obtained compounds were recorded on the Infra-Lum-FT 02 spectrometer (LUMEX, Russia) in the frequency range of 4200-400 cm⁻¹ (in a thin layer for liquid compounds).

1. Propylamine cyanethylation

A 69.4 g (1.18 mol) of distilled propylamine was added dropwise under stirring to a 106 g (2 mol) of acrylonitrile. Reaction mass stirred at room temperature for 10 hours. The reaction mass was dispersed in a vacuum of a water-jet and oil pumps.

Bis(2-cyanethyl)propylamine Yield 105 g (70%). bp 158-160 °C (3-4 mmHg); n_D²⁰ = 1.4627. IR (KBr, cm⁻¹): 2248 (CN), 2963, 2874, 2828 (CH₃, CH₂).

2. Synthesis of 1-propylpiperidin-4-one

A solution of bis(2-cyanethyl)propylamin (10 g, 0.06 mol) in 20 mL of toluene with sodium (0.83, 0.03 mol) was stirred under reflux in anhydrous toluene at 100-105 °C for 10 hours. After all of the sodium has completely reacted, 20 ml of hydrochloric acid solution are added dropwise to pH = 1. After separation, the aqueous layer was cooled, basified to pH = 10. The separated organic layer was repeatedly extracted with ether. The ether layer was dried over calcined potash, the ether was distilled off, and the residue was distilled in a vacuum of an oil pump.

1-Propylpiperidin-4-one Yield 4.1 g (41%). bp 158-160 °C (3-4 mmHg); n_D^{20} = 1.4566. IR (KBr, cm^{-1}): 1638 (C=O), 2959, 2934, 2873 (CH_3 , CH_2)

3 Synthesis of 3-mercaptopropinyl-5-amino-1,2,4-triazole

16.25 g (0.11 mol) of propargyl bromide in 20 ml of acetone were slowly added dropwise to a solution of 14.2 g (0.1 mol) of triazole in 50 ml of acetone heated to 50 °C. The next day, the reaction mass was filtered and the solvent was distilled on a rotary evaporator.

3-mercaptopropinyl-5-amino-1,2,4-triazole Yield 3.16 g (77%). mp 152 °C. ^1H NMR (400 MHz, DMSO- D_6) δ 7.52 (s, 1H), 6.11 (s, 1H), 3.73 (d, J = 12.2 Hz, 2H), 2.96 (d, J = 4.5 Hz, 1H). ^{13}C NMR (101 MHz, DMSO- D_6) δ 157.90 (s), 154.58 (s), 80.67 (d, J = 23.6 Hz), 73.59 (d, J = 20.1 Hz), 19.46 (s).

4 Synthesis of 1-propyl-4-(3'-amino-1'2'4'-triazolo-3'-thiopropinyl)-piperidin-4-ol by the Favorsky reaction

A mixture of 1.1 g (0.009 mol) of 1-propylpiperidin-4-one (2), 2.24 g (0.04 mol) of technical KOH and 200 mL of diethyl ether was stirred under heating (not more than 30 °C) for 1-2 hours. Next, 1.2 g (0.008 mol) of proparrilated triazole in 20 ml of ether was added dropwise at room temperature. After stirring for 2 hours, cold water was added to the reaction mixture, and the separated organic layer was extracted with ether. The ether layer was dried over calcined potash. The ether was distilled off, and the residue was washed repeatedly with acetonitrile until a precipitate formed.

1-propyl-4-(3'-amino-1'2'4'-triazolo-3'-thiopropinyl)-piperidin-4-ol Yield 1.75 g (76%). mp 185 °C. ^1H NMR (400 MHz, CDCl_3): δ 5.11 (s, 1H), 4.38 (s, J = 16.2 Hz, 1H), 2.82 (d, J = 58.0 Hz, 3H), 2.60 – 2.18 (m, 4H), 2.02 (s, 2H), 1.66 (s, 1H), 1.23 (s, 10H), 0.85 (d, J = 7.1 Hz, 4H). ^{13}C NMR (101 MHz, CDCl_3) δ 135.10 (s), 124.93 – 124.73 (m), 31.97 (s), 29.67 (d, J = 11.0 Hz), 29.33 (s), 26.18 (s), 23.19 (s), 22.41 (s), 14.03 (s).

REFERENCES

1. P. Ahmad; A. Hashem; E.F. Abd_Allah; A.A. Alqarawi; R. John; D. Egamberdieva; S. Gucel; *Front. Plant Sci.*, **2015**, 6, 868. <http://dx.doi.org/10.3389/fpls.2015.00868>.
2. S. Chakraborty; *Glob. Change Biol.*, **2013**, 19, 1985–2000. <http://dx.doi.org/10.1111/gcb.12205>.
3. B. Lugtenberg; F. Kamilova; *Ann. Rev. Microbiol.*, **2009**, 63, 541–556. <http://dx.doi.org/10.1146/annurev.micro.62.081307.162918>

4. G. Berg; J.L. Martinez; *Front. Microbiol.*, **2015**, 6, 241. <http://dx.doi.org/10.3389/fmicb.2015.00241>.
5. D. Egamberdieva; D. Jabborova; A. Hashem; *Saudi J. Biol.*, **2015**, 22, 773–779. <http://dx.doi.org/10.1016/j.sjbs.2015.04.019>.
6. D. Egamberdieva; D. Jabborova; G. Berg; *Plant Soil.*, **2015**, 405, 35. <http://dx.doi.org/10.1007/s11104-015-2661-8>.
7. D. Egamberdieva; Li. Li; K. Lindström; L. Räsänen; *Appl. Microbiol. Biotechnol.*, **2016**, 100, 2829–2841. <http://dx.doi.org/10.1007/s00253-015-7147-3>.
8. G. Berg; M. Alavi; C.S. Schmidt; C. Zachow; D. Egamberdieva; F. Kamilova; B. Lugtenberg; Biocontrol and osmoprotection for plants under saline conditions, in: Frans J. de Bruijn (Ed.), *Molecular Microbial Ecology of the Rhizosphere*; Wiley-Blackwell, USA, **2013**. <http://dx.doi.org/10.1002/9781118297674.ch55>.
9. E.F. Abd_Allah; A. Hashem; A.A. Alqarawi; A.H. Bahkali; M.S. Alwhibi; *Saudi J. Biol. Sci.*, **2015**, 22, 274–283.
10. M. Faisal; *J. Appl. Biotech.*, **2013**, 1, 45–53. <http://dx.doi.org/10.5296/jab.v1i1.3698>.
11. V.S. Meena; B.R. Maurya; J.P. Verma; A. Aeron; A. Kumar; K. Kim; V.K. Bajpai; *Ecol. Eng.*, **2015**, 81, 340–347. <http://dx.doi.org/10.1016/j.ecoleng.2015.04.065>.
12. D. Egamberdieva; Z. Kucharova; K. Davranov; G. Berg; N. Makarova; T. Azarova; V. Chebotar, I. Tikhonovich; F. Kamilova; S. Validov; B. Lugtenberg; *Biol. Fertil. Soils.*, **2011**, 47, 197–205. <http://dx.doi.org/10.1007/s00374-010-0523-3>.
13. J. Yadav; J.P. Verma; D.K. Jaiswal; A. Kumar; *Ecol. Eng.*, **2014**, 62, 123–128. <http://dx.doi.org/10.1016/j.ecoleng.2013.10.013>.
14. C.J. Wang; W. Yang; C. Wang; C. Gu; D.D. Niu; H.X. Liu; Y.P. Wang; J.H. Guo; *PLoS ONE.*, **2012**, 7, e52565. <http://dx.doi.org/10.1371/journal.pone.0052565>.
15. A.P. Parray; S. Jan; A.N. Kamili; R.A. Qadri; D. Egamberdieva; P. Ahmad; *Plant Growth Regul.*, **2016**, 35, 877–902. <http://dx.doi.org/10.1007/s00344-016-9583-4>.
16. D. Egamberdieva; S. Wirth; D. Jabborova; L.A. Räsänen; G. Berg; H. Liao; *J. Plant Inter.*, **2017**, 12, 100–107. <http://dx.doi.org/10.1080/17429145.2017.1294212>.
17. B.B. Landa; J.A. Navas-Cortés; R.M. Jiménez-Díaza; *Plant Pathol.*, **2004**, 53, 341–352. <http://dx.doi.org/10.1111/j.1365-3059.2004.01008.x>.
18. S. Ali; T.C. Charles; B.R. Glick; *Plant Physiol. Biochem.*, **2014**, 80, 160–167. <http://dx.doi.org/10.1016/j.plaphy.2014.04.003>.
19. A. Susilowati; A.T. Wahyudi; Y. Lestari; S. Wiyono; A. Suwanto; *Microbiol. Indones.*, **2010**, 4, 33–38. <http://dx.doi.org/10.5454/mi.4.1.7>.
20. D.K. Choudhary; A. Prakash; B.N. Johri; *Indian J. Microbiol.*, **2007**, 47, 289–297. <http://dx.doi.org/10.1007/s12088-007-0054-2>.
21. A. Hashem; E.F. Abd_Allah; A.A. Alqarawi; A. Aldebasi; D. Egamberdieva; *J. Plant Inter.*, **2015**, 10, 230–242. <http://dx.doi.org/10.1080/17429145.2015.1052025>.

22. A. Hashem; E.F. Abd_Allah; A. Alqarawi; A.A. Al-Huqail; S. Wirth; D. Egamberdieva; *Front. Plant Sci.*, **2016**, 7, 1089. [http://dx.doi.org/ 10.3389/fmicb.2016.01089](http://dx.doi.org/10.3389/fmicb.2016.01089).
23. Y. Jha; R.B. Subramanian; S. Patel; *Acta Physiol.Plant.*, **2011**, 33, 797–802. <http://dx.doi.org/10.1007/s11738-010-0604-9>.
24. M.A. Ahanger; A. Hashem; E.F. Abd_Allah; P. Ahmad, Arbuscular mycorrhiza in crop improvement under environmental stress, in: P. Ahmad, S. Rasool. Eds.; *Emerging Technologies and Management of Crop Stress Tolerance*, vol. 2, Academic Press, USA, **2014**, pp. 69–95.
25. B.B. Landa; J.A. Navas-Cortés; A. Hervás; R.M. Jiménez-Díaz; *Phytopathology*, **2001**, 91, 807–816. <http://dx.doi.org/10.1094/PHYTO.2001.91.8.807>.
26. S.Kh. Alimzhanova, Synthesis, stereochemistry and reactivity of new biologically active compounds of the piperidine series; Abstract of Doctor of Chemical Sciences: 02.00.03; Almaty, KazNU, **2000**, 50 p.
27. S.Kh. Alimzhanova; E. Sydykova; *Bulletin of the KazNU, chemical series*, **1994**, 92-96.

ULTRAVIOLET-VISIBLE (UV-VIS) SPECTROSCOPY AND CLUSTER ANALYSIS AS A RAPID TOOL FOR CLASSIFICATION OF MEDICINAL PLANTS

SIMONA CODRUȚA AURORA COBZAC^{a,b,*}, DORINA CASONI^{a,b},
MIHAELA BADEA^c, BILJANA BALABANOVA^d,
NATALIJA MARKOVA RUZDIK^e

ABSTRACT. The ultraviolet-visible (UV-Vis) spectroscopy coupled with cluster analysis (CA) was evaluated for the classification of some medicinal plants of different geographical growing area. To have a deeper view, the experiment was carried out on herbs belonging to different families. The UV-Vis spectra of hydroalcoholic extracts were acquired in the range of 200-800 nm. The hierarchical clustering analysis (HCA) was applied to the data matrix provided by unprocessed, normalized and standardized spectra respectively. Different types of distance measuring of (dis)similarity between the samples as well as different kinds of linkage or amalgamation rule were taken into account. The best results for the classification of the selected medicinal plants were obtained using *Ward's method* as the amalgamation rule combined with *1-Pearson r* clustering distance measurement. The obtained results reveal the ability of HCA with Ward and *1-Pearson r* algorithm to identify plant species even when the raw material has different provenience areas and different pedoclimatic growing conditions. In addition, this methodology revealed a direct link between herbs from different families.

Keywords: medicinal plants, classification/identification, UV-Vis spectroscopy, cluster analysis

^a Babeș-Bolyai University, Faculty of Chemistry and Chemical Engineering, 11 Arany Janos str., RO-400028, Cluj-Napoca, Romania

^b Research Center for Advanced Chemical Analysis, Instrumentation and Chemometrics – ANALYTICA, Babeș-Bolyai University 11 Arany Janos str., RO-400028, Cluj-Napoca, Romania

^c Faculty of Medicine, Transilvania University of Brasov, Nicolae Balcescu St., No. 56, Brasov, Romania

^d Department of Soil Chemistry and Hydrology, Faculty of Agriculture, Goce Delcev University, Krste Misirkov 10-A, 2000, Stip, Republic of North Macedonia

^e Department of Plant Production, Faculty of Agriculture, Goce Delcev University, Krste Misirkov 10-A, 2000, Stip, Republic of North Macedonia

* Corresponding author: csimona@chem.ubbcluj.ro

INTRODUCTION

The World Health Organization (WHO) encourages and promotes the integration of traditional medical practices into healthcare systems, and increasingly supports the countries producing medicinal plants [1]. Traditional medicine is often termed complementary or alternative medicine (CAM) and according to the WHO estimation, about 80% of the emerging world's population relies on herbal remedies (drugs) for therapy [2, 3].

Usually, the term *herbal drugs* denote medicinal plants or plant parts converted into phytopharmaceutical products (teas, tablets, tinctures and extracts) by means of simple processes involving harvesting, drying, storage, mincing/grinding, compressing or extraction of active compounds with different solvents. The parts of medicinal plants that may be used are root, leaf, flowers, fruit, seeds or even the whole plant. Regarding the composition, phytopharmaceuticals are mixtures of many compounds with the specific physiological effect that may act individually, additively, or in synergy to improve health and cure different ailments. The phyto-compounds that are responsible for the biological characteristics of plant species are the secondary metabolites. It is well known that for the same species, differences in geographical location and growing conditions may alter the composition by increasing/decreasing the content of the constituents responsible for the phytotherapeutic effect or appearance of other compounds. Also, different parts of the same plant contain different amounts of secondary metabolites. In this context, methods for correct identification/authentication and classification of plants with specific therapeutic actions are acquiring higher importance for consumers, producers, and the pharmaceutical industry. Usually, both identification and classification processes depend on the identification of physical, chemical and biochemical differences and similarities between samples [4].

Numerous analytical techniques have been developed for quality control and evaluate compliance with the standard requirements. Instead of this, the methods for classification and identification/authentication were less approached, because of the need for advanced methods for comparison of the analytical results with a huge volume of information from a database. Exploratory data analysis, unsupervised and supervised techniques are often used as pattern recognition methods for the classification of herbal products and reveal the similarities and dissimilarities of sample properties. The aim of the unsupervised pattern recognition methods is to detect similarities whereas supervised techniques make use of calibration or training sets with a priori known the information to build a classification model. Cluster analysis (CA) and principal component analysis (PCA) are widely applied for authenticating or classifying plants based on spectral data [5, 6]. The PCA method allows visualization of the difference between samples, whereas CA can classify

objects based on their characteristics. The combination of CA and PCA has been widely used in current quality assessment, classification and identification of different medicinal plants [7-9]. Usually, classification and identification/authentication of herbs extracts is carried out based on a chromatographic fingerprint [10-14]. Spectral analysis including ultraviolet-visible (UV-Vis) and infrared (IR) spectroscopy can also be used for these purposes [7, 15-17]. Their advantages consist in avoiding the time consumed by chromatographic separation while retaining sufficient information to obtain a correct classification [18]. The methods are based on the fact that samples with similar spectral responses have the same chemical and pharmaceutical properties. Starting from the spectral results, the application of pattern recognition methods is the first step of the data analysis for sample classification. The cost-effectiveness of spectroscopy combined with chemometrics was confirmed by numerous literature studies [19, 20]. Also, spectral data analyzed by chemometric methods better exploit the relationship between the plant spectra and properties [8].

Therefore, the aim of the present work was to identify the most appropriate cluster analysis methodology able to provide a rapid identification/classification of medicinal plants based on the UV-Vis spectra. For these investigations, seventeen medicinal plants belonging to various families and collected from Macedonia, Hungary and Romania were used.

RESULTS AND DISCUSSION

UV-Vis spectra of plant materials

UV-Vis spectral profile of hydroalcoholic extracts can provide qualitative and quantitative information upon the presence of different types of polyphenolic constituents [21, 22] that are the most common phytochemicals present in plants. The class of polyphenols includes phenolic acids (hydroxybenzoic acid derivatives and hydroxycinnamic acid derivatives), flavonoids (flavonols, flavones, flavanols, flavones, anthocyanidins, isoflavone), coumarins, stilbenes, tannins and lignans with specific absorbance values in the ultraviolet and visible spectral region.

A number of seventeen medicinal plants from spontaneous flora from Macedonia and different cultivars from Hungaria and Romania (Table 1) were selected for this study. The UV-Vis absorption spectra of their hydroalcoholic extracts were acquired in the range 200 – 800 nm. The obtained spectra profiles are presented in Figure 1. Two absorption bands were observed in the range from 200 to 250 nm and from 250 to 300 nm and a third broad absorption band is located between 300 and 400 nm. These absorption bands are related to different phenolic compounds present in the plant extracts that contain aromatic conjugated systems and absorb light in different UV spectral regions depending on the conjugations of the benzene rings.

Table 1. The name and provenience of the medicinal plants

No	Common name	Species	Part of the plant	Familly	Country of provenience (cultivar)	Code
1	Liquorice	<i>Glycyrrhiza glabra</i> L.	<i>radix</i> *	Fabaceae	Macedonia	Lq1
			<i>radix</i> **		Macedonia	Lq2
			<i>radix</i> **		Romania (Fares)	Lq3
2	Dandelion	<i>Taraxacum officinale</i> F.H.Wigg.	<i>radix</i> **	Asteraceae	Macedonia	Da4
			<i>radix</i> **		Hungary (Gyogyfu)	Da5
3	Comfrey	<i>Symphytum officinale</i> L.	<i>radix</i> **	Boraginaceae	Romania (Fares)	Co6
4	Valerian	<i>Valeriana officinalis</i> L.	<i>radix</i> **	Caprifoliaceae	Macedonia	Va7
			<i>radix</i> **		Romania (Fares)	Va8
5	Sweet fennel	<i>Feniculum vulgare</i> var. <i>dulcis</i> Mill.	<i>fructus</i>	Apiaceae	Macedonia	Fe9
			<i>fructus</i> TBC		Macedonia	Fe10
			<i>fructus</i>		Romania (Plafar)	Fe11
6	Dog rose	<i>Rosa canina</i> L.	<i>fructus</i> ***	Rosaceae	Macedonia	Dr12
			<i>fructus</i> ***		Macedonia	Dr13
			<i>fructus</i> **		Romania (Fares)	Dr14
7	Juniper	<i>Juniperus communis</i> L.	<i>fructus</i> ***	Cupresaceae	Macedonia	Ju15
			<i>fructus</i> ***		Romania (AdNatura)	Ju16
8	Bean	<i>Phaseolus vulgaris</i> L.	<i>pericarpum</i>	Fabaceae	Macedonia	Be17
			<i>pericarpum</i>		Romania (Fares)	Be18
9	Elderberry	<i>Sambucus nigra</i> L.	<i>flos</i> **	Adoxaceae	Macedonia	Eb19
			<i>flos</i> **		Romania (Fares)	Eb20
10	Wild thyme	<i>Thymus serpyllum</i> L.	<i>herba</i> **	Lamiaceae	Macedonia	Wt21
			<i>herba</i> **		Macedonia	Wt22
			<i>herba</i> **		Romania (Plafar)	Wt23
11	Horsetail	<i>Equisetum arvense</i> L.	<i>herba</i> ***	Equisetaceae	Macedonia	Ht24
			<i>herba</i> **		Romania (Fares)	Ht25
12	Oregano	<i>Origanum vulgare</i> L.	<i>herba</i> **	Lamiaceae	Macedonia	Or26
			<i>herba</i> **		Romania (Fares)	Or27
13	Peppermint	<i>Mentha x piperita</i> L.	<i>folium</i> **	Lamiaceae	Macedonia	Pm28
			<i>herba</i> **		Romania (Fares)	Pm29
			<i>folium</i> **		Romania	Pm30
14	Blackberry	<i>Rubus fruticosus</i> L.	<i>folium</i> **	Rosaceae	Macedonia	Bb31
			<i>folium</i> **		Romania (Plafar)	Bb32
15	St.John's wort	<i>Hypericum perforatum</i> L.	<i>herba</i> ***	Hypericaceae	Macedonia	Sw33
			<i>herba</i> **		Macedonia	Sw34
			<i>herba</i> **		Romania (Fares)	Sw35
16	Agrimony	<i>Agrimonia eupatoria</i> L.	<i>herba</i> **	Rosaceae	Macedonia	Ag36
			<i>herba</i> **		Romania (Fares)	Ag37
17	Stinging nettle	<i>Urtica dioica</i> L.	<i>semen</i>	Urticaceae	Macedonia	SnS38
			<i>folium</i> **		Macedonia	SnF39
			<i>herba</i> **		Romania (Fares)	SnH40

*-pulvis(powder); **-concis(pieces); ***-totus(entire)

Among the polyphenolic constituents usually present in medicinal plant extracts, different flavonoid subclasses show different shapes of spectra. According to the obtained spectral profile, most of the selected extracts are rich in flavonoids characterized by absorption band at around 240–290 nm (known as Band II) and flavones and flavonols characterized by absorption maximum around 310–370 nm (generally a longer wavelength for flavonols than for flavones).

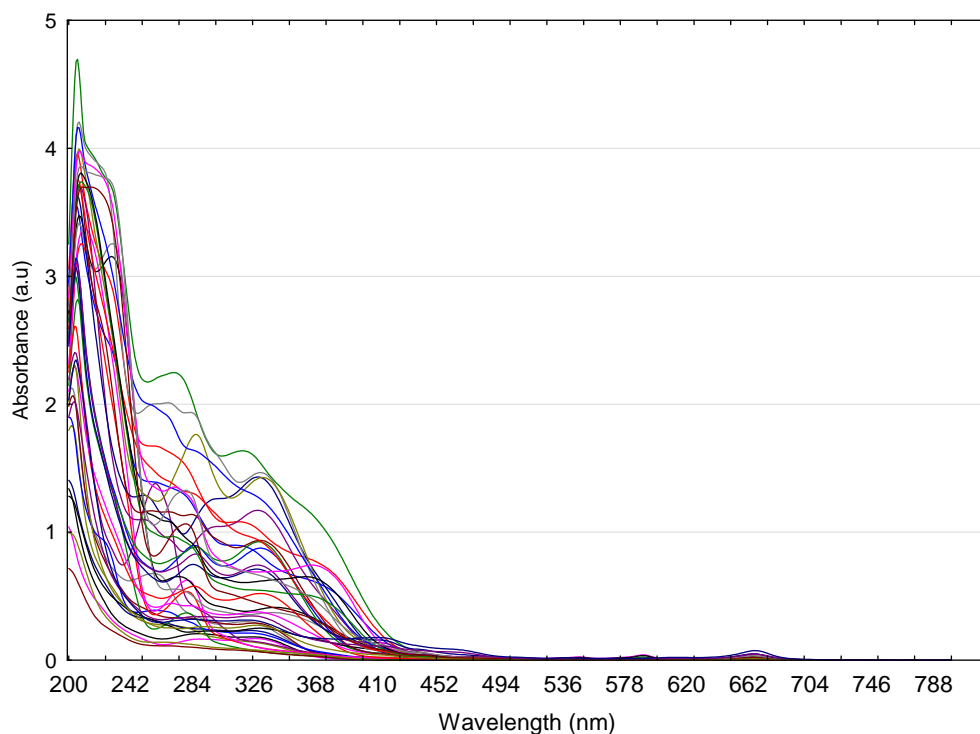


Figure 1. The absorption UV-Vis spectra of the investigated medicinal plant.

The absorption spectra profiles acquired in the range of 200–800 nm revealed that specific differences and similarities between the investigated samples are difficult to distinguish. Therefore, the cluster analysis was conducted to investigate the (dis)similarities in a spectral dataset and classify samples based on their characteristics.

Cluster analysis

Among the general categories of cluster analysis methods, hierarchical cluster analysis (HCA) with joining or tree clustering algorithm was applied on the digitized data matrix (40 samples x 601 variables) from unprocessed, normalized and standardized spectra respectively. The *Euclidean*, *Squared Euclidean*, *City-block (Manhattan)*, *Chebychev*, *Power*, *Percent disagreement* and *1-Pearson r* distance HCA algorithms were used for clustering distance measurements. Also, different linkage or amalgamation rule including *Single linkage* (nearest neighbor), *Complete linkage* (furthest neighbor), *Unweighted pair-group average (UWPGA)*, *Weighted pair-group average (WPGA)*, *Unweighted pair-group centroid (UWPGC)*, *Weighted pair-group centroid (WPGC)*, and *Ward's method* were applied in order to decide when two clusters are sufficiently similar to be linked together. The commonly applied, *Single (SL)* and *Complete linkage (CL)* algorithms used for clustering classification have not provided satisfactory results (Figure 2 **a,b**). In our case, the best results were obtained using *Ward's* amalgamation algorithm, when the highest similarity percent were revealed by short linkage distances (Figure 2, **c**).

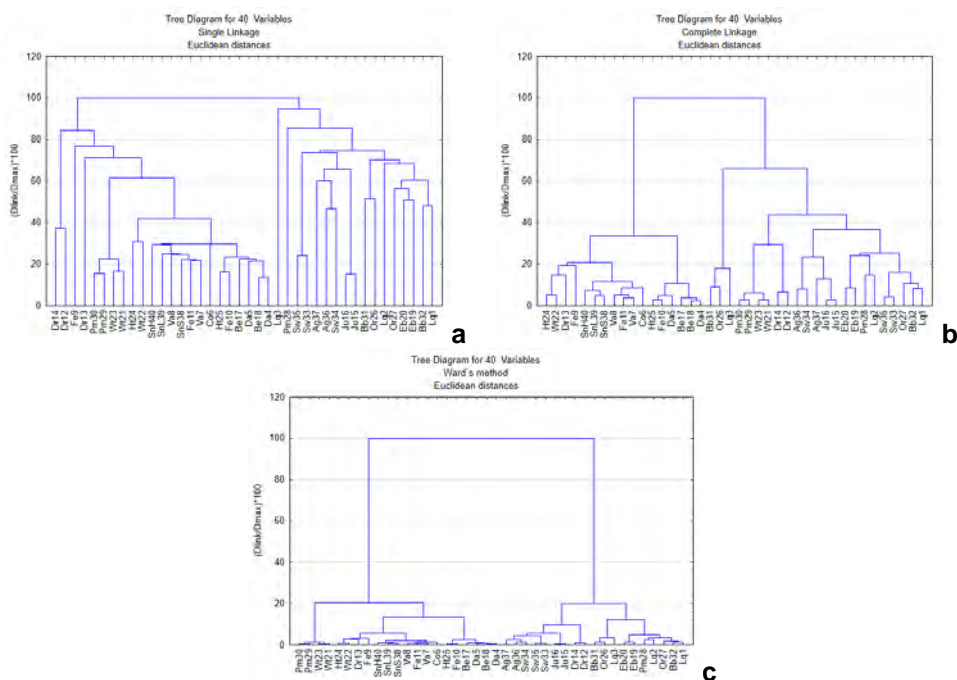


Figure 2. Dendrogram of investigated medicinal plant based on the UV-Vis spectral data using different linkage method (**a**-SL; **b**-CL; **c**-Ward's method) and Euclidian distance for clustering

In terms of distance measurement, among *Euclidean Square*, *Euclidean*, *City-block*, *Chebyshev*, *Power SUM(ABS(x-y)²)^{1/r}* and *1-Pearson r* applied methods, the *1-Pearson r* method was the most effective (Figure 3) since herbs from the same species were grouped together.

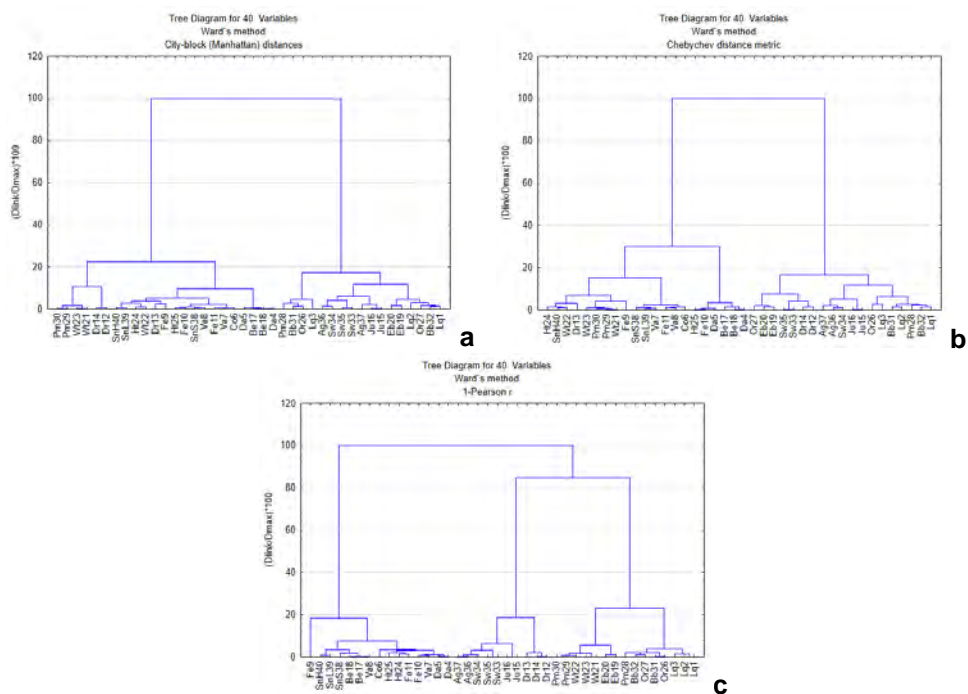


Figure 3. Dendrogram for classification of investigated medicinal plants based on the UV-Vis spectral data using *Ward's* method as linkage algorithm and different methods for distance measuring: (a)-*City-block (Manhattan)* distance; (b)-*Chebyshev*, (c)-*1-Pearson r*

The same protocol of statistical evaluation was applied to data obtained from spectra after their normalization and standardization. In comparison with the results obtained from unprocessed UV-Vis spectra, a better clustering of plants from the same species could be observed. Nevertheless, different clustering was highlighted depending on the method used for spectra processing (Figure 4).

It is noteworthy that using the combination *Ward's* / *1-Pearson r*, the same clustering of the samples was achieved both for unprocessed and processed spectra (Figure 5). The *Ward's* method is distinct from all other methods because it uses an analysis of variance approach to evaluate the distances between clusters and attempts to minimize the sum of squares of

any two (hypothetical) clusters that can be formed at each step. Moreover, the use of *1-Pearson r* distance is more efficient to find the similarity, providing small sub-clusters especially in case of correlated data such as those obtained from the UV-Vis spectra of the medicinal plant's extracts. So, we can conclude that if the input matrix is a correlation matrix, data would be transformed as *1-Pearson r* distances before the analysis.

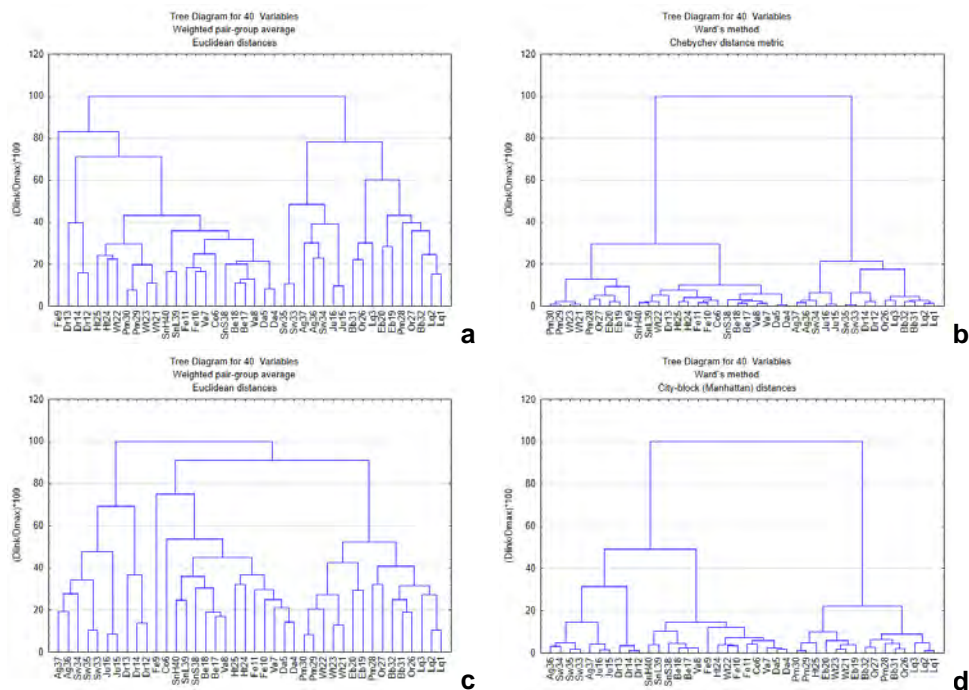


Figure 4. Classification dendrogram of investigated medicinal plants based on normalized (**a**; **b**) and standardized (**c**, **d**) spectra using *WPGA/Euclidian* (**a**, **c**) and *Ward's/City-block* (**b**, **d**) used as linkage algorithm/distance measuring mode

According to the obtained dendrogram (hierarchical tree clustering) (Figure 5), the investigated samples are divided into three principal clusters. A clear classification of the investigated plants according to the family could not be observed, but similarities in the composition of the plants belonging to different families could be taken into account. The most important result highlights a very good classification of the samples according to the species, despite their different geographical provenience area. Twelve of the investigated plant species (liquorice-Lq, dandelion-Da, dog rose-Dr, juniper-

Ju, bean-Be, elderberry-Eb, wild thyme-Wt, horsetail-Ht, St.John's wort-Sw, agrimony-Ag and stinging nettle-Sn) were classified in the individual sub-clusters. Plants rich in volatile oils, such as fennel-Fe, valerian-Va and peppermint-Pm were not grouped into sub-clusters but are included in the same principal cluster. Differences in spectra profiles could be assigned to possible variation in volatile oil content. An interesting clustering was observed in the case of blueberry-Bb and oregano-Or that were grouped according to the geographical growing area. This can be explained based on some similarities in their spectra.

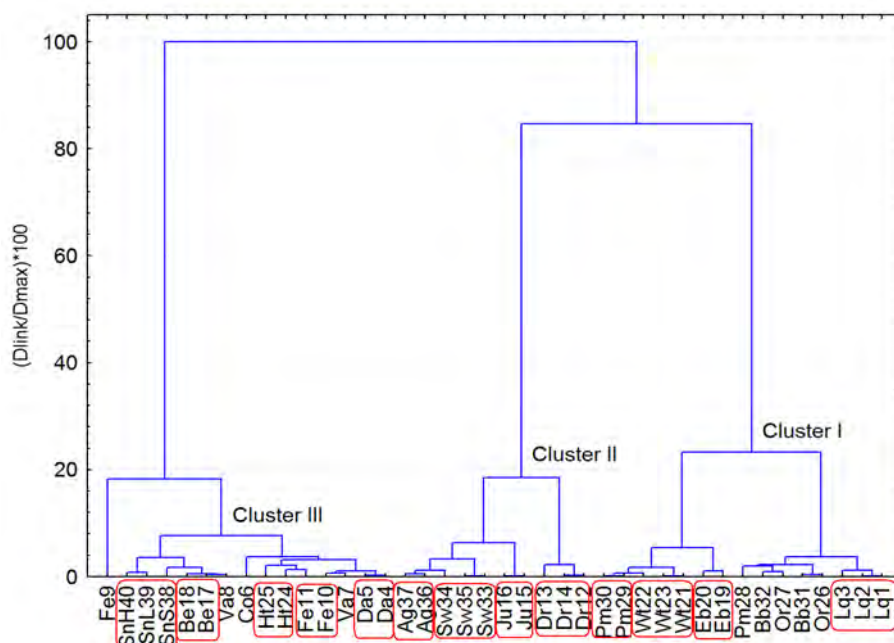


Figure 5. The dendrogram (hierarchical tree clustering) of the relationship between the investigated medicinal plant extracts based on the UV-Vis spectroscopy data using the $1-Pearson\ r$ distance as a measure of (dis)similarity between the samples and *Ward's* method as linkage or amalgamation rule specifying the (dis)similarity between the clusters

Although the HCA method has been widely used in the common approach for the medicinal plant's evaluation [23], to our best knowledge there is not concluded which would be the most appropriate combination of distance measurements/linkage methodology that can be used HCA analysis in order to provide a rapid identification / classification of the plant species even in cases in which the plant comes from different places and different

pedoclimatic conditions. During the investigations developed in the present study, it was demonstrated for the first time that using the *Ward's / 1-Pearson r* combination in HCA analysis of UV-Vis spectra, a rapid classification of plants can be obtained according to the species. Moreover this methodology has the ability to generally overcome the influences due to the pedoclimatic conditions, those related to the sample preparation (such as the degree of grinding) or those related to the use of the different parts of the plant. Examples can be revealed by classification of *Dog rose* (Dr) samples which are of different grinding and *Stinging nettle* samples that are of different part of plant provenience.

CONCLUSIONS

The ability of UV-Vis spectroscopy with hierarchic cluster analyses (HCA) was investigated for the rapid classification of medicinal plants. Using *Ward's method* as amalgamation rule combined with *1-Pearson r* for distance measurement, forty samples of medicinal plants from various families and of different geographical area provenience were grouped into individual sub-clusters according to their belonging species. The applied methodology revealed the same classification for the investigated samples in all cases using the original, normalized and standardized data provided by UV-Vis spectra respectively. Based on the obtained results, the proposed pattern recognition methodology combined with UV-Vis spectroscopy can be used for the rapid identification of plant species from different geographical areas.

EXPERIMENTAL SECTION

Materials and methods

The study was carried out on seventeen medicinal plants belonging to different families and having different European provenience areas (Macedonia, Hungary, and Romania). The Hungarian and Romanian vegetal material was purchased from a specialized store as phytoproducts for infusion. All phytoproducts are certified regarding the species and purity in concordance with regulations of Romanian and Hungarian Pharmacopoeias. The plants originated from North Macedonia were collected from three localities in the Osogovo mountains basin situated in the south-eastern part of the country. They were identified by determination key using the data from Matevski [24], a specimen is kept in the herbarium at the Department of Plant Production,

Faculty of Agriculture, Goce Delcev University in Shtip, Republic of North Macedonia. Depending on the part of plants that have a recognized therapeutic effect, forty hydroalcoholic extracts were obtained from roots (*radix*), leaves (*folium*), flowers (*flos*), fruits (*fructus*), seeds (*seeds*) or entire aerial parts (*herba*) (Table 1). The raw material was powdered using a mill, except sample Dr13 which was ground to coarse dimension. For each sample, 2 g of minced material was extracted with 20 mL of ethanol - water (7:3, v/v) mixture by a ten days maceration at room temperature. The extract was separated by centrifugation and the remained solid residue was two times centrifuged with 2 mL ethanol - water (7:3, v/v). The combined extracts were adjusted to 25 mL volumetric flask using a mixture of ethanol - water (7:3, v/v) in each case.

UV-Vis spectra acquisition and preprocessing

The molecular absorption UV-Vis spectra were recorded using the Jasco V-550 double beam spectrophotometer (Jasco Corporation, Japan). Spectra of the previously resulted extracts were collected in the region of 200 – 800 nm with 1 nm acquisition interval after 1:100 dilution. To remove any irrelevant information several spectral preprocessing techniques were applied before spectral data analysis. Usually scatter or baseline correction, signal enhancement and statistical filtering of signal noise preprocessing methods can be applied to the original spectra [25]. In this case, smoothing algorithms including the Savitzky–Golay method was used as a low-pass filter to correct additive and multiplicative effects in the spectral data and preserve the important features of information by removing random variations in spectra. Secondly, normalization and standardization processing techniques were applied. The standardization procedure was based on the transformation of initial spectral data by subtracting the mean from each value and dividing it by the standard deviation. All spectral values were replaced by standard values computed as $\text{Standardized value} = (\text{raw value} - \text{mean}) / \text{Standard deviation}$. Normalization was applied to eliminate the shifting of the peaks on the wavelength scale. For this the formula $(A - A_{\min}) / (A_{\max} - A_{\min})$, where A is absorbance value, A_{\min} is minimum value and A_{\max} is the maximum value of absorbance in the spectra.

Spectral data analysis

Cluster analysis (CA), an unsupervised pattern recognition method was used in order to detect similarities in the spectral dataset and classify the selected medicinal plants based on quantitative characteristics. The clustering techniques are divided into hierarchical and nonhierarchical type.

In the common approach for the medicinal plant's evaluation, the most popular clustering technique is hierarchical clustering analysis (HCA) due to the large flexibility to alter the similarity measurement criteria and the applied linkage methods to suit different applications. HCA technique is based on the creation of branched structures, called dendrograms which are qualitative in nature and permit visualization of clusters and correlations amongst samples. In order to decide when clusters should be merged or split, a measure of (dis)similarity between the samples as well as a linkage criterion specifying the (dis)similarity between the clusters is used. The result of this type of clustering is the hierarchical tree where the horizontal axis denotes the linkage distance between the obtained individual clusters. In this study, the *Euclidean*, *Squared Euclidean*, *City-block (Manhattan)*, *Chebyshev*, *Power* and *1-Pearson r* distance were used for distance measurements. The *Single Linkage*, *Complete Linkage*, *Unweighted Pair-Group Average*, *Weighted Pair-Group Average*, *Unweighted Pair-Group Centroid*, *Weighted Pair-Group Centroid (median)*, and *Ward's method* were used as different linkage or amalgamation rule in order to determine when two clusters are sufficiently similar to be linked together.

REFERENCES

- 1 WHO; WHO Guidelines on Good Agricultural and Collection Practices (GACP), 2003
- 2 WHO; Traditional Medicine. Growing Needs and Potential. WHO Policy Perspective on Medicine. WHO, Geneva, 2002
- 3 A. Gurib-Fakim; *Mol. Aspects Med.*, **2006**, 27, 1-93
- 4 O.Y. Rodionova; A.V. Titova; A.L. Polmerantsev; *Trends Anal. Chem.*, **2016**, 78, 17-22
- 5 M. Forina; P. Oliveri; S. Lanteri; M. Casale; *Chemom. Intell. Lab. Syst.*, **2008**, 93, 132-148
- 6 Y. Wei; W. Fan; X. Zhao; W. Wu; H. Lu; *Anal. Lett.*, **2015**, 48, 817-829
- 7 Z. Cao; Z. Wang; Z. Shang; J. Zhao; *PLOS ONE*, **2017**, 1-14
- 8 H.A. Gad; S.H. El-Ahmady; M.I. Abou-Shoer; M.M. Al-Azizi; *Phytochem. Anal.*, **2013**, 24, 1-24
- 9 I.M. Simion; C. Sârbu; *Spectrochim. Acta A: Mol. Biomol. Spectroscopy*, **2019**, Accepted manuscript, <http://doi.org.10.1016/j.saa.2019.04.038>
- 10 J. Fibigr; D. Satinsky; P. Solich; *Anal. Chim. Acta*, **2018**, 1036, 1-15
- 11 S.S. Chavan; V.M. Jadhav; V.J. Kadam; *Int. J. Pharm. Sci. Rev. Res.*, **2017**, 43, 161-168

- 12 X. Zhang; J. Zhang; S. Zhang; Z. Qian; S. Wu; J. Liu; Y. Ye; J. Si; *Ind. Crops Prod.*, **2018**, *124*, 707-718
- 13 G. Alvarez-Rivera; D. Ballesteros-Vivas; F. Parada-Alfonso; E. Ibañez; A. Cifuentes; *Trend. Anal. Chem.* **2019**, *112*, 87-101
- 14 M. Simion; D. Casoni; C. Sarbu; *J. Pharm. Biomed. Anal.* **2019**, *163*, 137-143
- 15 C. Cheng; J. Liu, W; Cao, R. Zheng; H, Wang; C. Zhang; *Vib. Spectrosc.*, **2010**, *54*, 50-55
- 16 T. Hu; W.Y. Jin; C.G. Cheng; *Spectroscopy*, **2011**, *25*, 271-285
- 17 A. Dankowska; W. Kowalewski; *Spectrochim. Acta A, Mol. Biomol. Spectroscopy*, **2019**, *211*, 195-202
- 18 D.D. Joshi; Herbal Drugs and Fingerprints. In *UV-Vis Spectroscopy: Herbal Drugs and Fingerprints*, Springer, New Delhi Heidelberg, 2012, Chapter 6, pp 101-105
- 19 L.A. Berrueta; R.M. Alonso-Salces; K. Heberger; *J. Chromatogr. A*, **2007**, *1158*, 196-214
- 20 J. Moros; *Trends Anal. Chem.* **2010**, *29*, 578-591
- 21 S.M. Dhivya; K. Kalaichelvi; *Int. J. Curr. Pharm. Res.*, **2017**, *9*, 46-49
- 22 K. Kalaichelvi; S. M. Dhivya; *Int. J. Herb. Med.*, **2017**, *5*, 40-44
- 23 D. Jing; W. Deguang; H. Linfang; C. Shilin; Q. Minjian; *J. Med. Plants Res.*, **2011**, *5*, 4001-4008
- 24 V. Matevski; Flora of the Republic of Macedonia, 1st Edition, Macedonian Academy of Science and Arts, Skopje, 2010 (in Macedonian)
- 25 A. Rinnan; F.W.J. van den Berg; S.B. Engelsens; *Trends Anal. Chem.*, **2009**, *28*, 1201-1222

FROM PHYTOCHEMISTRY TO METABOLOMICS: EIGHT DECADES OF RESEARCH IN PLANT AND FOOD SCIENCE

CARMEN SOCACIU^a

ABSTRACT. Phytochemistry represents a large interdisciplinary research area which apply the chemical knowledge in plant biology, biochemistry and physiology. Since centuries, the technology related to the isolation and characterization of phytochemicals (plant secondary metabolites) developed gradually towards a holistic approach of omics' technology, as part of the "systems biology" concept. This review underlines the scientific progress during the last eight decades, from "classical" phytochemistry to metabolomics, applied on plants and food and reflects not only the role of phytochemicals as key-molecules with essential roles in plants and with great benefits on animal and human health, but also their involvement in plant chemotaxonomy, food technology and authenticity. First, a selection of the major groups of phytochemicals and their main bioresources. The metabolomic technology is presented, as a high-throughput analytical platform to identify, by untargeted or targeted techniques, the fingerprint or key metabolites of a specific pathway in plants or for authentication of a food matrix. Updated literature data are presented, including a summary of eight decades of achievements of the research group related to Chemistry and Biochemistry of Natural Products at the University of Agricultural Sciences and Veterinary Medicine Cluj-Napoca, celebrating now 150 years of existence.

Keywords: *Phytochemistry, Metabolomics, Analytical platform*

INTRODUCTION

Phytochemicals

Since centuries, plants were studied as huge reservoir of valuable, small molecules, named phytochemicals. Phytochemistry was defined as being the study of these chemicals in plants and includes their isolation,

^a *University of Agricultural Sciences and Veterinary Medicine, 3-5 Manastur Street, 400372 Cluj-Napoca, Romania, e-mail: carmen.socaciu@usamvcluj.ro*

structural analysis, biosynthesis and their functions in plants, animals and humans, as reported by Lind since 1757, Eijkman in 1929 or Szent-Györgyi in 1939, recently cited [1]. Nearly 400,000 flowering plants have been classified so far, only around 5% being used for medicinal purposes, and only a minority were studied in detail with regard to the chemical composition and biological effects.

The Dictionary of Natural Products contains around 160,000 chemical entities isolated from plants and microorganisms [2]. Medicinal plants have always been used since ancient times to treat diseases, but the knowledge about active components of herbal preparations remained fragmentary since the biosynthetic pathways of many secondary metabolites of pharmacological importance have been elucidated only in a few species, while their chemodiversity remained largely unexplored [3, 4].

Phytochemistry adopts a phylogenetic approach and can be considered as an independent sub-field of botany or chemistry which analyses plants, identify and describe the structures of the large number of small molecules (secondary metabolites) produced by plants for their reproduction, insects' attraction and defense against pathogens. While primary metabolites (carbohydrates, proteins and amino acids, lipids) are related to the nutritional quality of plants and food, phytochemicals are "non-nutrients" but highly bioactive compounds with positive or negative effects on human health. Such secondary metabolites display a large structural diversity, reflecting the higher plants phenotype and adaptations to the various ecological environments [5] their biosynthesis and functions in plants being complemented by their actions, which determined the development of phytopharmacy and phytomedicine, providing the evidence of their health benefits [6].

There are three major groups of phytochemicals: phenolics (representing aprox. 45%), terpenoids and steroids (27%), alkaloids (18%) and other organo-sulfur or organo-nitrogen derivatives. Phenolics are water soluble compounds found in different plant and food sources while terpenes and terpenoids are lipophilic groups of major phytochemicals, as presented in Table 1. Alkaloids and sulfur- or nitrogen-containing phytochemicals are also included.

Table 1. Major groups of phytochemicals (classes, sub-classes, molecular species) and their main biosources

Group	Class	Sub-class	Molecular species	Main bioresources
Phenolics	Phenolic acids	Hydro benzoic acids	gallic acid, ellagic acid, vanillic acid	grape seed, raspberries, vanilla, tea, blackberries, pomegranate
		Hydroxy cinnamic acids	ferulic acid, o- and p-coumaric acid, caffeic acid, sinapic acid	wheat bran, cinnamon, coffee, kiwi fruit, plums, blueberries
	Flavonoids	Flavonols	quercetin, kaempferol	onions, kale, leeks, broccoli, buckwheat, red grapes, tea, apples
		Flavones	apigenin, luteolin	celery, herbs, parsley, chamomile, rooibos tea, capsicum pepper
		Isoflavones	genistein, daidzein, glycitein	soya, beans, chick peas, alfalfa, peanuts
		Flavanones	naringenin, hesperitin	citrus fruits
		Anthocyanidins and anthocyanins	cyanidin, delphinidin, malvidin, pelargonidin, peonidin, petunidin	red grapes, blueberries, cherries, strawberries, blackberries, raspberries, tea
		Flavan-3-ols	catechins, epicatechin, epigallocatechin gallate	green tea, chocolate, grape seeds
		Flavanolols	silymarin, silibinin	milk thistle, red onions, artichoke
		Dihydrochalcones	phloridzin, aspalathin	apples, rooibos tea
	Non-flavonoid polyphenols	Tannins	Condensed cathechins	cereals, fruits, berries, beans, red wine, cocoa
		Curcuminoids	curcumin	Turmeric root
		Stilbenes	cinnamic acid, resveratrol	grapes, wine, blueberries, raspberries
		Lignans	secoisolarici-resinol, sesamin	grains, flaxseed, sesame seeds
Terpenoids	Monoterpenes	C10	geraniol, limonen, citral, myrcen, menthol	lemon, orange, mentae leaves, hops
	Sesquiterpenes	C15	farnesol, cadinen	cassie, acacia, juniperus
	Diterpenes	C20	cafestol, phytol, vitamin A ginkgolide	green leaves, vegetable oils Ginkgo biloba
	Triterpenes	C30	squalene, ursolic acid, betuline and betulinic acid	birch, apples, cranberries, peppermint, oregano, thyme

Group	Class	Sub-class	Molecular species	Main bioresources
			Phytosterols (sitosterol, sitosterol, stigmasterol)	Vegetable oils, cereal grains, nuts, shoots, legumes
	Tetraterpenes	C40	Carotenes cryptoxanthin lycopene lutein zeaxanthin astaxanthin	sweet potato, carrots, pumpkin, tomatoes watermelon, guava, papaya corn, eggs, kale, spinach, red pepper, pumpkin, oranges, rhubarb, plum, mango, papaya) salmon, shrimp
		Saponins		chickpeas, soya beans
		Perillyl Alcohols		cherries, caraway seeds, mint
Alkaloids	Free alkaloids N-heterocycle		atropine, nicotine, morphine, cocaine	Atropa belladonna, tabac, coke leaves, poppyseed
	Polyamine alkaloids		palustrine, verbasceine	Horsetail, soy bean
	Pseudoalkaloids		caffeine, solanidine, aconitine	Coffee, Potatoes, tomatoes, Aconite
	Protoalkaloids		ephedrine, mescaline	Aconite, Bear's-Foot, Peyote
Sulfur- and non-Sulfur	Glucosinolates		Isothiocyanates (sulforaphane) and dithiolthiones	Cruciferous vegetables e.g. broccoli, Brussels sprouts, cauliflower, cabbage, radish, mustard
	Allylic sulfides		Allicin and S-allyl cysteine	garlic, leeks, onions
	Indoles		Indole-3-carbinol	Broccoli, Brussels sprouts
	Betaines		Betalaine	Beetroot
	Chlorophylls		Chlorophyll a and b	Green plant tissues
	Purgent compounds		Capsaicin, piperine	Chilli, black peppers

METABOLOMICS – AN EMERGING ANALYTICAL PLATFORM

Metabolomics, the newest, “apogee of omics’ technology”, is defined as a holistic qualitative and quantitative analysis of all small metabolites (of less than 1500 Daltons) found in a biological system [7, 8]. The term “metabolomics”

was mentioned for the first time in 1998 and developed tremendously as a valuable tool for advancing our understanding of primary and secondary metabolism in plants. It brings a holistic understanding of plant biology [9], as a complementary technology to functional genomics approaches such as transcriptomics and proteomics and contributes to a systems biology approach. Moreover, metabolomics as a post-genomics tool may offer distinct advantages when compared to other '-omics' technologies. (e.g. changes in the transcriptome or proteome do not always correlate to biochemical phenotypes).

Metabolomics technology involve advanced analytical tools that provide high degrees of sensitivity, selectivity and reproducibility are required. State-of-the-art of metabolomics comprises emerging analytical platforms such as gas chromatography and liquid chromatography–mass spectrometry-based techniques (GC–MS and HPLC–MS) and nuclear magnetic resonance (NMR) spectroscopy, Raman and FTIR spectroscopy. Each approach has its own advantages and disadvantages [10-13].

A Web of Science recent search, using the terms “metabolomics” or “metabonomics” found around 8800 publications. Such data provides high level information regarding the key-biomarkers for a specific plant or food, novel chemotaxonomic markers of biodiversity, plant-based drug discovery, food authenticity and traceability, as well the impacts of environmental stress or processing technology.

There are three different approaches to metabolomics that support the compound discovery efforts: targeted metabolomics, untargeted metabolomics and a hybrid technique of targeted-untargeted metabolomics.

Targeted metabolomics is a term used for the identification and quantification of one or more targeted molecules in a biological sample. Targeted analysis uses standards and/or spectroscopic data libraries, often in conjunction with other “omics” technologies in order to answer a specific research questions. It resembles to traditional phytochemical analysis which quantify specific molecules or classes of metabolites by optimizing their extraction, separation and detection methods.

The **untargeted metabolomics** is an unsupervised, data-driven approach, a process generating data sets which represents the whole chemical spectrum of a biological sample without bias, with predictive power. The untargeted analysis have a great potential in chemometric fingerprinting, compound and pathway discovery and hypothesis generation, but standardization is difficult and the potential for false discovery is high.

Targeted-untargeted metabolomics is a hybrid of analytical approach which combines technologies (chromatography, spectrometry) using available databases or other “omics” to target specific metabolites. Untargeted data sets are mined for known compounds from different species or tissues or

food matrices. The discovery of new metabolites and putative pathways is possible by these technologies, finding relationships between molecules in the data sets.

Metabolomics uses, beside advanced analytical technologies, subsequent multivariate data analyses and updated biostatistics tools (e.g. Profile Analysis, Metaboanalyst) [14]. Recently, available databases of metabolome and metabolic biomarkers (Lipid Gateway, Phenol Explorer, KEGG) became also *sine-qua-non* tools for adequate interpretation of biological significance [15]. Also, the Dr. Duke's Phytochemical and Ethnobotanical database facilitates in-depth searches of plants, chemicals, bioactivity and ethnobotany [16].

PLANT AND FOOD METABOLOMICS

Plant phenotyping and food authentication

Plant metabolomics was defined as a “large scale phytochemistry” [17], a “new frontier” in phytochemical analysis [18], a “missing link” in functional genomics [19, 20]. It provides an integrative view of endogenous metabolic patterns during plant growth, development and senescence but also responses to genetic events, environment and disease, gathering new information about the plant secondary metabolism. It covers new, interdisciplinary topics related to plant science, from chemotaxonomy, stress and biotic interactions, systemic pathogen resistance, induced resistance to diseases, plant and food authentication by specific biomarkers, biomarkers for biomedical applications (19, 21-23]. The metabolite profiling is also an aid to metabolic engineering in plants [24].

This technology differs from the classical phytochemical analysis in various fundamental aspects, being a holistic, data-driven approach with predictive power to assess all measurable metabolites without any pre-conception or pre-selection (as untargeted fingerprinting), possibly followed by targeted metabolite identification and quantitation. The phylogenetic approach of phytochemistry is completed by the performance of ‘omics’ tools based on advanced analysis, as reviewed recently [25, 26].

Plants have one of the largest metabolome (full set of metabolites), their leaves contain up to 30 000 phytochemicals, an arsenal prepared to survive and fight against abiotic and biotic environmental stressors. More than 200 000 different secondary metabolites have been isolated, purified, and identified from plants. In the past decade, around 1200 articles have been published describing plant metabolomes. The key factors in using efficiently the plant metabolomics data are the experimental design, authentic standard availability, extract standardization and statistical analysis.

Since abiotic and biotic stresses are the main reasons of substantial crop yield losses worldwide, recent researches were devoted to the mechanisms of plant interactions with the environment and the resistance to stress, especially using metabolomics technology based on mass spectrometry [27]. Among omics approaches, the metabolomics is the most complex and has received inadequate attention in crop science, particularly for trait mapping and plant selections [28]. An overview of the fundamental analytical technologies and subsequent multivariate data analyses involved in plant metabolomics was recently published [20]. The diverse omics platforms have great potential in improving the current understanding of important traits, enabling to develop new strategies for plant improvement. For the continued development of plant metabolomics, at least three objectives still need to be achieved: improvements in the elucidation of plant metabolome, comparisons of the results found in different laboratories and experiments, followed by the integration of plant metabolomics data with other functional genomics.

The plant metabolomic analysis developed rapidly in line with the new analytical tools for chemical separations (gas and liquid chromatography, capillary electrophoresis) and detection for molecular identification (mass spectrometry and NMR spectroscopy) which emerged the last decades, generating valuable metabolite databases [29], as presented above.

The general application of **metabolomics in food science and nutrition** has been also reviewed [30, 31] underlying the importance of improvements in food analytical chemistry, such as high-resolution mass spectrometry, NMR and advanced statistical techniques to process the large data sets [32, 33]. Plant and food metabolomics has improved our capacity to analyse the overall metabolome as well as helping to perform pathway analysis and metabolite identification [11,13]. Metabolomics tools are only now being used to identify different food components but also the food born derivatives, such as flavours during food processing. Recently, there were characterized the characteristics of the different groups of aroma-related metabolites and their relevant chemical and sensorial characteristics [33], including Maillard reaction pathways. Small phytochemical metabolites play a central role in food quality as they are coloured, fragrant or bioactive, contributing to nutritional value and to positive or negative sensory attributes (e.g. off-flavours). More than 20,000 compounds are identified in different foods (<http://www.Foodb.ca>). To understand the relationship between food quality and processing, a complete analysis of the metabolites present in a food sample is still needed [34]. Mass spectrometry (MS)-based techniques are the most widely used in food science either for volatile or non volatile, polar or unipolar molecules [35].

Food adulteration, mislabeling and fraud, is a worldwide growing concern. Current challenges associated with food authentication are influenced by the geographic origin, breed/variety identification, plant/animal production technology, food processing, etc. Accurate and reliable analytical methods are applied nowadays to monitor and control food authenticity and to guarantee correct and accurate labeling of foodstuffs, assuring that the components included in a food product are of the nature and quality declared by the seller. Omics' based technologies circumvent the limitations of traditional methodologies, being developed for the authentication of a wide range of food commodities. Recently it was reviewed the updated literature, since 2015, which applied omics-based technologies and especially metabolomics, for food authentication [36].

TRADITION AND MODERNITY

80 Years of Research at USAMV in Cluj-Napoca, Romania

The research group on "Chemistry and Biochemistry of Natural Compounds" was created since 80 years, at the former Institute of Agronomy in Cluj, known today as University of Agricultural Sciences and Veterinary Medicine, which celebrates this year 150 years of existence. The mentor of this group, professor Cornel Bodea (member of Romanian Academy and director of the Institute of Chemistry in Cluj) have had major contributions to the development of Phytochemistry in Romania, leading the most prominent group of Plant Science research in Romania, especially focused on secondary metabolites (carotenoid pigments), their biosynthesis, isolation and characterization from different bioresources, as well the beneficial effects on animals and humans. The scientific performance of this group, especially the last 5 decades is revealed by many international collaborations and publications in books, international journals. A prove of its international recognition was the organization, in 1972 of the 3rd International Carotenoid Symposium in Cluj. The scientific performance was continued by the followers Prof. G. Neamțu, prof. V. Tămaș and their collaborators, some of the most relevant publications being mentioned in Table 2.

The last 3 decades, another significant progress was noticed in this group, in-line to the diversification of phytochemistry areas and development of omics' technologies, as well due to the improvement of analytical facilities and formation of young scientists, approaching the plant and food metabolomics technology. Secondary metabolites, especially carotenoids, tocopherols, phytosterols, fatty acids, terpenoids, different polyphenols (from

phenolic acids to flavonoids, catechins and anthocyanins), but also terpenoids, glucosinolates from different plant sources enlarged the scientific areas of interest, being focused on the improvement of extraction procedures, separation by different chromatographic tools, isolation and characterization by different spectrometry tools, evaluation of their antioxidant/antitumor effects. Advanced biostatistics was developed for the proper classification (plant chemotaxonomy), confirmation of food authenticity or fraud identification. Table 2 reviews the most significant results, published in many international impact publications (more than 220, according to Web of Science) which prove the scientific performance reached nowadays. More than 40 PhD students were trained and involved in different projects and experiments related to Phytochemistry, Plant and Food metabolomics, including applications bio(nano)technology and in biomedical areas. The progress of this group' knowledge and expertise was significantly due to the performant metabolomic platform (HPLC-DAD-MS, GC-MS, Raman and FTIR Spectrometry) and advanced biostatistics/bioinformatics tools (multivariate combined with univariate data analyses) in the context of systems biology concept.

The previous and present studies, as well the results on applying omics' techniques are presented below, showing their impact on the new, emerging research areas such as bioeconomy, food industry, functional food and nutrition, phytomedicine [37].

Table 2. Relevant scientific areas and publications realized by the research group on Natural Product Chemistry from USAMV Cluj-Napoca

	Topics /Titles [reference]
Reviews and books	Treatise de Plant Biochemistry (vol I-VI) [38]
	Carotenod pigments and metabolites [39]
	Recent advances in the chemistry of phenothiazines [40]
	Food Chemistry [41]
	Molecular composition of carotenoid-lipo-protein structures of Seabuckthorn Berries [42]
	Xanthophyll Esters in Fruits and Vegetables [43]
	Food Colorants: Chemical And Functional Properties [44]
	Instruments to analyse food colors [45]
	Advances in natural food colorant chemistry. Part 1. Current technologies applied for pigments' extraction [46]
	Lipoxygenase-Quercetin Interaction: A Kinetic Study Through Biochemical and Spectroscopy Approaches [47]
	Phytochemical Antioxidants [48]

	Topics /Titles [reference]
	Antioxidant phytochemicals: Chemical characterization, functions and actions [49]
	Antioxidant Activity of European Mistletoe [50]
	Anthocyanins-Smart Molecules for Cancer Prevention [51]
	Plant and food metabolomics in the post genomic era: concepts, methodologies and applications [52]
	Plants and natural compounds with antidiabetic action [53]
	Pharmacological Benefits of Herbal Formulations in the Management of <i>Psoriasis vulgaris</i> [54]
	Plant metabolomics versus phytochemistry. What makes the difference? [55]
	Plant metabolomics beyond genomics [56]
	Screening of bioactive compounds synthesized by microalgae: a progress overview on extraction and chemical analysis [57]
	Bioactive ingredients from microalgae: food and feed application [58]
	Complementary advanced techniques applied for plant and food authentication [59]
	Challenges and impact of high-throughput targeted and untargeted plant/food medical metabolomics using UPLC-MS and FTIR technologies [60]
	Four Steps Metabolomic Characterization of Pigments as Biomarkers of Food Quality and Authenticity [61]
	Plant and food metabolomics: fingerprints of phytochemicals as authenticity markers of medicinal plant extracts and functional food [62]
	Applied metabolomics in Romania: from plant taxonomy to food quality, authenticity and traceability [63]
	Advances in Distilled Beverages Authenticity and Quality Testing [64]
	Foodomics: an advanced technology to integrate Food Analysis in the systems' biology approach [65]
Phytochemical analysis	Polar lipids and fatty acid distribution in carotenoprotein complexes extracted from <i>Sea Buckthorn</i> fruit [66]
	Qualitative analysis of phytosterols from different extracts [67]
	Structure of the carotenoid physoxanthin [68]
	Cyclization reactions of carotenoids [69]
	Enzymatic hydrolysis of zeaxanthin esters from <i>Physalis Alkekengi</i> [70]
	Gas-Chromatographic Analysis of Major Volatile Compounds Found in Traditional Fruit Brandies from Transylvania [71]
	Polyphenolic Content and Antioxidant Activities of Some Wild and Cultivated Blueberries from Romania [72]
	Fatty acid and phytosterol contents of some Romanian wild and cultivated berry pomaces [73]
	Evaluation of Betulin and Betulinic Acid Content in Birch Bark from Different Forestry Areas of Western Carpathians [74]
	Carotenoid composition of <i>Rosa canina</i> fruits determined by thin-layer chromatography and high-performance liquid chromatography [75]
	Carotenoids, tocopherols and antioxidant activity of lipophilic extracts from sea buckthorn berries (<i>Hippophae rhamnoides</i>) and apricots (<i>Prunus armeniaca</i>) [76]

	Topics /Titles [reference]
	Combined HPLC/UV-Vis/FTIR fingerprints of antioxidant phytochemicals as functional food authenticity, quality and functionality markers [77]
	Lipid Classes and Fatty Acid Regiodistribution in Triacylglycerols of Seed Oils of Two Sambucus Species (<i>S. nigra</i> L. and <i>S. ebulus</i> L.) [78]
	Total and individual carotenoids and phenolic acids content in fresh, refrigerated and processed spinach (<i>Spinacia oleracea</i> L.) [79]
Phytochemicals activity and effects	Antioxidant/prooxidant activity of a polyphenolic grape seed extract [80]
	Hydrophilic and Lipophilic Antioxidant Activities of Mistletoe (<i>Viscum album</i>) [81]
	Competitive carotenoid and cholesterol incorporation into liposomes: effect on membrane phase transition, fluidity, polarity and anisotropy [82]
	Carotenoids in DPPC vesicles: membrane dynamics [83]
	Carotenoid incorporation into biological membranes from artificial carriers: liposomes and beta-cyclodextrins [84]
	Incorporation of carotenoid esters in liposomes [85]
	HPLC analysis of carotenoids in four varieties of <i>Calendula Officinalis</i> L. Flowers [86]
	Chromatographic analysis (HPLC, GC) of Carotenol Fatty Acids Esters in <i>Physalis alkekengi</i> and <i>Hippophae rhamnoides</i> [87]
	Iron chelation properties of phenolic acids bearing catechol and galloyl groups [88]
	Antioxidant Activity Of Flavanols From Different Romanian Grape Seed Extracts [89]
	Lactic Acid Production by <i>Lactobacillus paracasei</i> 168 in Discontinuous Fermentation Using Lucerne Green Juice as Nutrient Substitute [90]
	Selenium enriched green tea coencapsulated with <i>B. infantis</i> or <i>B. breve</i> in chitosan coated alginate capsules improves survival of bacteria in simulated gastro-intestinal and refrigerated conditions [91]
	Catechin-rich green tea extract modulates the oxidative status of human retinal pigment epithelial cells [92]
	Inhibitory Effects Of Isoflavones on Soybean Lipoygenase-1 Activity [93]
	Comparative study about antioxidant activities of <i>Viscum album</i> from different, host trees, harvested in different seasons [94]
	Xanthophylls protect against induced oxidation in cultured human retinal pigment epithelial cells [95]
	Evaluation of Hydrolytic Activity of Different Pectinases on Sugar Beet (<i>Beta vulgaris</i>) Substrate Using FT-MIR Spectroscopy [96]
	Antioxidant Effect of Trans-Resveratrol in Cultured Human Retinal Pigment Epithelial Cells [97]
	Antioxidant activities of chokeberry extracts and the cytotoxic action of their anthocyanin fraction on HeLa human cervical tumor cells [98]
	Green tea increases the survival yield of Bifidobacteria in simulated gastrointestinal environment and during refrigerated conditions [99]
Anthocyanin determination in blueberry extracts from various cultivars and their antiproliferative and apoptotic properties in B16-F10 metastatic murine melanoma [100]	

	Topics /Titles [reference]
	Green synthesis of gold nanoparticles by <i>Allium sativum</i> extract and their assessment as SERS substrate [101]
	Selenium enriched green tea increase stability of <i>Lactobacillus casei</i> and <i>Lactobacillus plantarum</i> in chitosan coated alginate microcapsules during exposure to simulated gastrointestinal conditions [102]
	Structure and dose-related stability and antioxidant activity of catechins in abiotic vs cell environments: HPLC fingerprint and cellular markers [103]
	Antiproliferative and antioxidant properties of anthocyanin rich extracts from blueberry and blackcurrant juice [104]
	Chokeberry Anthocyanin Extract as Pancreatic β -Cell Protectors in Two Models of Induced Oxidative Stress [105]
	Effects of solid-state fermentation with two filamentous fungi on the total phenolic contents, flavonoids, antioxidant activities and lipid fractions of plum fruit (<i>Prunus domestica</i>) by-products [106]
	Melanoma inhibition by anthocyanins is associated with the reduction of oxidative stress biomarkers and changes in mitochondrial membrane potential [107]
	Thermal Stability Study of the Grape Seeds Extracts in the Aqueous Solutions [108]
Plant metabolomics	HPLC separation systems of flavonoids from several medicinal plants buds [109]
	HPLC analysis coupled with diode array detector used in determination of isoflavone aglycones from different Romanian varieties of soybeans [110]
	Composition in polyphenols and stability of the aqueous grape seed extract from the Romanian variety Merlot Recas [111]
	Comparative fingerprint and extraction yield of medicinal herb phenolics with hepatoprotective potential [112]
	Patterns of carotenoid pigments extracted from two orange peel wastes (<i>Valencia</i> & <i>Navel var.</i>) [113]
	HPLC Fingerprint of Bioactive Compounds and Antioxidant Activities of <i>Viscum album</i> from Different Host Trees [114]
	Chemometric discrimination of different tomato cultivars based on their volatile fingerprint in relation to lycopene and total phenolics content [115]
	In-tube extraction and GC-MS analysis of volatile components from wild and cultivated Sea Buckthorn (<i>Hippophae rhamnoides L. ssp Carpatica</i>) Berry Varieties and Juice [116]
	Glucosinolates profile and antioxidant capacity of Romanian <i>Brassica</i> vegetables obtained by organic and conventional agricultural practices [117]
	Carotenoid composition of berries and leaves from six Romanian Sea Buckthorn (<i>Hippophae rhamnoides L.</i>) varieties [118]
	Fingerprint and Quantification of Phenolic and Flavonoid Composition of Aqueous Leaf Extracts of <i>Cornus mas</i> and <i>Crataegus monogyna</i> [119]
	UHPLC/PDA-ESI/MS Analysis of the Main Berry and Leaf Flavonol Glycosides from Different Carpathian <i>Hippophae rhamnoides L.</i> Varieties [120]
	Untargeted metabolomics for Sea Buckthorn (<i>Hippophae rhamnoides ssp. carpatica</i>) berries and leaves: Fourier Transform Infrared Spectroscopy as a rapid approach for discrimination [121]

	Topics /Titles [reference]
	Comparative evaluation of phenolics' profile and recovery in spray dried powders obtained from rosemary and oregano extracts in relation to their antibacterial activity <i>in vitro</i> [122]
	Liberation and recovery of phenolic antioxidants and lipids in chokeberry (<i>Aronia melanocarpa</i>) pomace by solid-state bioprocessing using <i>Aspergillus niger</i> and <i>Rhizopus</i> [123]
	Comparative FTIR-ATR/HPLC metabolic profiles and quality assessment of herbal extracts of some medicinal plants originating from European countries [124]
	Comparative HPLC-ESI ⁺ -MS carotenoid profiles of <i>Chlorella sorokiniana</i> microalgae in aqueous suspensions and freeze milled powders [125]
Food metabolomics (authenticity)	Bioinformatics Tools for Metabolomic Data Processing and Analysis Using Untargeted Liquid Chromatography Coupled With Mass Spectrometry [126]
	Evaluation of the content and bioactivity of phenolic compounds in olive oil [127]
	UV-VIS spectrometry applied for the quality and authenticity evaluation of edible oils from Romania [128]
	Correlations of the phenolic compounds and the phenolic content in some spanish and French olive oils [129]
	Phytosterol and fatty acid profile of four edible oils processed in Romania [130]
	Photopyroelectric detection of vegetable oils' adulteration [131]
	HPLC fingerprint of organic acids in fruit juices [132]
	Free and esterified sterol distribution in four Romanian vegetable oil [133]
	Quantification of carbohydrates in fruit juices using FTIR spectroscopy and multivariate analysis [134]
	Prediction of Total Antioxidant Capacity of Fruit Juices using FTIR Spectroscopy and PLS regression [135]
	Rapid quantitative analysis of ethanol and prediction of methanol content in traditional fruit brandies from Romania, using FTIR spectroscopy and chemometrics [136]
	Romanian wines quality and authenticity using FT-MIR spectroscopy coupled with multivariate data analysis [137]
	HPLC fingerprinting of glucosinolates during fermentations assisted by chemometric analysis [138]
	Rapid, non-destructive determination of butter adulteration by means of photopyroelectric (PPE) calorimetry [139], and Discrimination of butter adulteration by ATR-FTIR spectroscopy [140]
Brown beer vinegar: A potentially functional product based on its phenolic profile and antioxidant activity [141]	

CONCLUSION

The scientific progress registered in phytochemistry and plant or food metabolomics, since eight decades was mainly due to the added-value knowledge and improvements of analytical platforms (from Infrared and

Raman spectrometry as rapid fingerprinting spectrometry techniques, gas- or liquid chromatography as main advanced separation techniques, coupled with mass-spectrometry or magnetic resonance), new biostatistics software and databases as well formation of a new generation of scientists trained in these emerging areas. This review shows not only the progress at international scale, related to plant and food phytochemistry and metabolomics, but reveals the Romanian contributions and significant achievements of the research group from the Departments and Research Centers related to Chemistry and Biochemistry of Natural Products. It is a welcomed occasion to celebrate the remarkable scientific quality brought by a synergic combination of “tradition and modernity” here in Cluj-Napoca, at the University of Agricultural Sciences and Veterinary Medicine which celebrates this year 150 years of existence.

ACKNOWLEDGEMENT

I would like to thank all my former and present collaborators, many of them my previous PhD students, who contributed significantly to the scientific performance of our group in Phytochemistry and Metabolomics research: Adela Pinteau, Elena Mudura, Fracisc Dulf, Andreea Bunea, Dan Vodnar, Constantin Bele, Madalina Neacsu, Sanda Andrei, Teodora Coldea, Sonia Socaci, Loredana Leopold, Cristina Coman, Lucian Cuius, Veronica Chedea, Dumitrița Rugina, Zorița Diaconeasa, Simona Vicaș, Raluca Pop, Oana Pop, Simona Zăvoi, Adina Chiș, Camelia Echim, Floricuta Ranga, Florinela Fetea as well to many collaborators from foreign universities: Hanspeter Pfander from University of Bern, George Britton from Liverpool University, Michel Gleizes from Bordeaux University, Roland Verhe, Mirjana Andjekovics and John Van Camp from Gent University, Horst A. Diehl from Bremen University, Harry Gruppen and Jean Paul Vinken from Wageningen University, Heiki Kallio from Turku University, Panos Kefalas from Mediterranean School Chania. These scientists had significant contributions to the training of our researchers in Phytochemistry, incl. Carotenoid Chemistry and Biochemistry, Biophysics, Food Chemistry and Biotechnology.

REFERENCES

1. R. Wayne; Plant Cell Biology (2nd Ed), Ed Elsevier, **2019**, 411-423.
2. J. Buckingham; Dictionary of Natural Products. Abingdon: Taylor & Francis, USA, **1993**.
3. F. Scossa; M. Benina; S. Alseekh; Y. Zhang; A.R. Fernie; *Planta Med.*, **2018**, *84*, 855-887.
4. J. Arnason; R.Mata; J.T.Romeo; *Phytochemistry of Medicinal Plants*. Springer Science & Business Media, **2013**.
5. E.T. Wurtzel; T.M. Kutchan; *Science*, **2016**, *353*, 1232-1236.

6. M.S. Meskin; *Phytochemicals in Nutrition and Health*, **2002**, CRC Press.
7. O. Fiehn; *Plant Mol. Biol.*, **2002**, *48*, 155-171.
8. G.J. Patti; O.Yanes; G.Siuzdak; *Nature Reviews*, **2012**, *13*, 263-269.
9. U. Roessner; D.A. Dias; (Eds.), *Metabolomics Tools for Natural Product Discovery, Methods and Protocols*, Humana Press, **2013**.
- 10.W. Weckwerth; *Metabolomics: methods-protocols in Methods in molecular biology*, Humana Press, **2007**.
- 11.A. Zhang; H. Sun; P. Wang; Y. Han; X. Wang; *The Analyst*, **2012**, *137*, 293-300.
- 12.S.D. Johanningsmeier; G.K. Harris; C.M. Klevorn; *Annual Review of Food Science and Technology*, **2016**, *7*, 413-438.
- 13.D.D. Marshall; R. Powers; (2017). *Progress in Nuclear Magnetic Resonance Spectroscopy*, **2017**, *100*, 1-16.
- 14.C. E. Turi; Jamie Finley; Paul R. Shipley; Susan J. Murch; P. N. Brown; *J. Nat. Prod.*, **2015**, *78*, 953-966.
- 15.P. Mendes; Brief. *Bioinform.*, **2002**, *3*, 134-145.
- 16.Dr. Duke's Phytochemical and Ethnobotanical Databases, <https://phytochem.nal.usda.gov/phytochem/plants>.
- 17.L.W. Sumner; P.Mendes; R.A. Dixon; *Phytochemistry*, **2003**, *62*, 817-836.
- 18.F. Tugizimana; L.Piater; I.Dubery; *South Afr. J.Sci.*, **2013**, *109*,1-11.
- 19.R. Hall; M. Beale; O. Fiehn; N.Hardy; L.Sumner; R.Bino; *Plant Cell*, **2002**, *14*, 1437-1440.
- 20.R.D. Hall (Ed.), *Annual Plant Reviews*; Wiley-Blackwell Publishing, Oxford, UK, **2011**, *43*, 448-465.
- 21.A.R. Fernie; *Funct Plant Biol*, **2003**, *30*,111-120.
- 22.J. Kopka; A. Fernie; W. Weckwerth; Y. Gibon; M. Stitt; *Genome Biol.*, **2004**, *5*, 109–117.
- 23.W. Weckwerth (ed.); *The Handbook of Plant Metabolomics*, Wiley-Blackwell, Guenter Kahl, **2013**.
- 24.R.N. Trethewey; *Curr. Opin. Plant Biol.*, **2004**, *7*, 196-201.
- 25.T. Tenenboim; Y. Brotman; *Trends in Plant Science*, **2016**, *21*, 781-792.
- 26.T. Garnatje et al.; *Trends in Plant Science*, **2017**, *22*, 187-198.
- 27.A. Piasecka; P. Kachlick; M. Stobiecki; *Int. J. Mol. Sci.*, **2019**, *20*, 379-397.
- 28.R. Kumar; A. Bohra; A.K.Pandey; M.K.Pandey; A.Kumar; *Frontiers in Plant Sci.*, **2017**, *8*, 1302-1309.
- 29.C. Deborde; J.X. Fontaine; D. Jacob; A. Botana; V. Nicaise; F. Richard-Forget; S. Lecomte; C. Decourtil; K. Hamade; F. Mesnard; A. Moing; R. Molinié; *Metabolomics*, **2019**, *15*, 28-36.
- 30.D.S. Wishart; *Trends Food Sci. Technol.*, **2008**, *19*, 482-493.
- 31.J.M. Cevallos-Cevallos; J.I. Reyes-De-Corcuera; E. Etxeberria; M.D. Danyluk; G.E. Rodrick; *Trends Food Sci. Technol*, **2009**, *20*, 557-566.
- 32.A. Scalbert; L. Brennan; O. Fiehn; T. Hankemeier; B.S. Kristal; B. van Ommen; *Metabolomics*, **2009**, *5*, 435-458.
- 33.J. Rubert; M. Zachariasova; J. Hajslova; *Food Additives and Contaminants- Part A Chemistry, Analysis, Control, Exposure and Risk Assessment*, **2015**, *32*, 1685-1708.

34. U. Thissen; L. Coulier; K.M. Overkamp; J. Jetten; B.J.C. van der Werff; T. Van de Ven; M.J. Van der Werf; *Food Quality and Preference*, **2011**, *22*, 499-512.
35. C. Diez-Simon; R. Mumm; R.D. Hall; *Metabolomics*, **2019**, *15*, 41-49.
36. K. Bohme; P. Calo-Mata; J. Barros-Velazquez; I. Ortea; *Trends Anal. Chem.*, **2019**, *110*, 221-234.
37. G. Ulrich-Merzenich; H. Zeitler; D. Jobst; D. Panek; H. Vetter; H. Wagner; *Phytomedicine*, **2007**, *14*, 70-82.
38. C. Bodea; *Tratat de Biochimie vegetală*, Ed. Academiei RSR, vol. I-VI, **1964-1984**.
39. G. Neamtu; V. Tămaș; *Pigmenți carotenoidici și metaboliti*, Ed. Ceres, București, **1986**.
40. C. Bodea; I. Silberg; *Adv. Heterocyclic Chem.*, **1968**, *9*, 321-332.
41. C. Socaciu; *Chimia Alimentelor*, Ed. Academic Press, Cluj-Napoca, **2017**, 126 pag.
42. C. Socaciu; A. Pinteaa; in *Seabuckthorn, A Multipurpose Wonder Plant* ed. V. Singh, Indus International, India, **2006**, pp. 342-360.
43. A. Bunea; C. Socaciu; A. Pinteaa; *Not. Bot. Horti. Agrobo*, **2014**, *42*, 310-324.
44. C. Socaciu (ed.); *Food Colorants: Chemical and Functional Properties*, CRC Press-Taylor and Francis Group, New York, **2008**, 633 pp.
45. C. Socaciu, H.A. Diehl; *Instruments to analyse food colors*, in *Handbook of Food Analysis Instruments*, S. Otles Ed., CRC Press-Taylor and Francis Group, New York, **2009**, chapter 1.
46. C. Socaciu; *Agrofood Industry Hi-tech*, **2009**, *20*, 43-46.
47. V.S. Chedea; S.I. Vicaș; C. Socaciu; T. Nagaya; H. J. Oduor Ogola; K. Yokota; K. Nishimura; M. Jisaka; *Lipoxygenase-Quercetin Interaction: A Kinetic Study Through Biochemical and Spectroscopy Approaches*, *Biochemical Testing*, **2012**, *InTech Publ*, pp. 29.
48. C. Socaciu; in *Alimentația funcțională cu componente bioactive naturale în sindromul metabolic*, Ed. Eurostampa, Timișoara, **2009**, pp. 95-127.
49. C. Socaciu; *Bull. USAMV-AGR*, **2002**, *58*, 22-29.
50. S.I. Vicas; D. Rugină; C. Socaciu; in *Phytochemicals as Nutraceuticals- Global Approaches to Their Role in Nutrition and Health*, *InTech Publ.*, **2012**, pp. 21.
51. Z. M. Diaconeasa; A. D. Frond; I. Stirbu; D. Rugina; C. Socaciu; *Anthocyanins- Smart Molecules for Cancer Prevention*, *InTech Publ.*, **2018**, chapter 5.
52. C. Socaciu; *Bull. USAMV-AGR*, **2006**, *62*, 352-359.
53. C. Coman; O. D. Rugină; C. Socaciu; *Not. Bot. Horti. Agrobo.*, **2012**, *40*, 314-325.
54. A.N. Boca; D. Tataru; A. Buzoianu; C. Pincelli; C. Socaciu; *Not. Bot. Horti. Agrobo.*, **2014**, *42*, 1-8.
55. C. Socaciu; 1st Int. Congr. Danube Reg. Bot. Gardens, Arad, 7-9.09. **2017**.
56. C. Socaciu; *Symp. Rom. Acad., University A.I. Cuza, Iași*, 15.10. **2010**.
57. D. Pătraș; C.V. Moraru; C. Socaciu; *Screening of bioactive compounds synthesized by microalgae: a progress overview on extraction and chemical analysis*, *Studia UBB Chemia*, **2018**, *63*, 21-35.
58. D. Pătraș; C.V. Moraru; C. Socaciu; *Bull. USAMV -FST*, **2019**, *76*, 1-15.
59. C. Socaciu; F. Ranga; F. Fetea; D. Leopold; F. Dulf; R. Parlog; *Czech J. Food Sci.*, **2009**, *27*, S70-S75.

- 60.C. Socaciu; R. Pop; F.Ranga; F. Fetea; Int. Conf. Rom. Soc. Biochemistry and Molecular Biology, Oradea, 5-6.06.**2014**.
- 61.C. Socaciu; 6th Int. Congr. Pigments in Food, Budapest, **2010**.
- 62.C. Socaciu; Fl.Ranga; F. Fetea; F.Dulf;, 5th Int. Conf. Plant Metabolomics, Yokohama, Japan, **2008**.
- 63.C.Socaciu; Fl.Ranga; F. Fetea; Metabomeeting, Lyon, **2008**.
- 64.T. E. Coldea; E. Mudura; C. Socaciu; Advances in Distilled Beverages Authenticity and Quality Testing, InTechopen Publ. **2017**, chapter 6.
- 65.C. Socaciu; C. Moraru; D. Patras 4th North and East Eur. Congr. on Food, Kaunas, 11-13.09. **2017**.
- 66.A. Pinteaa; A. Marpeau; M. Faye; C. Socaciu; M. Gleizes; *Phytochem. Anal.*, **2001**, 12, 293-298.
- 67.F. Dulf; C. Socaciu; C. Bele; *Bull. USAMV-VM*, **2005**, 61, 388-393.
- 68.C. Bodea; A.G. Andrewes; G. Borch; S. Liaaen-Jensen; *Phytochemistry*, **1978**, 17, 2037-2045.
- 69.C.Bodea; *Pure Appl. Chem.*, **1969**, 20, 517-527
- 70.A. Bunea; A. Pinteaa; S. Andrei; A. Lujerdean; C. Socaciu; *Bull. USAMV-Zoo*, **2006**, 62, 282-286.
- 71.T.E. Rusu; C. Socaciu; M. Parv; D.C. Vodnar; *Not. Bot. Horti. Agrobo.*, **2011**, 39, 109-116.
- 72.Bunea; D. O. Ruginã; A.M. Pinteaa; Z. Sconța; C.I. Bunea; C. Socaciu;, *Not. Bot. Horti. Agrobo.*, **2011**, 39, 70-76.
- 73.F. Dulf; S. Andrei; A. Bunea; C. Socaciu; *Chem. Papers*, **2012**, 66, 925-934.
- 74.L. Holonec; F.Ranga; D. Crainic; A. Truța; C. Socaciu; *Not. Bot. Horti. Agrobo.*, **2012**, 40, 99-105.
- 75.T. Hodisan; C. Socaciu; I. Ropan; G. Neamtu; *J. Pharm. Biomed. Anal.*, **1997**, 25, 256-262.
- 76.E.A. Pop; Z.M. Diaconeasa; F.Fetea; A. Bunea; F. Dulf; A. Pinteaa; C.Socaciu; *Bull. USAMV-FST*, **2015**, 72, 169-175.
- 77.C. Socaciu; S.Drăgan; F.Ranga; F. Fetea; D.Preda; 3rd Int. Conf. Polyphenols and Health, Kyoto, Japan, **2007**.
- 78.F.V. Dulf; I. Oroian; D.C. Vodnar; C. Socaciu; A. Pinteaa; *Molecules*, **2013**, 18, 11768-11785.
- 79.A. Bunea; M. Andjelkovic; C. Socaciu; O. Bobis; M. Neacsu; R. Verhé; J. Van Camp; *Food Chemistry*, **2008**, 108, 649-656.
- 80.V.S. Chedea; C. Braicu; C. Socaciu; *Food Chemistry*, **2010**, 121, 132-139.
- 81.S. Vicas; J. Prokisch; D. Rugina; C. Socaciu; *Not. Bot. Horti. Agrobo.*, **2009**, 37, 112-116.
- 82.C. Socaciu; R. Jessel; H.A. Diehl; *Chem. Phys Lipids*, **2000**, 106, 79-88.
- 83.C. Socaciu, S. Haertel; H. A. Diehl; *Spectrochimica Acta, part A*, **1999**, 55, 2289-2297.
- 84.I. Lancrajan, H. A. Diehl; C. Socaciu; M. Engelke; M. Zorn-Kruppa; *Chem. Phys. Lipids*, **2001**, 112, 1-10.
- 85.A. Pinteaa; C. Socaciu; H. A. Diehl; *Biophys. Chem.*, **2005**, 118, 7-14.

- 86.A. Pinteaa; C. Bele; S. Andrei; C. Socaciu; *Acta Biol. Szegediensis*, **2003**, *47*, 37-40.
- 87.A. Pinteaa; A. Varga; P. Stepnowski; C. Socaciu; M. Culea; H.A. Diehl; *Phytochemical Analysis*, **2005**, *16*, 188-195.
- 88.M. Andjelkovic; J. Van Camp; B. De Meulenaer; G. Depaemelaere; C. Socaciu; M. Verloo ; R. Verhe; *Food Chemistry*, **2006**, *98*, 23-31.
- 89.D. Ruginã; S. Vicaș; C. Momeu; C. Socaciu; *Chem. Listy*, **2008**, *99*, 1234-1235.
- 90.D.C. Vodnar, J. Venus ; R. Schneider ; C. Socaciu; *Chem. Eng. & Technol.*, **2010**, *33*, 468-474.
- 91.D.C. Vodnar; C. Socaciu; *International J. Food Sci. & Technol.*, **2010**, *45*, 2345-2351.
- 92.A. Pinteaa; D. Rugina; R. Parlog; C. Socaciu; *Rom. Biotechnol. Lett.*, **2010**, *15*, 4964-4978.
- 93.S. Vicas; V. Chedea; C.Socaciu; *J. Food Biochem.*, **2011**, *35*, 613-627.
- 94.S. Vicaș; D. Rugina; C. Socaciu; *J. Med. Plant Res.*, **2011**, *5*, 2237-2244.
- 95.A. Pinteaa; D. Rugina; A. Bunea; R. Pop; C. Socaciu, *J. Food Comp. Anal.*, **2011**, *24*, 830-836.
- 96.A. Chis; F. Fetea; H. Matei; C. Socaciu; *Not. Bot. Horti. Agrobi.*, **2011**, *39*, 99-104.
- 97.A. Pinteaa; D. Rugina; R. Pop; A. Bunea; C. Socaciu; H.A. Diehl; *J. Ocular Pharmacol. & Ther.*, **2011**, *27*, 315-321.
- 98.D. Ruginã; Z. Sconța; L. Leopold; A. Pinteaa; A. Bunea; C. Socaciu; *J. Med. Food*, **2012**, *15*, 700-706.
- 99.D.C. Vodnar; C. Socaciu; *Chem. Central J.*, **2012**, 61-69.
100. Bunea; D. Ruginã; Z. Sconța; R. M. Pop; A. Pinteaa; C. Socaciu; F.Tăbăran; C. Grootaert; K.Struijs; J. VanCamp; *Phytochemistry*, **2013**, *95*, 436-444.
101. C. Coman; L.F. Leopold; O.D. Ruginã; L.Barbu-Tudoran; N. Leopold; M. Tofanã; C. Socaciu; *J. Nanopart. Res.*, **2013**, *16*, 2158-2167.
102. D.C. Vodnar; C. Socaciu; *LWT-Food Sci.Technol.*, **2014**, *57*, 406-411.
103. D.Preda; I. Berindan Neagoe; O.Balacescu; 3rd Int. Conf. on Polyphenols and Health, Kyoto, Japan, **2007**.
104. Z. Diaconeasa; L. Leopold; D. Rugina; C. Socaciu; *Int. J. Mol. Sci.*, **2015**, *16*, 2352-2365.
105. D. Ruginã; Z. Diaconeasa; C. Coman; A. Bunea; C. Socaciu; A. Pinteaa; *Oxidative Med. Cellular Longevity*, **2015**, 1-10.
106. F.V. Dulf; D.C. Vodnar; C. Socaciu; *Food Chemistry*, **2016**, *209*, 27-36.
107. Z. Diaconeasa; H. Ayvaz; D. Ruginã; L. Leopold; A. Stănilă; C. Socaciu; *Plant Foods for Human Nutr.*, **2017**, *72*, 404-410.
108. C. Pop; A. M. Rotar; L. Salanța; S. Socaci; F.Ranga; C. Socaciu; *Bull. USAMV-FST*, **2015**, *72*, 91-98.
109. M. Neacsu; C. Socaciu; M. Tamas; C. Blidar; *Bull. USAMV-AGR*, **2002**, *58*, 37-43.
110. M. Neacsu; S.Vicas; C. Socaciu; *Bull. USAMV-AGR*, **2008**, *65*, 310-315
111. V. Chedea; C. Echim; C. Socaciu; *J. Food Biochem.*, **2011**, *35*, 92-108.
112. S. Zavoi; F. Fetea; F. Ranga; R. Pop; A. Baci; C. Socaciu; *Not. Bot. Horti. Agrobi.*, **2011**, *39*, 82-89.

113. V.S. Chedea; P. Kefalas; C. Socaciu; *Journal of Food Biochemistry*, **2010**, *34*, 101-110.
114. S. Vicas; D. Rugina; L. Leopold; A.Pintea A.; C. Socaciu; *Not. Bot. Horti. Agrobio.*, **2011**, *39*, 48-57.
115. S.A. Socaci; C. Socaciu; C. Mureşan; A. Fărcaş; M.Tofană; S. Vicaş; A. Pintea; *Phytochem. Anal.*, **2014**, *25*, 165-169.
116. S.A. Socaci; C. Socaciu; M. Tofana; V. Rati; A. Pintea; *Phytochem. Anal.*, **2013**, *24*, 319-328.
117. S.I. Vicas; A.C.Teusdea; M. Carbutar; S. Socaci; C. Socaciu; *Plant Foods Human Nutr.*, **2013**, *68*, 313-321.
118. R.M. Pop; Y. Weesepeel; C. Socaciu; A. Pintea; J.P. Vincken; H.Gruppen; *Food Chemistry*, **2014**, *42*, 1-8.
119. M. Badalica-Petrescu; S. Dragan; F. Ranga; F. Fetea; C. Socaciu; *Not. Bot. Horti. Agrobio.*, **2014**, *42*, 9-18.
120. R. M. Pop; C. Socaciu; A. Pintea; A.D. Buzoianu; M.D. Sanders; H. Gruppen; J.P. Vincken; *Phytochem. Anal.*, **2013**, *24*, 484-492.
121. R. M. Pop; A. Buzoianu; V. Rati; C. Socaciu; *Not. Bot. Horti. Agrobio.*, **2014**, *42*, 545-550.
122. F.Bunghez; A. M. Rotar; D.C. Vodnar; G.M. Cătuşescu; C. Socaciu; *Rom. Biotechnol. Lett.*, **2016**, *21*, 1-15.
123. F.V. Dulf; D.C. Vodnar; E.H. Dulf; Z. Diaconeasa; C. Socaciu; *LWT-Food Sci. Technol.*, **2018**, *87*, 241-249.
124. C.Socaciu; F.Ranga; F. Fetea; 5th Int. Conf. on Plant Metabolomics Pacifico, Yokohama, Japan, **2008**.
125. C. Moraru; K. Skjanes; D. Patras; C. Socaciu; C.J.J.Spetz; 18th Int. Symposium on Carotenoids, Luzern, 9-14 July **2017**.
126. A.G. Lazar; F.Romanciuc; M.A. Socaciu; C. Socaciu; *Bull. USAMV-FST*, **2015**, *72*, 103-115.
127. M. Andjelković; J. Van Camp; C. Socaciu; R. Verhe; *Commun. Agric. Appl. Biol. Sci.*, **2006**, *71*, 19-23.
128. C. Socaciu; F. Ranga; H. A. Diehl; *Bull. USAMV-AGR*, **2005**, *61*, 295-300.
129. M. Andjelkovic; J Van Camp; M. Pedra; K. Renders; C. Socaciu; R. Verhe; *J. Agric. Food Chem.*, **2008**, *56*, 5181-5187.
130. F. Dulf; C. Socaciu; C. Bele; A. Pintea; M. Unguresan; *Chem. Listy*, 2008, *102*, s265–s309.
131. M. Streza; D. Dadarlat; C. Socaciu; C. Bele; F. Dulf; V. Simon; *Food Biophys.*, **2009**, *4*,147-150.
132. L.F. Leopold; H.A. Diehl; C. Socaciu; *Bull. USAMV-AGR*, **2006**, *62*, 288-293.
133. F. Dulf; M. Unguresan; D. Vodnar; C. Socaciu; *Not. Bot. Horti. Agrobio.*, **2010**, *38*, 91-97.
134. L.F. Leopold; N. Leopold; H.A. Diehl; C. Socaciu; *Spectroscopy-Int J.*, IOS Press, **2011**, 112.
135. L.F. Leopold; N. Leopold; H.A. Diehl; C. Socaciu; *Food Anal. Meth.*, **2012**, *5*, 405-407.

136. T.E. Coldea; C. Socaciu; F. Fetea; F. Ranga; R.M. Pop; M. Florea; *Not. Bot. Horti. Agrobio.*, **2013**, *41*, 143-149.
137. R. Banc; F. Loghin; D. Miere; F. Fetea; C. Socaciu; *Not. Bot. Horti. Agrobio.*, **2014**, *42*, 556-564.
138. S. I. Vicas; A. C. Teusdea; M. Carbutar; C. Socaciu; *Rom. Biotech. Lett.*, **2015**, *20*, 1067-1075.
139. L. Cuibus; D. Dadarlat; M. Streza; F.V. Dulf; Z. Diaconeasa; C. Socaciu; *J. Therm. Anal. Calorim.*, **2017**, *127*, 1193-1200.
140. L. Cuibus; R. Maggio; V. Mureşan; Z. Diaconeasa; O.L. Pop; C. Socaciu; *Bull. USAMV-FST*, **2015**, *72*, 70-76.
141. E. Mudura; T.E. Coldea; C. Socaciu; F. Ranga; C. Pop; A.M. Rotar; A. Pasqualone; *J. Serbian Chem. Soc.*, **2018**, *83*, 19-30.